

UC Santa Barbara

UC Santa Barbara Electronic Theses and Dissertations

Title

Manipulation of the Uranyl (UO₂²⁺) Moiety: New Routes to Reduction and O-U-O Angle Perturbation

Permalink

<https://escholarship.org/uc/item/5qz6f3rq>

Author

Owens, Elizabeth Anne

Publication Date

2016

Peer reviewed|Thesis/dissertation

UNIVERSITY OF CALIFORNIA

Santa Barbara

Manipulation of the Uranyl (UO_2^{2+}) Moiety: New Routes to Reduction and O-U-O Angle
Perturbation

A dissertation submitted in partial satisfaction of the
requirements for the degree Doctor of Philosophy
in Chemistry

by

Elizabeth Anne Owens

Committee in charge:

Professor Trevor Hayton, Chair

Professor Peter Ford

Professor Ram Seshadri

Professor Steve Buratto

September 2016

The dissertation of Elizabeth Anne Owens is approved.

Peter Ford

Ram Seshadri

Steve Buratto

Trevor Hayton, Committee Chair

June 2016

Manipulation of the Uranyl (UO_2^{2+}) Moiety: New Routes to Reduction and O-U-O Angle
Perturbation

Copyright © 2016

by

Elizabeth Anne Owens

ACKNOWLEDGEMENTS

There are many people I would like to thank for my tenure in graduate school. First, I have to thank Dr. Toni Barstis at St. Mary's College for inspiring me early on to love chemistry, and my undergraduate advisor, Dr. Nicholas Leadbeater at UConn, for introducing me to the world of research and motivating me to pursue graduate studies at UCSB in chemistry.

Of course, I would like to thank my research advisor Dr. Trevor Hayton, for letting me join his group, and pushing me to always do my best. I am truly grateful for his guidance with research, as well as with all areas of my life. The multiple trips to China we went on will be seared in my mind forever, and I loved going on all the group activities: hikes, camping trips, curling and ice-skating. In addition to my time at UCSB, I had the opportunity to perform research at the Shanghai Institute of Organic Chemistry with Dr. Yaofeng Chen, who really went out of his way to make me feel welcome in his group.

I would also like to thank all of my labmates for helping to create an amazing work environment. Specifically, Dr. Lani Seaman and Dr. Jessie Brown for mentoring me, and sharing an office with me. You both made my workdays so much brighter and full of laughter. I also started graduate school at the same time as Danil Smiles, and through these past five years, he has become one of my best friends. He has always been a constant source of helpful advice and inspiration. I also had the pleasure of mentoring six undergraduate students, who were a tremendous help with my research

projects: Jessica Tuck, Shawn Lu, Leonel Griego, Joshua Scott, Megan Wakefield, and Mikaela Kosich.

Outside of the laboratory, I would like to thank my family for all of their encouragement and support over the years. My parents have always been amazing role models in everything they do, and have helped me become the person I am today. Without them, I never could have achieved this. Delaina and Wyatt are my two wonderful siblings, who have always been incredibly supportive. I would also like to thank my 'In-Laws' for all of their encouragement, as they are some of the kindness, and most genuinely good-natured people I've ever met. I really feel lucky to be surrounded by such a great family.

Importantly, I want to thank the person who has helped me the most during my graduate career, my husband Dr. Shawn Owens. We met during my first year at UCSB, and ever since he has given me unwavering love and support. I owe all the things I've achieved in graduate school to him. I look forward to all the days ahead, and the many adventures we will share together.

VITA OF ELIZABETH ANNE OWENS
June 2016

EDUCATION

Doctor of Philosophy in Chemistry (expected) June 2016

University of California, Santa Barbara

Advisor: Professor Trevor W. Hayton

Dissertation: "Manipulation of the Uranyl (UO_2^{2+}) Moiety: New Routes to
Reduction and O-U-O Angle Perturbation"

Bachelor of Science in Chemistry and German May 2011

University of Connecticut

PROFESSIONAL EMPLOYMENT

2011-present: Graduate Student Researcher, Department of Chemistry, University of California, Santa Barbara

2011-2013: Teaching Assistant, Department of Chemistry, University of California, Santa Barbara

2010-2011: Undergraduate Student Researcher, Department of Chemistry, University of Connecticut

PUBLICATIONS

Elizabeth A. Pedrick, Jason W. Schultz, Guang Wu, Liviu Mirica, and Trevor W. Hayton, "Perturbation of the O-U-O Angle in Uranyl by Coordination to a 12-Membered Macrocycle" *Inorganic Chemistry*, **2016**, *55*, 5693-5701.

Elizabeth A. Pedrick, Lani A. Seaman, Joshua C. Scott, Leonel Griego, Guang Wu, and Trevor W. Hayton, "Synthesis and Reactivity of a U(IV) Dibenzoyne Complex" *Organometallics*, **2016**, *35*, 494-502.

Elizabeth A. Pedrick, Peter Hrobárik, Lani A. Seaman, Guang Wu, and Trevor W. Hayton, "Synthesis, Structure and Bonding of Hexaphenyl Thorium(IV): Observation of a Non-Octahedral Structure" *Chemical Communications*, **2016**, *52*, 689-692.

Elizabeth A. Pedrick, Guang Wu, and Trevor W. Hayton, "Oxo Ligand Substitution in a Cationic Uranyl Complex: Synergistic Interaction of an Electrophile and a Reductant" *Inorganic Chemistry*, **2015**, *54*, 7038-7044.

Elizabeth A. Pedrick, Guang Wu, Trevor W. Hayton, "Reductive Silylation of the Uranyl Ion with Ph_3SiOTf ", *Inorganic Chemistry*, **2014**, *53*, 12237-12239.

Elizabeth A. Pedrick, Guang Wu, Nikolas Kaltsoyannis, and Trevor W. Hayton, "Reductive Silylation of a Uranyl Dibenzoylmethanate Complex: A Controlled Example of Uranyl Oxo Cleavage" *Chemical Science*, **2014**, *5*, 3204-3213.

Lani A. Seaman, Elizabeth A. Pedrick, Takashi Tsuchiya, Guang Wu, Elena Jakubikova, and Trevor W. Hayton, "Comparison of the Reactivity of 2-Li-C₆H₄CH₂NMe₂ with MCl_4 (M = Th, U): Isolation of a Thorium Aryl Complex or a Uranium Benzyne Complex" *Angewandte Chemie*, **2013**, *52*, 10589-10592.

Christopher (Xiang) Lee, Elizabeth A. Pedrick, and Nicholas E. Leadbeater, "Preparation of Arene Chromium Tricarbonyl Complexes Using Continuous-Flow Processing" *Journal of Flow Chemistry*, **2012**, *2(4)*, 115-117.

Elizabeth A. Pedrick, and Nicholas E. Leadbeater, "Preparation of Cisplatin Using Microwave Heating and Continuous-Flow Processing as Tools" *Inorganic Chemistry Communications*, **2011**, *14*, 4B1-4B3.

AWARDS

First Place Winner of the 2015 DOE, Office of Nuclear Energy, Innovations in Fuel Cycle Research Award in Separations. Awarded for the work in the published paper, "Reductive Silylation of a Uranyl Dibenzoylmethanate Complex: A Controlled Example of Uranyl Oxo Cleavage"

Recipient of a 2013-2014 University of California, Santa Barbara PIRE-ECCI fellowship, resulting in a collaboration with Dr. Yaofeng Chen at the State Key Laboratory of Organic Chemistry in Shanghai, China. This also funded a research trip to Shanghai for two months.

Recipient of a 2010-2011 UConn Catherine Destefano-Rossi Scholarship for outstanding academic achievement in chemistry

FIELDS OF STUDY

Major Field: Inorganic Chemistry

Studies in Reduction Silylation of Uranyl / Organometallic Actinide Chemistry

ABSTRACT

Manipulation of the Uranyl (UO_2^{2+}) Moiety: New Routes to Reduction and O-U-O Angle Perturbation

by

Elizabeth Anne Owens

Treatment of $\text{UO}_2(\text{dbm})_2(\text{THF})$ with 1 equiv of R_3SiH ($\text{R} = \text{Ph}, \text{Et}$), in the presence of $\text{B}(\text{C}_6\text{F}_5)_3$, results in the formation of $\text{U}(\text{OB}\{\text{C}_6\text{F}_5\}_3)(\text{OSiR}_3)(\text{dbm})_2(\text{THF})$ ($\text{R} = \text{Ph}, \text{Et}$) in good yields. Interestingly, the addition of 1 equiv of $\text{H}(\text{dbm})$ to $\text{U}(\text{OB}\{\text{C}_6\text{F}_5\}_3)(\text{OSiEt}_3)(\text{dbm})_2(\text{THF})$ results in substitution of the $-\text{OSiEt}_3$ ligand to form $\text{U}(\text{OB}\{\text{C}_6\text{F}_5\}_3)(\text{dbm})_3$ and HOSiEt_3 . Furthermore, addition of HOSiEt_3 and 1 equiv of THF to $\text{U}(\text{OB}\{\text{C}_6\text{F}_5\}_3)(\text{dbm})_3$, results in the formation $\text{U}(\text{OB}\{\text{C}_6\text{F}_5\}_3)(\text{OSiEt}_3)(\text{dbm})_2(\text{THF})$, revealing that this process is reversible. In addition, reaction of $\text{U}(\text{OB}\{\text{C}_6\text{F}_5\}_3)(\text{OSiPh}_3)(\text{dbm})_2(\text{THF})$ with excess HOSiPh_3 also results in the formation of the substituted oxo product, $\text{U}(\text{OSiPh}_3)_3(\text{dbm})_2$.

Reaction of $[\text{UO}_2(\text{dppmo})_2(\text{OTf})][\text{OTf}]$ with 4 equiv of Ph_3SiOTf and 2 equiv of Cp_2Co , generates the $\text{U}(\text{IV})$ complex, $\text{U}(\text{OTf})_4(\text{dppmo})_2$, in excellent yield, along with $\text{Ph}_3\text{SiOSiPh}_3$ and $[\text{Cp}_2\text{Co}][\text{OTf}]$. This reaction proceeds via two $\text{U}(\text{IV})$ silyloxo intermediates, $[\text{U}(\text{OSiPh}_3)_2(\text{dppmo})_2(\text{OTf})][\text{OTf}]$ and $[\text{U}(\text{OSiPh}_3)(\text{dppmo})_2(\text{OTf})_2][\text{OTf}]$. Similarly, reaction of $[\text{UO}_2(\text{TPPO})_4][\text{OTf}]_2$ with 6 equiv of Me_3SiOTf and 2 equiv Cp_2Co ,

generates the U(IV) complex, $[\text{Cp}_2\text{Co}][\text{U}(\text{OTf})_5(\text{TPPO})_2]$, in good yield, concomitant with formation of $\text{Me}_3\text{SiOSiMe}_3$, $[\text{Ph}_3\text{POSiMe}_3][\text{OTf}]$, and $[\text{Cp}_2\text{Co}][\text{OTf}]$. These transformations represent novel examples of one-pot reductions of uranyl to U(IV), at ambient temperatures and pressures.

Addition of 2 equiv of Ph_3SiOTf to $\text{UO}_2(\text{dbm})_2(\text{THF})$ or $\text{UO}_2(\text{Aracnac})_2$, results in the formation of $\text{U}(\text{OSiPh}_3)_2(\text{dbm})_2(\text{OTf})$ and $[\text{U}(\text{OSiPh}_3)_2(\text{Aracnac})_2][\text{OTf}]$, respectively, in good yields. This suggests that Ph_3SiOTf could be used as a general reagent for the reductive silylation of uranyl, as it does not require the addition of a Lewis acid activator. In addition, treatment of $\text{UO}_2(\text{dbm})_2(\text{THF})$ with 2 equiv of Me_3SiOTf results in the formation of $[\text{U}(\text{OSiMe}_3)_2(\text{dbm})_2(\text{THF})][\text{OTf}]$.

Reaction of $\text{UO}_2(\text{N}(\text{SiMe}_3)_2)_2(\text{THF})_2$ with 1 or 2 equiv of the 14-membered macrocycle, tmtaaH_2 , generates the protonolysis products $\text{UO}_2(\text{tmtaaH})(\text{N}(\text{SiMe}_3)_2)(\text{THF})$ or $\text{UO}_2(\text{tmtaaH})_2$, respectively, in excellent yields. In addition, reaction of $[\text{UO}_2\text{Cl}_2(\text{THF})_2]_2$ with 2 equiv of $\text{Li}_2(\text{tmtaa})$, affords the complex, $[\text{Li}]_2[\text{Li}(\text{THF})_3\text{Cl}]_2[\text{UO}_2\text{Cl}_2\{\text{tmtaa}\}_2\text{UO}_2\text{Cl}_2]$, in good yield. The $\{\text{tmtaa}\}_2^{2-}$ dimer, contained within this complex, is a $1e^-$ oxidation product of the $[\text{tmtaa}]^{2-}$ ligand. Similarly, addition of 2 equiv of K_2tmtaa to $[\text{UO}_2\text{Cl}_2(\text{THF})_2]_2$, results in the formation of the $2e^-$ oxidized ligand product, a β -diketiminate pyrazolium macrocycle, in modest yield. The isolation of oxidized ligand products suggests *cis*- $\text{UO}_2(\text{tmtaa})$ is a likely intermediate in these transformations, as it would be very unstable and readily undergo ligand oxidation.

Addition of 2 equiv of the 12-membered macrocycles, $^{\text{H}}\text{N}_4$ or $^{\text{Me}}\text{N}_4$, to $[\text{UO}_2\text{Cl}_2(\text{THF})_2]_2$ in MeCN, results in the formation of $\text{UO}_2\text{Cl}_2(\text{RN}_4)$ ($\text{R} = \text{H}, \text{Me}$), which

were isolated as yellow-orange solids in good yields. Similarly, reaction of $\text{UO}_2(\text{OTf})_2(\text{THF})_3$ with $^{\text{H}}\text{N}_4$ in MeCN results in the formation of $\text{UO}_2(\text{OTf})_2(^{\text{H}}\text{N}_4)$, in good yield. Finally, reaction of $\text{UO}_2(\text{OTf})_2(\text{THF})_3$ with $^{\text{Me}}\text{N}_4$ in THF results in the formation of $[\text{UO}_2(\text{OTf})(\text{THF})(^{\text{H}}\text{N}_4)][\text{OTf}]$, in good yield. These complexes exhibit the smallest O-U-O bond angles measured to date, a consequence of the small binding pocket of the $^{\text{RN}}_4$ ligands, along with its relative rigidity.

Reaction of UCl_4 with 6 equiv of 2-Li- $\text{C}_6\text{H}_4\text{CH}_2\text{NMe}_2$ affords dark blue crystals of $[\text{Li}]_2[\text{U}(2\text{-C}_6\text{H}_3\text{CH}_2\text{NMe}_2)_2(2\text{-C}_6\text{H}_4\text{CH}_2\text{NMe}_2)_2]$ in good yield, which can be converted to $[\text{Li}][\text{Li}(\text{THF})_2[\text{U}(2\text{-C}_6\text{H}_3\text{CH}_2\text{NMe}_2)_2(2\text{-C}_6\text{H}_4\text{CH}_2\text{NMe}_2)_2]$ by dissolving in THF. Using 2 equiv of benzophenone with $[\text{Li}]_2[\text{U}(2\text{-C}_6\text{H}_3\text{CH}_2\text{NMe}_2)_2(2\text{-C}_6\text{H}_4\text{CH}_2\text{NMe}_2)_2]$ affords the double insertion product, $[\text{Li}][\text{U}(2\text{-C}_6\text{H}_3\text{CH}_2\text{NMe}_2\text{-3-COPh}_2)_2(2\text{-C}_6\text{H}_4\text{CH}_2\text{NMe}_2)]$, in good yield, as well as 1 equiv of 2- $\text{C}_6\text{H}_4\text{CH}_2\text{NMe}_2$. Addition of 2 equiv of AdN_3 to $[\text{Li}]_2[\text{U}(2\text{-C}_6\text{H}_3\text{CH}_2\text{NMe}_2)_2(2\text{-C}_6\text{H}_4\text{CH}_2\text{NMe}_2)_2]$, in the presence of 2 equiv of 12-crown-4 ether, yields the double insertion product, $[\text{Li}(12\text{-crown-4})_2][\text{Li}][\text{U}(5\text{-C}_6\text{H}_3\text{CH}_2\text{NMe}_2\text{-2-}N_3\text{Ad})_2(2\text{-C}_6\text{H}_4\text{CH}_2\text{NMe}_2)_2]$, in good yield. Finally, reaction of $[\text{Li}]_2[\text{U}(2\text{-C}_6\text{H}_3\text{CH}_2\text{NMe}_2)_2(2\text{-C}_6\text{H}_4\text{CH}_2\text{NMe}_2)_2]$ with 2 equiv of PhCN, affords the single insertion product, $[\text{Li}][\text{Li}(\text{Et}_2\text{O})][\text{U}(2,3\text{-C}_6\text{H}_3\text{CH}_2\text{NMe}_2)(5\text{-C}_6\text{H}_3\text{CH}_2\text{NMe}_2\text{-2-NCPh})(2\text{-C}_6\text{H}_4\text{CH}_2\text{NMe}_2)_2]$, in modest yield.

TABLE OF CONTENTS

Acknowledgements	iv
Vita of Elizabeth Anne Owens.....	vi
Abstract.....	viii
Table of Contents.....	xi
List of Figures.....	xxi
List of Schemes.....	xxvi
List of Tables	xxix
List of Abbreviations	xxxii
Chapter 1. Introduction.....	1
1.1. The Uranyl Moiety	2
1.2. Uranyl Oxo Functionalization.....	4
1.3. Uranyl Oxo Substitution	8
1.4. <i>Cis</i> -Uranyl.....	10
1.5. General Remarks	15
1.6. References	17
Chapter 2. Borane-Mediated Reductive Silylation of a Uranyl	
Dibenzoylmethanate Complex: An Example of Controlled Uranyl Oxo Ligand	
Substitution	20
2.1. Introduction	22
2.2. Results and Discussion	26
2.2.1. Synthesis, Characterization, and Electrochemical Studies of	

UO ₂ (dbm) ₂ (THF) (2.1).....	26
2.2.2. Synthesis and Characterization of U(OB{C ₆ F ₅ } ₃)(OSiPh ₃)(dbm) ₂ (THF) (2.2) and U(OB{C ₆ F ₅ } ₃)(OSiEt ₃)(dbm) ₂ (THF) (2.3)	30
2.2.3. Synthesis and Characterization of	
U(κ^2 - <i>O,F</i> -OB{C ₆ F ₅ } ₃)(OSiEt ₃)(dbm) ₂ (2.4)	35
2.2.4. Synthesis and Characterization of U(OB{C ₆ F ₅ } ₃)(dbm) ₃ (2.5)	37
2.2.5. Synthesis of U(OSiPh ₃) ₃ (dbm) ₂ (2.6) and	
U(OB{C ₆ F ₅ } ₃)(OSiEt ₃)(dbm) ₂ (HOPh) (2.7)	41
2.3. Summary	46
2.4. Experimental Section	47
2.4.1. General Procedures	47
2.4.2. Cyclic Voltammetry Measurements	48
2.4.3. Synthesis of UO ₂ (dbm) ₂ (THF) (2.1).....	48
2.4.4. Synthesis of U(OB{C ₆ F ₅ } ₃)(OSiPh ₃)(dbm) ₂ (THF) (2.2).....	49
2.4.5. Synthesis of U(OB{C ₆ F ₅ } ₃)(OSiEt ₃)(dbm) ₂ (THF) (2.3).....	50
2.4.6. Synthesis of U(κ^2 - <i>O,F</i> -OB{C ₆ F ₅ } ₃)(OSiEt ₃)(dbm) ₂ (2.4)	51
2.4.7. Synthesis of U(OB{C ₆ F ₅ } ₃)(dbm) ₃ (2.5).....	52
2.4.8. Synthesis of U(OSiPh ₃) ₃ (dbm) ₂ (2.6)	52
2.4.9. Synthesis of U(OB{C ₆ F ₅ } ₃)(OSiEt ₃)(dbm) ₂ (HOPh) (2.7)	53
2.4.10. X-Ray Crystallography	54
2.5. Acknowledgements.....	58
2.6. References	58

Chapter 3. Oxo Ligand Substitution in a Cationic Uranyl Complex: Synergistic

Interaction of an Electrophile and a Reductant	61
3.1. Introduction	63
3.2. Results and Discussion	66
3.2.1. Borane-Mediated Reductive Silylation of [$\text{UO}_2(\text{dppmo})_2(\text{OTf})][\text{OTf}]$	66
3.2.1.1. Synthesis and Characterization of [$\text{U}^{\text{IV}}(\text{OSiPh}_3)(\text{dppmo})_2(\text{OTf})_2][\text{OTf}]$ (3.1)	66
3.2.1.2. Identification of [$\text{UO}_2(\text{dppmo})_2(\text{OTf})][\text{HB}(\text{C}_6\text{F}_5)_3]$ and Ph_3SiOTf	69
3.2.2. Reductive Silylation of [$\text{UO}_2(\text{dppmo})_2(\text{OTf})][\text{OTf}]$ and [$\text{UO}_2(\text{TPPO})_4][\text{OTf}]_2$ with Cp_2Co	73
3.2.2.1. Synthesis and Characterization of $\text{U}^{\text{IV}}(\text{OTf})_4(\text{dppmo})_2$ (3.3)	73
3.2.2.2. Synthesis and Characterization of [$\text{U}^{\text{IV}}(\text{OSiPh}_3)_2(\text{dppmo})_2(\text{OTf})][\text{OTf}]$ (3.4)	78
3.2.2.3. Synthesis and Characterization of [$\text{Cp}_2\text{Co}][\text{U}^{\text{IV}}(\text{OTf})_5(\text{TPPO})_2]$ (3.5)	81
3.2.3. Synthesis of U(IV) Triflate Complexes from $\text{U}(\text{IV})\text{Cl}_4$	85
3.2.3.1. Synthesis and Characterization of [$\text{U}^{\text{IV}}(\text{OTf})_2(\text{dppmo})_3][\text{OTf}]_2$ (3.6)	85
3.2.3.2. Synthesis, Characterization and Reactivity of [$\text{U}^{\text{IV}}(\text{OTf})_2(\text{TPPO})_4][\text{OTf}]_2$ (3.7)	88
3.3. Summary	91

3.4. Experimental Section	93
3.4.1. General Procedures	93
3.4.2. Synthesis of $[\text{UO}_2(\text{dppmo})_2(\text{OTf})][\text{OTf}]$	93
3.4.3. Synthesis of $[\text{UO}_2(\text{TPPO})_4][\text{OTf}]_2$	94
3.4.4. Synthesis of $[\text{U}^{\text{IV}}(\text{OSiPh}_3)(\text{dppmo})_2(\text{OTf})_2][\text{OTf}]$ (3.1)	95
3.4.5. Synthesis of 3.1 using Cp_2Co	95
3.4.6. Synthesis of $[\text{Na}(12\text{-crown-}4)_2][\text{HB}(\text{C}_6\text{F}_5)_3]$ (3.2)	96
3.4.7. Synthesis of $\text{U}^{\text{IV}}(\text{OTf})_4(\text{dppmo})_2$ (3.3).....	97
3.4.8. Synthesis of $[\text{U}^{\text{IV}}(\text{OSiPh}_3)_2(\text{dppmo})_2(\text{pyr})][\text{OTf}]_2$ (3.4-pyr).....	98
3.4.9. Synthesis of $[\text{Cp}_2\text{Co}][\text{U}^{\text{IV}}(\text{OTf})_5(\text{TPPO})_2]$ (3.5).....	99
3.4.10. Synthesis of 3.5 using Ph_3SiOTf	100
3.4.11. Synthesis of $[\text{U}^{\text{IV}}(\text{OTf})_2(\text{dppmo})_3][\text{OTf}]_2$ (3.6)	101
3.4.12. Synthesis of $[\text{U}^{\text{IV}}(\text{OTf})_2(\text{TPPO})_4][\text{OTf}]_2$ (3.7)	102
3.4.13. NMR-Scale Reaction of Ph_3SiOTf with Cp_2Co	103
3.4.14. NMR-Scale Reaction of $[\text{UO}_2(\text{dppmo})_2(\text{OTf})][\text{OTf}]$ with Cp_2Co .	103
3.4.15. NMR-Scale Reaction of $[\text{UO}_2(\text{dppmo})_2(\text{OTf})][\text{OTf}]$ with Ph_3SiOTf	104
3.4.16. NMR-Scale Reaction of $[\text{UO}_2(\text{TPPO})_4][\text{OTf}]_2$ with Cp_2Co	104
3.4.17. NMR-Scale Reaction of $[\text{UO}_2(\text{TPPO})_4][\text{OTf}]_2$ with Me_3SiOTf	104
3.4.18. NMR-Scale Reaction of Me_3SiOTf with Cp_2Co	105
3.4.19. X-Ray Crystallography	105
3.5. References	109

Chapter 4. Reductive Silylation of the Uranyl Ion with R₃SiOTf

(R = Ph, Me)	112
4.1. Introduction	113
4.2. Results and Discussion	115
4.2.1. Synthesis and Characterization of U(OSiPh ₃) ₂ (dbm) ₂ (OTf) (4.1) and [U(OSiPh ₃) ₂ (^{Ar} acnac) ₂][OTf] (4.2)	115
4.2.2. Reactions with Me ₃ SiOTf	120
4.2.3. Synthesis and Characterization of UO ₂ (dbm ^{Me}) ₂ (THF) (4.3).....	121
4.2.4. Synthesis and Characterization of U(OSiPh ₃) ₂ (dbm ^{Me}) ₂ (OTf) (4.4).....	123
4.2.5. Synthesis and Characterization of UO ₂ (dbm) ₂ (DMPO) (4.5).....	126
4.3. Summary	129
4.4. Experimental Section	131
4.4.1. General Procedures	131
4.4.2. Synthesis of U(OSiPh ₃) ₂ (dbm) ₂ (OTf) (4.1)	131
4.4.3. Synthesis of 4.1 with 1 equiv Ph ₃ SiOTf.....	132
4.4.4. Reaction of 4.1 with Me ₃ SiOTf	133
4.4.5. Synthesis of [U(OSiPh ₃) ₂ (^{Ar} acnac) ₂][OTf] (4.2).....	133
4.4.6. Synthesis of H(dbm ^{Me})	134
4.4.7. Synthesis of UO ₂ (dbm ^{Me}) ₂ (THF) (4.3)	135
4.4.8. Synthesis of U(OSiPh ₃) ₂ (dbm ^{Me}) ₂ (OTf) (4.4)	136
4.4.9. Synthesis of UO ₂ (dbm) ₂ (DMPO) (4.5)	136
4.4.10. Synthesis of 4.1 from 4.5	137

4.4.11. X-Ray Crystallography	138
4.5. Acknowledgements	140
4.6. References	140
Chapter 5. Coordination of a Tetra(aza)macrocyclic to the Uranyl Ion....	143
5.1. Introduction	145
5.2. Results and Discussion	148
5.2.1. Synthesis and Characterization of $\text{UO}_2(\text{tmtaaH})(\text{N}(\text{SiMe}_3)_2)(\text{THF})$ (5.1) and $\text{UO}_2(\text{tmtaaH})_2$ (5.2)	148
5.2.2. Synthesis and Characterization of the β -diketiminato pyrazolium macrocyclic (<i>Z</i> -isomer: 5.3 ; <i>E</i> -isomer: 5.4)	153
5.2.3. Synthesis and Characterization of $[\text{Li}]_2[\text{Li}(\text{THF})_3\text{Cl}]_2[\text{UO}_2\text{Cl}_2\{\text{tmtaa}\}_2\text{UO}_2\text{Cl}_2]$ (5.5).....	157
5.2.4. Synthesis and Characterization of $[\text{Li}(\text{THF})]_2[\text{UO}_2(\text{N}(\text{SiMe}_3)_2)_2(\text{tmtaa})]$ (5.6).....	160
5.3. Summary	163
5.4. Experimental Section	165
5.4.1. General Procedures	165
5.4.2. Raman Spectroscopy.....	165
5.4.3. Synthesis of Li_2tmtaa	166
5.4.4. Synthesis of $\text{UO}_2(\text{tmtaaH})(\text{N}(\text{SiMe}_3)_2)(\text{THF})$ (5.1)	166
5.4.5. Synthesis of $\text{UO}_2(\text{tmtaaH})_2$ (5.2).....	167
5.4.6. Synthesis of the β -diketiminato pyrazolium macrocyclic (<i>Z</i> -isomer: 5.3)	168

5.4.7. Synthesis of the β -diketiminato pyrazolium macrocycle (<i>E</i> -isomer: 5.4)	170
5.4.8. Synthesis of $[\text{Li}]_2[\text{Li}(\text{THF})_3\text{Cl}]_2[\text{UO}_2\text{Cl}_2\{\text{tmtaa}\}_2\text{UO}_2\text{Cl}_2]$ (5.5)	170
5.4.9. Synthesis of $[\text{Li}(\text{THF})]_2[\text{UO}_2(\text{N}(\text{SiMe}_3)_2)_2(\text{tmtaa})]$ (5.6).....	171
5.4.10. X-Ray Crystallography	171
5.5. Acknowledgements	176
5.6. References	176
Chapter 6. Perturbation of the O-U-O Angle in Uranyl by Coordination to a 12-membered Macrocycle.....	179
6.1. Introduction	180
6.2. Results and Discussion	182
6.2.1. Synthesis and Characterization of $\text{UO}_2\text{Cl}_2(\text{H}^+\text{N}4)$ (6.1) and $\text{UO}_2\text{Cl}_2(\text{Me}^+\text{N}4)$ (6.2)	182
6.2.2. Synthesis and Characterization of $\text{UO}_2(\text{OTf})_2(\text{H}^+\text{N}4)$ (6.3) and $[\text{UO}_2(\text{OTf})(\text{THF})(\text{Me}^+\text{N}4)][\text{OTf}]$ (6.4).....	187
6.2.3. Raman U=O ν_{sym} Stretch Comparison.....	189
6.2.4. Solution Phase Behavior of Complexes 6.1 - 6.4	192
6.3. Summary	194
6.4. Experimental Section	196
6.4.1. General Procedures	196
6.4.2. Raman Spectroscopy.....	196
6.4.3. Characterization of $[\text{UO}_2\text{Cl}_2(\text{THF})_2]_2$	197
6.4.4. Characterization of $\text{UO}_2(\text{OTf})_2(\text{THF})_3$	197

6.4.5. Synthesis of $\text{UO}_2\text{Cl}_2(\text{HN4})$ (6.1)	197
6.4.6. Synthesis of $\text{UO}_2\text{Cl}_2(\text{MeN4})$ (6.2)	198
6.4.7. Synthesis of $\text{UO}_2(\text{OTf})_2(\text{HN4})$ (6.3)	199
6.4.8. Synthesis of $[\text{UO}_2(\text{OTf})(\text{THF})(\text{MeN4})][\text{OTf}]$ (6.4)	200
6.4.9. X-Ray Crystallography.....	201
6.5. Acknowledgements	205
6.6. References	205
Chapter 7. Synthesis and Reactivity of a U(IV) Dibenzynes Complex	208
7.1. Introduction	210
7.1.1. Actinide Aryl Complexes	210
7.1.2. Metal-Stabilized Benzynes.....	212
7.2. Results and Discussion	218
7.2.1. Synthesis and Characterization of $[\text{Li}]_2[\text{U}(2,3\text{-C}_6\text{H}_3\text{CH}_2\text{NMe}_2)_2(2\text{-C}_6\text{H}_4\text{CH}_2\text{NMe}_2)_2]$ (7.1) and $[\text{Li}][\text{Li}(\text{THF})_2][\text{U}(2,3\text{-C}_6\text{H}_3\text{CH}_2\text{NMe}_2)_2(2\text{-C}_6\text{H}_4\text{CH}_2\text{NMe}_2)_2]$ (7.2).....	218
7.2.2. Synthesis and Characterization of $[\text{Li}][\text{U}(2\text{-C}_6\text{H}_3\text{CH}_2\text{NMe}_2\text{-3-COPh})_2(2\text{-C}_6\text{H}_4\text{CH}_2\text{NMe}_2)]$ (7.3).....	223
7.2.3. Synthesis and Characterization of $[\text{Li}][\text{Li}(\text{Et}_2\text{O})][\text{U}(2,3\text{-C}_6\text{H}_3\text{CH}_2\text{NMe}_2)(2\text{-C}_6\text{H}_3\text{CH}_2\text{NMe}_2\text{-3-C(Ph)=N})(2\text{-C}_6\text{H}_4\text{CH}_2\text{NMe}_2)_2]$ (7.4)	227
7.2.4. Synthesis and Characterization of $[\text{Li}][\text{Li}(\text{Et}_2\text{O})][\text{U}(2,3\text{-C}_6\text{H}_3\text{CH}_2\text{NMe}_2)(5\text{-C}_6\text{H}_3\text{CH}_2\text{NMe}_2\text{-2-S})(2\text{-C}_6\text{H}_4\text{CH}_2\text{NMe}_2)_2]$ (7.5).....	230
7.2.5. Reactivity of 7.1 with Unsaturated Hydrocarbons	232

7.2.6. Synthesis and Characterization of [Li(12-crown-4) ₂][Li][U(2-C ₆ H ₃ CH ₂ NMe ₂ -3-(<i>N-N=N</i> -Ad)) ₂ (2-C ₆ H ₄ CH ₂ NMe ₂) ₂] (7.6)	233
7.3. Summary	237
7.4. Experimental Section	239
7.4.1. General Procedures	239
7.4.2. Synthesis of [Li] ₂ [U(2,3-C ₆ H ₃ CH ₂ NMe ₂) ₂ (2-C ₆ H ₄ CH ₂ NMe ₂) ₂] (7.1)	239
7.4.3. Synthesis of [Li][U(2-C ₆ H ₃ CH ₂ NMe ₂ -3-COPh) ₂ (2-C ₆ H ₄ CH ₂ NMe ₂) ₂] (7.3)	241
7.4.4. Synthesis of [Li][Li(Et ₂ O)][U(2,3-C ₆ H ₃ CH ₂ NMe ₂)(2-C ₆ H ₃ CH ₂ NMe ₂ -3-C(Ph)=N)(2-C ₆ H ₄ CH ₂ NMe ₂) ₂] (7.4)	242
7.4.5. Synthesis of [Li][Li(Et ₂ O)][U(2,3-C ₆ H ₃ CH ₂ NMe ₂)(5-C ₆ H ₃ CH ₂ NMe ₂ -2- <i>S</i>)(2-C ₆ H ₄ CH ₂ NMe ₂) ₂] (7.5)	243
7.4.6. Synthesis of [Li(12-crown-4) ₂][Li][U(2-C ₆ H ₃ CH ₂ NMe ₂ -3-(<i>N-N=N</i> -Ad)) ₂ (2-C ₆ H ₄ CH ₂ NMe ₂) ₂] (7.6)	244
7.4.7. X-Ray Crystallography	245
7.5. Acknowledgements	249
7.6. References	249
Appendix A	253
Appendix B. Synthesis of U(IV) Aryl Complexes and Sc(III) Ketimide	
Complexes	266
B.1. Synthesis of [Li(Et ₂ O)] ₂ [Li(THF)] ₂ [U(C ₆ H ₄) ₂ (C ₆ H ₅) ₄] (B.1)	267
B.2. Synthesis of [Li(Et ₂ O)] ₄ [LiCl][U(C ₆ H ₄) ₂ (C ₆ H ₅) ₃ (OC ₄ H ₉)] (B.2)	269

B.3. Synthesis of $\text{Sc}^{\text{III}}(\text{L1})(\text{N}=\text{C}^t\text{Bu}_2)(\text{Cl})$ (B.4)	272
B.4. Synthesis of $[\text{Sc}^{\text{III}}(\text{N}=\text{C}^t\text{Bu}_2)_3]_2$ (B.5)	275
B.5. X-ray Crystallography	278
B.6. References	281

LIST OF FIGURES

Figure 1.1. a) General molecular structure of the uranyl ion. b) π and σ bonding in the uranyl ion	2
Figure 1.2. Proposed reaction for the bioreduction of uranyl to U(IV) by <i>Geobacter sulfurreducens</i>	4
Figure 1.3. A comparison of the uranyl(IV) reduction potential (vs. Fc/Fc ⁺) and the U=O symmetric stretching frequency (ν_1) for several uranyl complexes	5
Figure 2.1. a) Room temperature cyclic voltammogram of 2.1 . b) Solid-state Raman spectrum of 2.1	29
Figure 2.2. Solid-state structures of U(OB{C ₆ F ₅ } ₃)(OSiPh ₃)(dbm) ₂ THF (2.2) and U(OB{C ₆ F ₅ } ₃)(OSiEt ₃)(dbm) ₂ (THF)·C ₇ H ₈ ·0.5C ₆ H ₁₄ (2.3 ·C ₇ H ₈ ·0.5C ₆ H ₁₄)	32
Figure 2.3. ¹⁹ F{ ¹ H} NMR spectrum of 2.3 in CD ₂ Cl ₂ at 25 °C	34
Figure 2.4. Solid-state structure of U(κ^2 -O,F-OB{C ₆ F ₅ } ₃)(OSiEt ₃)(dbm) ₂ (2.4)	36
Figure 2.5. Solid-state structure of U(OB{C ₆ F ₅ } ₃)(dbm) ₃ ·2C ₇ H ₈ ·C ₆ H ₁₄ (2.5 ·2C ₇ H ₈ ·C ₆ H ₁₄)	40
Figure 2.6. Solid-state structure of U(OSiPh ₃) ₃ (dbm) ₂ ·CH ₂ Cl ₂ (2.6 ·CH ₂ Cl ₂)	43
Figure 2.7. Solid-state structure of U(OB{C ₆ F ₅ } ₃)(OSiEt ₃)(dbm) ₂ (HOPh)·C ₆ H ₁₄ (2.7 ·C ₆ H ₁₄)	45
Figure 3.1. Solid-state structure of [U ^{IV} (OSiPh ₃)(dppmo) ₂ (OTf) ₂][OTf]·3CH ₂ Cl ₂ ·C ₄ H ₁₀ O (3.1 ·3CH ₂ Cl ₂ ·C ₄ H ₁₀ O)	68

Figure 3.2. Solid-state structure of $[U^{IV}(OTf)_4(dppmo)_2][Cp_2Co][OTf] \cdot 1.5C_7H_8 \cdot C_6H_{14}$ ([3.3][Cp₂Co][OTf]·1.5C₇H₈·C₆H₁₄)	75
Figure 3.3. Solid-state structure of $[U^{IV}(OSiPh_3)_2(dppmo)_2(pyr)][OTf]_2 \cdot 2C_5H_5N$ $\cdot C_4H_{10}O$ ([3.4-pyr]·2C₅H₅N·C₄H₁₀O)	80
Figure 3.4. Solid state Raman spectrum of $[UO_2(TPPO)_4][OTf]_2$	83
Figure 3.5. Solid-state structure of $[Cp_2Co][U^{IV}(OTf)_5(TPPO)_2]$ (3.5)	84
Figure 3.6. Solid-state structure of $[U^{IV}(OTf)_2(dppmo)_3][OTf]_2 \cdot 4CH_2Cl_2$ (3.6·4CH₂Cl₂)	87
Figure 3.7. Solid-state structure of $[U^{IV}(OTf)_2(TPPO)_4][OTf]_2 \cdot CH_2Cl_2$ (3.7·CH₂Cl₂)	90
Figure 4.1. Examples of reductive silylation of the uranyl ion with various silylating reagents	114
Figure 4.2. Solid-state structures of $U(OSiPh_3)_2(dbm)_2(OTf)$ (4.1) and $[U(OSiPh_3)_2(Aracnac)_2][OTf] \cdot THF$ (4.2·THF)	118
Figure 4.3. Solid-state Raman spectrum of 4.3	123
Figure 4.4. Solid-state structure of $U(OSiPh_3)_2(dbm^{Me})_2(OTf)$ (4.4).....	125
Figure 5.1. Solid-state structures of $UO_2(tmtaaH)(N(SiMe_3)_2)(THF)$ (5.1) and $UO_2(tmtaaH)_2$ (5.2)	151
Figure 5.2. Solid-state structures of $C_{22}H_{22}N_4$ (5.3) and $C_{22}H_{22}N_4 \cdot C_4H_8O$ (5.4·C₄H₈O)	155
Figure 5.3. Solid-state structure of $[Li]_2[Li(THF)_3Cl]_2[UO_2Cl_2\{tmtaa\}_2UO_2Cl_2] \cdot C_4H_8O$ (5.5·C₄H₈O)	159

Figure 5.4. Solid-state structure of $[\text{Li}(\text{THF})_2[\text{UO}_2(\text{N}(\text{SiMe}_3)_2)_2(\text{tmtaa})]] \cdot 2\text{C}_6\text{D}_6$ (5.6 · $2\text{C}_6\text{D}_6$)	162
Figure 6.1. Solid-state structures of 6.1 - 6.4	184
Figure 6.2. Solid-state structures of 6.2 and 6.2a , highlighting the difference between the O-U-O and $\text{N}_{\text{pyr}}\text{-U-N}_{\text{pyr}}$ planes.....	186
Figure 6.3. Solid-state Raman spectrum of 6.3	192
Figure 6.4. ^1H NMR spectrum of complex 6.2 in CD_2Cl_2	193
Figure 7.1. Solid-state structures of $[\text{Li}]_2[\text{U}(2,3\text{-C}_6\text{H}_3\text{CH}_2\text{NMe}_2)_2(2\text{-C}_6\text{H}_4\text{CH}_2\text{NMe}_2)_2]$ (7.1) and $[\text{Li}][\text{Li}(\text{THF})_2][\text{U}(2,3\text{-C}_6\text{H}_3\text{CH}_2\text{NMe}_2)_2(2\text{-C}_6\text{H}_4\text{CH}_2\text{NMe}_2)_2]$ (7.2).....	221
Figure 7.2. Solid-state structure of $[\text{Li}][\text{U}(2\text{-C}_6\text{H}_3\text{CH}_2\text{NMe}_2\text{-3-COPh}_2)_2(2\text{-C}_6\text{H}_4\text{CH}_2\text{NMe}_2)] \cdot 0.5\text{C}_6\text{H}_{14}$ (7.3 · $0.5\text{C}_6\text{H}_{14}$)	225
Figure 7.3. ^1H NMR spectrum of complex 7.3 in C_6D_6	226
Figure 7.4. Solid-state structure of $[\text{Li}][\text{Li}(\text{Et}_2\text{O})][\text{U}(2,3\text{-C}_6\text{H}_3\text{CH}_2\text{NMe}_2)(2\text{-C}_6\text{H}_3\text{CH}_2\text{NMe}_2\text{-3-C}(\text{Ph})=\text{N})(2\text{-C}_6\text{H}_4\text{CH}_2\text{NMe}_2)_2]$ (7.4)	229
Figure 7.5. Solid-state structure of $[\text{Li}][\text{Li}(\text{Et}_2\text{O})][\text{U}(2,3\text{-C}_6\text{H}_3\text{CH}_2\text{NMe}_2)(5\text{-C}_6\text{H}_3\text{CH}_2\text{NMe}_2\text{-2-S})(2\text{-C}_6\text{H}_4\text{CH}_2\text{NMe}_2)_2]$ (7.5).....	232
Figure 7.6. Solid-state structure of $[\text{Li}(12\text{-crown-4})_2][\text{Li}][\text{U}(2\text{-C}_6\text{H}_3\text{CH}_2\text{NMe}_2\text{-3-(N=N=N-Ad)})_2(2\text{-C}_6\text{H}_4\text{CH}_2\text{NMe}_2)_2] \cdot \text{OC}_4\text{H}_{10}$ (7.6 · OC_4H_{10})	235
Figure A.1. $^{19}\text{F}\{^1\text{H}\}$ NMR spectrum of the <i>in situ</i> reaction of $\text{UO}_2(\text{dbm})_2(\text{THF})$ with 1 equiv of $\text{B}(\text{C}_6\text{F}_5)_3$ and 2 equiv HSiEt_3 in CD_2Cl_2 ; after 24 h at 25 °C.....	254
Figure A.2. $^{19}\text{F}\{^1\text{H}\}$ NMR spectrum of the <i>in situ</i> reaction of $[\text{UO}_2(\text{dppmo})_2\text{OTf}][\text{OTf}]$ with 2 equiv Ph_3SiH and $\text{B}(\text{C}_6\text{F}_5)_3$ in $\text{TCE-}d_2$; after 5 min at 25 °C.	255

Figure A.3. Partial $^{19}\text{F}\{^1\text{H}\}$ NMR spectrum of the <i>in situ</i> reaction of $[\text{UO}_2(\text{dppmo})_2\text{OTf}][\text{OTf}]$ with 2 equiv Ph_3SiH and $\text{B}(\text{C}_6\text{F}_5)_3$ in $\text{TCE-}d_2$; after 72 h at 105 °C	256
Figure A.4. ^1H NMR spectra of the <i>in situ</i> reaction of $[\text{UO}_2(\text{dppmo})_2(\text{OTf})][\text{OTf}]$ with 4 equiv of Ph_3SiOTf and 2 equiv of Cp_2Co in CD_2Cl_2	257
Figure A.5. ^1H NMR spectrum of “ $[\text{U}(\text{OSiMe}_3)_2(\text{dbm})_2(\text{THF})][\text{OTf}]$ ” in CD_2Cl_2 at 25 °C	258
Figure A.6. $^{19}\text{F}\{^1\text{H}\}$ NMR spectrum of “ $[\text{U}(\text{OSiMe}_3)_2(\text{dbm})_2(\text{THF})][\text{OTf}]$ ” in CD_2Cl_2 at 25 °C	259
Figure A.7. Solid-state ball and stick structure of $\text{UO}_2(\text{dbm})_2(\text{DMPO})$ (4.5).....	260
Figure A.8. ^1H NMR spectrum of a mixture of the two isomers of $\text{C}_{22}\text{H}_{22}\text{N}_4$ (<i>Z</i> -isomer: 5.3 ; <i>E</i> -isomer: 5.4) in a 2:3 ratio in C_6D_6	261
Figure A.9. $^{13}\text{C}\{^1\text{H}\}$ NMR spectrum of a mixture the two isomers of $\text{C}_{22}\text{H}_{22}\text{N}_4$ (<i>Z</i> - isomer: 5.3 ; <i>E</i> -isomer: 5.4) in a 2:3 ratio in C_6D_6	262
Figure A.10. ^1H NMR spectrum of $[\text{Li}(\text{THF})]_2[\text{UO}_2(\text{N}(\text{SiMe}_3)_2)_2(\text{tmtaa})]$ (5.6) in C_6D_6 at 25 °C	263
Figure A.11. $^7\text{Li}\{^1\text{H}\}$ NMR spectrum of $[\text{Li}(\text{THF})]_2[\text{UO}_2(\text{N}(\text{SiMe}_3)_2)_2(\text{tmtaa})]$ (5.6) in C_6D_6 at 25 °C	264
Figure A.12. Temperature dependence of μ_{eff} for $[\text{Li}][\text{U}(2,3\text{-C}_6\text{H}_3\text{CH}_2\text{NMe}_2)(2\text{-}$ $\text{C}_6\text{H}_4\text{CH}_2\text{NMe}_2)_3]$ from 4 K to 300 K	265
Figure B.1. Solid-state structure of $[\text{Li}(\text{Et}_2\text{O})]_2[\text{Li}(\text{THF})]_2[\text{U}(\text{C}_6\text{H}_4)_2(\text{C}_6\text{H}_5)_4]$ (B.1)	268

Figure B.2. Solid-state structure of $[\text{Li}(\text{Et}_2\text{O})]_4[\text{LiCl}][\text{U}(\text{C}_6\text{H}_4)_2(\text{C}_6\text{H}_5)_3(\text{OC}_4\text{H}_9)]$ (B.2)	270
Figure B.3. Solid-state structure of $[\text{Li}(\text{THF})]_4[\text{C}_6\text{H}_5]_4$ (B.3)	271
Figure B.4. Solid-state structure of $\text{Sc}^{\text{III}}(\text{L1})(\text{N}=\text{C}^t\text{Bu}_2)(\text{Cl})$ (B.4)	273
Figure B.5. ^1H NMR spectrum of complex B.4 in C_6D_6	274
Figure B.6. Solid-state structure of $[\text{Sc}^{\text{III}}(\text{N}=\text{C}^t\text{Bu}_2)_3]_2$ (B.5)	276
Figure B.7. ^1H NMR spectrum of complex B.5 in C_6D_6	277

LIST OF SCHEMES

Scheme 1.1. Sequential addition of silylamide ligands to the uranyl ion	6
Scheme 1.2. a) Functionalization of an oxo ligand in a uranyl bisbenzaminato complex with B(C ₆ F ₅) ₃ . b) Reductive silylation of uranyl utilizing the Arnold group ‘Pacman’ polypyrrrolic macrocycle ligand	7
Scheme 1.3. Examples of uranyl oxo substitution at room temperature.....	10
Scheme 1.4. Previous attempts to make the <i>cis</i> -uranyl complex, <i>cis</i> -Cp’ ₂ UO ₂ (Cp’ = η ⁵ - C ₅ Me ₅ , 1,2,4-C ₅ H ₂ ^t Bu ₃)	12
Scheme 1.5. Previous attempts to make a <i>cis</i> -uranyl complex, from a U(VI) starting material.....	13
Scheme 2.1. Borane-catalyzed silylation of a ketone.....	23
Scheme 2.2. Proposed catalytic cycle for the reductive silylation of uranyl to U(IV).....	24
Scheme 2.3. Reductive Silylation of UO ₂ (^{Ar} acnac) ₂ with B(C ₆ F ₅) ₃ and Et ₃ SiH	26
Scheme 2.4. Synthesis of UO ₂ (dbm) ₂ (THF) (2.1).....	27
Scheme 2.5. Synthesis of U(OB{C ₆ F ₅ } ₃)(OSiPh ₃)(dbm) ₂ (THF) (2.2) and U(OB{C ₆ F ₅ } ₃)(OSiEt ₃)(dbm) ₂ (THF) (2.3)	30
Scheme 3.1. Rare examples of reductive silylation of uranyl to U(IV).....	64
Scheme 3.2. Borane-mediated reductive silylation of [UO ₂ (dppmo) ₂ (OTf)][OTf]	67
Scheme 3.3. Proposed catalytic cycle for reductive silylation of uranyl to U(IV).....	72

Scheme 3.4. Synthesis of complex 3.3 and the proposed mechanism for the formation of 3.3	73
Scheme 3.5. Synthesis of complex 3.5	81
Scheme 3.6. Synthesis of complex 3.6	86
Scheme 3.7. Synthesis of complex 3.7	88
Scheme 4.1. Synthesis of complexes 4.1 and 4.2	116
Scheme 4.2. Synthesis of $\text{UO}_2(\text{dbm}^{\text{Me}})_2(\text{THF})$ (4.3).....	122
Scheme 5.1. Synthesis of complexes 5.1 and 5.2	149
Scheme 5.2. Bond length comparison for complexes 5.1 , 5.2 , and 5.5	152
Scheme 5.3. Synthesis of compounds 5.3 and 5.4	153
Scheme 6.1. Synthesis of complexes 6.1 and 6.2	182
Scheme 6.2. Synthesis of complexes 6.3 and 6.4	187
Scheme 7.1. Synthesis of a) $(\eta^5\text{-Cp}^*)_2[\text{U}(\text{N},\text{C})\text{-}(o\text{-C}_6\text{H}_4)\text{NPh}]$, b) $(\eta^5\text{-Cp}^*)_2\text{U}(\eta^2\text{-TeC}_6\text{H}_4)$, c) $[\eta^5\text{-1,2,4-(Me}_3\text{C)}_3\text{C}_5\text{H}_2]_2\text{Th}[\eta^2\text{-N},\text{C}\text{-}\{\text{N}(p\text{-MeC}_6\text{H}_3)(\text{SiHPh}_2)\}]$, and d) $(\eta^5\text{-Cp}^*)_2\text{U}(\text{hpp})(\text{C}_6\text{H}_5)$	211
Scheme 7.2. Synthesis of $\text{Th}(2\text{-C}_6\text{H}_4\text{CH}_2\text{NMe}_2)_4$	212
Scheme 7.3. Reactivity of aryl complexes of a) zirconium and b) germanium and c) uranium.....	214
Scheme 7.4. Synthesis of $[\text{Li}(\text{THF})_2][\text{UCl}_2(2,3\text{-C}_6\text{H}_3\text{CH}_2\text{NMe}_2)(2\text{-C}_6\text{H}_4\text{CH}_2\text{NMe}_2)_2]$ and $[\text{Li}][\text{U}(2,3\text{-C}_6\text{H}_3\text{CH}_2\text{NMe}_2)(2\text{-C}_6\text{H}_4\text{CH}_2\text{NMe}_2)_3]$	216
Scheme 7.5. Reactivity of a thorium metalla-cyclopropene complex.....	217
Scheme 7.6. Synthesis of complexes 7.1 and 7.2	218
Scheme 7.7. Reactivity of complex 7.1	223

Scheme 7.8. Insertion chemistry of tetrabenzyluranium	224
Scheme B.1. Synthesis of B.1 and B.3	267
Scheme B.2. Synthesis of complex B.2	270
Scheme B.3. Synthesis of complex B.4	272
Scheme B.4. Synthesis of complex B.5	275

LIST OF TABLES

Table 2.1. Electrochemical Data for Selected Uranyl(VI) Complexes.....	29
Table 2.2. Selected Bond Lengths (Å) and Angles (deg) for Complexes 2.2 - 2.6	33
Table 2.3. X-ray Crystallographic Data for Complexes 2.2 – 2.4	56
Table 2.4. X-ray Crystallographic Data for Complexes 2.5 – 2.7	57
Table 3.1. U=O ν_{sym} Stretch Comparison in Several Uranyl Complexes	66
Table 3.2. Selected Bond Lengths (Å) and Angles (deg) for Complexes 3.1 - 3.4	69
Table 3.3. X-ray Crystallographic Information for 3.1, 3.3 and 3.4-pyr	107
Table 3.4. X-ray Crystallographic Information for 3.5, 3.6 and 3.7	108
Table 4.1. Selected Bond Lengths (Å) and Angles (deg) for Complexes 4.1, 4.2, and 4.4	119
Table 4.2. X-Ray Crystallographic Data for Complexes 4.1, 4.2 and 4.4	139
Table 5.1. Selected bond lengths (Å) and angles (deg) for complexes 5.1, 5.2, 5.5, and 5.6	151
Table 5.2. X-ray Crystallographic Information for 5.1, 5.2, and 5.5	174
Table 5.3. X-ray Crystallographic Information for 5.3, 5.4, and 5.6	175
Table 6.1. Selected bond lengths (Å) and angles (deg) for complexes 6.1 -	185
Table 6.2. Comparison of the U=O ν_{sym} Stretch for a Series of Uranyl Complexes.....	191

Table 6.3. X-ray Crystallographic Information for 6.1 – 6.2a	203
Table 6.4. X-ray Crystallographic Information for 6.3 and 6.4	204
Table 7.1. Selected bond lengths (Å) for complexes 7.1 and 7.2	221
Table 7.2. X-ray Crystallographic Information for 7.1 – 7.3	247
Table 7.3. X-ray Crystallographic Information for 7.4 – 7.6	248
Table A.1. Electrochemical parameters for UO ₂ (dbm) ₂ (THF) (2.1) in CH ₂ Cl ₂ (vs. Fc/Fc ⁺ , [NBu ₄][PF ₆] as supporting electrolyte)	253
Table B.1. X-ray Crystallographic Information for B.1 , B.2 and B.3	279

LIST OF ABBREVIATIONS

°	degree
°C	degree Celsius
12-crown-4	1,4,7,10-tetraoxacyclododecane
$^{13}\text{C}\{^1\text{H}\}$	13-C-proton decoupled
18-crown-6	1,4,7,10,13,16-hexaoxacyclooctadecane
^1H	hydrogen-1
2-Li-C ₆ H ₄ CH ₂ NMe ₂	2-lithium- <i>N,N</i> -dimethylbenzylamine
^2H	hydrogen-2, deuterium
$^7\text{Li}\{^1\text{H}\}$	lithium-7-proton decoupled
Å	angstrom, 10 ⁻¹⁰ m
acac	acetylacacetate
AdN ₃	1-azidoadamantane
An	actinide
AO	atomic orbital
Ar	aryl
Ar ₂ nacnac	(2,6- ^{<i>i</i>} Pr ₂ C ₆ H ₃)NC(Me)CHC(Me)N(2,6- ^{<i>i</i>} Pr ₂ C ₆ H ₃)
Ar ₁ acnac	ArNC(Ph)CHC(Ph)O, Ar = 3,5- ^{<i>t</i>} Bu ₂ C ₆ H ₃
avg.	average
BDE	bond dissociation enthalpy
bipy	2,2'-bipyridine
Bn	benzyl
br	broad
Bu	butyl
C ₄ mpyr	<i>N</i> -methyl- <i>N</i> -propylpyrrolidinium
ca.	circa
calcd.	calculated
CCD	charge-coupled-device
cm ⁻¹	wavenumber

COSY	homonuclear correlation spectroscopy
Cp	$\eta^5\text{-C}_5\text{H}_5$
Cp*	$\eta^5\text{-C}_5\text{Me}_5$
CV	cyclic voltammetry
d	doublet <i>or</i> days
dbm	dibenzoyl methanate
dbm ^{Me}	PhC(O)CCH ₃ C(O)Ph
DFT	density functional theory
Dipp	2,6-diisopropylphenyl
DMAP	4-dimethylaminopyridine
DME	1,2-dimethoxyethane
DMF	dimethylformamide
DMSO	dimethylsulfoxide
<i>d_n</i>	deuterated in <i>n</i> positions
dppmo	bis(diphenylphosphino) methane oxide
e ⁻	electron
eq	equation
equiv	equivalent
Et	ethyl
Et ₂ O	diethylether
Fc	ferrocene
fcdc	1,2-ferrocenedicarboxylate
FTIR	Fourier transform infrared
g	gram
GOF	goodness of fit
<i>H</i>	enthalpy
h	hour
hfac	hexafluoroacetylacetonate
^H N4	2,11-diaza[3,3](2,6) pyridinophane
hpp	1,3,4,6,7,8-hexahydro-2 <i>H</i> -pyrimido[1,2- <i>a</i>]pyrimidinato

Hz	hertz
<i>i</i> Pr	<i>iso</i> -propyl
IR	infrared
<i>J</i>	NMR coupling constant
J	Joule
K	Kelvin
k	kilo
L	liter <i>or</i> ligand
L1	CH ₃ C(2-6-(<i>i</i> Pr) ₂ -C ₆ H ₃ N)CHC(CH ₃)(NCH ₂ CH ₂ NMe ₂)
M	molar
m	meter <i>or</i> multiplet <i>or</i> medium
<i>m</i>	meta
<i>m/z</i>	mass-to-charge ratio
Me	methyl
Me-N-Sal	<i>p</i> -CH ₃ -salicylideneaniline
MeN ₄	<i>N,N'</i> -dimethyl-2,11-diaza[3,3](2,6) pyridinophane
Mes	mesityl
MesPDI ^{Me}	2,6-((Mes)N=CMe) ₂ C ₅ H ₃ N
min	minute
mL	milliliter
mmol	millimole
MO	molecular orbital
mol	mol
ⁿ Bu	<i>n</i> -butyl
NCN	Me ₃ Si(N)CPh(N)SiMe ₃
NIR	near-infrared
NMR	nuclear magnetic resonance
<i>o</i>	ortho
OAc	acetate
OAr	aryloxide

OR	alkoxide
OTf	Trifluoromethylsulfonate
<i>p</i>	para
Ph	phenyl
PhCN	benzyl nitrile
ppm	parts per million
py	pyridine
q	quartet
R	alkyl
redox	reduction-oxidation
RT	room temperature
s	singlet <i>or</i> strong <i>or</i> second
sal- <i>p</i> -phdn	<i>N,N'</i> - <i>p</i> -phenylene-bis(salicylideneiminato)
sh	shoulder
SQUID	superconducting quantum interference device
T	Tesla
t	triplet
Tbt	2,4,6-tris[bis(trimethylsilyl)methyl]phenyl
^t Bu	<i>tert</i> -butyl
^t Bu-MesPDI ^{Me}	2,6-((Mes)N=CMe) ₂ - <i>p</i> -C(CH ₃) ₃ C ₅ H ₂ N
Tf ₂ N	bistriflylamide
THF	tetrahydrofuran
TMEDA	<i>N,N,N',N'</i> -tetramethylethylenediamine
tmtaaH ₂	dibenzotetramethyltetraaza[14]annulene
Tp ^{Ms}	[HB(3-Mspz) ₃] ⁻ (Ms = mesityl)
TPPO	triphenylphosphine oxide
UV	ultraviolet
V	volt
vis	visible
vs	versus

VT	variable temperature
w	weak
xs	excess
Δ	heat <i>or</i> difference
δ	chemical shift in ppm
ϵ	extinction coefficient
η^x	hapticity of order x
μ	micro <i>or</i> denotes a bridging atom

“EVERYTHING IS AWESOME!

Everything is cool when you’re part of a team.”

- The Lego Movie

Chapter 1. Introduction

1.1. The Uranyl Moiety.....	2
1.2. Uranyl Oxo Functionalization	4
1.3. Uranyl Oxo Substitution.....	8
1.4. <i>Cis</i>-Uranyl.....	10
1.5. General Remarks.....	15
1.6. References	17

1.1 The Uranyl Moiety

The uranyl moiety (UO_2^{2+}) is the major form of uranium present in spent nuclear fuel and is a water-soluble environmental contaminant. The moiety has a strictly linear $\text{O}=\text{U}=\text{O}$ geometry, which can be explained by a combination of uranium 6d and 5f atomic orbitals bonding with oxygen 2p atomic orbitals in the $\text{U}=\text{O}$ bond (Figure 1.1).^{1,2} This gives rise to very strong $\text{U}=\text{O}$ interactions, which have a bond orders of 3,³ and short $\text{U}-\text{O}$ bond lengths (ca. 1.78 Å). The $\text{U}=\text{O}$ bond dissociation energy is 604 kJ/mol,¹ which is 72 kJ/mol larger than that observed for CO_2 (532 kJ/mol).⁴

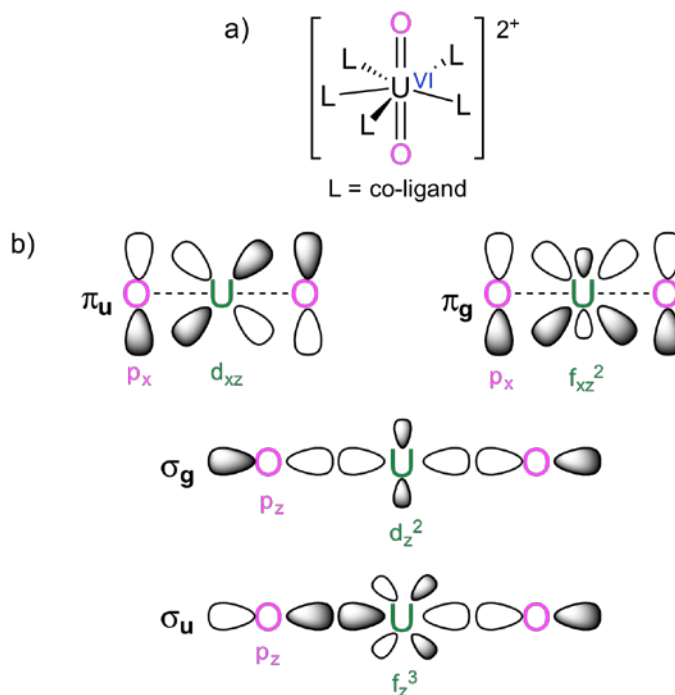


Figure 1.1. a) General molecular structure of the uranyl ion. b) π and σ bonding in the uranyl ion. (Figure adapted from references 1 and 2).

These oxo ligands tend to be unreactive and resistant towards functionalization.⁵ For example, when UO_3 is treated with neat triflic acid at 110 °C, only one of the oxo

ligands becomes protonated to form water and $\text{UO}_2(\text{OTf})_2$.⁶ There is no further protonation observed and the uranyl moiety remains completely unscathed.

Due to the solubility of the uranyl species in water, it is an established environmental danger, and therefore has been receiving increased attention.^{5,7-9} Strategies to control its release into groundwater, usually involve reduction of the U(VI) moiety to a less soluble U(IV) species, UO_2 .¹⁰⁻¹⁶ Certain bacteria in nature, such as *Geobacter sulfurreducens*, can facilitate the reduction of uranyl(VI) to an insoluble, tetravalent form, through U=O bond activation (Figure 1.2).⁹ The reaction pathway is proposed to happen stepwise, first through reduction to a U(V) intermediate, followed by reduction to the U(IV) species (Figure 1.2).⁹ The most important step involves the coordination of a Lewis acidic uranium center of one uranyl moiety to an oxo ligand of another uranyl moiety, which results in weakening of the activated U=O bond, and allows for reduction of the uranium center. Additionally, the activation of a second “exo” oxo ligand, through protonation, is also an important step, and facilitates the disproportionation of two U(V) centers to one U(VI) and one U(IV) center.⁹ Clearly, functionalization of the uranyl oxo ligands plays an important role in the reduction of uranyl to U(IV). While this transformation may seem facile, a controlled one-pot reduction of uranyl to U(IV), where all the intermediates are fully characterized, has yet to be realized in a laboratory setting.

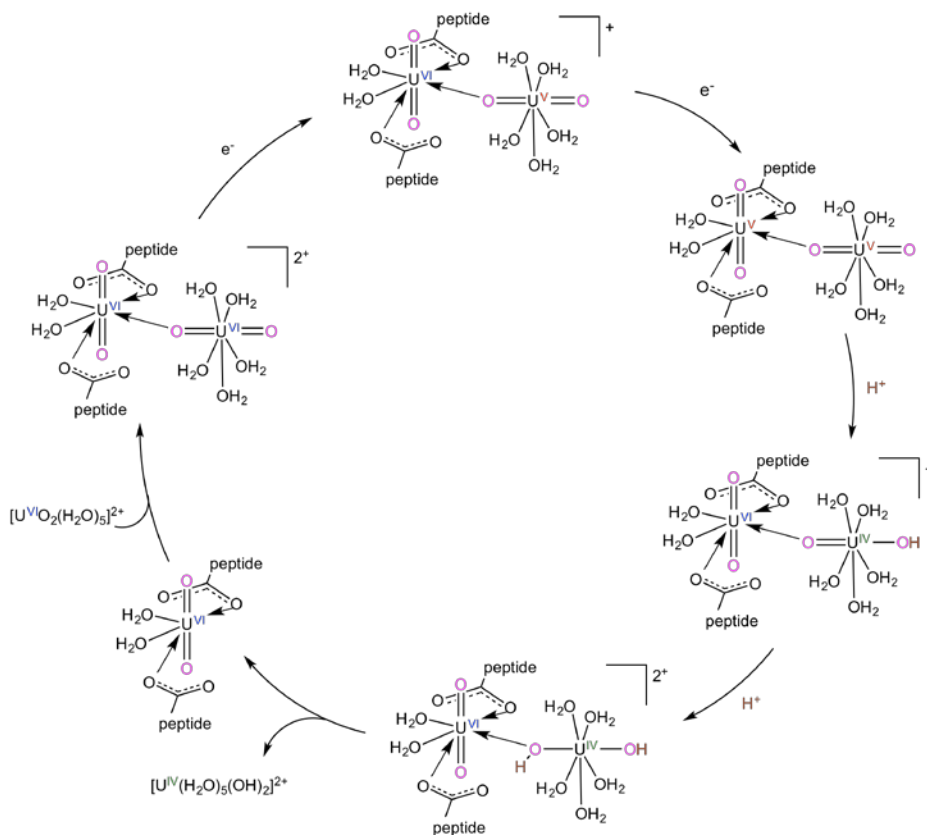


Figure 1.2. Proposed reaction for the bioreduction of uranyl to U(IV) by *Geobacter sulfurreducens*. (Figure recreated from reference 9).

1.2 Uranyl Oxo Functionalization

Functionalization of the uranyl oxo ligands can be facilitated through use of strongly electron donating equatorial co-ligands,^{17,18} which weaken the U=O interaction, and increase the reactivity of the oxo ligands. Interestingly, the symmetric stretching frequency of the uranyl moiety can be used as a convenient measure for the extent of oxo ligand activation from the co-ligands.⁵ Coordination of a strongly electron donating co-ligand results in a red shifting of the U=O stretching frequency, which can

be observed by IR and Raman spectroscopy. This trend is easily visualized by plotting the uranyl(VI)/(V) reduction potential vs. the U=O symmetric stretching frequency (ν_1) for a number of uranyl complexes (Figure 1.3). There appears to be a relatively linear relationship between the reduction potentials and the ν_1 values. This indicates that ν_1 values can be used to identify the extent of U=O bond activation from the equatorial ligands. Notably, $\text{UO}_2(\text{}^t\text{Buacnac})(\text{THF})$ does not fit this trend, for reasons we do not yet understand.^{5,17,19} In contrast to the trend exhibited by the ν_1 values, there appears to be no correlation between the U=O asymmetric stretches (ν_3) and reduction potential, likely due to difficulty in assigning this stretch.⁵

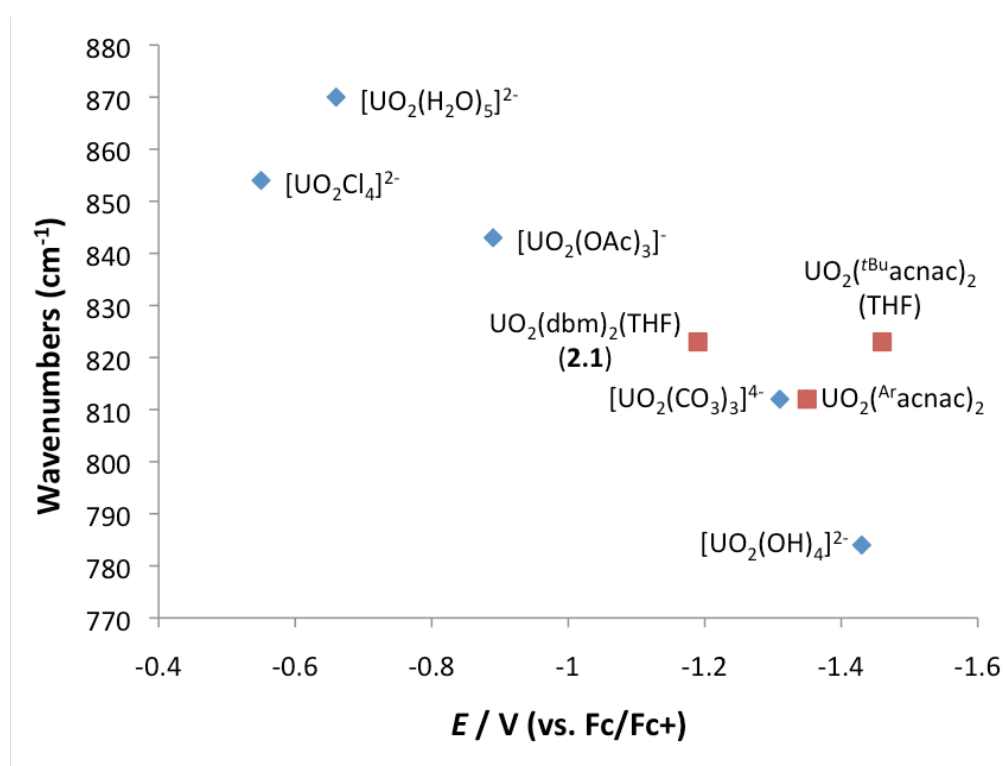
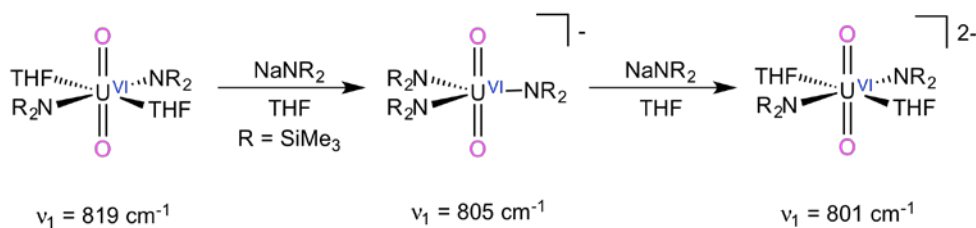


Figure 1.3. A comparison of the uranyl(IV) reduction potential (vs. Fc/Fc⁺) and the U=O symmetric stretching frequency (ν_1) for several uranyl complexes. Raman data and reduction potentials for $[\text{UO}_2\text{Cl}_4]^{2-}$, $[\text{UO}_2(\text{H}_2\text{O})_5]^{2+}$, $[\text{UO}_2(\text{OAc})_3]^-$, $[\text{UO}_2(\text{CO}_3)_3]^{4-}$, and

$[\text{UO}_2(\text{OH})_4]^{2-}$ were taken from reference 5. Reduction potentials were converted to Fc/Fc^+ by subtracting 0.49 V from the original Ag/AgCl values.²⁰ Reduction potentials for $\text{UO}_2(\text{Aracnac})_2$,²¹ $\text{UO}_2(\text{t}^{\text{Bu}}\text{acnac})_2(\text{THF})$,¹⁹ and $\text{UO}_2(\text{dbm})_2(\text{THF})$ (**2.1**) (Synthesis and full discussion in Chapter 2) were recorded in CH_2Cl_2 (■). Raman data for $\text{UO}_2(\text{Aracnac})_2$ and $\text{UO}_2(\text{t}^{\text{Bu}}\text{acnac})_2(\text{THF})$ were taken from reference 19.

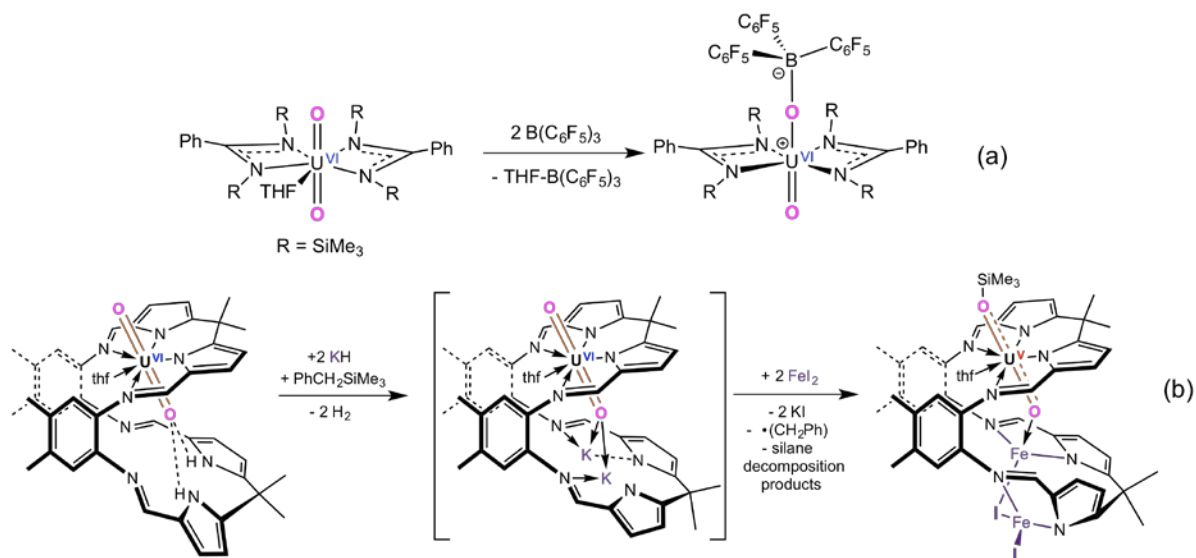
A trend between the extent of electron donation from the equatorial ligands and ν_1 values is nicely demonstrated in the complexes $[\text{UO}_2(\text{N}(\text{SiMe}_3)_2)_n]^{2-n}$ ($n=2-4$), where consecutive addition of the electron donating silylamide ligand, results in a decrease in the ν_1 values (Scheme 1.1).²² The increased Lewis basicity of the oxo ligands upon coordination of a strongly electron donating co-ligand to the uranium center can be explained by either the increased Coulombic charge repulsion between the uranium and the oxo ligands, or the competition between the oxo ligands and the co-ligand for uranium 6d and 5f orbitals, resulting in a weakening of the $\text{U}=\text{O}$ bond.^{5,17,23}



Scheme 1.1. Sequential addition of silylamide ligands to the uranyl ion. (scheme recreated from reference 22).

Sarsfield and Helliwell have also demonstrated that the electron rich ligand, benzaminato, can disrupt the uranyl bonding framework.¹⁸ The uranyl complex, $\text{UO}_2(\text{NCN})_2(\text{THF})$ [$\text{NCN} = \text{Me}_3\text{Si}(\text{N})\text{CPh}(\text{N})\text{SiMe}_3$] exhibits a ν_1 of 803 cm^{-1} , which is red

shifted from the starting material ($[\text{UO}_2\text{Cl}_2(\text{THF})_2]_2$, ν_1 840 cm^{-1}), and indicates an increased nucleophilicity of the oxo ligands. The weakening of the $\text{U}=\text{O}$ interaction facilitates the functionalization of one of the uranyl oxo ligands with $\text{B}(\text{C}_6\text{F}_5)_3$, a strong electrophile (Scheme 1.2a).¹⁸ $\text{B}(\text{C}_6\text{F}_5)_3$ coordination displaces electron density away from the $\text{U}=\text{O}$ bond, and weakens the $\text{U}=\text{O}$ bond even further. This is evidenced by the elongated $\text{U}=\text{O}$ bond length (1.898(3) Å) and a red shifted Raman stretching frequency of 780 cm^{-1} for $\text{UO}\{\text{OB}(\text{C}_6\text{F}_5)_3\}(\text{NCN})_2$. Utilization of strong electrophiles, such as $\text{B}(\text{C}_6\text{F}_5)_3$, to functionalize uranyl has been seen in several examples.^{18,24,25}



Scheme 1.2. **a)** Functionalization of an oxo ligand in a uranyl bisbenzaminato complex with $\text{B}(\text{C}_6\text{F}_5)_3$ (scheme reproduced from reference 18). **b)** Reductive silylation of uranyl utilizing the Arnold group ‘Pacman’ polypyrrolic macrocycle ligand (scheme reproduced from reference 26).

Another method for the functionalization of uranyl is reductive silylation, which has been the most successful and features the widest scope.^{5,19,26-33} It was first

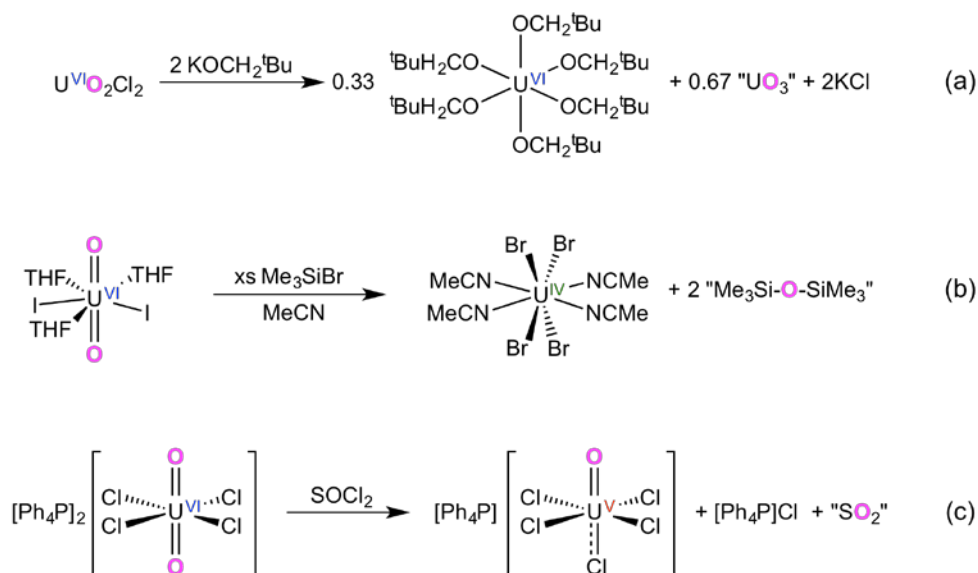
developed by Arnold and co-workers in 2008, when they showed their electron donating polypyrrolic macrocycle ligand allowed for the reductive silylation of $\text{UO}_2(\text{THF})(\text{H}_2\text{L})$ ($\text{L} =$ 'Pacman' polypyrrolic macrocycle), to produce the U(V) silyloxide, $[\text{U}(\text{OSiMe}_3)(\text{THF})\text{Fe}_2\text{I}_2\text{L}]$ (Scheme 1.2b).^{26,27,32,33} In this example, the uranium center is reduced from U(VI) to U(V), and one of the oxo ligands has been silylated. These two steps acting together have become known as 'reductive silylation'. Since 2008, reductive silylation of uranyl has also been achieved in our group using β -ketoiminate co-ligands.^{29,30} For example, reaction of $\text{UO}_2(\text{Aracnac})_2$ ($\text{Aracnac} = \text{ArNC}(\text{Ph})\text{CHC}(\text{Ph})\text{O}$, $\text{Ar} = 3,5\text{-tBu}_2\text{C}_6\text{H}_3$),²⁴ with a mixture of $\text{B}(\text{C}_6\text{F}_5)_3$ and HSiR_3 ($\text{R} = \text{Ph}, \text{Et}$), results in formation of the U(V) reductive silylation products, $\text{U}^{\text{V}}(\text{OSiPh}_3)(\text{OB}\{\text{C}_6\text{F}_5\}_3)(\text{Aracnac})_2$ and $[\text{U}^{\text{V}}(\text{OSiEt}_3)_2(\text{Aracnac})_2][\text{HB}(\text{C}_6\text{F}_5)_3]$.^{29,30} Other methods of reductive functionalization of the uranyl ion have also been reported, including reductive lithiation,³⁴ reduction and functionalization with lanthanide amides,^{35,36} and oxo ligand metalation.³⁷⁻⁴¹

1.3 Uranyl Oxo Substitution

While actinide chemists now have several procedures in place for functionalizing the uranyl oxo ligand (Section 1.2), there are only a few examples of complete uranyl oxo bond substitution, which could be a vital step for achieving controlled reduction of uranyl to U(IV). Uranyl oxo substitution usually requires harsh conditions, such as elevated temperatures and pressures, and the mechanism is still poorly understood.^{9,31,42,43} One example of U=O bond substitution, occurs during the

reaction of $\text{Ni}(\text{OAc})_2$ and $\text{UO}_2(\text{OAc})_2$ in the presence of HF, resulting in the formation of $[\text{Ni}^{\text{II}}(\text{H}_2\text{O})_6\text{U}^{\text{IV}}_3\text{F}_{16}\cdot 3\text{H}_2\text{O}]$.⁴² In this reaction, there is no apparent correlation between the stoichiometry of the reactants and products, and it requires the highly corrosive HF, elevated temperatures (200 °C), and long reaction times (72 h).

There are only a handful of instances of U=O bond substitution at room temperature.⁴⁴ In one example, the metathesis of $[\text{UO}_2\text{Cl}_2(\text{THF})_2]_2$ with 6 equiv of the potassium alkoxide, $\text{KOCH}_2\text{C}(\text{CH}_3)_3$, results in the formation of the homoleptic U(VI) species, $\text{U}[\text{OCH}_2\text{C}(\text{CH}_3)_3]_6$, along with a UO_3 precipitate (Scheme 1.3a).¹⁷ It is speculated that the UO_3 is the destination of the substituted oxo ligands, however, the mechanism is still unknown. Additionally, Ephritikhine and co-workers demonstrated that addition of excess Me_3SiX (X = Cl, Br, I) to $\text{UO}_2\text{I}_2(\text{THF})_3$ in MeCN resulted in formation of $\text{UX}_4(\text{MeCN})_4$ in good yields (Scheme 1.3b).³¹ This reaction is not well understood, as all the original bonds to the uranium have been broken, and no intermediates have been isolated. In addition, the fate of the oxo ligands of the uranyl fragment are not certain, but the reaction was recently re-investigated by our group and thought to be converted into $\text{Me}_3\text{SiOSiMe}_3$.²⁸ In another example, the reaction of $[\text{Ph}_4\text{P}]_2[\text{UO}_2\text{Cl}_4]$ with thionyl chloride generated the U(VI) mono-oxo, $[\text{Ph}_4\text{P}][\text{UOCl}_5]$ (Scheme 1.3c).²⁵ While this synthesis results in U=O bond substitution at ambient conditions, the mechanism by which this reaction proceeds, and the fate of the missing oxo ligand, are not certain.



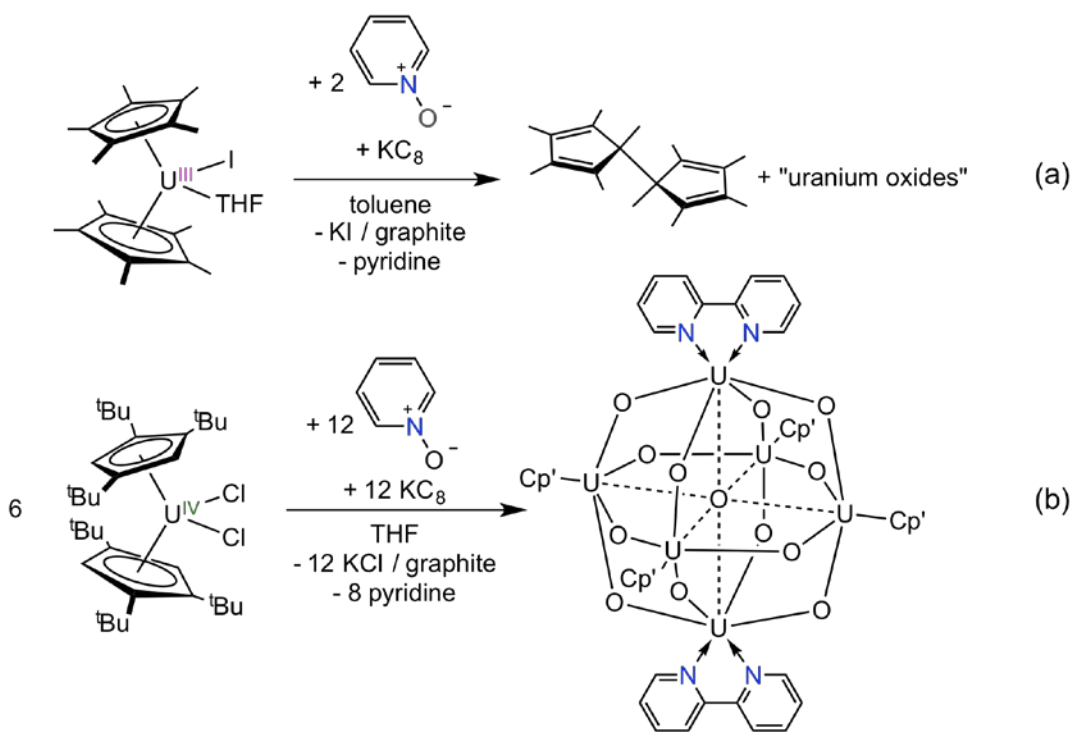
Scheme 1.3. Examples of uranyl oxo substitution at room temperature. **a)** reproduced from reference 17. **b)** reproduced from reference 31. **c)** reproduced from reference 25.

1.4 *Cis*-Uranyl

In contrast to the *trans*-uranyl fragment, the *cis*-uranyl ion is unknown, and all attempts to synthesize a *cis*-uranyl complex have been unsuccessful thus far.⁴⁵⁻⁴⁹ In fact, the O-U-O angle of uranyl rarely deviates past 170° (Figure 1.1), which is unusual considering that transition metal dioxo complexes typically feature *cis*-stereochemistry.⁵⁰⁻⁵⁴ The linear geometry of the uranyl moiety has been rationalized by the mixing of the 5f_z³ and 6p_z uranium AOs in the O-U-O σ-bonding framework, which turns the U-O σ_u⁺ MO into a “superlative σ donor”,⁵⁵ and consequently destabilizes the valence σ_u-antibonding MO (Figure 1.1), which is the highest occupied orbital.⁵⁵ The overlap of the 6p_z and 5f_z³ AOs could not take place if the O-U-O angle was not linear (Figure 1.1). Subsequent calculations have also confirmed the uranium

$6p_z$ AO, stabilizes the linear geometry of uranyl, however, the order of the valence orbitals are still being debated.^{1,2} The isolation of a *cis*-uranyl complex could provide some more insight into the exact orbital combination responsible for the stabilization of a linear O-U-O geometry.

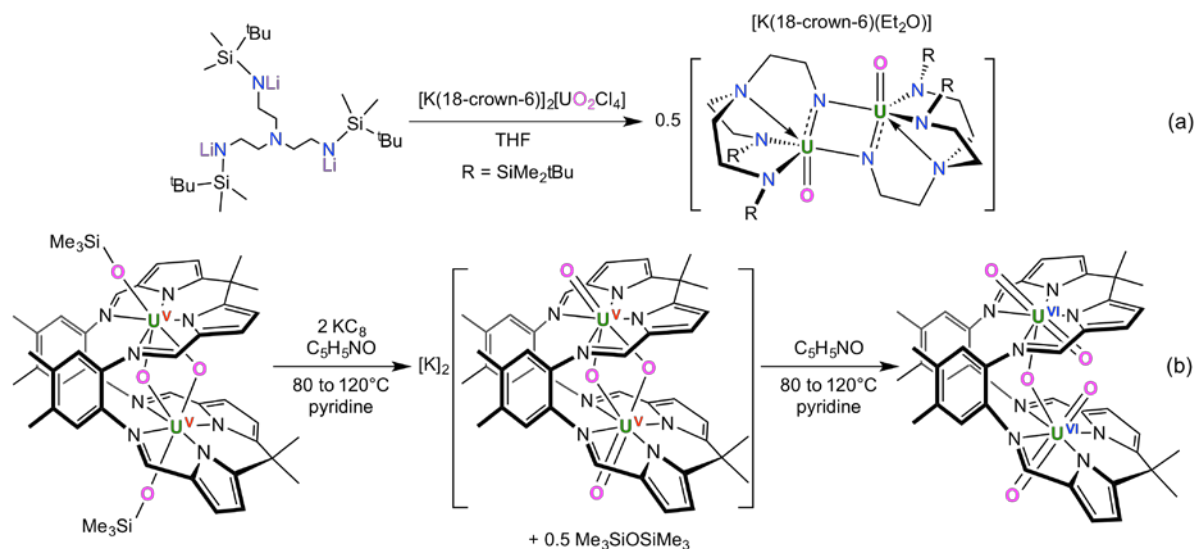
Several attempts have been made to generate a *cis*-uranyl complex, however, most have been thwarted by unwanted ligand oxidation or ligand decomposition. For example, reaction of $\text{Cp}^*_2\text{UI}(\text{THF})$ with KC_8 and pyridine-*N*-oxide, in an attempt to generate the *cis*-uranyl complex, *cis*- Cp^*_2UO_2 , resulted in formation of the pentamethylcyclopentadienyl dimer and unidentified “uranium oxides” (Scheme 1.4a).⁵⁶ Similarly, reaction of $\text{Cp}'_2\text{UCl}_2$ ($\text{Cp}' = 1,2,4\text{-C}_5\text{H}_2\text{tBu}_3$) with pyridine-*N*-oxide and KC_8 afforded a mixed-valent uranium oxo cluster (Scheme 1.4b).⁵⁷ In both instances, a *cis*-uranyl intermediate is likely formed, but it is unstable and decomposes via spontaneous ligand oxidation.



Scheme 1.4. Previous attempts to make the *cis*-uranyl complex, *cis*-Cp'₂UO₂ (Cp' = η⁵-C₅Me₅, 1,2,4-C₅H₂^tBu₃). **a)** reproduced from reference 56. **b)** reproduced from reference 57.

Clark and co-workers approached generating a *cis*-uranyl complex differently, by trying to force a *trans*-uranyl moiety to exhibit *cis*-oxo stereochemistry through ligation of a tripodal ligand. However, reaction of [Li]₃[N(CH₂CH₂NSi^tBuMe₂)₃] with [K(18-crown-6)]₂[*trans*-UO₂Cl₄] only resulted in formation of a mixed-valent U(V/VI) oxo-imido dimer, [K(18-crown-6)(Et₂O)][UO(μ₂-NCH₂CH₂N(CH₂CH₂NSi^tBuMe₂)₂)]₂ (Scheme 1.5a).⁴⁵ In this example, a *cis*-uranyl intermediate is also likely formed, however, it is probably unstable, and results in abstraction of a silyl group from the tripodal ligand and U=O cleavage. The mechanism of this reaction is not well

understood, however, it is clear that this particular tripodal ligand is not robust enough to stabilize a *cis*-uranyl complex.



Scheme 1.5. Previous attempts to make a *cis*-uranyl complex, from a U(VI) starting material. **a)** reproduced from reference 45. **b)** reproduced from references 58 and 59.

Although a true *cis*-uranyl complex as yet to be synthesized, Arnold and co-workers have demonstrated that the thermolysis of a mixture of $UO_2(N\{SiMe_3\}_2)(pyr)_2$ and $UO_2(pyridine)(H_2L)$ leads to the binuclear U(V) oxo complex, $[(Me_3SiOU^VO)_2(L)]$ ($L =$ polypyrrole macrocycle), where the pacman ligand enforces the binuclear U(V) complex to form *cis*-oxo ligands ($O-U-O$ angle of $73.3(2)^\circ$) (Scheme 1.5b).⁵⁸ Reduction of both the uranium ions to U(V) and silylation of the “exo” oxo ligands, weakens the U-O σ - and π -bonds, which likely lowers the energy needed for *cis/trans* isomerization. More recently, Arnold and co-workers demonstrated that the one-pot reduction and oxidation of the binuclear U(V) oxo complex, $[(Me_3SiOU^VO)_2(L)]$ with KC_8 or potassium metal and pyridine-*N*-oxide, results in the formation of the doubly desilylated

binuclear U(V) complex, $[K]_2[(OUO)_2(L)]$ ($L =$ polypyrrole macrocycle), which is formally generated by coupling of a *trans*- $[U^VO_2]^+$ fragment with a *cis*- $[U^VO_2]^+$ fragment within the binding pocket of the polypyrrole macrocycle (Scheme 1.5b).^{58,59} Similar to $[(Me_3SiOU^VO)_2(L)]$, the reduced U(V) ions in $[K]_2[(OUO)_2(L)]$ likely lower the energy penalty required for *cis/trans* isomerization. This is nicely demonstrated, when oxidation of this complex with pyridine-*N*-oxide results in rearrangement of the *cis*-di(oxo) fragment back to the original *trans* structure (Scheme 1.5b).^{58,59}

Furthermore, a *cis*-uranyl coordination polymer, $cis-[UO_2(fcdc)(THF) \cdot (Fc)]_n$ ($fcdc = 1,2$ -ferrocenedicarboxylate), was reported by Duval and co-workers in 2007,⁴⁸ but not even a year later Ephritikhine and co-workers showed this result was unreproducible,⁴⁷ and is likely incorrect. A similar 2015 report of a *cis*-uranyl coordination polymer is also probably incorrect.⁴⁹

Interestingly, density functional theory (DFT) studies of $[UO_2(OH)_4]^{2-}$ reveal that the *cis* isomer is 18-20 kcal/mol higher in energy than the *trans* isomer, depending on the method used.^{60,61} Similar calculations by Schelter and co-workers reveal that the *cis* isomer of $[UO_2(N(SiH_3)_2)_3]^-$ is 31.4 kcal/mol higher in energy than the *trans* isomer.⁶² Even though these *cis*-uranyl isomers are higher in energy than the *trans*-isomers, they still represent local minima on the energy landscape, indicating their isolation should be possible. These large destabilizations likely reflect the lack of an Inverse Trans Influence (ITI) in the *cis*- UO_2^{2+} fragment,⁶³⁻⁶⁷ and further highlight the challenges inherent in isolating a *cis*-uranyl complex.

1.5 General Remarks

This dissertation is divided into 7 chapters and 2 appendices, and covers three primary areas of research: 1) the reductive silylation of uranyl to U(IV) and examples of uranyl oxo ligand substitution, 2) attempts to synthesize a *cis*-uranyl complex, and 3) the synthesis and reactivity of a U(IV) dibenzene complex.

Chapters 2, 3 and 4 explore the reductive silylation of uranyl using various co-ligands, such as dbm, dppmo and TPPO. Both chapters 2 and 3 contain rare examples of uranyl oxo ligand substitution under ambient conditions. Chapter 3 contains the first reported one-pot reduction under ambient conditions of uranyl to U(IV), where the fate of the substituted oxo ligands have been explicitly identified. This work is especially interesting because it displays a close resemblance to the proposed mechanism for the biological reduction of uranyl by *Geobacter sulfurreducens*.⁹ The understanding of reduction and remediation of uranyl in the environment is a crucial consideration when planning for storage of spent nuclear fuel. Chapter 4 explores the effectiveness of various silylating reagents, R₃SiOTf (R = Ph, Me).

Chapters 5 and 6 discuss several attempts to generate a *cis*-uranyl complex, by reacting *trans*-uranyl with small macrocycle ligands that occupy only one hemisphere of the metal ion, in order to force *cis*-stereochemistry of the uranyl oxo ligands. Although true *cis*-uranyl complexes were not isolated, the results presented do give insight into new strategies for the generation of a *cis*-uranyl complex in the future.

Chapter 7 describes the synthesis and the in-depth reactivity studies of the first isolable U(IV) dibenzene complex, and its comparison to transition metal benzene complexes.

Appendix A contains supplementary information for several chapters. Appendix B describes the synthesis of several molecules not mentioned in the main body of this dissertation.

1.6 References

- (1) Denning, R. G. *J. Phys. Chem. A* **2007**, *111*, 4125.
- (2) Kaltsoyannis, N. *Inorg. Chem.* **2000**, *39*, 6009.
- (3) Kaltsoyannis, N.; Scott, P. *The f elements*; Oxford University Press: New York, 1999.
- (4) deB. Darwent, B. *Nat. Stand. Ref. Data Ser.* **1970**, *31*, 1.
- (5) Fortier, S.; Hayton, T. W. *Coord. Chem. Rev.* **2010**, *254*, 197.
- (6) Berthet, J.-C.; Lance, M.; Nierlich, M.; Ephritikhine, M. *Eur. J. Inorg. Chem.* **2000**, 1969
- (7) Katz, J. J.; Seaborg, G. T.; Morss, L. R. *The Chemistry of the Actinide Elements*; Second ed.; Chapman and Hall: New York, 1986; Vol. 1.
- (8) Anderson, R. T.; Vrionis, H. A.; Ortiz-Bernad, I.; Resch, C. T.; Long, P. E.; Dayvault, R.; Karp, K.; Marutzky, S.; Metzler, D. R.; Peacock, A.; White, D. C.; Lowe, M.; Lovley, D. R. *Appl. Environ. Microbiol.* **2003**, *69*, 5884
- (9) Sundararajan, M.; Campbell, A. J.; Hillier, I. H. *J. Phys. Chem. A* **2008**, *112*, 4451.
- (10) Wu, W.-M.; Carley, J.; Fienen, M.; Mehlhorn, T.; Lowe, K.; Nyman, J.; Luo, J.; Gentile, M. E.; Rajan, R.; Wagner, D.; Hickey, R. F.; Gu, B.; Watson, D.; Cirpka, O. A.; Kitanidis, P. K.; Jardine, P. M.; Criddle, C. S. *Environ. Sci. Technol.* **2006**, *40*, 3978.
- (11) Wu, W.-M.; Carley, J.; Gentry, T.; Ginder-Vogel, M. A.; Fienen, M.; Mehlhorn, T.; Yan, H.; Caroll, S.; Pace, M. N.; Nyman, J.; Luo, J.; Gentile, M. E.; Fields, M. W.; Hickey, R. F.; Gu, B.; Watson, D.; Cirpka, O. A.; Zhou, J.; Fendorf, S.; Kitanidis, P. K.; Jardine, P. M.; Criddle, C. S. *Environ. Sci. Technol.* **2006**, *40*, 3986.
- (12) Renshaw, J. C.; Butchins, L. J. C.; Livens, F. R.; May, I.; Charnock, J. M.; Lloyd, J. R. *Environ. Sci. Technol.* **2005**, *39*, 5657.
- (13) Gu, B.; Wu, W.-M.; Ginder-Vogel, M. A.; Yan, H.; Fields, M. W.; Zhou, J.; Fendorf, S.; Criddle, C. S.; Jardine, P. M. *Environ. Sci. Technol.* **2005**, *39*, 4841.
- (14) Ilton, E. S.; Haiduc, A.; Cahill, C. L.; Felmy, A. R. *Inorg. Chem.* **2005**, *44*, 2986.
- (15) Williams, K. H.; Bargar, J. R.; Lloyd, J. R.; Lovley, D. R. *Curr. Opin. Biotechnol.* **2013**, *24*, 489.
- (16) Noubactep, C.; Meinrath, G.; Dietrich, P.; Merkel, B. *Environ. Sci. Technol.* **2003**, *37*, 4304.
- (17) Wilkerson, M. P.; Burns, C. J.; Dewey, H. J.; Martin, J. M.; Morris, D. E.; Paine, R. T.; Scott, B. L. *Inorg. Chem.* **2000**, *39*, 5277.
- (18) Sarsfield, M. J.; Helliwell, M. *J. Am. Chem. Soc.* **2004**, *126*, 1036.
- (19) Brown, J. L.; Mokhtarzadeh, C. C.; Lever, J. M.; Wu, G.; Hayton, T. W. *Inorg. Chem.* **2011**, *50*, 5105.
- (20) Wang, W.; Zhao, N.; Geng, Y.; Cui, S.-B.; Hauser, J.; Decurtins, S.; Liu, S.-X. *RSC Adv.* **2014**, *4*, 32639.
- (21) Hayton, T. W.; Wu, G. *Inorg. Chem.* **2009**, *48*, 3065.
- (22) Burns, C. J.; Clark, D. L.; Donohoe, R. J.; Duval, P. B.; Scott, B. L.; Tait, C. D. *Inorg. Chem.* **2000**, *39*, 5464.
- (23) Fillaux, C.; Guillaumont, D.; Berthet, Jean C.; Copping, R.; Shuh, D. K.; Tylliszczak, T.; Auwer, C. D. *Phys. Chem. Chem. Phys.* **2010**, *12*, 14253.

- (24) Schnaars, D. D.; Wu, G.; Hayton, T. W. *J. Am. Chem. Soc.* **2009**, *131*, 17532.
- (25) Bagnall, K. W.; du Preez, J. G. H. *Chem. Commun.* **1973**, 820.
- (26) Arnold, P. L.; Patel, D.; Wilson, C.; Love, J. B. *Nature* **2008**, *451*, 315.
- (27) Arnold, P. L.; Love, J. B.; Patel, D. *Coord. Chem. Rev.* **2009**, *253*, 1973
- (28) Brown, J. L.; Wu, G.; Hayton, T. W. *J. Am. Chem. Soc.* **2010**, *132*, 7248
- (29) Schnaars, D. D.; Wu, G.; Hayton, T. W. *Inorg. Chem.* **2011**, *50*, 4695.
- (30) Schnaars, D. D.; Wu, G.; Hayton, T. W. *Inorg. Chem.* **2011**, *50*, 9642.
- (31) Berthet, J.-C.; Siffredi, G.; Thuéry, P.; Ephritikhine, M. *Eur. J. Inorg. Chem.* **2007**, 4017.
- (32) Yahia, A.; Arnold, P. L.; Love, J. B.; Maron, L. *Chem. Commun.* **2009**, 2402.
- (33) Yahia, A.; Arnold, P. L.; Love, J. B.; Maron, L. *Chem. Eur. J.* **2010**, *16*, 4881.
- (34) Arnold, P. L.; Pécharman, A.-F.; Love, J. B. *Angew. Chem. Int. Ed.* **2011**, *50*, 9456.
- (35) Arnold, P. L.; Hollis, E.; Nichol, G. S.; Love, J. B.; Griveau, J.-C.; Caciuffo, R.; Magnani, N.; Maron, L.; Castro, L.; Yahia, A.; Odoh, S. O.; Schreckenbach, G. *J. Am. Chem. Soc.* **2013**, *135*, 3841.
- (36) Arnold, P. L.; Hollis, E.; White, F. J.; Magnani, N.; Caciuffo, R.; Love, J. B. *Angew. Chem. Int. Ed.* **2011**, *50*, 887.
- (37) Nocton, G.; Horeglad, P.; Vetere, V.; Pecaut, J.; Dubois, L.; Maldivi, P.; Edelstein, N. M.; Mazzanti, M. *J. Am. Chem. Soc.* **2010**, *132*, 495.
- (38) Nocton, G.; Horeglad, P.; Pecaut, J.; Mazzanti, M. *J. Am. Chem. Soc.* **2008**, *130*, 16633.
- (39) Mougél, V.; Biswas, B.; Pecaut, J.; Mazzanti, M. *Chem. Commun.* **2010**, *46*, 8648.
- (40) Natrajan, L.; Burdet, F.; Pecaut, J.; Mazzanti, M. *J. Am. Chem. Soc.* **2006**, *128*, 7152.
- (41) Mougél, V.; Pecaut, J.; Mazzanti, M. *Chem. Commun.* **2012**, *48*, 868.
- (42) Bean, A. C.; Sullens, T. A.; Runde, W.; Albrecht-Schmitt, T. E. *Inorg. Chem.* **2003**, *42*, 2628.
- (43) Berthet, J.-C.; Thuery, P.; Ephritikhine, M. *Inorg. Chem.* **2005**, *44*, 1142.
- (44) Gong, Y.; Vallet, V.; del Carmen Michelini, M.; Rios, D.; Gibson, J. K. *J. Phys. Chem. A* **2014**, *118*, 325.
- (45) Duval, P. B.; Burns, C. J.; Buschmann, W. E.; Clark, D. L.; Morris, D. E.; Scott, B. L. *Inorg. Chem.* **2001**, *40*, 5491.
- (46) Arney, D. S. J.; Burns, C. J. *J. Am. Chem. Soc.* **1995**, *117*, 9448.
- (47) Villiers, C.; Thuéry, P.; Ephritikhine, M. *Angew. Chem. Int. Ed.* **2008**, *47*, 5892.
- (48) Vaughn, A. E.; Barnes, C. L.; Duval, P. B. *Angew. Chem. Int. Ed.* **2007**, *46*, 6622.
- (49) Guan, Q. L.; Bai, F. Y.; Xing, Y. H.; Liu, J.; Zhang, H. Z. *Inorg. Chem. Commun.* **2015**, *59*, 36.
- (50) Haiges, R.; Skotnitzki, J.; Fang, Z.; Dixon, D. A.; Christe, K. O. *Angew. Chem. Int. Ed.* **2015**, *54*, 9581.
- (51) Correia, I.; Pessoa, J. C.; Duarte, M. T.; da Piedade, M. F. M.; Jackush, T.; Kiss, T.; Castro, M. M. C. A.; Geraldes, C. F. G. C.; Avecilla, F. *Eur. J. Inorg. Chem.* **2005**, *2005*, 732.

- (52) Wong, Y.-L.; Yang, Q.; Zhou, Z.-Y.; Lee, H. K.; Mak, T. C. W.; Ng, D. K. P. *New J. Chem.* **2001**, *25*, 353.
- (53) Lippert, C. A.; Arnstein, S. A.; Sherrill, C. D.; Soper, J. D. *J. Am. Chem. Soc.* **2010**, *132*, 3879.
- (54) Demachy, I.; Jean, Y. *Inorg. Chem.* **1997**, *36*, 5956.
- (55) Tatsumi, K.; Hoffmann, R. *J. Am. Chem. Soc.* **1980**, *19*, 2656.
- (56) Cantat, T.; Graves, C. R.; Scott, B. L.; Kiplinger, J. L. *Angew. Chem. Int. Ed.* **2009**, *48*, 3681.
- (57) Duval, P. B.; Burns, C. J.; Clark, D. L.; Morris, D. E.; Scott, B. L.; Thompson, J. D.; Werkema, E. L.; Jia, L.; Andersen, R. A. *Angew. Chem. Int. Ed.* **2001**, *40*, 3357.
- (58) Arnold, P. L.; Jones, G. M.; Odoh, S. O.; Schreckenbach, G.; Magnani, N.; Love, J. B. *Nat. Chem.* **2012**, *4*, 221.
- (59) Jones, G. M.; Arnold, P. L.; Love, J. B. *Angew. Chem. Int. Ed.* **2012**, *51*, 12584.
- (60) Schreckenbach, G.; Hay, P. J.; Martin, R. L. *Inorg. Chem.* **1998**, *37*, 4442.
- (61) Bühl, M.; Schreckenbach, G. *Inorg. Chem.* **2010**, *49*, 3821.
- (62) Mullane, K. C.; Lewis, A. J.; Yin, H.; Carroll, P. J.; Schelter, E. J. *Inorg. Chem.* **2014**, *53*, 9129.
- (63) La Pierre, H. S.; Meyer, K. *Inorg. Chem.* **2013**, *52*, 529.
- (64) Kovács, A.; Konings, R. J. M. *Chem. Phys. Chem.* **2006**, *7*, 455.
- (65) Lam, O. P.; Franke, S. M.; Nakai, H.; Heinemann, F. W.; Hieringer, W.; Meyer, K. *Inorg. Chem.* **2012**, *51*, 6190.
- (66) Lewis, A. J.; Carroll, P. J.; Schelter, E. J. *J. Am. Chem. Soc.* **2013**, *135*, 511.
- (67) Pedrick, E. A.; Wu, G.; Kaltsoyannis, N.; Hayton, T. W. *Chem. Sci.* **2014**, *5*, 3204.

Chapter 2. Borane-Mediated Reductive Silylation of a Uranyl

Dibenzoylmethanate Complex: An Example of Controlled Uranyl Oxo Ligand Substitution

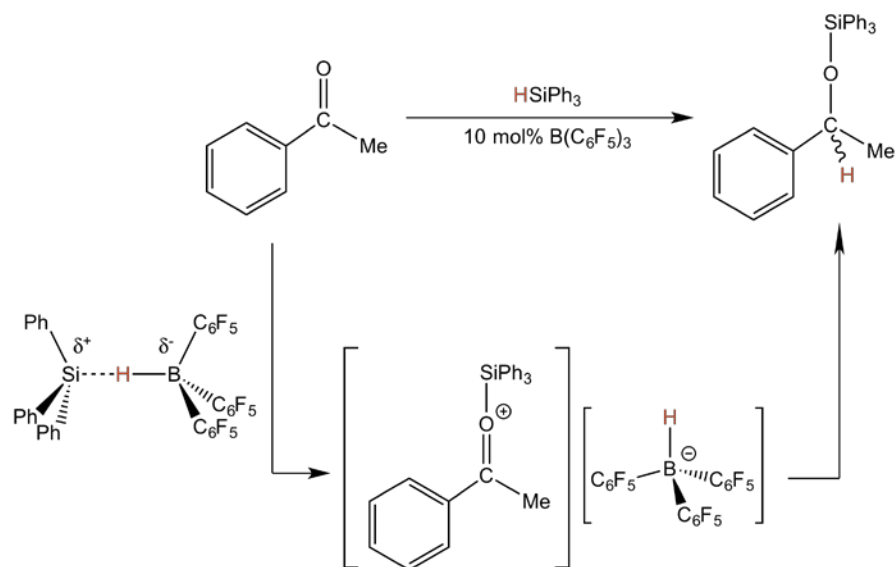
2.1. Introduction	22
2.2. Results and Discussion	26
2.2.1. Synthesis, Characterization, and Electrochemical Studies of $\text{UO}_2(\text{dbm})_2(\text{THF})$ (2.1).....	26
2.2.2. Synthesis and Characterization of $\text{U}(\text{OB}\{\text{C}_6\text{F}_5\}_3)(\text{OSiPh}_3)(\text{dbm})_2(\text{THF})$ (2.2) and $\text{U}(\text{OB}\{\text{C}_6\text{F}_5\}_3)(\text{OSiEt}_3)(\text{dbm})_2(\text{THF})$ (2.3)	30
2.2.3. Synthesis and Characterization of $\text{U}(\kappa^2\text{-O,F-OB}\{\text{C}_6\text{F}_5\}_3)(\text{OSiEt}_3)(\text{dbm})_2$ (2.4).....	35
2.2.4. Synthesis and Characterization of $\text{U}(\text{OB}\{\text{C}_6\text{F}_5\}_3)(\text{dbm})_3$ (2.5).....	37
2.2.5. Synthesis of $\text{U}(\text{OSiPh}_3)_3(\text{dbm})_2$ (2.6) and $\text{U}(\text{OB}\{\text{C}_6\text{F}_5\}_3)(\text{OSiEt}_3)(\text{dbm})_2(\text{HOPh})$ (2.7).....	41
2.3. Summary	46
2.4. Experimental Section	47
2.4.1. General Procedures	47
2.4.2. Cyclic Voltammetry Measurements.....	48
2.4.3. Synthesis of $\text{UO}_2(\text{dbm})_2(\text{THF})$ (2.1).....	48
2.4.4. Synthesis of $\text{U}(\text{OB}\{\text{C}_6\text{F}_5\}_3)(\text{OSiPh}_3)(\text{dbm})_2(\text{THF})$ (2.2)	49
2.4.5. Synthesis of $\text{U}(\text{OB}\{\text{C}_6\text{F}_5\}_3)(\text{OSiEt}_3)(\text{dbm})_2(\text{THF})$ (2.3)	50
2.4.6. Synthesis of $\text{U}(\kappa^2\text{-O,F-OB}\{\text{C}_6\text{F}_5\}_3)(\text{OSiEt}_3)(\text{dbm})_2$ (2.4).....	51
2.4.7. Synthesis of $\text{U}(\text{OB}\{\text{C}_6\text{F}_5\}_3)(\text{dbm})_3$ (2.5).....	52

2.4.8. Synthesis of $U(OSiPh_3)_3(dbm)_2$ (2.6).....	52
2.4.9. Synthesis of $U(OB\{C_6F_5\}_3)(OSiEt_3)(dbm)_2(HOPh)$ (2.7)	53
2.4.10. X-Ray Crystallography	54
2.5. Acknowledgements	58
2.6. References	58

2.1 Introduction

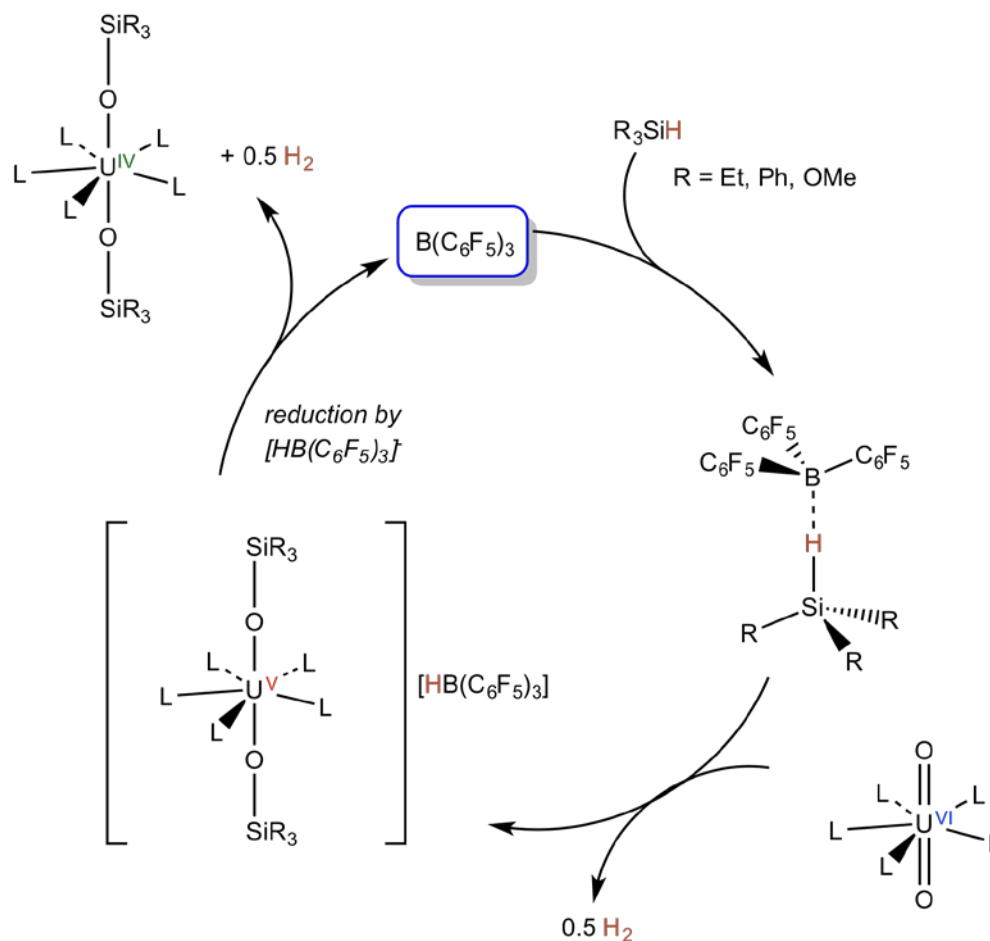
The reduction of uranyl(VI) to U(IV) has proven to be a viable strategy for the treatment of contaminated legacy sites,¹⁻⁷ and can be achieved through functionalization or substitution of the uranyl oxo ligands.⁸ Oxo ligand functionalization and substitution of the uranyl ion can be rather challenging,⁹ however, both can be facilitated through the use of strongly electron donating equatorial co-ligands,^{10,11} utilization of strong electrophiles,¹¹⁻¹³ or reductive silylation.^{9,14-22}

Interestingly, B(C₆F₅)₃-activated silanes have been shown to reduce a variety of organic substrates, including ketones, enols and imines.²³⁻²⁸ In this type of silylation process, studied extensively by Piers and co-workers, the Lewis acidic perfluoroaryl borane, B(C₆F₅)₃, forms a proposed borane-silane adduct with an electron rich silane, Ph₃SiH, which activates the silicon towards nucleophilic attack from the oxygen by abstracting a hydride (Scheme 2.1).^{24,29} In 2014, a similar borane-silane adduct between 1,2,3-tris(pentafluorophenyl)-4,5,6,7-tetrafluoro-1-bora-indene and Et₃SiH was crystallographically characterized for the first time.²⁹



Scheme 2.1. Borane-catalyzed silylation of a ketone (Scheme reproduced from reference 24).

Drawing inspiration from the reductive silylation work done by Arnold and co-workers (Scheme 1.2b), as well as the work done by Piers and co-workers (Scheme 2.1), our group developed a proposed catalytic method for uranyl functionalization using B(C₆F₅)₃ (Scheme 2.2). We hypothesize that reaction of a uranyl complex, UO₂L_x (L = co-ligand), with a borane-silane adduct, SiPh₃ would promote a double silylation to generate a U(V) bis-silyloxy complex, where the charge is balanced by the borohydride counterion, [HB(C₆F₅)₃]⁻.^{18,19} Then, by optimizing the redox potential of the U(V) intermediate by modifying the co-ligands, it would be possible for [HB(C₆F₅)₃]⁻, which is a competent reducing agent,³⁰ to further reduce the U(V) center to U(IV), whilst regenerating the B(C₆F₅)₃ catalyst (Scheme 2.2). However, we still need to find the ideal co-ligands (L) to facilitate the unprecedented catalytic ‘reductive silylation’ of uranyl.

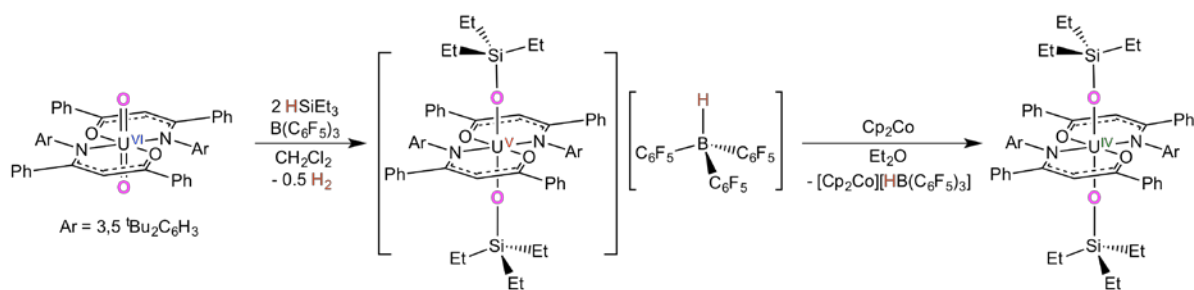


Scheme 2.2. Proposed catalytic cycle for the reductive silylation of uranyl to U(IV).

Our group has previously probed the utility of the electron rich, β -ketoiminate ligand, $^{Ar}acnac$ ($^{Ar}acnac = ArNC(Ph)CHC(Ph)O$, $Ar = 3,5\text{-}^tBu_2C_6H_3$), for its use as a co-ligand in the proposed cycle (Scheme 2.2).¹⁸ The uranyl complex, $UO_2(^{Ar}acnac)_2$, was shown to react with $HSiR_3$ ($R = Ph, Et$), in combination with $B(C_6F_5)_3$, to generate the U(V) silyloxo complexes, $U(OSiPh_3)(OB\{C_6F_5\}_3)(^{Ar}acnac)_2$ ¹⁸ and $[U(OSiEt_3)_2(^{Ar}acnac)_2][HB(C_6F_5)_3]$ ¹⁹ (Scheme 2.3). In both cases, the strong electron donating ability of $^{Ar}acnac$ ligand activated the uranyl oxo groups toward functionalization. Other researchers have also hypothesized that strongly donating

equatorial groups weaken the U=O bond and activate the oxo ligands toward functionalization and/or substitution.³¹⁻³⁴ This hypothesis is supported by vibrational data, which shows a clear correlation between donor ability and the U=O ν_{sym} stretch (Figure 1.3).⁹

It is important to note, however, in both examples, there was no evidence for reduction to U(IV), the desired product. In fact, Cp₂Co, an external reductant, was needed to achieve complete reduction to U(IV), which is not practical for large-scale catalytic reductions.¹⁹ Since the borane reagent is also consumed in the reaction, either by coordination to an unfunctionalized uranyl oxo, U(OSiPh₃)(OB{C₆F₅})₃(^{Ar}acnac)₂,¹⁸ or trapped as a borohydride anion, [U(OSiEt₃)₂(^{Ar}acnac)₂][HB(C₆F₅)₃],¹⁹ we hypothesize that the reduction process was stopped at U(V) due to the strong electron donating properties of the ^{Ar}acnac ligand. While a strong electron donating co-ligand is ideal for activating the oxo ligands in uranyl towards functionalization, it appears to be simultaneously thwarting the complete reduction to U(IV). A slightly weaker donating equatorial ligand might be better suited for this process. Finding the right amount of electron donation from the co-ligands to balance both oxo ligand activation and metal center reduction is key for this process to work.



Scheme 2.3. Reductive Silylation of $\text{UO}_2(\text{Aracnac})_2$ with $\text{B}(\text{C}_6\text{F}_5)_3$ and Et_3SiH . (Scheme reproduced from reference 19).

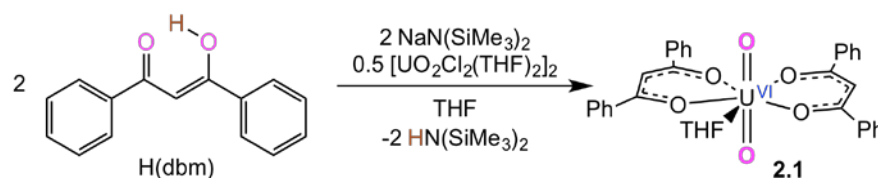
In this chapter, we report a new example of reductive silylation, using a $\text{B}(\text{C}_6\text{F}_5)_3$ -activated silane to functionalize the oxo ligands of a dibenzoylmethanate-supported uranyl complex. In addition, we demonstrate a two-step procedure for the controlled substitution of a uranyl oxo ligand under ambient conditions.

2.2 Results and Discussion

2.2.1. Synthesis, Characterization, and Electrochemical Studies of $\text{UO}_2(\text{dbm})_2(\text{THF})$ (2.1)

To expand the scope of borane-mediated silylation of uranyl, the utility of dbm (dbm = $\text{OC}(\text{Ph})\text{CHC}(\text{Ph})\text{O}$) as a uranyl supporting ligand was probed. Several $\text{UO}_2(\text{dbm})_2(\text{L})$ -type complexes have been reported in the literature, however, they typically feature Lewis base co-ligands that could be incompatible with our reductive silylation protocol (e.g., H_2O , dmsO, dmf).³⁵⁻³⁷ Thus, we endeavored to synthesize a uranyl dibenzoylmethanate complex that contained THF as a co-ligand. Reaction of 2

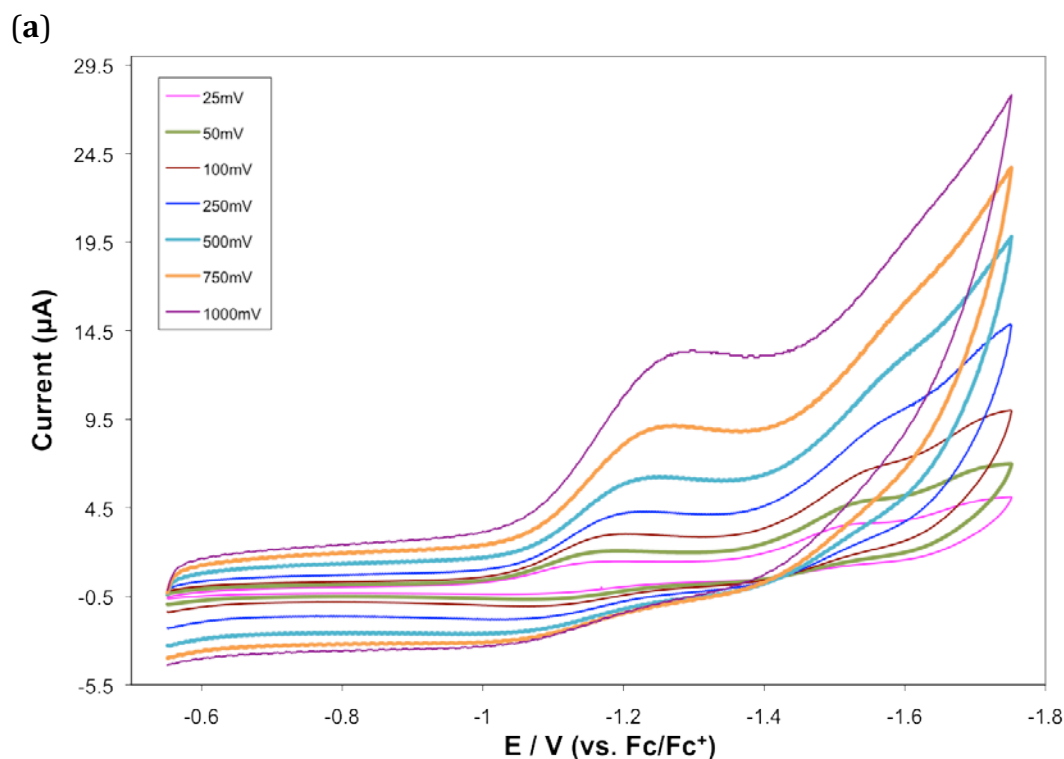
equiv of Na(dbm), generated *in situ*, with $\text{UO}_2\text{Cl}_2(\text{THF})_3$ results in formation of a light orange solution, from which $\text{UO}_2(\text{dbm})_2(\text{THF})$ (**2.1**) can be isolated as an orange powder in 71% yield (Scheme 2.4). This complex features a singlet at 7.32 ppm in its ^1H NMR spectrum (CD_2Cl_2), which is assignable to the γ -CH of the dbm ligand. In addition, broad singlets at 4.99 and 2.47 ppm, confirm the presence of THF in the uranyl coordination sphere. Complex **2.1** had been reported previously,³⁸ but had not been fully characterized. It is closely related to several other uranyl bis(β -diketonate) complexes that have been reported in the literature,^{37,39} including $\text{UO}_2(\text{acac})_2(\text{THF})$,⁴⁰ $\text{UO}_2(\text{dbm})_2(\text{dmsO})$,³⁶ and $\text{UO}_2(\text{dbm})_2(\text{H}_2\text{O})$.³⁵



Scheme 2.4. Synthesis of $\text{UO}_2(\text{dbm})_2(\text{THF})$ (**2.1**)

We evaluated the strength of the U=O bonds in complex **2.1** relative to the previously characterized β -ketoiminate complex, $\text{UO}_2(\text{Aracnac})_2$. The room temperature cyclic voltammogram of **2.1** in CH_2Cl_2 reveals an irreversible reduction feature at $E_{1/2} = -1.19$ V (vs. Fc/Fc^+), measured at a scan rate of 0.1 V/s, which we attribute to the U(VI/V) redox couple (Figure 2.1a). This feature is irreversible at all scan rates. Additionally, reduction of **2.1** to U(IV) was not observed within the range of the solvent window. Importantly, this value is less negative than that observed for $\text{UO}_2(\text{Aracnac})_2$ ($\text{Ar} = 3,5\text{-}^t\text{Bu}_2\text{C}_6\text{H}_3$) ($E_{1/2} = -1.35$ V vs. Fc/Fc^+),⁴¹ confirming that the dbm

equatorial ligand is less electron donating than the ^{Ar}acnac ligand, and suggesting a lesser degree of oxo ligand activation in **2.1** (Table 2.1). For further comparison, $\text{UO}_2(\text{dbm})_2(\text{dmsO})$ features a reversible $\text{UO}_2^{2+}/\text{UO}_2^+$ redox couple at $E_{1/2} = -1.36$ V (vs. Fc/Fc^+ , in dmsO),³⁶ while $\text{UO}_2(\text{dbm})_2(\text{dmf})$ features a reversible $\text{UO}_2^{2+}/\text{UO}_2^+$ redox couple at $E_{1/2} = -1.46$ V (vs. Fc/Fc^+ , in dmf).³⁷ These lower redox potentials reflect the strong donating ability of dmsO and dmf vs. THF. In addition, **2.1** features a $\text{U}=\text{O}$ ν_{sym} mode of 823 cm^{-1} in its Raman spectrum (Figure 2.1b). For comparison, the $\text{U}=\text{O}$ ν_{sym} mode for $\text{UO}_2(\text{Aracnac})_2$ was determined to be 812 cm^{-1} ,¹⁷ which reveals that the $\text{U}=\text{O}$ bonds in $\text{UO}_2(\text{dbm})_2(\text{THF})$ are stronger than those in $\text{UO}_2(\text{Aracnac})_2$, and further supports the claim that the dbm ligand is less electron donating.



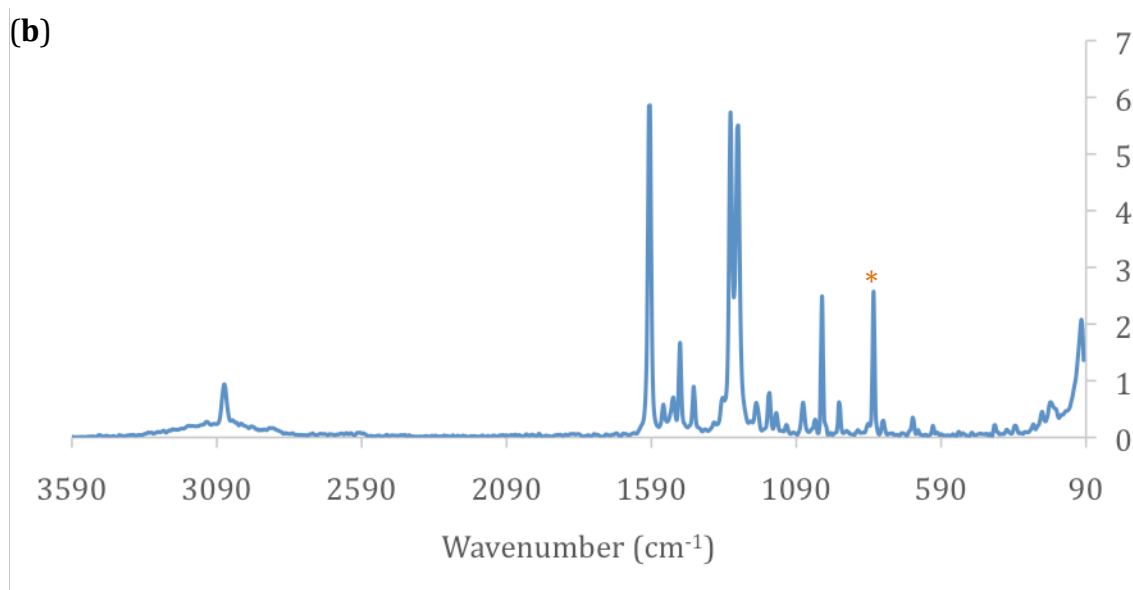


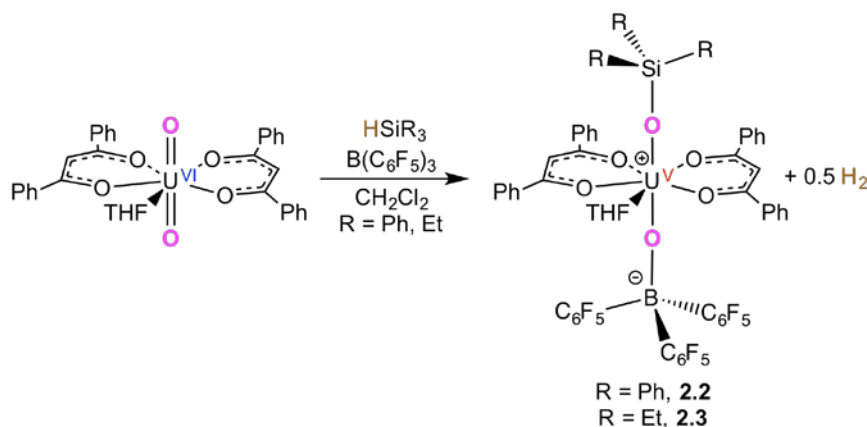
Figure 2.1. (a) Room temperature cyclic voltammogram of **2.1**. Measured in CH₂Cl₂ with 0.1 M [NBu₄][PF₆] as supporting electrolyte. Electrochemical parameters presented in Table A.1. (b) Solid-state Raman spectrum of **2.1**. U=O ν_{sym} stretch is observed at 823 cm⁻¹ (*).

Table 2.1. Electrochemical Data for Selected Uranyl(VI) Complexes

	E_{1/2} (V) (vs. Fc/Fc⁺)	Ref.
UO ₂ (Ar ₂ nacnac) ₂ (acac) (Ar = 2,6- <i>i</i> Pr ₂ C ₆ H ₃)	-1.82* (CH ₂ Cl ₂)	42
UO ₂ (salen) ₂ (DMF)	-1.67 (DMF)	37
UO ₂ (Ar ₂ nacnac) ₂ (dbm) (Ar = 2,6- <i>i</i> Pr ₂ C ₆ H ₃)	-1.65* (CH ₂ Cl ₂)	42
UO ₂ (^{Ar} acnac) ₂ (Ar = 2,4,6-Me ₃ C ₆ H ₂)	-1.52 (CH ₂ Cl ₂)	41
UO ₂ (^t Buacnac) ₂ (THF)	-1.46 (CH ₂ Cl ₂)	17
UO ₂ (dbm) ₂ (DMF)	-1.461 (DMF)	43
UO ₂ (Ar ₂ nacnac) ₂ (hfac) (Ar = 2,6- <i>i</i> Pr ₂ C ₆ H ₃)	-1.39* (CH ₂ Cl ₂)	42
UO ₂ (dbm) ₂ (DMSO)	-1.36 (DMSO)	36
UO ₂ (^{Ar} acnac) ₂ (Ar = 3,5- ^t Bu ₂ C ₆ H ₃)	-1.35 (CH ₂ Cl ₂)	41
UO ₂ (dbm) ₂ (THF) (2.1)	-1.19* (CH ₂ Cl ₂)	this work

* measured at a scan rate of 0.1 V/s.

2.2.2. Synthesis and Characterization of $\text{U}(\text{OB}\{\text{C}_6\text{F}_5\}_3)(\text{OSiPh}_3)(\text{dbm})_2(\text{THF})$ (2.2**) and $\text{U}(\text{OB}\{\text{C}_6\text{F}_5\}_3)(\text{OSiEt}_3)(\text{dbm})_2(\text{THF})$ (**2.3**)**



Scheme 2.5. Synthesis of $\text{U}(\text{OB}\{\text{C}_6\text{F}_5\}_3)(\text{OSiPh}_3)(\text{dbm})_2(\text{THF})$ (**2.2**) and $\text{U}(\text{OB}\{\text{C}_6\text{F}_5\}_3)(\text{OSiEt}_3)(\text{dbm})_2(\text{THF})$ (**2.3**).

Upon establishing that dbm was a weaker donor than Aracnac , we subjected $\text{UO}_2(\text{dbm})_2(\text{THF})$ to our reductive silylation protocol. Thus, addition of 1 equiv of HSiPh_3 to $\text{UO}_2(\text{dbm})_2(\text{THF})$, in the presence of 1 equiv of $\text{B}(\text{C}_6\text{F}_5)_3$, results in the formation a deep red solution, from which $\text{U}(\text{OB}\{\text{C}_6\text{F}_5\}_3)(\text{OSiPh}_3)(\text{dbm})_2(\text{THF})$ (**2.2**) can be isolated as a dark red crystalline material in 62% yield (Scheme 2.5). Similarly, addition of 1 equiv HSiEt_3 to $\text{UO}_2(\text{dbm})_2(\text{THF})$, in the presence of 1 equiv of $\text{B}(\text{C}_6\text{F}_5)_3$, results in the formation of a deep red solution, from which $\text{U}(\text{OB}\{\text{C}_6\text{F}_5\}_3)(\text{OSiEt}_3)(\text{dbm})_2(\text{THF})$ (**2.3**) can be isolated as a red-orange crystalline material in 55% yield (Scheme 2.5). Isolation of **2.2** and **2.3** proceed with higher yield, if 0.25 equiv of THF is added to the mother liquor. Also important to note, in the case of **2.3**, a higher yield can be obtained, if excess silane is used.

A similar activation of $\text{UO}_2(\text{Aracnac})_2$, was observed previously in our group,^{18,19}

where the formation of H₂ gas was speculated. Even though the formation of gas bubbles were not observed, during the reactions to obtain **2.2** and **2.3**, it is assumed that **2.2** and **2.3** are formed via a similar mechanism. Most importantly, the observation that the stronger U=O bonds of UO₂(dbm)₂(THF) are susceptible to reductive silylation, relative to UO₂(Aracnac)₂, shows that the scope of this transformation is broader than originally thought.

Complexes **2.2** and **2.3** both crystallize in the triclinic space group P-1 as a hexane solvate, **2.2**·C₆H₁₄, and a toluene and hexane solvate, **2.3**·C₇H₈·0.5C₆H₁₄, respectively (Figure 2.2). Both **2.2** and **2.3** exhibit pentagonal bipyramidal geometries, as determined from the inter-ligand bond angles. For instance, complex **2.2** exhibits an O_B-U-O_{Si} bond angle of 175.06(8)°, while the O_{eq}-U-O_{ax} bond angles range from 84.06(8) to 95.42(8)°. ⁴⁴⁻⁴⁶ In complexes **2.2** and **2.3**, one uranyl oxo ligand has been converted to a silyloxy group, while the other oxo ligand is coordinated to a molecule of B(C₆F₅)₃, as was observed for U(OB{C₆F₅}₃)(OSiPh₃)(Aracnac)₂.¹⁸ For complex **2.2**, the U-O_{Si} and U-O_B bond lengths are 2.024(2) and 1.952(2) Å, respectively, while for **2.3**, they are 2.011(2) and 1.960(2) Å, respectively (Table 2.2). These values are comparable to those previously reported for U(V)-silyloxy and U(V)-OB(C₆F₅)₃ distances,^{14,16,18,19} and are indicative of a substantial reduction of the U=O bond order. Interestingly, the U-O_{dbm} bond lengths in **2.2** (av. U-O = 2.281 Å) and **2.3** (av. U-O = 2.282 Å) (Table 2.2) are shorter than those observed in other uranyl dbm complexes (ca. 2.35 Å).⁴⁷ Finally, both **2.2** and **2.3** feature a THF molecule coordinated to the uranium center. This contrasts with the reductive silylation product of UO₂(Aracnac)₂, for which no coordinated solvent is observed, a consequence of the reduced steric

profile of the dbm ligand vs. the much bulkier ^{Ar}acnac ligand.

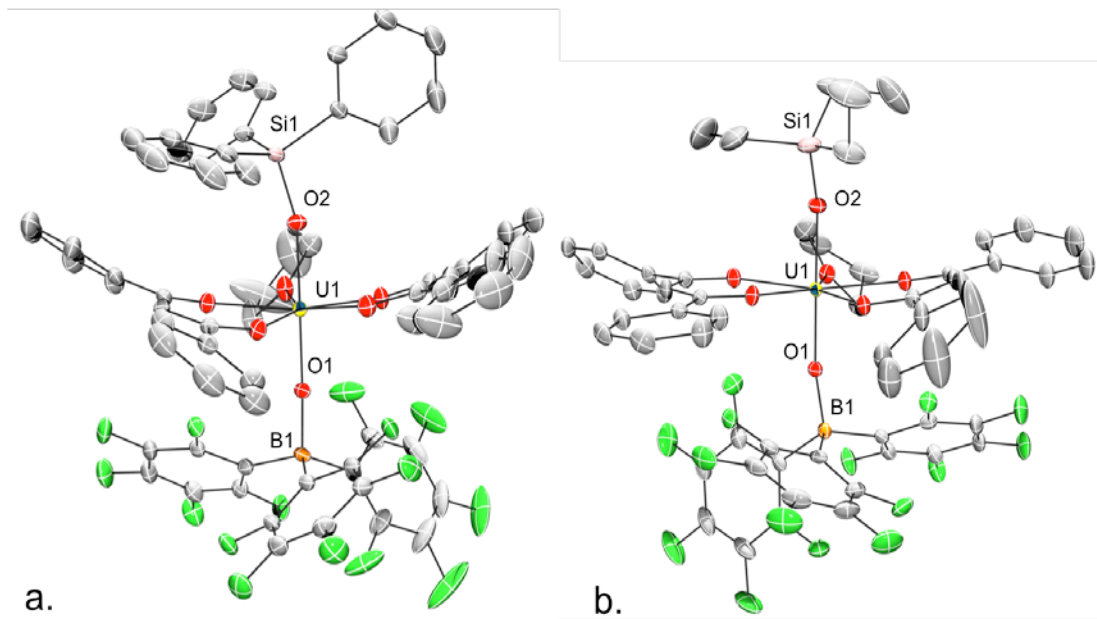


Figure 2.2. A) Solid-state structure of $\text{U}(\text{OB}\{\text{C}_6\text{F}_5\}_3)(\text{OSiPh}_3)(\text{dbm})_2\text{THF}$ (**2.2**) with 50% probability ellipsoids. A hexane molecule and all hydrogens have been removed for clarity. B) Solid-state structure of $\text{U}(\text{OB}\{\text{C}_6\text{F}_5\}_3)-(\text{OSiEt}_3)(\text{dbm})_2(\text{THF})\cdot\text{C}_7\text{H}_8\cdot 0.5\text{C}_6\text{H}_{14}$ (**2.3** $\cdot\text{C}_7\text{H}_8\cdot 0.5\text{C}_6\text{H}_{14}$) with 50% probability ellipsoids. Solvate molecules and hydrogen atoms have been omitted for clarity.

Table 2.2. Selected Bond Lengths (Å) and Angles (deg) for Complexes **2.2** – **2.6**

	2.2	2.3	2.4	2.5^a	2.6
U-O _{Si-trans}	2.024(2)	2.011(2)	1.981(3)		2.075(3) 2.065(3)
U-O _{Si-cis}					2.105(3)
U-O _B	1.952(2)	1.960(2)	1.915(2)	1.96(2), 1.93(2)	
U-O _{dbm-cis}	2.246(2)	2.250(2)	2.235(3)	2.23(2), 2.19(1)	2.297(3)
	2.280(2)	2.258(2)	2.252(3)	2.24(2), 2.27(2)	2.299(3)
	2.280(2)	2.301(2)	2.257(3)	2.26(2), 2.28(2)	2.314(3)
	2.317(2)	2.320(2)	2.277(3)	2.30(1), 2.28(1) 2.37(2), 2.27(2)	2.359(3)
U-O _{dbm-trans}				2.14(2), 2.25(2)	
U-F			2.654(2)	2.88(2), 2.93(2)	
O-Si	1.665(2)	1.681(2)	1.720(3)		1.606(3) 1.641(3) 1.648(3)
O-B	1.525(4)	1.503(4)	1.546(5)	1.52(4), 1.50(4)	
O _{Si} -U-O _B	175.06(8)	178.43(8)	169.3(1)		
O _{Si} -U-O _{Si}					167.2(1) 156.4(2) 167.0(2) 170.3(2)
U-O-Si	164.0(1)	153.5(1)	148.7(2)		
U-O-B	172.0(2)	165.8(2)	151.6(2)	160(2), 161(2)	

^a two independent molecules in the asymmetric unit.

The ¹H NMR spectrum of **2.2** in CD₂Cl₂ consists of four broad resonances at 10.76, 4.75, 4.54, and 3.60 ppm in a 4:4:2:1 ratio, respectively, which correspond to the four proton environments of the dbm ligand. Additionally, three sharper resonances are observed at 7.53, 7.41, and 6.22 ppm in a 2:1:2 ratio, which correspond to the *m*-, *p*-, and *o*-proton atoms of the Ph₃Si group. Similarly, the ¹H NMR spectrum of **2.3** in CD₂Cl₂ consists of four broad resonances at 7.40, 6.66, 6.26 and 4.54 ppm in a 2:4:4:1 ratio, respectively, as well as two broad resonances at 4.94 and 3.48 ppm, which correspond to the two Et₃Si proton environments. The ¹⁹F{¹H} NMR spectrum of **2.2** consists of three resonances at -136.21, -160.49, and -165.75 ppm, in a 2:1:2 ratio,

corresponding to the *o*-, *p*-, and *m*-fluorine atoms of the C₆F₅ groups. Similarly, the ¹⁹F{¹H} NMR spectrum of **2.3** consists of three resonances at -135.00, -160.69, and -165.86 ppm, in a 2:1:2 ratio (Figure 2.3). Finally, the near-IR spectra for **2.2** and **2.3** are similar to those of other U(V) complexes,^{12,16,18,19} supporting the presence of a 5f¹ ion.

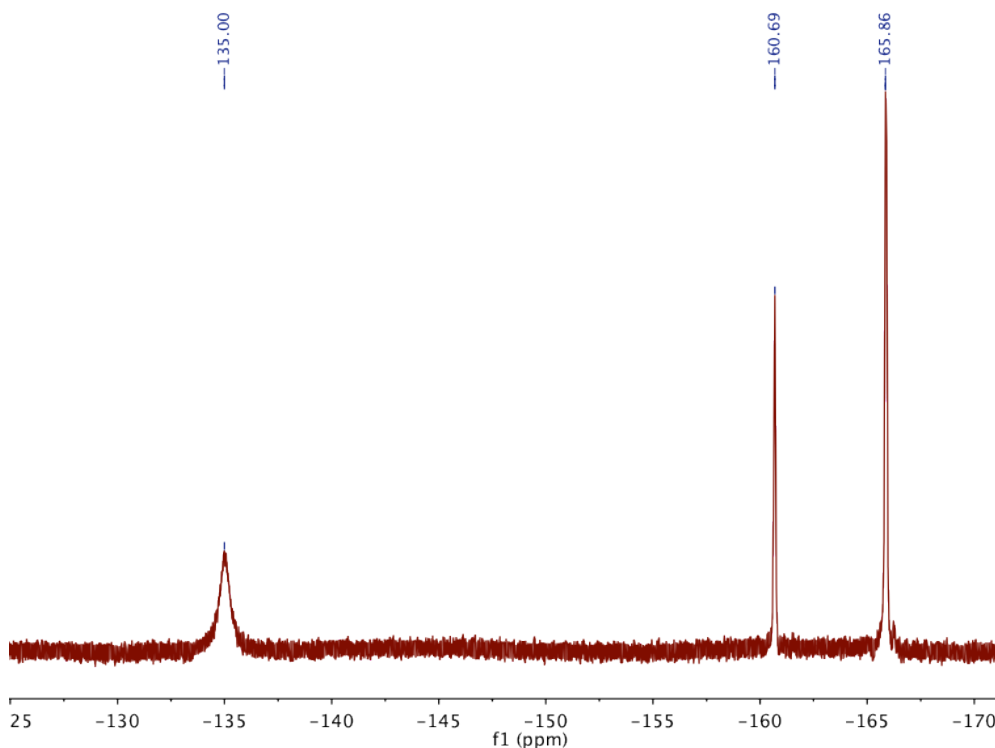
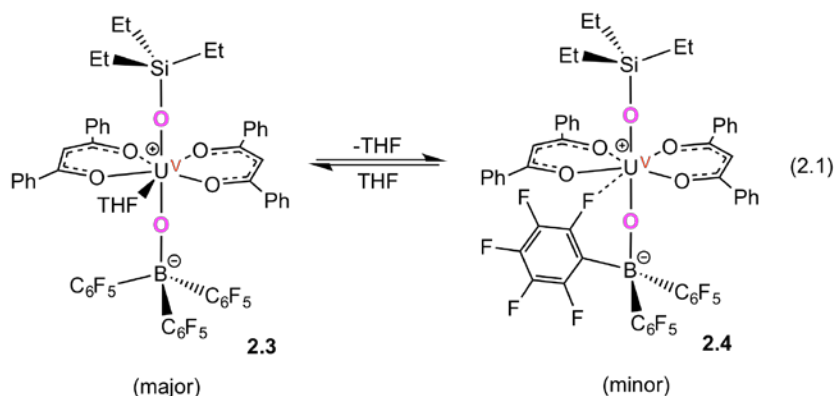


Figure 2.3. ¹⁹F{¹H} NMR spectrum of **2.3** in CD₂Cl₂ at 25 °C.

In both **2.2** and **2.3**, the *o*-fluorine resonances are slightly broadened in comparison to the *m*- and *p*-fluorine resonances (Figure 2.3). We attribute this to the proximity of the *o*-fluorines to the unpaired e⁻ on the paramagnetic U(V) centers, which shortens the T₂ relaxation time, and results in broadness in the ¹⁹F NMR resonances.

2.2.3. Synthesis and Characterization of $U(\kappa^2-O,F-OB\{C_6F_5\}_3)(OSiEt_3)(dbm)_2$ (**2.4**)



Interestingly, crystallization of **2.3** without the addition of 0.25 equiv of THF to the supernatant led to the isolation of a second, minor product, $U(\kappa^2-O,F-OB\{C_6F_5\}_3)(OSiEt_3)(dbm)_2$ (**2.4**), as red-orange crystals in low yield (eq 2.1). Complex **2.4** crystallizes in the triclinic space group P-1 and its solid-state molecular structure is shown in Figure 2.4. The U–O_{Si} and U–O_B bond lengths of **2.4**, 1.981(3) and 1.915(2) Å, respectively, are comparable to those observed in complexes **2.2** and **2.3**. In contrast, the U–O–B bond angle (151.6(2)°) in **2.4** is considerably smaller than those observed in **2.2** (172.0(2)°) and **2.3** (165.8(2)°), likely due to the presence of a F → U dative interaction between an *o*-fluorine atom of the B(C₆F₅)₃ moiety and the uranium center, which occurs in place of ligation of the THF solvate molecule. Interestingly, F → U dative interactions are quite rare and to our knowledge have only been observed in four other complexes. [Cp*₂Co][U{OB(C₆F₅)₃}₂(^{Ar}acnac)(OEt₂)]¹² exhibits two F → U dative interactions, while U^{IV}(NPh^F)₄ (Ph^F = C₆F₅), U^{IV}(NPhPh^F)₄, and U^{III}(NPh^F)₃(THF)₂ exhibit three or more F → U interactions each.⁴⁸ The U–F distance for complex **2.4** (2.654(2) Å) falls on the shorter end of U–F dative interactions, which range from ~2.60 – 2.93 Å.^{12,48}

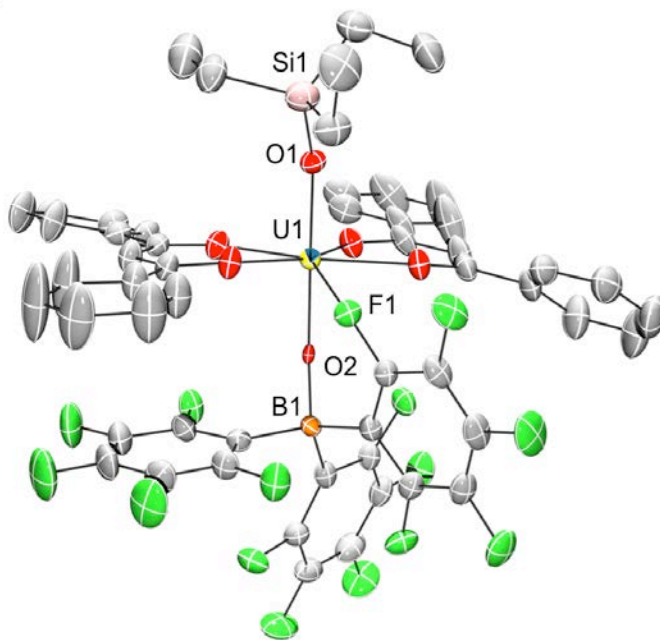
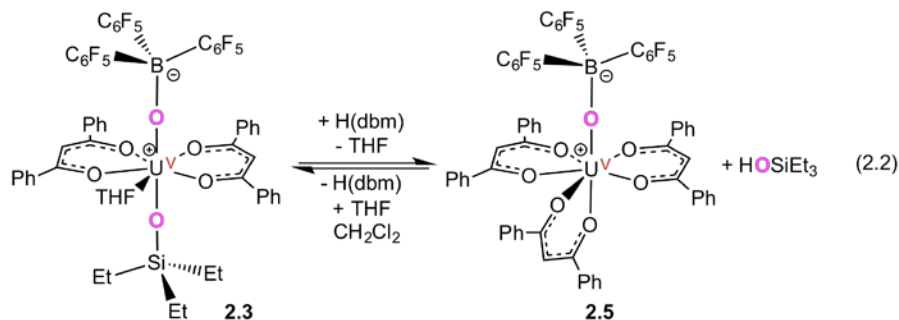


Figure 2.4. Solid-state structure of $U(\kappa^2\text{-}O,F\text{-}OB\{C_6F_5\}_3)(OSiEt_3)(dbm)_2$ (**2.4**) with 50% probability ellipsoids. Hydrogen atoms have been omitted for clarity.

The 1H NMR spectrum of **2.4** in CD_2Cl_2 consists of four broad resonances corresponding to the equatorial dbm protons at 7.47, 6.59, 6.53 and 5.75 ppm in a 2:1:4:4 ratio, and two broad resonances corresponding to the Et_3Si - protons at 5.36 and 2.72 ppm in a 2:3 ratio. The $^{19}F\{^1H\}$ NMR spectrum of **2.4** consists of two resonances at -160.20 and -165.53 ppm in a 1:2 ratio, which are assignable to the *p*- and *m*-fluorine atoms of the C_6F_5 groups. In addition, a very broad resonance assignable to the *o*-fluorine atoms is observed at -149.25 ppm. Notably, this resonance is shifted significantly upfield in comparison to those observed for **2.2** and **2.3**, suggestive of some interaction with the paramagnetic U(V) center.⁴⁸ However, the observation of only a single peak for the *o*-fluorine atoms is indicative of free rotation about the B-C bond. Also present in the spectrum are resonances at 161.6 and 166.3

ppm, which are attributable to complex **2.3**. Interestingly, complexes **2.3** and **2.4** are also both observed in the *in situ* $^{19}\text{F}\{^1\text{H}\}$ NMR spectrum of the reaction between $\text{UO}_2(\text{dbm})_2(\text{THF})$, HSiEt_3 , and $\text{B}(\text{C}_6\text{F}_5)_3$ (Figure A.1). We suggest that complexes **2.3** and **2.4** are in equilibrium, and addition of THF to the mother liquor during crystallization favors the formation **2.3**, permitting its isolation in higher yields.

2.2.4. Synthesis and Characterization of $\text{U}(\text{OB}\{\text{C}_6\text{F}_5\}_3)(\text{dbm})_3$ (**2.5**)



Since we did not see any evidence for reduction to U(IV) during the formation of **2.2** and **2.3**, as expected from our proposed catalytic cycle (Scheme 2.2), we explored the ligand exchange reactivity of this new family of functionalized uranyl complexes, given the rarity of well-defined oxo ligand substitution reactions for the uranyl moiety.^{10,13,16,20,49} We hypothesized that the small steric profile of the equatorial dbm ligands would allow for facile axial ligand exchange. Thus, addition of 1 equiv H(dbm) to **2.3** led to an equilibrium between **2.3** and the U(V) tris(dibenzoylmethanate) complex, $\text{U}(\text{OB}\{\text{C}_6\text{F}_5\}_3)(\text{dbm})_3$ (**2.5**), from which complex **2.5** could be isolated as dark red crystals in 33% yield (eq 2.2). The isolation of complex **2.5** represents a rare

example of controlled uranyl oxo ligand substitution at ambient temperature and pressure.

Complex **2.5** crystallizes in the triclinic space group $P1$, as a toluene and hexane solvate, $2.5 \cdot 2C_7H_8 \cdot C_6H_{14}$, with two separate molecules in the asymmetric unit. Its solid-state molecular structure is shown in Figure 2.5. The uranium ion in complex **2.5** is coordinated by three dbm ligands and a $B(C_6F_5)_3$ -capped oxo ligand. Interestingly, there is also a $F \rightarrow U$ dative interaction between an *o*-fluorine atom of the $B(C_6F_5)_3$ moiety and the uranium center, given that the U–F distances for the two independent molecules of complex **2.5** are 2.88(2) and 2.93(2) Å (Table 2.2). These are much longer in comparison to complex **2.4**, however, they do fall in the range of U–F dative interactions, $\sim 2.60 - 2.93$ Å.^{12,48} Similar to the U–F distances, the U–O–B bond angles in **2.5** (161(2) and 160(2)°) also fall between complexes **2.3** (165.8(2)°) and **2.4** (151.6(2)°). While the geometry about the uranium center in complex **2.5** can be described as a distorted triangular dodecahedron (CSM = 2.25), according to the continuous shape measure developed by Alvarez and co-workers,⁵⁰ it is probably better described as a biaugmented trigonal prism J50 (CSM = 1.86). The U–O_B bond lengths of the two independent molecules (1.96(2) and 1.93(2) Å) are comparable to those observed for complexes **2.2**, **2.3**, and **2.4**, but longer than that observed for the U(V) mono-oxo complex, $U(O)(NR_2)_3$ (R = SiMe₃), which features a U–O bond length of 1.817(1) Å.⁵¹ The elongated U–O bond in **2.5** is clearly the result of borane coordination to the oxo ligand. The U–O distances associated with the dbm oxygen atoms that are situated *trans* to the $O(B\{C_6F_5\}_3)$ ligand are 2.14(2) and 2.25(2) Å, while the average U–O_{dbm-*cis*} bond length is 2.27(4) Å. The average *trans* U–O_{dbm} bond length is 0.071 Å

shorter than the average *cis* bond (averaged over the two independent molecules in the asymmetric unit), and could be indicative of the presence of the Inverse Trans Influence (ITI), which was first proposed by Denning in 1992⁶² and typically occurs in high-valent U(V) and U(IV) systems with multiply bonded imido and oxo ligands.^{45,52-54} However, it should be noted that the diffraction data for **2.5** are of modest quality, and leads to large uncertainties in the metrical parameters. We therefore turned to computational chemistry in the form of density functional theory to explore the possibility of an ITI in **2.5** (calculated bond lengths in Table 2.2). Geometry optimization using the hybrid PBE0 functional showed a *trans* shortening of 0.063 Å, suggesting the presence of ITI. The mean absolute deviation (MAD) between the calculated and experimental U–O bond lengths is only 0.012 Å, which implies good agreement between the theoretical and experiment values.

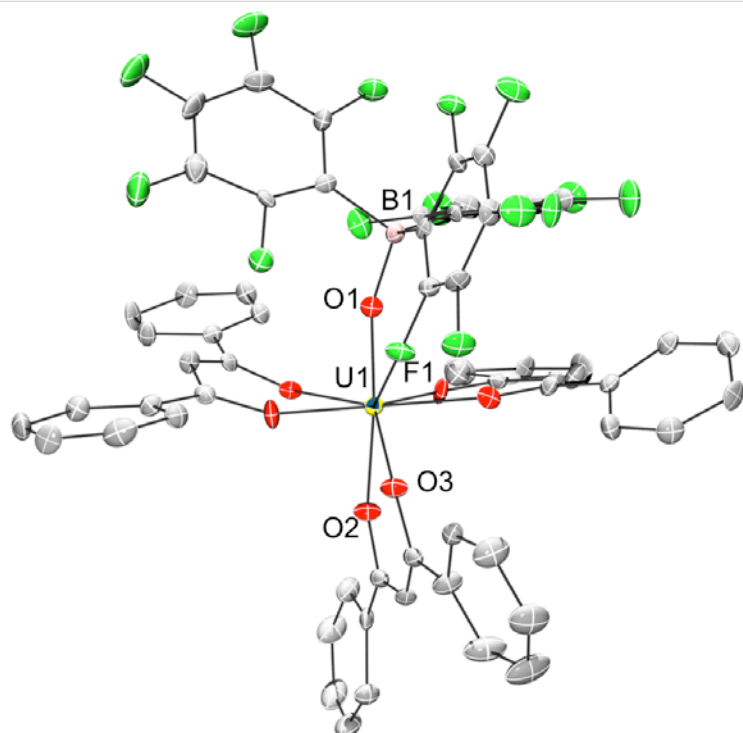


Figure 2.5. Solid-state structure of $\text{U}(\text{OB}\{\text{C}_6\text{F}_5\}_3)(\text{dbm})_3 \cdot 2\text{C}_7\text{H}_8 \cdot \text{C}_6\text{H}_{14}$ (**2.5**· $2\text{C}_7\text{H}_8 \cdot \text{C}_6\text{H}_{14}$) with 50% probability ellipsoids. Complex **2.5** crystallizes with two independent molecules in the asymmetric unit; only one is pictured here. Solvate molecules and hydrogen atoms have been omitted for clarity.

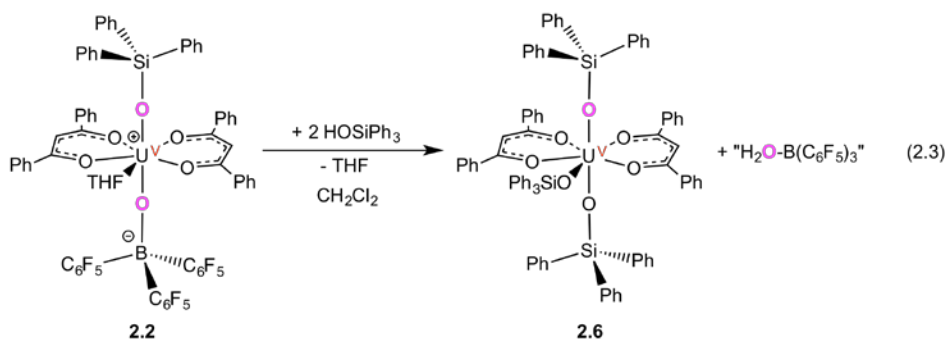
The ^1H NMR spectrum of **2.5** in CD_2Cl_2 consists of four broad resonances at 8.22, 7.68, 6.70 and 6.24 ppm in a 1:2:4:4 ratio, which corresponds to the four dbm proton environments and indicates that there is only one dbm environment observed at room temperature. In addition, the $^{19}\text{F}\{^1\text{H}\}$ NMR spectrum of **2.5** consists of three resonances at -144.72, -160.57, and -165.98 ppm, in a 2:1:2 ratio, corresponding to the *o*-, *p*-, and *m*-fluorine atoms of the C_6F_5 groups. Notably, the *o*-fluorine resonance (-144.72 ppm) is broad and shifted upfield in comparison to those observed for **2.2** and **2.3**, but not as upfield shifted as complex **2.4**, suggestive of some interaction with the paramagnetic U(V) center.⁴⁸ Similar to complex **2.4**, the observation of only a single peak for the *o*-fluorine atoms is indicative of free rotation about the B-C bond. Finally, the near-IR spectrum for **2.5** is similar to those of other U(V) complexes,^{12,16,18,19} supporting the presence of a $5f^1$ ion.

To determine the fate of the missing Et_3SiO - group upon formation of **2.5**, we monitored the reaction of **2.3** with 1 equiv of $\text{H}(\text{dbm})$ by NMR spectroscopy. The *in situ* $^{19}\text{F}\{^1\text{H}\}$ NMR spectrum of the reaction mixture revealed the formation of complex **2.5**, as evidenced by a characteristic resonance at -144.8 ppm, along with the presence of complex **2.3**. Complexes **2.3** and **2.5** were observed in a 3:1 ratio, respectively, according to the integrations of their *o*-fluorine resonances. Most importantly, the in

situ $^{13}\text{C}\{^1\text{H}\}$ NMR spectrum of the reaction mixture reveals the formation of HOSiEt_3 , as evidenced by resonances at 6.21 and 5.56 ppm.⁵⁵ The proposed reaction stoichiometry was further confirmed by following the reaction of **2.5** with 1 equiv of HOSiEt_3 , and 1 equiv of THF, in CD_2Cl_2 by ^1H and $^{19}\text{F}\{^1\text{H}\}$ NMR spectroscopies, which reveals the formation of complex **2.3** and $\text{H}(\text{dbm})$, along with complete consumption of complex **2.5**. This transformation represents a rare example of a controlled, reversible uranyl $\text{U}=\text{O}$ bond substitution, in which the fate of the substituted oxo ligand has been explicitly determined.^{10,13,20,56,57}

2.2.5. Synthesis of $\text{U}(\text{OSiPh}_3)_3(\text{dbm})_2$ (**2.6**) and $\text{U}(\text{OB}\{\text{C}_6\text{F}_5\}_3)(\text{OSiEt}_3)(\text{dbm})_2$ - (HOPh) (**2.7**).

Reaction of **2.2** with 1 equiv of $\text{H}(\text{dbm})$ in CD_2Cl_2 also results in formation of **2.5**, as determined by ^1H and $^{19}\text{F}\{^1\text{H}\}$ NMR spectroscopies. This experiment reveals the presence of complexes **2.2** and **2.5** in a 3:2 ratio, respectively. However, in one instance, crystallization of a similar reaction mixture led to the isolation of the $\text{U}(\text{V})$ trisilyloxy complex, $\text{U}(\text{OSiPh}_3)_3(\text{dbm})_2$ (**2.6**), as red plate crystals. Since complex **2.6** was not readily identified in the *in situ* NMR spectra, we attempted to prepare **2.6** purposefully. Thus, reaction of excess HOSiPh_3 with complex **2.2** in dichloromethane, gratifyingly, led to the isolation of complex **2.6** as red-orange crystals in 56% yield (eq 2.3). Although we were unable to observe the proposed by-product, " $\text{H}_2\text{O}-\text{B}(\text{C}_6\text{F}_5)_3$ ",⁵⁸ in the *in situ* NMR spectra, the isolation of complex **2.6** represents another rare example of uranyl oxo ligand substitution at ambient temperature and pressure.



Complex **2.6** crystallizes in the triclinic space group *P*-1, as the dichloromethane solvate, **2.6**·CH₂Cl₂ (Figure 2.6). Complex **2.6** features three triphenyl-silyloxy groups and two dbm ligands coordinated to the U⁵⁺ ion, leading to a pentagonal bipyramidal geometry around the uranium center, as determined from the inter-ligand bond angles. For example, complex **2.6** exhibits an O_{Si}-U1-O_{Si} bond angle of 167.2(1)°, while the O_{eq}-U-O_{ax} bond angles range from 82.0(1) to 104.3(1)°.⁴⁴⁻⁴⁶ The axial-OSiPh₃ groups have U-O_{Si} bond lengths of 2.075(3) and 2.065(3) Å, and are comparable to those observed in complexes **2.2** and **2.3**, as well as those previously reported for other U(V)-silyloxides.^{14,16,18,19} These axial U-O_{Si} bond lengths in **2.6** are comparable to the U-O_{Si} bond length exhibited by the equatorial *cis*-OSiPh₃ group (2.105(3) Å). A larger difference in U-O_{Si} bond lengths between the two silyloxy environments was expected, as a difference between axial and equatorial U(V) silyloxy U-O_{Si} bond lengths has been seen before in the complexes, [K(18-crown-6)][U(NR)(OSi(O^{*t*}Bu)₃)₄] (R = Ad, SiMe₃), which have average equatorial U-O_{Si} bond lengths of 2.212 Å (R = Ad) and 2.173 Å (R = SiMe₃), and shorter axial U-O_{Si} bond lengths of 2.180(6) Å (R = Ad) and 2.130(7) Å (R = SiMe₃).⁵⁹

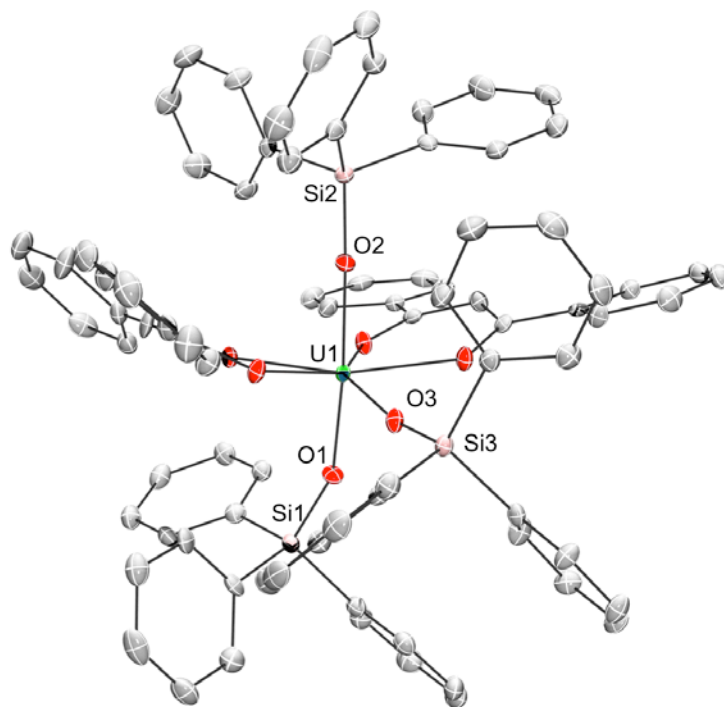
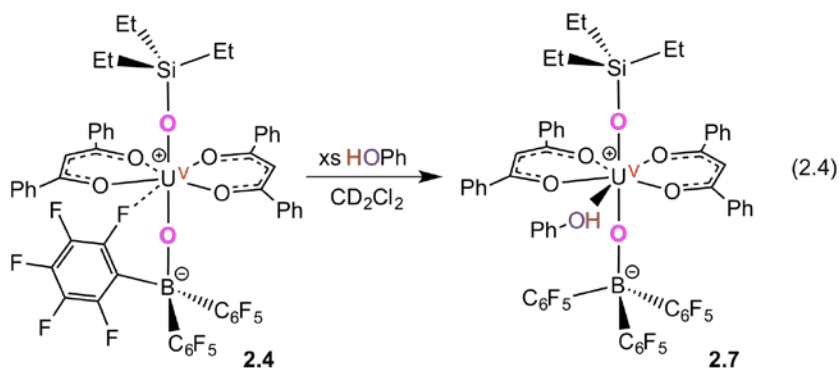


Figure 2.6. Solid-state structure of $\text{U}(\text{OSiPh}_3)_3(\text{dbm})_2 \cdot \text{CH}_2\text{Cl}_2$ (**2.6**· CH_2Cl_2) with 50% probability ellipsoids. CH_2Cl_2 solvate and all hydrogen atoms have been omitted for clarity.

We also endeavored to demonstrate another example of uranyl oxo ligand substitution, by exploring the reactivity of HOPh with **2.4**. From an examination of the *in situ* ^1H and $^{19}\text{F}\{^1\text{H}\}$ NMR spectra from the reaction of complex **2.4** with excess HOPh, it was clear that a new paramagnetic uranium containing product was formed. We hypothesized that its formula was $\text{U}(\text{OSiEt}_3)(\text{OPh})(\text{dbm})_2(\text{L})$, which could be formed by replacement of the $-\text{OB}(\text{C}_6\text{F}_5)_3$ ligand in **2.4** with an an $-\text{OPh}$ ligand; however, we were unable to observe the proposed by-product, “ $\text{H}_2\text{O}-\text{B}(\text{C}_6\text{F}_5)_3$ ”,⁵⁸ in the *in situ* NMR spectra. Dark orange crystals were isolated from this NMR experiment, which were, surprisingly, revealed to be the U(V) complex, $\text{U}(\text{OB}\{\text{C}_6\text{F}_5\}_3)(\text{OSiEt}_3)(\text{dbm})_2(\text{HOPh})$

(2.7). To our dismay, oxo ligand substitution did not occur; instead, the HOPh coordinated to the equatorial plane of the uranium center, displacing the coordinated *o*-fluorine atom (eq 2.4).



Complex **2.7** crystallizes in the triclinic space group *P*-1 as the hexane solvate, $\text{U}(\text{OB}\{\text{C}_6\text{F}_5\}_3)(\text{OSiEt}_3)(\text{dbm})_2(\text{HOPh})\cdot\text{C}_6\text{H}_{14}$ (**2.7**· C_6H_{14}) (Figure 2.7), with pentagonal bipyramidal geometry about the uranium center. The $\text{U}-\text{O}_{\text{Si}}$ bond length of 2.003(3) Å and the $\text{U}-\text{O}_{\text{B}}$ bond length of 1.951(3) Å are almost identical to complex **2.3**, along with most of the other bond lengths. The $\text{U}-\text{O}_{\text{Ph}}$ bond length is 2.573(3) Å, which is comparable to other $\text{U}-\text{HOR}$ bond lengths,^{60,61} indicating there is probably a proton attached to the OPh group.

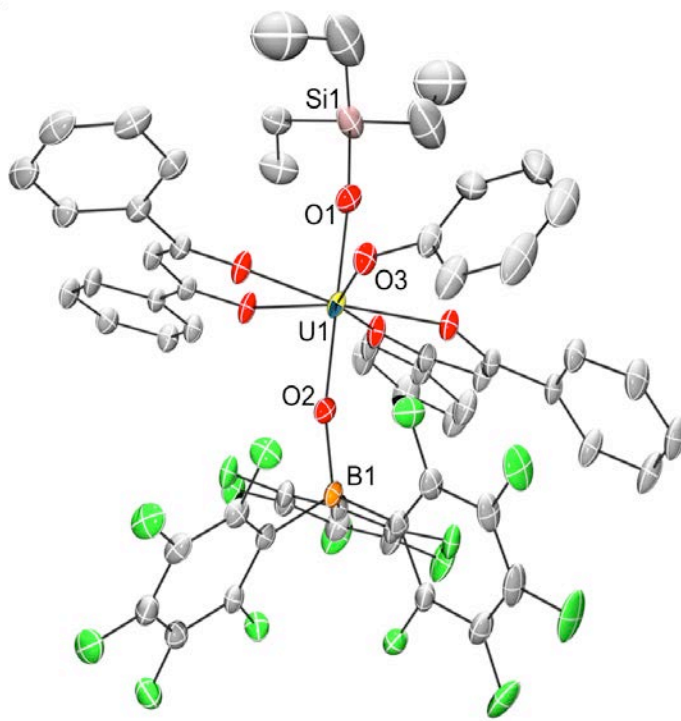


Figure 2.7. Solid-state structure of $\text{U}(\text{OB}\{\text{C}_6\text{F}_5\}_3)(\text{OSiEt}_3)(\text{dbm})_2(\text{HOPh}) \cdot \text{C}_6\text{H}_{14}$ ($2.7 \cdot \text{C}_6\text{H}_{14}$) with 50% probability ellipsoids. Hexane solvate and all hydrogen atoms have been omitted for clarity. Selected bond lengths (Å) and angles (°): $\text{U1-O1} = 2.003(3)$, $\text{U1-O2} = 1.951(3)$, $\text{U1-O3} = 2.573(3)$, $\text{O1-Si1} = 1.684(3)$, $\text{O2-B1} = 1.517(5)$, $\text{O1-U1-O2} = 177.3(1)$.

2.3 Summary

Reaction of $\text{UO}_2(\text{dbm})_2(\text{THF})$ (**2.1**) with 2 equiv HSiR_3 ($\text{R} = \text{Ph}, \text{Et}$), in the presence of 1 equiv of $\text{B}(\text{C}_6\text{F}_5)_3$, results in the formation of $\text{U}(\text{OB}\{\text{C}_6\text{F}_5\}_3)(\text{OSiR}_3)(\text{dbm})_2(\text{THF})$ ($\text{R} = \text{Ph}$, **2.2**; Et , **2.3**) via oxo ligand silylation. The isolation of complexes **2.2** and **2.3** demonstrates that the borane-activated silylation of the uranyl oxo ligand does not require the highly donating β -ketoiminate ligand, Aracnac , to proceed. Instead, oxo ligand silylation can be achieved with weaker donors attached to the uranyl equatorial sites, revealing the generality of this borane-mediated reductive silylation protocol. However, since we did not see any evidence for further reduction of **2.2** and **2.3** to U(IV), the utility of other co-ligands should be explored.

Interestingly, both complexes **2.2** and **2.3** exhibit uranyl oxo substitution chemistry. For example, complex **2.3** reacts with 1 equiv $\text{H}(\text{dbm})$ to form $\text{U}(\text{OB}\{\text{C}_6\text{F}_5\}_3)(\text{dbm})_3$ (**2.5**) and HOSiEt_3 , in which the silylated oxo has been replaced by the dbm ligand via protonation. In addition, complex **2.2** reacts with 2 equiv HOSiPh_3 to afford $\text{U}(\text{OSiPh}_3)_3(\text{dbm})_2$ (**2.6**), where the $-\text{OB}(\text{C}_6\text{F}_5)_3$ ligand has been replaced by a silyloxy group. We propose this oxo ligand substitution chemistry is unique to the dbm equatorial ligand vs. the Aracnac ligand, because of the narrow steric profile of the dbm ligand.

2.4 Experimental Section

2.4.1 General Procedures. All reactions and subsequent manipulations were performed under anaerobic and anhydrous conditions under an atmosphere of nitrogen. Hexanes, diethyl ether, and toluene were dried using a Vacuum Atmospheres DRI-SOLV solvent purification system, and stored over 3Å molecular sieves for 24 h prior to use. CH₂Cl₂ and CD₂Cl₂ were dried over activated 3 Å molecular sieves for 24 h before use. THF was distilled twice, first from calcium hydride and then from sodium benzophenone ketyl, and stored over 3Å molecular sieves for 24 h prior to use. UO₂Cl₂(THF)₃ was synthesized by the published procedure.⁶⁵ UO₂(dbm)₂(THF) was synthesized by modifying the previously reported procedure for the preparation of UO₂(hfac)₂(THF) (see below).^{40,66,67} All other reagents were purchased from commercial suppliers and used as received.

NMR spectra were recorded on a Varian UNITY INOVA 400 MHz spectrometer or a Varian UNITY INOVA 500 MHz spectrometer. ¹H and ¹³C{¹H} NMR spectra are referenced to external SiMe₄ using the residual protio solvent peaks as internal standards (¹H NMR experiments) or the characteristic resonances of the solvent nuclei (¹³C NMR experiments). ¹⁹F{¹H} NMR spectra were referenced to external CFCl₃ in C₆D₆. Raman and IR spectra were recorded on a Mattson Genesis FTIR/Raman spectrometer with a NXR FT Raman Module. IR samples were recorded as KBr pellets, while Raman samples were recorded in an NMR tube as neat solids. UV-vis/NIR experiments were performed on a UV-3600 Shimadzu spectrophotometer. Elemental analyses were performed by the Microanalytical Laboratory at UC Berkeley.

2.4.2 Cyclic Voltammetry Measurements. CV experiments were performed with a CH Instruments 600c Potentiostat, and the data were processed using CHI software (version 6.29). All experiments were performed in a glove box using a 20 mL glass vial as the cell. The working electrode consisted of a platinum disk embedded in glass (2 mm diameter), the counter electrode was a platinum wire, and the reference electrode consisted of AgCl plated on Ag wire. Solutions employed during CV studies were typically 1 mM in the metal complex and 0.1 M in [Bu₄N][PF₆]. All potentials are reported versus the [Cp₂Fe]^{0/+} couple. For all trials, $i_{p,a}/i_{p,c} = 1$ for the [Cp₂Fe]^{0/+} couple, while $i_{p,c}$ increased linearly with the square root of the scan rate (i.e., \sqrt{v}).

2.4.3 Synthesis of UO₂(dbm)₂(THF) (2.1). To a stirring THF (3 mL) solution of [UO₂Cl₂(THF)₂]₂ (435.2 mg, 0.448 mmol) was added dropwise a solution of H(dbm) (343.4 mg, 1.545 mmol) and NaN(SiMe₃)₂ (291.4 mg, 1.587 mmol) in THF (3 mL). This resulted in formation of a light orange solution. This solution was stirred for 24 h, whereupon the solution was filtered through a Celite column supported on glass wool (0.5 cm × 2 cm) to remove NaCl. The solution was then concentrated *in vacuo*, layered with hexanes (3 mL), and stored at -25 °C for 24 h, which resulted in the deposition of an orange powder. The solid was then extracted into dichloromethane (6 mL), and filtered through a Celite column supported on glass wool (0.5 cm × 2 cm). The filtrate was then concentrated *in vacuo*, layered with hexanes (3 mL), and stored at -25 °C for 24 h, which resulted in the deposition of an orange powder (440.2 mg, 71% yield). Anal. Calcd UO₇C₃₄H₃₀: C, 51.78; H, 3.83; N, 0.00. Found: C, 51.55; H, 3.45; N, <0.2. ¹H NMR (CD₂Cl₂, 25 °C, 400 MHz): δ 8.50 (br s, 8H, ortho CH), 7.66 (br s, 8H, meta CH),

7.64 (br s, 4H, para CH), 7.32 (br s, 2H, γ -CH), 4.99 (br s, 4H, THF), 2.47 (br s, 4H, THF). $^{13}\text{C}\{^1\text{H}\}$ NMR (CD_2Cl_2 , 25 °C, 126 MHz): δ 189.03 (s, C=O), 140.37 (s, ipso C), 132.88 (s, para CH), 129.46 (s, ortho CH), 128.98 (s, meta CH), 98.59 (s, γ -CH), 74.76 (s, THF), 27.43 (s, THF). IR (KBr pellet, cm^{-1}): 1597(sh w), 1591(m), 1549(sh m), 1535(vs), 1520(vs), 1477(m), 1452(m), 1440(w), 1360(s), 1348(m), 1313(m), 1298(m), 1224(sh w), 1221(w), 1180(w), 1159(w), 1122(w), 1067(w), 1022(sh w), 1024(w), 939(w), 906(s), 873(w), 840(w), 785(w), 750(m), 717(m), 684(m), 617(w), 604(w), 519(m). Raman (cm^{-1}): 3061(w), 1595(s), 1522(w), 1514(w), 1491(m), 1444(w), 1333(sh w), 1317(s), 1290(s), 1225(w), 1182(w), 1155(w), 1063(w), 1001(m), 939(w), 823(m, U=O ν_{sym}), 685(w), 561(w).

2.4.4 Synthesis of $\text{U}(\text{OB}(\text{C}_6\text{F}_5)_3)(\text{OSiPh}_3)(\text{dbm})_2(\text{THF})$ (2.2). To a stirring orange dichloromethane (3 mL) solution of $\text{UO}_2(\text{dbm})_2(\text{THF})$ (143.3 mg, 0.181 mmol) was added dropwise a solution of Ph_3SiH (47.3 mg, 0.182 mmol) and $\text{B}(\text{C}_6\text{F}_5)_3$ (91.9 mg, 0.179 mmol) in dichloromethane (2 mL). This resulted in the immediate formation of a dark red solution. This solution was stirred for 15 h, whereupon the deep red solution was filtered through a Celite column supported on glass wool (0.5 cm \times 2 cm). The solution was then concentrated *in vacuo*, THF (4 μL , 0.049 mmol) was added, and the solution was layered with hexanes (2 mL) and stored at -25 °C for 24 h, which resulted in the deposition of brown-red crystals (184.8 mg, 62% yield). Anal. Calcd $\text{UO}_7\text{SiBF}_{15}\text{C}_{70}\text{H}_{45}$: C, 53.89; H, 2.91. Found: C, 53.62; H, 3.02. ^1H NMR (CD_2Cl_2 , 25 °C, 400 MHz): δ 10.76 (br s, 8H, dbm CH), 7.53 (s, 6H, Ph_3Si meta CH), 7.41, (t, $J_{\text{HH}} = 5.6$ Hz, 3H, Ph_3Si para CH), 6.22 (s, 6H, Ph_3Si ortho CH), 4.75 (br s, 8H, dbm CH), 4.54 (br s, 4H, dbm para CH), 3.60 (br s, 2H, γ -CH), -1.21(br s, 4H, THF), -1.96 (br s, 4H, THF). $^{19}\text{F}\{^1\text{H}\}$

NMR: (CD₂Cl₂, 25 °C, 376 MHz): δ -136.24 (br s, 6F, ortho CF), -160.50 (s, 3F, para CF), -165.76 (s, 6F, meta CF). UV-vis/NIR (CH₂Cl₂, 3.85 × 10⁻³ M, L·mol⁻¹·cm⁻¹): 894 (ε = 12), 1114 (ε = 17), 1146 (sh, ε = 12), 1300 (sh, ε = 9), 1362 (ε = 19), 1438 (sh, ε = 12), 1462 (sh, ε = 11), 1606 (ε = 75). IR (KBr pellet, cm⁻¹): 1643(w), 1595(sh w), 1589(m), 1518(vs), 1486(sh m), 1479(m), 1466(s), 1441(m), 1429(w), 1381(vw), 1373(vw), 1340(m), 1317(m), 1296(m), 1280(m), 1225(w), 1180(vw), 1157(vw), 1117(m), 1093(m), 1068(w), 1022(w), 993(sh vw), 978(m), 941(w), 875(sh w), 847(m), 820(s), 814(sh m), 787(w), 768(sh w), 764(w), 742(w), 714(w), 698(w), 683(w), 671(sh w), 617(w), 601(w), 574(vw), 528(m), 511(m), 461(sh m), 445(sh m), 418(sh vs), 414(vs), 407(vs).

2.4.5 Synthesis of U(OB{C₆F₅}₃)(OSiEt₃)(dbm)₂(THF) (2.3). To a stirring orange dichloromethane (3 mL) solution of UO₂(dbm)₂THF (127.0 mg, 0.160 mmol) was added dropwise a solution of Et₃SiH (26 μL, 0.162 mmol) and B(C₆F₅)₃ (81.9 mg, 0.160 mmol) in dichloromethane (2 mL), which resulted in the immediate formation of a dark red solution. The solution was stirred for 24 h, whereupon the deep red solution was filtered through a Celite column supported on glass wool (0.5 cm × 2 cm). The solution was then concentrated *in vacuo*. THF (4 μL, 0.049 mmol) was added, and the solution was layered with hexanes (2 mL) and stored at -25 °C for 24 h, which resulted in the deposition of red-orange crystals (126.1 mg, 55% yield). Anal. Calcd UO₇SiBF₁₅C₅₈H₄₅: C, 49.20; H, 3.20. Found: C, 49.24; H, 3.36. ¹H NMR (CD₂Cl₂, 25 °C, 400 MHz): δ 7.40 (t, *J*_{HH} = 6.0 Hz, 4H, para CH), 6.66 (br s, 8H, ortho CH), 6.26 (s, 8H, meta CH), 4.94 (br s, 6H, CH₂CH₃), 4.54 (br s, 2H, γ-CH), 3.48 (br s, 9H, CH₂CH₃), -1.10 (br s, 4H, THF), -2.03 (br s, 4H, THF). ¹⁹F{¹H} NMR (CD₂Cl₂, 25 °C, 376 MHz): δ -135.00 (br s, 6F, ortho CF), -

160.69 (t, $J_{\text{FF}} = 13.9$ Hz, 3F, para CF), -165.86 (d, $J_{\text{FF}} = 16.2$ Hz, 6F, meta CF). UV-vis/NIR (CH_2Cl_2 , 4.15×10^{-3} M, $\text{L}\cdot\text{mol}^{-1}\cdot\text{cm}^{-1}$): 878 ($\epsilon = 11$), 1118 ($\epsilon = 17$), 1334 ($\epsilon = 18$), 1438 (sh, $\epsilon = 12$), 1420 (sh, $\epsilon = 7$), 1608 ($\epsilon = 103$). IR (KBr pellet, cm^{-1}): 1643(w), 1595(sh w), 1589(w), 1525(vs), 1518(sh vs), 1489(m), 1481(m), 1466(s), 1441(m), 1342(m), 1317(m), 1296(w), 1281(w), 1227(w), 115(sh w), 1094(m), 1068(w), 1022(w), 978(m), 941(w), 820(m), 810(m), 766(sh w), 760(w), 746(w), 717(w), 685(w), 669(sh w), 601(w), 527(w).

2.4.6 Synthesis of $\text{U}(\text{OB}(\text{C}_6\text{F}_5)_3)(\text{OSiEt}_3)(\text{dbm})_2$ (2.4). To a stirring orange dichloromethane (3 mL) solution of $\text{UO}_2(\text{dbm})_2\text{THF}$ (264.6 mg, 0.335 mmol) was added dropwise a solution of Et_3SiH (100 μL , 0.626 mmol) and $\text{B}(\text{C}_6\text{F}_5)_3$ (171.6 mg, 0.335 mmol) in dichloromethane (2mL), which resulted in formation of a dark red solution. The solution was stirred for 24 h, whereupon the deep red solution was filtered through a Celite column supported on glass wool (0.5 cm \times 2 cm). The solvent was removed *in vacuo*, which resulted in formation of a dark red oil. The oil was triturated with Et_2O (2 \times 4 mL), and then extracted into dichloromethane (4 mL). The solution was then concentrated *in vacuo* and layered with hexanes (2 mL). Storage at -25 $^\circ\text{C}$ for 24 h produced a dark red oil, which was discarded. The supernatant was further concentrated and layered with more hexanes (2 mL). Storage at -25 $^\circ\text{C}$ for another 24 h resulted in the deposition of a red-orange crystalline solid (106.5 mg, 24% yield). ^1H NMR (CD_2Cl_2 , 25 $^\circ\text{C}$, 400 MHz): δ 7.47 (br t, $J_{\text{HH}} = 6.6$ Hz, 4H, para CH), 6.59 (br s, 2H, γ -CH), 6.53 (br s, 8H, meta CH), 5.75 (br s, 8H, ortho CH), 5.36 (br s, 6H, CH_2CH_3), 2.72 (br s, 9H, CH_2CH_3). $^{19}\text{F}\{^1\text{H}\}$ NMR (CD_2Cl_2 , 25 $^\circ\text{C}$, 376 MHz): δ -151.05 (br s, 6F, ortho CF), -160.01 (t, $J_{\text{FF}} = 17.7$ Hz, 3F, para CF), -165.38 (d, $J_{\text{FF}} = 19.2$ Hz, 6F, meta CF).

2.4.7 Synthesis of U(OB{C₆F₅})₃(dbm)₃ (2.5). To a stirring dark red-orange dichloromethane solution (3 mL) of **2.3** (92.6 mg, 0.065 mmol) was added dropwise a dichloromethane (1 mL) solution of H(dbm) (16.5 mg, 0.073 mmol). The solution was stirred for 1 h, whereupon the solution was filtered through a Celite column supported on glass wool (0.5 cm × 2 cm). The solution was then concentrated *in vacuo*, layered with hexanes (2 mL), and stored at -25 °C for 24 h, which resulted in the deposition of a dark red solid (18.5 mg, 33% yield). X-ray quality crystals were grown out of toluene solution layered with hexanes. Anal. Calcd UO₇BF₁₅C₆₃H₃₃: C, 52.70; H, 2.32. Found: C, 52.65; H, 1.97. ¹H NMR (CD₂Cl₂, 25 °C, 400 MHz): δ 8.24 (br s, 3H, γ-CH), 7.68 (t, 6H, para CH), 6.71 (d, 12H, ortho CH), 6.22 (br s, 12H, meta CH). ¹⁹F{¹H} NMR (CD₂Cl₂, 25 °C, 376 MHz): δ -144.79 (br s, 6F, ortho CF), -160.54 (t, *J*_{FF} = 19.7 Hz, 3F, para CF), -166.01 (d, *J*_{FF} = 19.9 Hz, 6F, meta CF). UV-vis/NIR (CH₂Cl₂, 2.75 × 10⁻³ M, L·mol⁻¹·cm⁻¹): 714 (sh, ε = 30), 950 (ε = 27), 1128 (sh, ε = 12), 1164 (sh, ε = 27), 1202 (ε = 36), 1482 (ε = 108), 1904 (ε = 34). IR (KBr pellet, cm⁻¹): 1643(w), 1591(sh m), 1587(m), 1522(sh vs), 1514(vs), 1487(sh m), 1470(s), 1466(s), 1437(m), 1371(w), 1340(sh w), 1317(m), 1294(m), 1280(m), 1225(w), 1184(w), 1109(sh w), 1095(m), 1067(m), 1024(w), 974(m), 939(w), 870(w), 831(w), 768(sh w), 758(w), 721(sh w), 717(w), 685(m), 602(w), 532(w), 523(sh w).

2.4.8 Synthesis of U(OSiPh₃)₃(dbm)₂ (2.6). To a stirring red-orange solution of **2.2** (70.3 mg, 0.042 mmol) in dichloromethane (2 mL), was added a white slurry of HOSiPh₃ (24.1 mg, 0.087 mmol) in dichloromethane (1 mL), dropwise, which resulted in no visible change. The mixture was allowed to stir at room temperature for 1 h, whereupon all the solid appeared to have dissolved. The red-orange solution was

filtered through a Celite column supported on glass wool (0.5 cm × 2 cm), and the filtrate was concentrated *in vacuo*, and layered with ether (2 mL). Storage at -25 °C for 24 h resulted in the deposition of red-orange crystals (4.2 mg). The supernatant was concentrated *in vacuo* and stored at -25 °C for 24 h, which resulted in the deposition of more red-orange crystals (16.4 mg). A third crop was also isolated in a similar fashion (15.2 mg), for a combined 56% yield. IR (KBr pellet, cm⁻¹): 1589(w), 1518(s), 1489(sh w), 1479(m), 1439(w), 1427(m), 1327(m), 1313(sh w), 1294(w), 1227(w), 1186(w), 1115(s), 1105(sh m), 1066(w), 1028(w), 1001(w), 987(m), 935(w), 860(vs), 741(w), 710(s), 698(s), 684(sh w), 536(sh w), 524(sh w), 511(s).

2.4.9 Synthesis of U(OB{C₆F₅}₃)(OSiEt₃)(dbm)₂(HOPh) (2.7). A red orange CD₂Cl₂ solution (1 mL) containing **2.4** (17.4 mg, 0.013 mmol) was sealed in a J. Young NMR tube, and the ¹H and ¹⁹F{¹H} NMR spectra were recorded. Then a colorless CD₂Cl₂ solution (0.5 mL) of HOPh (2.1 mg, 0.022 mmol) was added drop-wise, resulting in a color change to dark orange. The tube was sealed, and the ¹H and ¹⁹F{¹H} NMR spectra were re-recorded after 1 h at 25 °C. These spectra revealed the presence of a new paramagnetic uranium-containing product. This reaction mixture was filtered through a Celite column supported on glass wool (0.5 cm × 2 cm), and dried *in vacuo*, which resulted in a dark orange solid. The solid was extracted into toluene (~1 mL) and layered with hexanes (< 1 mL). Storage of the mixture for 1 month at -25 °C, resulted in the formation of dark orange crystals of **2.7**. ¹⁹F{¹H} NMR (CD₂Cl₂, 25 °C, 376 MHz): δ -134.95 (br s, 6F, ortho CF), -160.71 (s, 3F, para CF), -166.91 (s, 6F, meta CF).

2.4.10 X-ray Crystallography. The solid-state molecular structures of complexes **2.2** – **2.7** were determined similarly with exceptions noted in the following paragraph. Crystals were mounted on a cryoloop under Paratone-N oil. Data collection was carried out on a Bruker KAPPA APEX II diffractometer equipped with an APEX II CCD detector using a TRIUMPH monochromator with a Mo K α X-ray source ($\lambda = 0.71073 \text{ \AA}$). Data for **2.2**, **2.3**, **2.5**, **2.6**, and **2.7** were collected at 100(2) K, while data for **2.4** were collected at 150(2) K, using an Oxford nitrogen gas cryostream system. A hemisphere of data was collected using ω scans with 0.3° frame widths. Frame exposures of 5, 10, 10, 10, 10 and 10 seconds were used for complexes **2.2**, **2.3**, **2.4**, **2.5**, **2.6** and **2.7** respectively. Data collection and cell parameter determination were conducted using the SMART program.⁶⁸ Integration of the data frames and final cell parameter refinement were performed using SAINT software.⁶⁹ Absorption correction of the data was carried out empirically based on reflection ψ -scans using the multi-scan method SADABS.⁷⁰ Subsequent calculations were carried out using SHELXTL.⁷¹ Structure determination was done using direct or Patterson methods and difference Fourier techniques. All hydrogen atom positions were idealized, and rode on the atom of attachment. Structure solution, refinement, graphics, and creation of publication materials were performed using SHELXTL.⁷¹

Complex **2.3** exhibits positional disorder of the toluene solvent molecule. The positional disorder was addressed by modeling the molecule in two orientations, in a 50:50 ratio. The EADP, DFIX, and FLAT commands were used to constrain both orientations of the toluene molecule. For complex **2.5**, every non-hydrogen atom in one of the uranium molecule was constrained using the EADP command to its symmetry

equivalent atom on the other uranium molecule. Two toluene solvent molecules were not refined anisotropically. In addition, the C-C bonds of the toluene rings were constrained with the DFIX command, while the rings were constrained with the FLAT command. Hydrogen atoms were not assigned to disordered carbon atoms. Complex **2.7** exhibits a disordered hexanes solvate. The disordered carbon atoms were not refined anisotropically, and hydrogen atoms were not assigned to disordered carbon atoms. A hydrogen atom was also not assigned to the OPh group, as this resulted in an error message during refinement. A summary of relevant crystallographic data for **2.2** – **2.7** is presented in Tables 2.3-2.4. Complexes **2.2** – **2.5** have been deposited in the Cambridge Structural Database (**2.2**: CCDC 994968; **2.3**: CCDC 994969; **2.4**: CCDC 994970; **2.5**: CCDC 994971).

Table 2.3. X-ray Crystallographic Data for Complexes **2.2** – **2.4**

	2.2 ·C ₆ H ₁₄	2.3 ·C ₇ H ₈ ·0.5C ₆ H ₁₄	2.4
empirical formula	UO ₇ BF ₁₅ SiC ₇₆ H ₅₉	UO ₇ BF ₁₅ SiC ₆₈ H ₆₀	UO ₆ BF ₁₅ SiC ₅₄ H ₃₇
Crystal habit, color	plate, red-orange	plate, red	plate, red-orange
crystal size (mm)	0.35 × 0.30 × 0.30	0.40 × 0.30 × 0.10	0.10 × 0.08 × 0.05
crystal system	triclinic	triclinic	triclinic
space group	<i>P</i> -1	<i>P</i> -1	<i>P</i> -1
vol (Å ³)	3411.96(16)	3202.79(11)	2555.2(2)
a (Å)	13.6767(4)	12.8552(3)	12.0721(6)
b (Å)	15.7946(4)	15.7463(3)	12.2867(7)
c (Å)	16.3191(4)	16.5535(3)	17.8840(11)
α (deg)	102.448(2)	100.009(1)	89.672(4)
β (deg)	93.042(2)	103.592(1)	80.120(4)
γ (deg)	96.154(2)	90.593(1)	78.024(4)
Z	2	2	2
fw (g/mol)	1646.16	1551.09	1343.77
density (calcd) (Mg/m ³)	1.602	1.608	1.747
abs coeff (mm ⁻¹)	2.493	2.650	3.305
F ₀₀₀	1634	1540	1310
Total no. reflections	35645	31034	30650
Unique reflections	13946	15762	12728
final R indices [I > 2σ(I)]	R ₁ = 0.0266 wR ₂ = 0.0647	R ₁ = 0.0281 wR ₂ = 0.0783	R ₁ = 0.0388 wR ₂ = 0.1047
largest diff peak and hole (e ⁻ Å ⁻³)	1.960 and -1.180	2.493 and -0.716	6.198 and -1.785
GOF	1.032	1.097	1.047

Table 2.4. X-ray Crystallographic Data for Complexes **2.5** – **2.7**

	2.5 ·2C ₇ H ₈ ·C ₆ H ₁₄	2.6 ·CH ₂ Cl ₂	2.7 ·C ₆ H ₁₄
empirical formula	UO ₇ BF ₁₅ C ₇₃ H ₄₈	UO ₇ Cl ₂ Si ₃ C ₈₅ H ₆₉	UO ₇ BF ₁₅ SiC ₆₆ H ₅₇
Crystal habit, color	plate, red	plate, red	plate, dark orange
crystal size (mm)	0.20 × 0.15 × 0.10	0.25 × 0.05 × 0.05	0.3 × 0.2 × 0.05
crystal system	triclinic	triclinic	triclinic
space group	<i>P</i> 1	<i>P</i> -1	<i>P</i> -1
vol (Å ³)	3157.04(16)	3538.7(8)	3005.3(7)
a (Å)	15.1204(4)	13.922(2)	12.307(2)
b (Å)	16.1764(5)	14.726(2)	13.357(2)
c (Å)	16.4479(5)	18.173(2)	19.531(3)
α (deg)	112.966(2)	77.965(3)	104.550(2)
β (deg)	96.391(2)	85.649(3)	91.364(2)
γ (deg)	115.286(2)	76.288(3)	103.834(2)
Z	2	2	2
fw (g/mol)	1570.95	1595.60	1524.05
density (calcd) (Mg/m ³)	1.653	1.497	1.684
abs coeff (mm ⁻¹)	2.672	2.477	2.822
F ₀₀₀	1548	1606	1510
Total no. reflections	32024	16083	18817
Unique reflections	24983	13131	16048
final R indices [<i>I</i> > 2σ(<i>I</i>)]	R ₁ = 0.0468 wR ₂ = 0.1062	R ₁ = 0.0425 wR ₂ = 0.1074	R ₁ = 0.0460 wR ₂ = 0.1124
largest diff peak and hole (e ⁻ Å ⁻³)	1.486 and -2.212	3.833 and -3.301	5.537 and -3.006
GOF	0.975	0.812	1.053

2.5 Acknowledgements

I would like to thank our collaborator, Dr. Nik Kaltsoyannis, at University College London for collection and analysis of the DFT data for complex **2.5**.

2.6 References

- (1) Wu, W.-M.; Carley, J.; Fienen, M.; Mehlhorn, T.; Lowe, K.; Nyman, J.; Luo, J.; Gentile, M. E.; Rajan, R.; Wagner, D.; Hickey, R. F.; Gu, B.; Watson, D.; Cirpka, O. A.; Kitanidis, P. K.; Jardine, P. M.; Criddle, C. S. *Environ. Sci. Technol.* **2006**, *40*, 3978.
- (2) Wu, W.-M.; Carley, J.; Gentry, T.; Ginder-Vogel, M. A.; Fienen, M.; Mehlhorn, T.; Yan, H.; Carroll, S.; Pace, M. N.; Nyman, J.; Luo, J.; Gentile, M. E.; Fields, M. W.; Hickey, R. F.; Gu, B.; Watson, D.; Cirpka, O. A.; Zhou, J.; Fendorf, S.; Kitanidis, P. K.; Jardine, P. M.; Criddle, C. S. *Environ. Sci. Technol.* **2006**, *40*, 3986.
- (3) Renshaw, J. C.; Butchins, L. J. C.; Livens, F. R.; May, I.; Charnock, J. M.; Lloyd, J. R. *Environ. Sci. Technol.* **2005**, *39*, 5657.
- (4) Gu, B.; Wu, W.-M.; Ginder-Vogel, M. A.; Yan, H.; Fields, M. W.; Zhou, J.; Fendorf, S.; Criddle, C. S.; Jardine, P. M. *Environ. Sci. Technol.* **2005**, *39*, 4841.
- (5) Ilton, E. S.; Haiduc, A.; Cahill, C. L.; Felmy, A. R. *Inorg. Chem.* **2005**, *44*, 2986.
- (6) Williams, K. H.; Bargar, J. R.; Lloyd, J. R.; Lovley, D. R. *Curr. Opin. Biotechnol.* **2013**, *24*, 489.
- (7) Noubactep, C.; Meinrath, G.; Dietrich, P.; Merkel, B. *Environ. Sci. Technol.* **2003**, *37*, 4304.
- (8) Sundararajan, M.; Campbell, A. J.; Hillier, I. H. *J. Phys. Chem. A* **2008**, *112*, 4451.
- (9) Fortier, S.; Hayton, T. W. *Coord. Chem. Rev.* **2010**, *254*, 197.
- (10) Wilkerson, M. P.; Burns, C. J.; Dewey, H. J.; Martin, J. M.; Morris, D. E.; Paine, R. T.; Scott, B. L. *Inorg. Chem.* **2000**, *39*, 5277.
- (11) Sarsfield, M. J.; Helliwell, M. *J. Am. Chem. Soc.* **2004**, *126*, 1036.
- (12) Schnaars, D. D.; Wu, G.; Hayton, T. W. *J. Am. Chem. Soc.* **2009**, *131*, 17532.
- (13) Bagnall, K. W.; du Preez, J. G. H. *Chem. Commun.* **1973**, 820.
- (14) Arnold, P. L.; Patel, D.; Wilson, C.; Love, J. B. *Nature* **2008**, *451*, 315.
- (15) Arnold, P. L.; Love, J. B.; Patel, D. *Coord. Chem. Rev.* **2009**, *253*, 1973
- (16) Brown, J. L.; Wu, G.; Hayton, T. W. *J. Am. Chem. Soc.* **2010**, *132*, 7248
- (17) Brown, J. L.; Mokhtarzadeh, C. C.; Lever, J. M.; Wu, G.; Hayton, T. W. *Inorg. Chem.* **2011**, *50*, 5105.

- (18) Schnaars, D. D.; Wu, G.; Hayton, T. W. *Inorg. Chem.* **2011**, *50*, 4695.
- (19) Schnaars, D. D.; Wu, G.; Hayton, T. W. *Inorg. Chem.* **2011**, *50*, 9642.
- (20) Berthet, J.-C.; Siffredi, G.; Thuéry, P.; Ephritikhine, M. *Eur. J. Inorg. Chem.* **2007**, 4017.
- (21) Yahia, A.; Arnold, P. L.; Love, J. B.; Maron, L. *Chem. Commun.* **2009**, 2402.
- (22) Yahia, A.; Arnold, P. L.; Love, J. B.; Maron, L. *Chem. Eur. J.* **2010**, *16*, 4881.
- (23) Parks, D. J.; Piers, W. E. *J. Am. Chem. Soc.* **1996**, *118*, 9440
- (24) Parks, D. J.; Blackwell, J. M.; Piers, W. E. *J. Org. Chem.* **2000**, *65*, 3090
- (25) Blackwell, J. M.; Sonmor, E. R.; Scoccitti, T.; Piers, W. E. *Org. Lett.* **2000**, *2*, 3921
- (26) Blackwell, J. M.; Morrison, D. J.; Piers, W. E. *Tetrahedron* **2002**, *58*, 8247
- (27) Blackwell, J. M.; Foster, K. L.; Beck, V. H.; Piers, W. E. *J. Org. Chem.* **1999**, *64*, 4887
- (28) Berkefeld, A.; Piers, W. E.; Parvez, M. *J. Am. Chem. Soc.* **2010**, *132*, 10660.
- (29) Houghton, A. Y.; Hurmalainen, J.; Mansikkamäki, A.; Piers, W. E.; Tuononen, H. M. *Nat. Chem.* **2014**, *6*, 983.
- (30) Erker, G.; Stephan, D. W. *Frustrated Lewis Pairs I: Uncovering and Understanding*; Springer: Heidelberg New York Dordrecht London, 2013.
- (31) Clark, D. L.; Conradson, S. D.; Donohoe, R. J.; Keogh, D. W.; Morris, D. E.; Palmer, P. D.; Rogers, R. D.; Tait, C. D. *Inorg. Chem.* **1999**, *38*, 1456.
- (32) McGlynn, S. P.; Smith, J. K.; Neely, W. C. *J. Chem. Phys.* **1961**, *35*, 105.
- (33) Allen, P. G.; Bucher, J. J.; Clark, D. L.; Edelstein, N. M.; Ekberg, S. A.; Gohdes, J. W.; Hudson, E. A.; Kaltsoyannis, N.; Lukens, W. W.; Neu, M. P.; Palmer, P. D.; Reich, T.; Shuh, D. K.; Tait, C. D.; Zwick, B. D. *Inorg. Chem.* **1995**, *34*, 4797.
- (34) Ingram, K. I. M.; Haller, L. J. L.; Kaltsoyannis, N. *Dalton Trans* **2006**, 2403.
- (35) Abubacker, K. M.; Prasad, N. S. K. *J. Inorg. Nucl. Chem.* **1961**, *16*, 296.
- (36) Mizuguchi, K.; Lee, S.-H.; Ikeda, Y.; Tomiyasu, H. *J. Alloys Compd.* **1998**, *271/273*, 163.
- (37) Kim, S.-Y.; Tomiyasu, H.; Ikeda, Y. *J. Nucl. Sci. Technol.* **2002**, *39*, 160.
- (38) Yayamura, T.; Iwata, S.; Iwamaru, S.-i.; Tomiyasu, H. *J. Chem. Soc., Faraday Trans.* **1994**, *90*, 3253.
- (39) Sacconi, L.; Giannoni, G. *J. Chem. Soc.* **1954**, 2368.
- (40) Tahir, A. A.; Hamid, M.; Mazhar, M.; Zeller, M.; Hunter, A. D. *Acta Crystallogr. Sec. E* **2006**, *E62*, m1780.
- (41) Hayton, T. W.; Wu, G. *Inorg. Chem.* **2009**, *48*, 3065.
- (42) Hayton, T. W.; Wu, G. *Inorg. Chem.* **2008**, *47*, 7415
- (43) Kim, S.-Y.; Asakura, T.; Morita, Y.; Ikeda, Y. *J. Alloys Compounds* **2006**, *408-412*, 1291.
- (44) Wester, D.; Palenik, G. J. *J. Am. Chem. Soc.* **1973**, *95*, 6505.
- (45) La Pierre, H. S.; Meyer, K. *Inorg. Chem.* **2013**, *52*, 529.
- (46) Jiang, J.; Sarsfield, M. J.; Renshaw, J. C.; Livens, F. R.; Collison, D.; Charnock, J. M.; Helliwell, M.; Eccles, H. *Inorg. Chem.* **2002**, *41*, 2799.
- (47) Kannan, S.; Pillai, M. R. A.; Venugopal, V.; Droege, P. A.; Barnes, C. L. *Inorg. Chim. Acta* **1997**, *254*, 113.
- (48) Yin, H.; Lewis, A. J.; Williams, U. J.; Carroll, P. J.; Schelter, E. J. *Chem. Sci.* **2013**, *4*, 798.

- (49) Gong, Y.; Vallet, V.; del Carmen Michelini, M.; Rios, D.; Gibson, J. K. *J. Phys. Chem. A* **2014**, *118*, 325.
- (50) Casanova, D.; Alemany, P.; Bofill, J. M.; Alvarez, S. *Chem. Eur. J.* **2003**, *9*, 1281.
- (51) Fortier, S.; Brown, J. L.; Kaltsoyannis, N.; Wu, G.; Hayton, T. W. *Inorg. Chem.* **2012**, *51*, 1625.
- (52) Kovács, A.; Konings, R. J. M. *Chem. Phys. Chem.* **2006**, *7*, 455.
- (53) Lam, O. P.; Franke, S. M.; Nakai, H.; Heinemann, F. W.; Hieringer, W.; Meyer, K. *Inorg. Chem.* **2012**, *51*, 6190.
- (54) Lewis, A. J.; Carroll, P. J.; Schelter, E. J. *J. Am. Chem. Soc.* **2013**, *135*, 511.
- (55) Chauhan, B. P. S.; Sarkar, A.; Chauhan, M.; Roka, A. *Appl. Organomet. Chem.* **2009**, *23*, 385.
- (56) Bean, A. C.; Sullens, T. A.; Runde, W.; Albrecht-Schmitt, T. E. *Inorg. Chem.* **2003**, *42*, 2628.
- (57) Berthet, J.-C.; Thuéry, P.; Ephritikhine, M. *Chem. Commun.* **2005**, 3415.
- (58) Bergquist, C.; Bridgewater, B. M.; Harlan, C. J.; Norton, J. R.; Friesner, R. A.; Parkin, G. *J. Am. Chem. Soc.* **2000**, *122*, 10581.
- (59) Camp, C.; Pécaut, J.; Mazzanti, M. *J. Am. Chem. Soc.* **2013**, *135*, 12101.
- (60) Salmon, L.; Thuery, P.; Ephritikhine, M. *Chem. Commun.* **2006**, 856.
- (61) Salmon, L.; Thuéry, P.; Ephritikhine, M. *Eur. J. Inorg. Chem.* **2006**, *2006*, 4289.
- (62) Denning, R. *Struct. Bonding* **1992**, *79*, 215.
- (63) Bartleet, J. M.; Denning, R. G.; Morrison, I. D. *Mol. Phys.* **1992**, *75*, 601.
- (64) O'Grady, E.; Kaltsoyannis, N. *Dalton Trans.* **2002**, 1233.
- (65) Wilkerson, M. P.; Burns, C. J.; Paine, R. T.; Scott, B. L. *Inorg. Chem.* **1999**, *38*, 4156.
- (66) Kramer, G. M.; Dines, M. B.; Hall, R. B.; Kaldor, A.; Jacobson, A. J.; Scanlon, J. C. *Inorg. Chem.* **1980**, *19*, 1340.
- (67) Alagar, M.; Rajagopal, K.; Krishnakumar, R. V.; Subha Nandhini, M.; Kannan, S.; Natarajan, S. *Acta Crystallogr. Sec. E* **2003**, *E59*, m524.
- (68) SMART, Apex II, Version 2.1; Bruker AXS Inc.: Madison, WI, 2005.
- (69) SAINT, Software User's Guide, Version 7.34a; Bruker AXS Inc.: Madison, WI, 2005.
- (70) Sheldrick, G. M. *SADABS*, University of Gottingen: Germany, 2005.
- (71) SHELXTL PC, Version 6.12; Bruker AXS Inc.: Madison, WI, 2005.

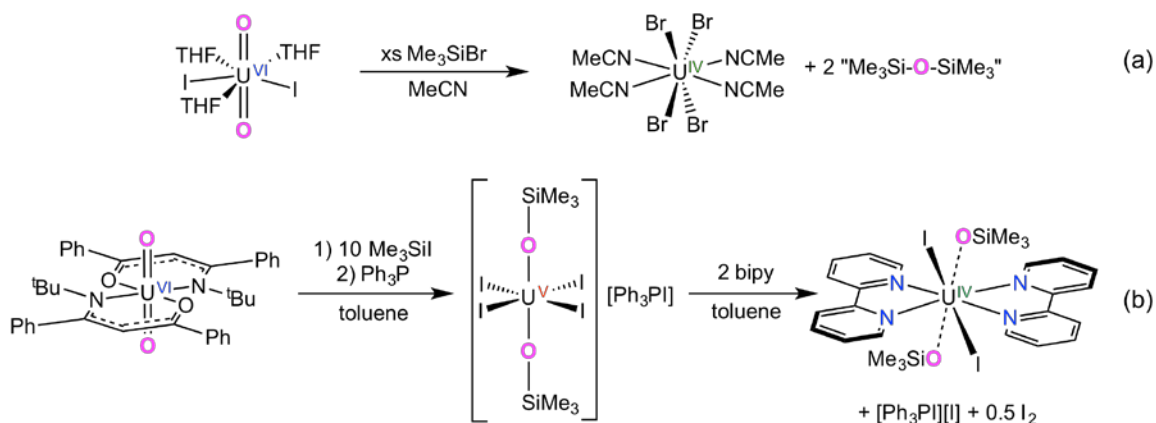
Chapter 3. Oxo Ligand Substitution in a Cationic Uranyl Complex: Synergistic Interaction of an Electrophile and a Reductant

3.1. Introduction	63
3.2. Results and Discussion	66
3.2.1. Borane-Mediated Reductive Silylation of $[\text{UO}_2(\text{dppmo})_2(\text{OTf})][\text{OTf}]$	66
3.2.1.1. Synthesis and Characterization of $[\text{U}^{\text{IV}}(\text{OSiPh}_3)(\text{dppmo})_2(\text{OTf})_2][\text{OTf}]$ (3.1).....	66
3.2.1.2. Identification of $[\text{UO}_2(\text{dppmo})_2(\text{OTf})][\text{HB}(\text{C}_6\text{F}_5)_3]$ and Ph_3SiOTf	69
3.2.2. Reductive Silylation of $[\text{UO}_2(\text{dppmo})_2(\text{OTf})][\text{OTf}]$ and $[\text{UO}_2(\text{TPPO})_4][\text{OTf}]_2$ with Cp_2Co	73
3.2.2.1. Synthesis and Characterization of $\text{U}^{\text{IV}}(\text{OTf})_4(\text{dppmo})_2$ (3.3)	73
3.2.2.2. Synthesis and Characterization of $[\text{U}^{\text{IV}}(\text{OSiPh}_3)_2(\text{dppmo})_2(\text{OTf})][\text{OTf}]$ (3.4).....	78
3.2.2.3. Synthesis and Characterization of $[\text{Cp}_2\text{Co}][\text{U}^{\text{IV}}(\text{OTf})_5(\text{TPPO})_2]$ (3.5).....	81
3.2.3. Synthesis of U(IV) Triflate Complexes from $\text{U}(\text{IV})\text{Cl}_4$	85
3.2.3.1. Synthesis and Characterization of $[\text{U}^{\text{IV}}(\text{OTf})_2(\text{dppmo})_3][\text{OTf}]_2$ (3.6).....	85
3.2.3.2. Synthesis, Characterization and Reactivity of $[\text{U}^{\text{IV}}(\text{OTf})_2(\text{TPPO})_4][\text{OTf}]_2$ (3.7)	88
3.3. Summary	91
3.4. Experimental Section	93
3.4.1. General Procedures	93

3.4.2. Synthesis of $[\text{UO}_2(\text{dppmo})_2(\text{OTf})][\text{OTf}]$	93
3.4.3. Synthesis of $[\text{UO}_2(\text{TPPO})_4][\text{OTf}]_2$	94
3.4.4. Synthesis of $[\text{U}^{\text{IV}}(\text{OSiPh}_3)(\text{dppmo})_2(\text{OTf})_2][\text{OTf}]$ (3.1).....	95
3.4.5. Synthesis of 3.1 using Cp_2Co	95
3.4.6. Synthesis of $[\text{Na}(12\text{-crown-}4)_2][\text{HB}(\text{C}_6\text{F}_5)_3]$ (3.2).....	96
3.4.7. Synthesis of $\text{U}^{\text{IV}}(\text{OTf})_4(\text{dppmo})_2$ (3.3)	97
3.4.8. Synthesis of $[\text{U}^{\text{IV}}(\text{OSiPh}_3)_2(\text{dppmo})_2(\text{pyr})][\text{OTf}]_2$ (3.4-pyr).....	98
3.4.9. Synthesis of $[\text{Cp}_2\text{Co}][\text{U}^{\text{IV}}(\text{OTf})_5(\text{TPPO})_2]$ (3.5)	99
3.4.10. Synthesis of 3.5 using Ph_3SiOTf	100
3.4.11. Synthesis of $[\text{U}^{\text{IV}}(\text{OTf})_2(\text{dppmo})_3][\text{OTf}]_2$ (3.6).....	101
3.4.12. Synthesis of $[\text{U}^{\text{IV}}(\text{OTf})_2(\text{TPPO})_4][\text{OTf}]_2$ (3.7).....	102
3.4.13. NMR-Scale Reaction of Ph_3SiOTf with Cp_2Co	103
3.4.14. NMR-Scale Reaction of $[\text{UO}_2(\text{dppmo})_2(\text{OTf})][\text{OTf}]$ with Cp_2Co	103
3.4.15. NMR-Scale Reaction of $[\text{UO}_2(\text{dppmo})_2(\text{OTf})][\text{OTf}]$ with Ph_3SiOTf	104
3.4.16. NMR-Scale Reaction of $[\text{UO}_2(\text{TPPO})_4][\text{OTf}]_2$ with Cp_2Co	104
3.4.17. NMR-Scale Reaction of $[\text{UO}_2(\text{TPPO})_4][\text{OTf}]_2$ with Me_3SiOTf	104
3.4.18. NMR-Scale Reaction of Me_3SiOTf with Cp_2Co	105
3.4.19. X-Ray Crystallography	105
3.5. References	109

3.1 Introduction

Reductive silylation of the uranyl ion was first reported in 2008,¹ and has since been described for a variety of co-ligand types and silylating reagents.²⁻⁷ For example, Arnold and co-workers demonstrated that sequential reaction of $U^{VI}O_2(THF)(H_2L)$ ($L =$ polypyrrolic macrocycle) with $KN(SiMe_3)_2$ and FeI_2 resulted in formation of the $U(V)$ silyloxy, $[U^{VO}(OSiMe_3)(THF)Fe_2I_2L]$ (Scheme 1.2b).⁷ Similarly, our research group has demonstrated that reaction of $UO_2(Aracnac)_2$ ($Aracnac = ArNC(Ph)CHC(Ph)O$, $Ar = 3,5\text{-}^tBu_2C_6H_3$),⁸ or $UO_2(dbm)_2(THF)$ (**2.1**) ($dbm = OC(Ph)CHC(Ph)O$), with a mixture of $B(C_6F_5)_3$ and $HSiR_3$ ($R = Ph, Et$), results in formation of the reductive silylation products, $U^V(OSiPh_3)(OB\{C_6F_5\}_3)(Aracnac)_2$,^{9,10} and $U^V(OSiR_3)(OB\{C_6F_5\}_3)(dbm)_2(THF)$ ($R = Ph$ (**2.2**), Et (**2.3**)).¹¹ In contrast to these oxo functionalization reactions, examples of complete oxo substitution remain rare (Section 1.3). For instance, Ephritikhine and co-workers reported that reaction of UO_2I_2 with Me_3SiX ($X = Cl, Br, I$) in $MeCN$ resulted in formation of $U^{IV}X_4(MeCN)_4$ (Scheme 3.1a).^{12,13} In addition, we demonstrated a two-step procedure for the controlled removal of a uranyl oxo ligand in chapter 2, wherein a uranyl oxo in **2.1** was converted into a silyloxy that was subsequently protonated with a weak acid, $H(dbm)$, to generate $U^V(OB\{C_6F_5\}_3)(dbm)_3$ (**2.5**).¹¹



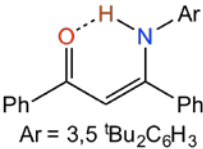
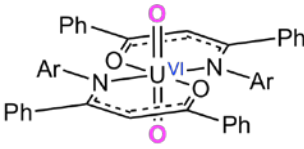
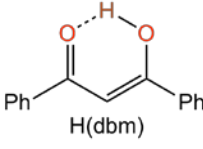
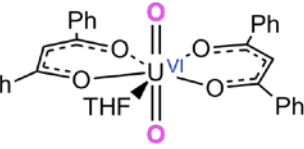
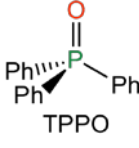
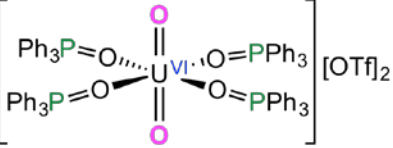

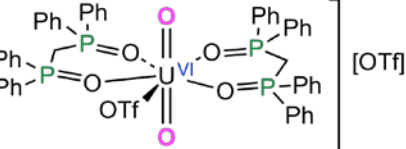
Scheme 3.1. Rare examples of reductive silylation of uranyl to U(IV). **a)** (Scheme reproduced from reference 12). **b)** (Scheme reproduced from reference 15).

It is notable that many reductive silylation reactions can only achieve a 1e⁻ reduction of the metal center.^{1,2,9,10} Achieving a 2e⁻ reduction, which would allow for isolation of a U(IV) product, appears to be more difficult, and only a few examples are known, including the Ephritikhine example discussed in the preceding paragraph (Scheme 3.1a).¹² Other examples include the reaction of $\text{UO}_2(\text{tBuacnac})_2$ ($\text{tBuacnac} = \text{tBuNC(Ph)CHC(Ph)O}$) with $\text{Me}_3\text{SiI}/\text{Ph}_3\text{P}$, followed by addition of bipy (Scheme 3.1b),¹⁵ and the stepwise reaction of $\text{UO}_2(\text{Aracnac})_2$ with $\text{B}(\text{C}_6\text{F}_5)_3/\text{HSiR}_3$ ($\text{R} = \text{Ph, Et}$) and Cp_2Co (Scheme 2.3).^{9,10} These three transformations result in the formation of U(IV) bis(silyloxy) complexes as the final products; however, the transformations are two step processes that require the isolation of an intermediate. This paucity of examples can be rationalized on the basis of the strongly electron donating ligands, such as Aracnac or the pacman macrocycle,¹ which are often used in this chemistry, as these tend to stabilize higher oxidation states. As a result, the products of these reactions often have U(V)/U(IV) redox potentials that are a challenge to access chemically. For

example, the U(V) reductive silylation product, $U^V(OSiPh_3)(OB\{C_6F_5\}_3)(^{Ar}acnac)_2$, features a rather low U(V)/U(IV) redox potential of -0.72 V (vs. Fc/Fc⁺).⁹ These strongly-donating ligands are nonetheless beneficial because they weaken the axial ligand field, thereby rendering the oxo ligands more nucleophilic and making the initial silylation step easier.

Herein, we describe our attempts to perform reductive silylation on $[UO_2(dppmo)_2(OTf)][OTf]$ (dppmo = $Ph_2P(O)CH_2P(O)Ph_2$) and $[UO_2(TPPO)_4][OTf]_2$ (TPPO = Ph_3PO). These complexes were chosen, in part, because their cationic charges should make reduction to U(IV) more facile, potentially enabling a 2e⁻ reductive silylation reaction. These favorable redox properties are evidenced indirectly by their U=O(sym) vibrational modes, as it has been previously demonstrated that less negative uranyl 1e⁻ reduction potentials correlate with higher energy U=O(sym) stretches.¹⁶ In particular, $[UO_2(dppmo)_2(OTf)][OTf]$ and $[UO_2(TPPO)_4][OTf]_2$ feature U=O(sym) stretches of 849 cm⁻¹,¹⁷ and 839 cm⁻¹, respectively (Table 3.1), which are notably higher in energy than those exhibited by $UO_2(^{Ar}acnac)_2$ (812 cm⁻¹),¹⁵ or $UO_2(dbm)_2(THF)$ (823 cm⁻¹).¹¹ However, their higher energy uranyl U=O(sym) stretches also suggests that their oxo ligands will be less nucleophilic, which will disfavor oxo ligand silylation. It is clearly important to find the right balance of electron donation from the co-ligands, to facilitate U=O bond activation, while still allowing for reduction to U(IV).

Table 3.1. U=O ν_{sym} Stretch Comparison in Several Uranyl Complexes

Ligand	Uranyl Complex	U=O ν_{sym} stretch (cm^{-1})	Ref.
 Ar = 3,5 ^t Bu ₂ C ₆ H ₃		812	15
 H(dbm)		823	Ch. 2
 TPPO		839	This chapter
 dppmo		849	17

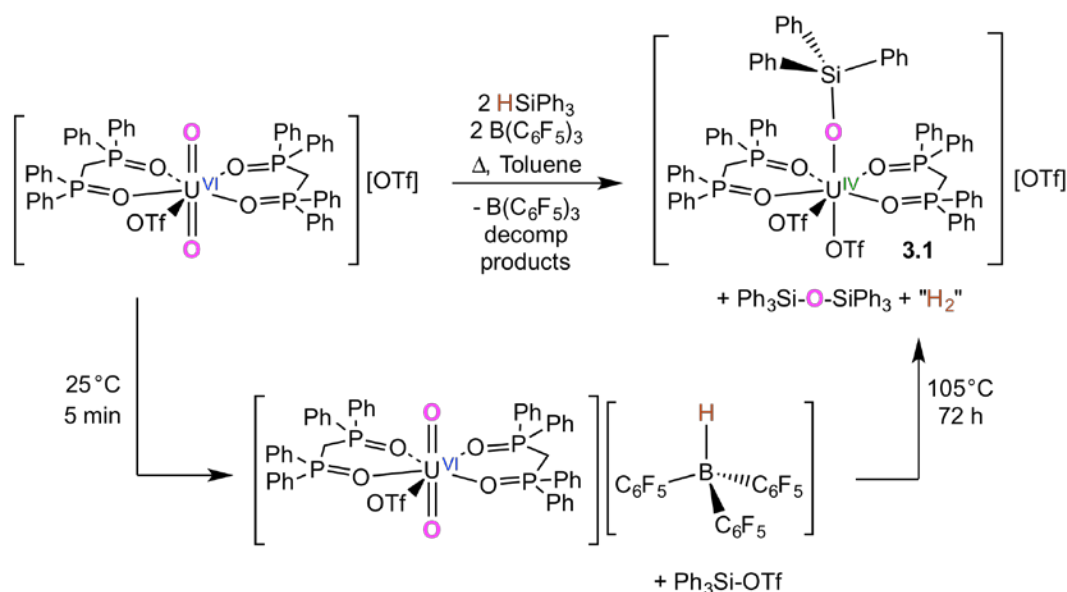
3.2 Results and Discussion

3.2.1. Borane-Mediated Reductive Silylation of [UO₂(dppmo)₂(OTf)][OTf]

3.2.1.1. Synthesis and Characterization of [U^{IV}(OSiPh₃)(dppmo)₂(OTf)₂][OTf] (3.1).

Once it was established that dppmo was a weaker donor than both Aracnac and dbm, we exposed [UO₂(dppmo)₂(OTf)][OTf] to our typical reductive silylation protocol. Unexpectedly, addition of 2 equiv of HSiPh₃ and 2 equiv of B(C₆F₅)₃ to

$[\text{UO}_2(\text{dppmo})_2(\text{OTf})][\text{OTf}]$ (Scheme 3.2), at room temperature, did not generate any reduced uranium-containing products, as determined by the *in situ* ^1H NMR spectra. However, heating these reaction mixtures at $105\text{ }^\circ\text{C}$ for 72 h, results in a conversion to the U(IV) mono-silyloxide, $[\text{U}^{\text{IV}}(\text{OSiPh}_3)(\text{dppmo})_2(\text{OTf})_2][\text{OTf}]$ (**3.1**), which can be isolated as sea-foam green crystals in very modest yields (Scheme 3.2). The isolation of complex **3.1** represents a rare example of uranyl oxo ligand substitution as well as a one-pot reduction of uranyl to U(IV).



Scheme 3.2. Borane-mediated reductive silylation of $[\text{UO}_2(\text{dppmo})_2(\text{OTf})][\text{OTf}]$.

Complex **3.1** crystallizes in the monoclinic space group $P2_1/n$ as a dichloromethane and Et_2O solvate, $\mathbf{3.1} \cdot 3\text{CH}_2\text{Cl}_2 \cdot \text{C}_4\text{H}_{10}\text{O}$ (Figure 3.1). Selected bond lengths and angles can be found in Table 3.2. In the solid state, complex **3.1** features two dppmo ligands, a $[\text{OSiPh}_3]^-$ ligand, an $\eta^1\text{-OTf}$ ligand, and an $\eta^2\text{-OTf}$ ligand, in a bi-capped trigonal prismatic geometry, according to the continuous shape measure developed by Alvarez and co-workers (CSM = 1.91).¹⁸ The U- O_{Si} distance is $2.073(6)\text{ \AA}$,

which is comparable to other U(IV) silyloxide distances,⁹ including those of $\text{U}^{\text{IV}}(\text{OSiMe}_3)_2\text{I}_2(\text{bipy})_2$ (2.084(4) Å),¹⁵ $\text{U}^{\text{IV}}(\text{OSiEt}_3)_2(\text{Aracnac})_2$ (2.129(2) Å),¹⁰ and $\text{Cp}_3\text{U}^{\text{IV}}(\text{OSiPh}_3)$ (2.135(8) Å).¹⁹ The U-O distance of the η^1 -bound OTf moiety (2.391(7) Å) is similar to that of the uranyl starting material, $[\text{UO}_2(\text{dppmo})_2(\text{OTf})][\text{OTf}]$ (2.408(3) Å),¹⁷ while the U-O distances of the η^2 -bound OTf ligand (2.614(9) and 2.622(8) Å) are substantially longer. Finally, the average U-O_{dppmo} bond length (av. U-O = 2.35 Å) is similar to that of the uranyl starting material (av. U-O = 2.38 Å).¹⁷

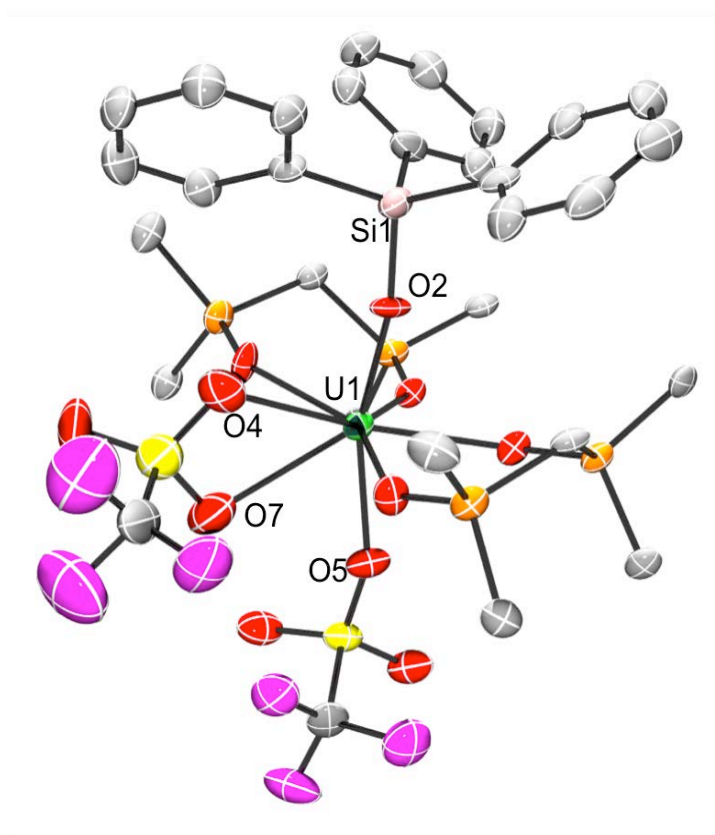


Figure 3.1. Solid-state structure of $[\text{U}^{\text{IV}}(\text{OSiPh}_3)(\text{dppmo})_2(\text{OTf})_2][\text{OTf}] \cdot 3\text{CH}_2\text{Cl}_2 \cdot \text{C}_4\text{H}_{10}\text{O}$ ($3.1 \cdot 3\text{CH}_2\text{Cl}_2 \cdot \text{C}_4\text{H}_{10}\text{O}$) with 50% probability ellipsoids. Solvates, hydrogen atoms, and the triflate counter ion have been removed for clarity. In addition, only the ipso carbons of the dppmo phenyl rings are shown for clarity.

Table 3.2. Selected Bond Lengths (Å) and Angles (deg) for Complexes **3.1** – **3.4**

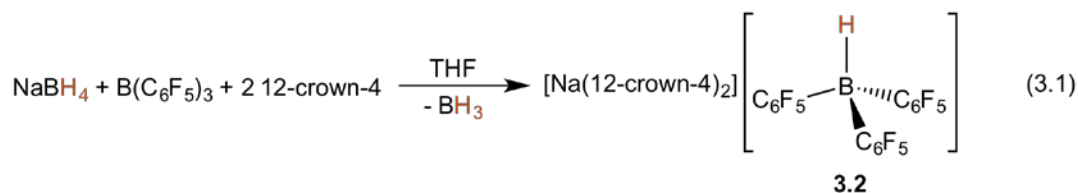
	3.1	3.3	3.4-pyr	3.5
U-O _{Si}	2.073(6)		2.125(3) 2.135(3)	
U-O _{OTf} (η^2)	2.614(9) 2.622(8)			
U-O _{OTf} (η^1)	2.391(7)	2.36(1) 2.36(1) 2.40(1) 2.44(1)		2.308(5) 2.312(4) 2.337(4) 2.340(4) 2.341(4)
U-O _{dppmo/TPPO}	2.341(6) 2.346(6) 2.354(6) 2.359(6)	2.27(2) 2.28(1) 2.30(2) 2.38(1)	2.352(3) 2.393(2) 2.394(3) 2.397(2)	2.186(4) 2.197(4)
O-Si	1.647(7)		1.634(3) 1.649(3)	
O _{Si} -U-O _{OTf}	163.2(3)			
O _{Si} -U-O _{Si}			159.0(1)	
U-O-Si	166.6(4)		168.0(2) 165.4(2)	

The ¹H NMR spectrum of **3.1** in CD₂Cl₂ consists of three sharp paramagnetically shifted resonances at 38.48, 12.69, and 11.82 ppm, which correspond to the *o*-, *m*-, and *p*-proton atoms of the Ph₃Si- group, respectively. Additionally, there are four resonances at 6.36, 5.90, -1.61, and -12.79 in a 2:4:4:1 ratio, corresponding to the various dppmo proton environments. The ¹⁹F{¹H} and ³¹P{¹H} resonances were presumably too broad to be observed.

3.2.1.2. Identification of [UO₂(dppmo)₂(OTf)][HB(C₆F₅)₃] and Ph₃SiOTf

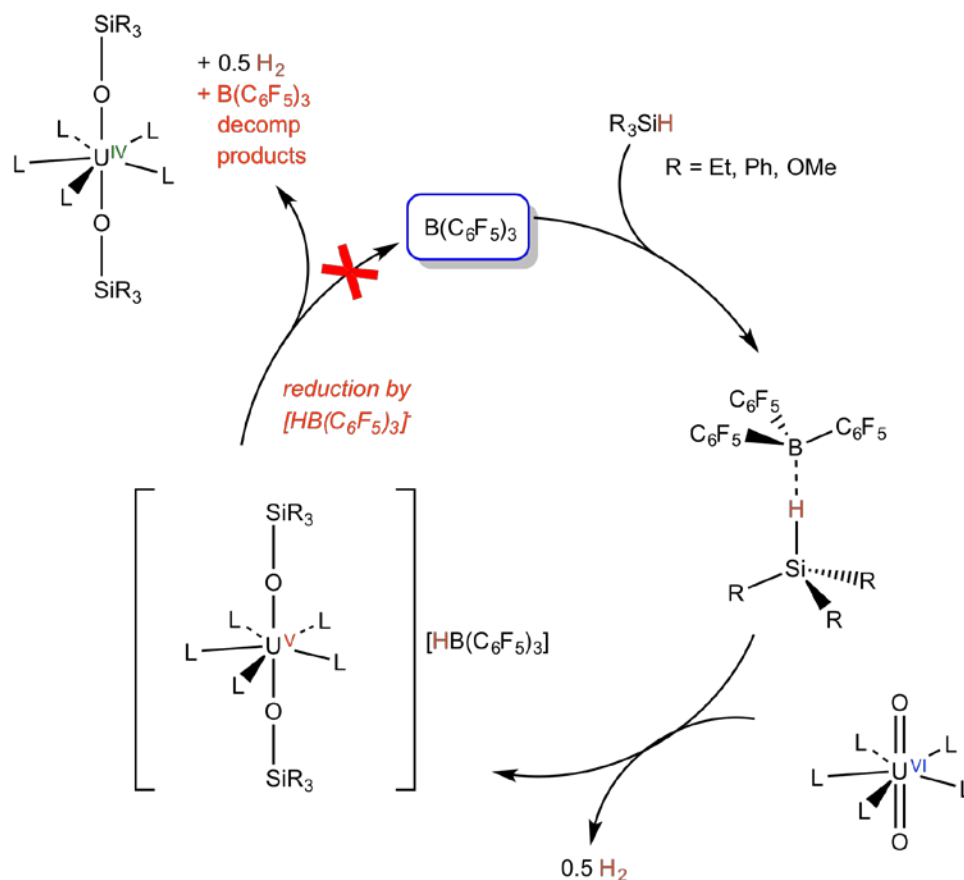
According to the *in situ* ¹H and ¹⁹F NMR spectra there is complete conversion of the uranium-containing material from [UO₂(dppmo)₂(OTf)][OTf] to complex **3.1**. However, we found that **3.1** is extremely difficult to isolate cleanly in high yields, due to the formation of numerous non-uranium containing side products. Therefore, we

wanted to investigate the mechanism of the transformation and identify as many of the side products as possible. In this regard, the synthesis of complex **3.1** was followed by NMR spectroscopy in TCE-*d*₂ (TCE = 1,1,2,2-tetrachloroethane). Immediately, at room temperature an anion exchange reaction is observed, as evidenced by the *in situ* ¹⁹F{¹H} NMR spectrum (Figure A.2), which exhibits three new fluorine resonances at -133.73, -163.66, and -166.65 ppm, corresponding to the presence of [HB(C₆F₅)₃]⁻.²⁰⁻²⁵ Additionally, there are two resonances at -77.36 ppm, corresponding to the OTf species in the newly proposed uranyl complex, [UO₂(dppmo)₂(OTf)][HB(C₆F₅)₃], and -76.71 ppm, corresponding to Ph₃SiOTf.²⁶ [HB(C₆F₅)₃]⁻ formation was further confirmed by studying the *in situ* ¹¹B NMR spectrum at room temperature, which features a broad singlet at -25.71 ppm, consistent with reported chemical shifts of [HB(C₆F₅)₃]⁻.²⁰⁻²⁵ To corroborate this assignment, we independently prepared the complex, [Na(12-crown-4)₂][HB(C₆F₅)₃] (**3.2**). Reaction of NaBH₄ and B(C₆F₅)₃ in the presence of 2 equiv of 12-crown-4, results in the formation of **3.2** as a white powder in 25% yield (eq 3.1). Complex **3.2** exhibits a boron resonance at -25.48 ppm (MeCN-*d*₃) in its ¹¹B NMR spectrum. These observations confirm that at room temperature, reaction of [UO₂(dppmo)₂(OTf)][OTf] with 2 equiv HSiPh₃ and 2 equiv B(C₆F₅)₃ results in the formation of [UO₂(dppmo)₂(OTf)][HB(C₆F₅)₃] and Ph₃SiOTf (Scheme 3.2). All attempts to crystallize [UO₂(dppmo)₂(OTf)][HB(C₆F₅)₃] were unsuccessful.



Once the reaction mixture to form **3.1** was heated for 72 h at 105 °C, another set of NMR spectra were collected. A number of $B(C_6F_5)_3$ decomposition products have been identified in the *in situ* $^{19}F\{^1H\}$ NMR spectrum (Figure A.3). For instance, the resonance at -169.50 ppm, corresponds to Ph_3SiF (literature values: -170.4 ppm in DME and -169.2 ppm in C_6D_6).^{27,28} In addition, the resonances at -138.37, -153.53, and -161.82 ppm have been assigned to pentafluorobenzene (literature values: -140.3, -155.3, -163.8 ppm in C_6D_{12}).²⁹ Lastly, we have also been able to assign the chemical shifts at -134.10, -163.98, and -166.98 ppm to $[B(C_6F_5)_4]^-$.^{30,31} The formation of $[B(C_6F_5)_4]^-$ was further confirmed by studying the *in situ* ^{11}B NMR spectrum after heating, which features a sharp singlet at -17.46 ppm.³¹ Clearly, $B(C_6F_5)_3$ is unstable under these reaction conditions. Moreover, we suggest that these decomposition products make the isolation of complex **3.1** particularly difficult.

Given these reaction intermediates, we hypothesized that Ph_3SiOTf was acting as the silylating reagent and $[HB(C_6F_5)_3]^-$ was acting as the reducing reagent in the reaction to form **3.1**. Since Ph_3SiOTf is required to form complex **3.1**, we decided to perform the same reaction to form **3.1** with 1 equiv of independently prepared Ph_3SiOTf . Thus, addition of 2 equiv of $HSiPh_3$, 2 equiv of $B(C_6F_5)_3$ and 1 equiv Ph_3SiOTf to $[UO_2(dppmo)_2(OTf)](OTf)$, results in the formation of a small amount of complex **3.1** at room temperature, however, the reaction still required heating to go to completion, and there appeared to be just as many by-products according to the *in situ* 1H and ^{19}F NMR spectra. Also, it is important to note that addition of 2 equiv Ph_3SiOTf to $[UO_2(dppmo)_2(OTf)](OTf)$, resulted in no reaction, demonstrating that Ph_3SiOTf alone cannot reductively silylate $[UO_2(dppmo)_2(OTf)](OTf)$.



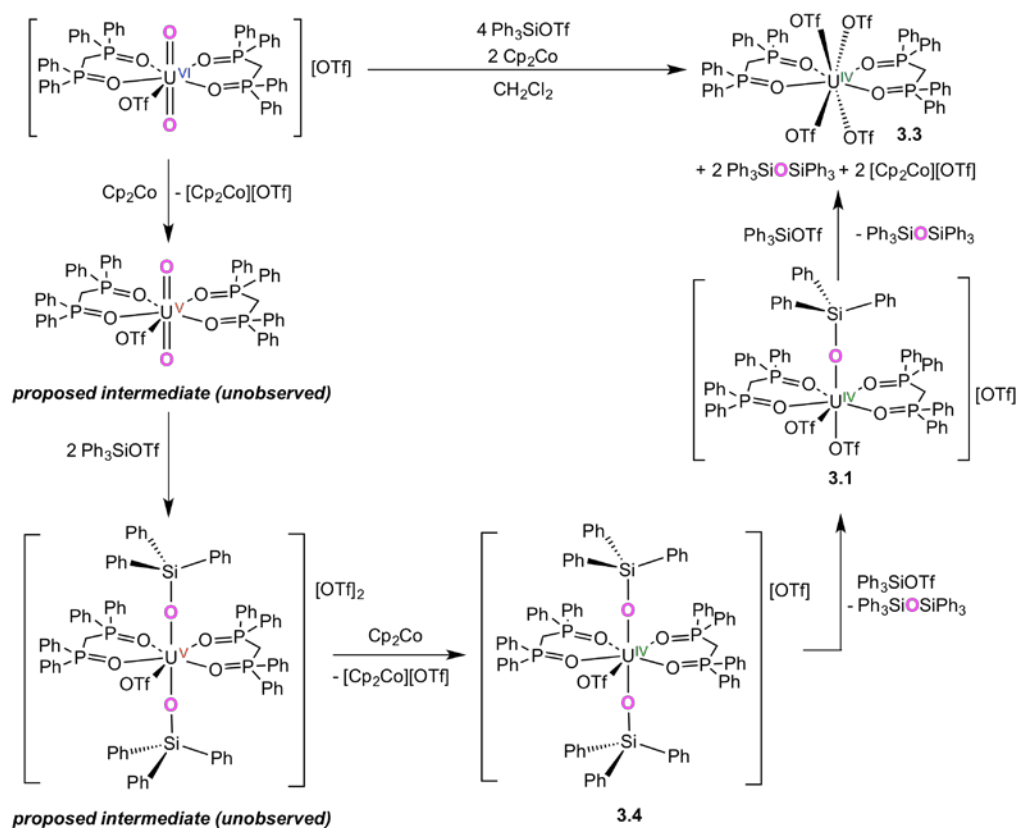
Scheme 3.3. Proposed catalytic cycle for reductive silylation of uranyl to U(IV).

Since B(C₆F₅)₃ is not stable at elevated temperatures (105 °C), it cannot be regenerated in the reaction to make **3.1**, and therefore cannot be used as a catalyst (Scheme 3.3). This work, and previous reports of uranyl reductive silylation using B(C₆F₅)₃,^{9,10} lead us to the conclusion that the activation barrier for the reduction of the U(V) disilyloxyde by [HB(C₆F₅)₃]⁻ is so high that overcoming it ultimately destroys the B(C₆F₅)₃ in the process. Accordingly, the next step was to find a reducing agent with a smaller activation barrier. We turned our attention to Cp₂Co, due to its previous success with reducing U(V) complexes to U(IV) complexes.^{9,10}

3.2.2. Reductive Silylation of $[\text{UO}_2(\text{dppmo})_2(\text{OTf})][\text{OTf}]$ and $[\text{UO}_2(\text{TPPO})_4][\text{OTf}]_2$ with Cp_2Co

3.2.2.1. Synthesis and Characterization of $\text{U}^{\text{IV}}(\text{OTf})_4(\text{dppmo})_2$ (**3.3**)

Gratifyingly, reaction of $[\text{UO}_2(\text{dppmo})_2(\text{OTf})][\text{OTf}]$ with 4 equiv of Ph_3SiOTf , in the presence of 2 equiv of Cp_2Co , results in a rapid reaction at room temperature, as evidenced by a color change from pale yellow to dark yellow-green. Work-up of the reaction mixture after 24 h results in the isolation of the U(IV) triflate complex, $\text{U}^{\text{IV}}(\text{OTf})_4(\text{dppmo})_2$ (**3.3**), as a lime green powder in an 83% yield (Scheme 3.4). Complex **3.3** is the result of complete oxo ligand removal from the uranyl ion, concomitant with a $2e^-$ reduction.



Scheme 3.4. Synthesis of complex **3.3** and the proposed mechanism for the formation of **3.3**.

Complex **3.3** co-crystallizes with 1 equiv of cobaltocenium triflate in the lattice as a toluene and hexane solvate, $[\mathbf{3.3}][\text{Cp}_2\text{Co}][\text{OTf}] \cdot 1.5\text{C}_7\text{H}_8 \cdot \text{C}_6\text{H}_{14}$. Its solid-state molecular structure is shown in Figure 3.2 and selected bond lengths and angles are collected in Table 3.2. The uranium center is coordinated by two dppmo ligands and four OTf ligands, and features a square antiprism geometry (CSM = 0.32),¹⁸ wherein the two square faces are defined by O1, O4, O7, and O8, and O2, O3, O5, and O6, respectively. The average U-O_{OTf} distance (av. U-O = 2.39 Å) in complex **3.3** is similar to other U(IV)-O_{OTf} distances,³²⁻³⁴ but is slightly longer than those observed in the structurally related complex, U^{IV}(OTf)₄(DME)₂ (av. U-O = 2.28 Å),³⁵ which is probably a result of the steric bulk of the dppmo ligands. In addition, the average U-O_{dppmo} bond length (av. U-O = 2.31 Å) is slightly shorter than the average U-O_{dppmo} distance in the uranyl starting material, [UO₂(dppmo)₂(OTf)][OTf] (av. U-O = 2.38 Å),¹⁷ but is similar to other U(IV) phosphine oxide complexes.³⁶⁻³⁸ Notably, there are only a few metal complexes in the literature with four coordinated OTf ligands,³⁹⁻⁴³ such as the neutral complexes, U^{IV}(OTf)₄(DME)₂, U^{IV}(OTf)₄(TPPO)₃,⁴⁴ and the chromium complex, [Cr(OTf)₄(C₆H₄{NH₂})₂],⁴⁵ as well as the anionic species [Fe(OTf)₄]²⁻,⁴⁶ [Na(OTf)₄]³⁻,⁴⁷ and [CpTi(OTf)₄]⁻.⁴⁸

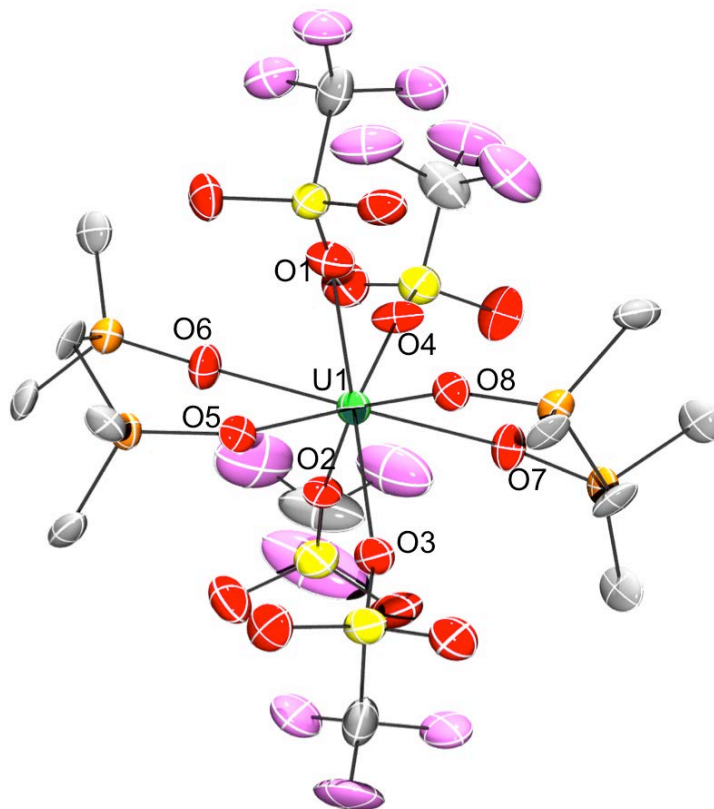


Figure 3.2. Solid-state structure of $[\text{U}^{\text{IV}}(\text{OTf})_4(\text{dppmo})_2][\text{Cp}_2\text{Co}][\text{OTf}] \cdot 1.5\text{C}_7\text{H}_8 \cdot \text{C}_6\text{H}_{14}$ (**[3.3]** $[\text{Cp}_2\text{Co}][\text{OTf}] \cdot 1.5\text{C}_7\text{H}_8 \cdot \text{C}_6\text{H}_{14}$) with 50% probability ellipsoids. All hydrogens, the co-crystallized cobaltocenium triflate, and the toluene and hexane solvates have been removed for clarity. In addition, only the ipso carbons of the dppmo phenyl rings are shown for clarity.

The ^1H NMR spectrum of complex **3.3** in CD_2Cl_2 exhibits a broad resonance at 32.75 ppm, corresponding to the γ -proton environment on the dppmo ligands. In addition, this spectrum features singlets at 15.25, 8.89, and 8.67 ppm, which correspond to the *o*-, *p*-, and *m*- resonances of the phenyl rings on the dppmo backbone, respectively. Finally, a singlet at 5.70 ppm is assignable to the co-crystallized $[\text{Cp}_2\text{Co}]^+$ moiety. The $^{19}\text{F}\{^1\text{H}\}$ NMR spectrum of **3.3** exhibits two extremely broad

resonances at -97.26 and -77.18 ppm, which can be attributed to the OTf environment in complex **3.3** and the OTf anion in $[\text{Cp}_2\text{Co}][\text{OTf}]$,⁴⁹ respectively. The broadness of these resonances is suggestive of exchange of the inner- and outer-sphere triflate moieties at a rate that is comparable to the NMR time scale. The $^{31}\text{P}\{^1\text{H}\}$ NMR spectrum of **3.3** does not feature any resonances, possibly because they are too broad to be observed. In addition, the near-IR spectrum for **3.3** is similar to those of other U(IV) complexes,^{9,10,50,51} supporting the presence of a $5f^2$ ion.

To better understand the mechanism of formation of complex **3.3**, and determine the fate of the “yl” oxygen atoms, we followed the reaction of $[\text{UO}_2(\text{dppmo})_2(\text{OTf})][\text{OTf}]$ with 4 equiv of Ph_3SiOTf and 2 equiv of Cp_2Co , in CD_2Cl_2 , by ^1H and $^{19}\text{F}\{^1\text{H}\}$ NMR spectroscopies. The ^1H NMR spectrum after 20 min reveals the formation of $[\text{Cp}_2\text{Co}]^+$, as evidenced by a resonance at 5.35 ppm,⁴⁹ as well as complex **3.1**, with the *ortho*-CH resonances of the $[\text{OSiPh}_3]^-$ ligand at 36.91 ppm (Figure A.4). In addition, two new uranium-containing intermediates are also present in the reaction mixture, as evidenced by the appearance of downfield resonances at 47.85 and 41.70 ppm, which we have assigned to the *ortho*-CH resonances of the $[\text{OSiPh}_3]^-$ ligand. We have tentatively assigned the resonance at 47.85 ppm to the U(IV) bis-silyloxy complex, $[\text{U}^{\text{IV}}(\text{OSiPh}_3)_2(\text{dppmo})_2(\text{OTf})][\text{OTf}]$ (**3.4**) (see below). Complexes **3.1** and **3.4** are likely intermediates formed along the reaction pathway to **3.3**, which is not present in the reaction mixture at these short reaction times. Consistent with this hypothesis, the ^1H NMR spectrum of the reaction mixture after 2 h reveals the complete disappearance **3.4**, the continued presence of **3.1**, and the appearance of complex **3.3**, as evidenced by the observation of a broad resonance at 33.41 ppm, which is

assignable to the γ -CH₂ environment of the dppmo ligand (Figure A.4). After 24 h, the ¹H NMR spectrum of the reaction mixture reveals the complete disappearance of complex **3.1**, along with the expected presence of complex **3.3** (Figure A.4). Interestingly, complex **3.3** is not very soluble under these conditions and it partially precipitates from solution. The *in situ* ¹⁹F{¹H} NMR spectra are consistent with this reaction sequence. For example, the *in situ* ¹⁹F{¹H} NMR spectrum after 20 min reveals the presence of outer sphere [OTf]⁻, along with a resonance at -114.19 ppm, which we have tentatively assigned to the OTf environment of complex **3.4**. After 2 h, this resonance disappears, concomitant with the appearance of a new resonance 97.24 ppm, which is assignable to complex **3.3**. Finally, a ²⁹Si{¹H} NMR spectrum of the reaction mixture, in TCE-*d*₂ (TCE = 1,1,2,2-tetrachloroethane), consists of a singlet at -17.83 ppm, which is assignable to Ph₃SiOSiPh₃,⁵² confirming the final fate of the uranyl oxo ligands.

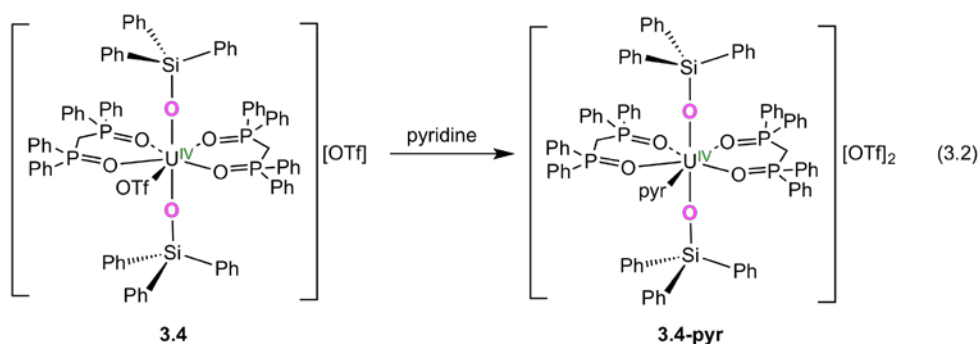
Interestingly, addition of 2 equiv of Cp₂Co to a solution of [UO₂(dppmo)₂(OTf)][OTf] results in the consumption of the uranyl starting material and the formation of free dppmo and [Cp₂Co][OTf]; however, we have been unable to identify the uranium-containing products of this reaction. Moreover, addition of 1 equiv of Cp₂Co to Ph₃SiOTf in CD₂Cl₂ results in no reaction over the course of 30 min. When combined with the knowledge that [UO₂(dppmo)₂(OTf)][OTf] does not react with Ph₃SiOTf, these experiments reveal the synergistic relationship between Cp₂Co and Ph₃SiOTf that is required to form **3.3**. To explain these observations, and rationalize the observed *in situ* NMR spectra, we postulate that **3.3** is formed via a series of intermediate steps (Scheme 3.4). First, Cp₂Co reduces

[UO₂(dppmo)₂(OTf)][OTf], transiently forming U^VO₂(dppmo)₂(OTf), which is then captured by 2 equiv of Ph₃SiOTf to form a U(V) bis(silyloxy) intermediate. In the absence of Ph₃SiOTf, U^VO₂(dppmo)₂(OTf) likely decomposes, as evidenced by the formation of free dppmo in the reaction of [UO₂(dppmo)₂(OTf)][OTf] with 2 equiv of Cp₂Co. The U(V) bis(silyloxy) intermediate subsequently reacts with a further equivalent of Cp₂Co to generate the complex **3.4** and [Cp₂Co][OTf]. Complex **3.4** then reacts with a third equiv of Ph₃SiOTf, to generate complex **3.1** and 1 equiv of Ph₃SiOSiPh₃, whereupon complex **3.1** reacts with the final equiv of Ph₃SiOTf, to afford complex **3.3** and the second equiv of Ph₃SiOSiPh₃. Most importantly, the reduction of [UO₂(dppmo)₂(OTf)][OTf] to a neutral U(V) complex should render the uranyl oxo ligands more nucleophilic, which nicely rationalizes why Ph₃SiOTf is an ineffective silylating reagent in the absence of Cp₂Co.

3.2.2.2. Synthesis and Characterization of [U^{IV}(OSiPh₃)₂(dppmo)₂(OTf)][OTf] (3.4)

In an attempt to isolate the hypothesized U(IV) silyloxy intermediates, and buttress the proposed mechanism, the reaction of [UO₂(dppmo)₂(OTf)][OTf] with 2 equiv of Ph₃SiOTf and 2 equiv of Cp₂Co was stirred at room temperature for 2 h. Work-up of this reaction mixture results in isolation of a light green solid that contained the U(IV) bis-silyloxy complex, [U^{IV}(OSiPh₃)₂(dppmo)₂(OTf)][OTf] (**3.4**), complex **3.1** and [Cp₂Co][OTf], in a 2:1:3 ratio, respectively, as determined by ¹H and ¹⁹F NMR spectroscopies. Notably, complex **3.3** was not formed in this reaction, according to a ¹H NMR spectrum of the reaction mixture, which may be a function of the insufficient

amount of Ph₃SiOTf and shorter reaction time. Recrystallization of this mixture from pyridine layered with Et₂O, afforded yellow crystals of [U^{IV}(OSiPh₃)₂(dppmo)₂(pyr)][OTf]₂ (**3.4-pyr**). Exposure of **3.4** to pyridine likely displaces the inner-sphere triflate moiety in favor of the coordinated pyridine solvate (eq 3.2).



Complex **3.4-pyr** crystallizes in the monoclinic space group $P2_1/c$, as the pyridine and Et₂O solvate, **3.4-pyr**·2C₅H₅N·C₄H₁₀O (Figure 3.3). Selected bond lengths and angles can be found in Table 3.2. Complex **3.4-pyr** features a capped trigonal prism geometry (CSM = 1.49),¹⁸ wherein the two dppmo ligands and the two [OSiPh₃]⁻ ligands define the trigonal prism and the coordinated pyridine solvate forms the capping group. The two U-O_{Si} distances are 2.125(3) and 2.135(3) Å, which are comparable to complex **3.1** (2.073(6) Å), and other U(IV) silyloxide distances.^{9,10,15,19} The average U-O_{dppmo} bond length (av. U-O = 2.384 Å) is similar to complex **3.1** and the uranyl starting material (av. U-O = 2.38 Å).¹⁷

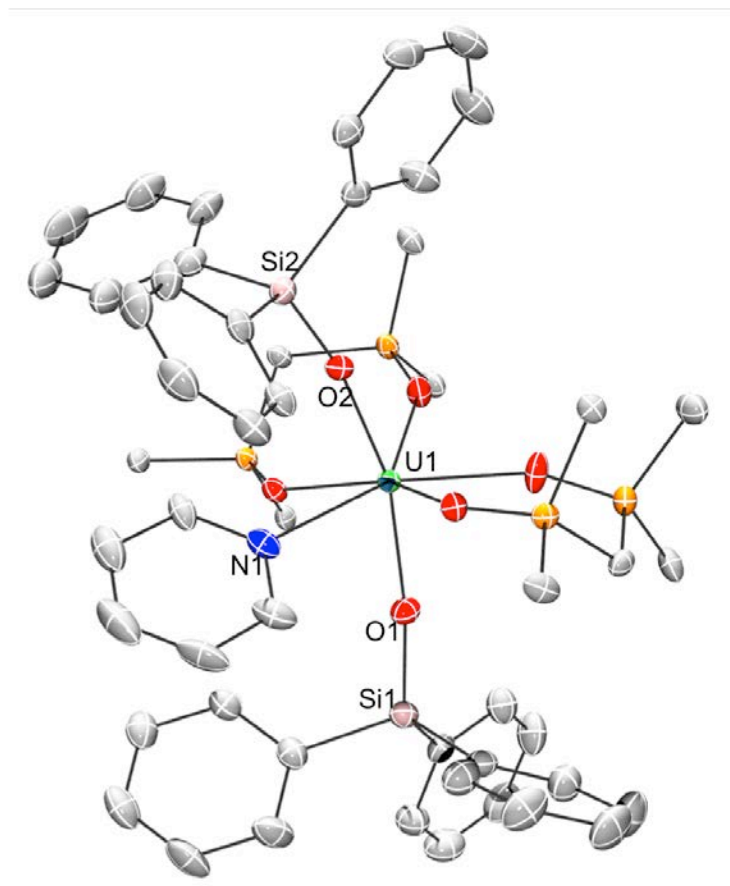
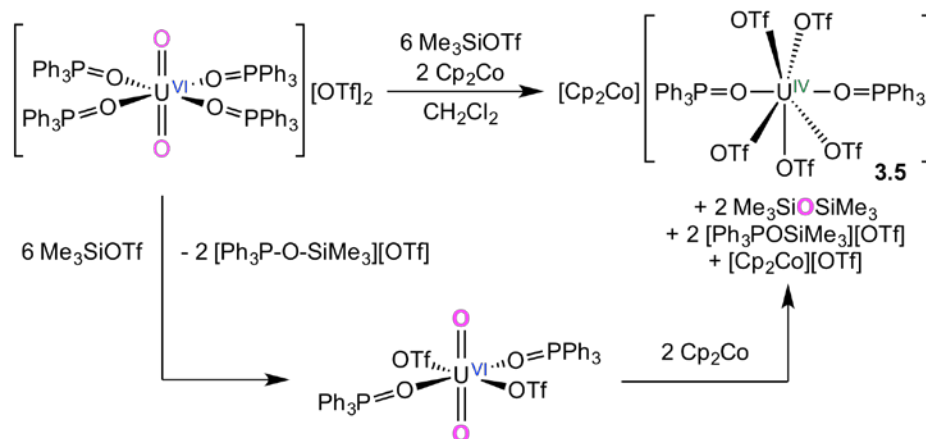


Figure 3.3. Solid-state structure of $[\text{U}^{\text{IV}}(\text{OSiPh}_3)_2(\text{dppmo})_2(\text{pyr})][\text{OTf}]_2 \cdot 2\text{C}_5\text{H}_5\text{N} \cdot \text{C}_4\text{H}_{10}\text{O}$ (**[3.4-pyr]**· $2\text{C}_5\text{H}_5\text{N} \cdot \text{C}_4\text{H}_{10}\text{O}$) with 50% probability ellipsoids. Solvates, all hydrogens, and the triflate counterions have been removed for clarity. In addition, only the ipso carbons of the dppmo phenyl rings are shown for clarity.

The ^1H NMR spectrum of **3.4-pyr** in CD_2Cl_2 consists of three broad paramagnetically shifted resonances at 48.01, 14.90, and 13.61 ppm, which correspond to the *o*-, *m*-, and *p*-proton atoms of the Ph_3Si - groups, respectively. Additionally, there are four resonances at 4.00, 3.17, -11.81, and -17.31 ppm in a 1:4:2:4 ratio, corresponding to the various dppmo proton environments. The coordinated pyridine resonances were not observed, possibly due to overlap with the uncoordinated

pyridine solvent resonances. Surprisingly, the $^{19}\text{F}\{^1\text{H}\}$ NMR spectrum features two broad resonances at -81.21 and -113.72 ppm in a 3:1 ratio, respectively. We tentatively, assign the former resonance the outer sphere OTf anions, while the latter resonance is likely due to a uranium-coordinated OTf ligand. To explain this result, we suggest that complex **3.4-pyr** undergoes partial $[\text{OTf}]^-$ association in solution, to form a mixture of **3.4** and **3.4-pyr**.

3.2.2.3. Synthesis and Characterization of $[\text{Cp}_2\text{Co}][\text{U}^{\text{IV}}(\text{OTf})_5(\text{TPPO})_2]$ (**3.5**)



Scheme 3.5. Synthesis of complex **3.5**.

To further our insight into the reductive silylation of cationic uranyl complexes, we attempted the reductive silylation of $[\text{UO}_2(\text{TPPO})_4][\text{OTf}]_2$. This complex features a $\text{U}=\text{O}$ ν_{sym} value of 839 cm^{-1} in its Raman spectrum (Figure 3.4), which is comparable to that of $[\text{UO}_2(\text{dppmo})_2(\text{OTf})][\text{OTf}]$ (849 cm^{-1}), suggesting that it is a similarly difficult substrate for the reductive silylation reaction. Thus, addition of 6 equiv of Me_3SiOTf and 2 equiv of Cp_2Co to a cold CH_2Cl_2 solution of $[\text{UO}_2(\text{TPPO})_4][\text{OTf}]_2$ results in

formation of $[\text{Cp}_2\text{Co}][\text{U}^{\text{IV}}(\text{OTf})_5(\text{TPPO})_2]$ (**3.5**), which can be isolated as a yellow-green crystalline material in a 76% yield (Scheme 3.5). Also formed in this reaction are $\text{Me}_3\text{SiOSiMe}_3$ ⁵³ and $[\text{Ph}_3\text{POSiMe}_3][\text{OTf}]$,⁵⁴⁻⁵⁶ according to the $^{29}\text{Si}\{^1\text{H}\}$ and $^{31}\text{P}\{^1\text{H}\}$ NMR spectra of the reaction mixture. Interestingly, the reagents must be cooled to $-25\text{ }^\circ\text{C}$ before the reaction, otherwise significant amounts of intractable black precipitate (possibly UO_2) are formed instead. Complex **3.5** can also be formed by addition of 6 equiv of Ph_3SiOTf , and 2 equiv of Cp_2Co , to $[\text{UO}_2(\text{TPPO})_4][\text{OTf}]_2$; however, the by-products formed in this case proved difficult to separate from complex **3.5**. Importantly, reaction of $[\text{UO}_2(\text{TPPO})_4][\text{OTf}]_2$ with only Me_3SiOTf results in formation of $[\text{Ph}_3\text{POSiMe}_3][\text{OTf}]$ and $\text{UO}_2(\text{OTf})_2(\text{TPPO})_2$, but does not result in any oxo ligand silylation. (Yellow block crystals of $\text{UO}_2(\text{OTf})_2(\text{TPPO})_2$ were isolated once from the reaction mixture and characterized by X-ray crystallography; however, they were very disordered and only connectivity was determined.) In addition, reaction of $[\text{UO}_2(\text{TPPO})_4][\text{OTf}]_2$ with only Cp_2Co results in a slow transformation, similar to that observed between $[\text{UO}_2(\text{dppmo})_2(\text{OTf})][\text{OTf}]$ and Cp_2Co , while no reaction is observed between Me_3SiOTf and Cp_2Co . Overall, these data point to a synergistic relationship between Me_3SiOTf and Cp_2Co during the conversion of uranyl to U(IV), similar to that observed during formation of **3.3**.

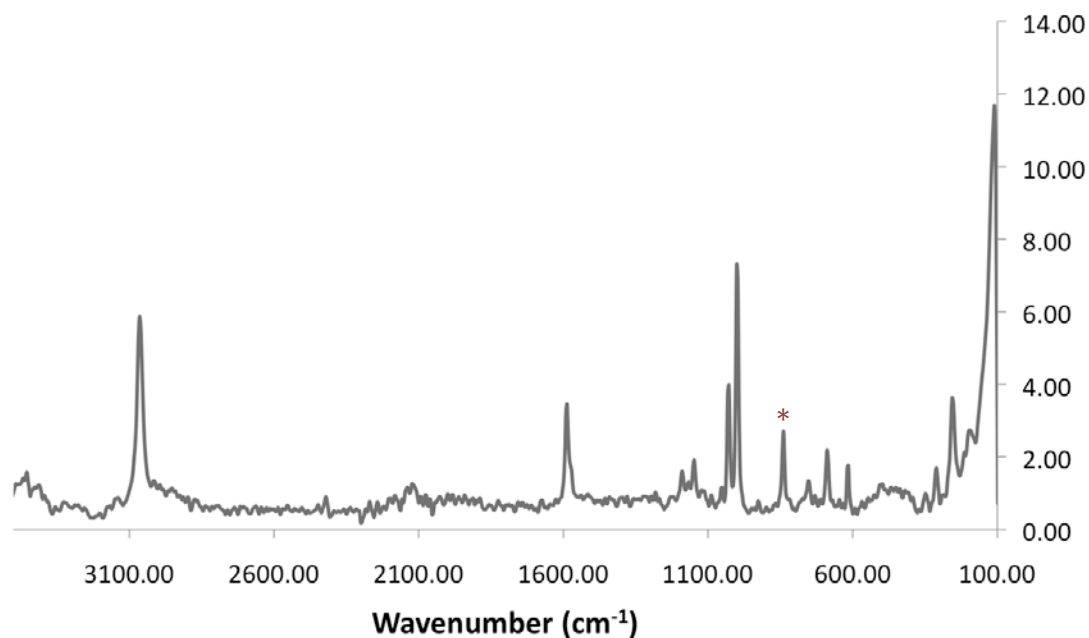


Figure 3.4. Solid state Raman spectrum of $[\text{UO}_2(\text{TPPO})_4][\text{OTf}]_2$. U=O ν_{sym} stretch is observed at 839 cm^{-1} (*).

Complex **3.5** crystallizes in the monoclinic space group $P2_1/c$ as a discrete cation/anion pair. Its solid-state molecular structure is shown in Figure 3.5 and selected bond lengths and angles are collected in Table 3.2. The U(IV) center in **3.5** features a pentagonal bipyramidal (CSM = 1.74) geometry,¹⁸ wherein two TPPO ligands occupy the axial positions and the five η^1 -OTf ligands occupy the equatorial plane. To our knowledge, complex **3.5** is the only crystallographically characterized metal complex with five coordinated OTf ligands; however, three crystal structures of metal complexes with six coordinated OTf ligands have been determined, including: the anionic Th(IV) complex, $[\text{Th}^{\text{IV}}(\text{H}_2\text{O})_3(\text{OTf})_6]^{2-}$,⁵⁷ and the two examples of the Y(III) hexatriflate anion, $[\text{C}_4\text{mpyr}]_3[\text{Yb}^{\text{III}}(\text{OTf})_6]$ and $[\text{C}_4\text{mpyr}]_4[\text{Yb}^{\text{III}}(\text{OTf})_6][\text{Tf}_2\text{N}]$.⁵⁸ The average U-O_{OTf} distance (av. U-O = 2.33 Å) in complex **3.5** is typical of those in other

U(IV)-triflate complexes,³²⁻³⁴ but is slightly shorter than those seen in complex **3.3**, which we attribute to the reduced steric bulk of TPPO vs. dppmo. In addition, the two U-O_{TPPO} bond lengths (2.186(4) and 2.197(4) Å) are both shorter than the U-O_{dppmo} distance observed for **3.3**, which is also consistent with the reduced steric profile of TPPO vs. dppmo.

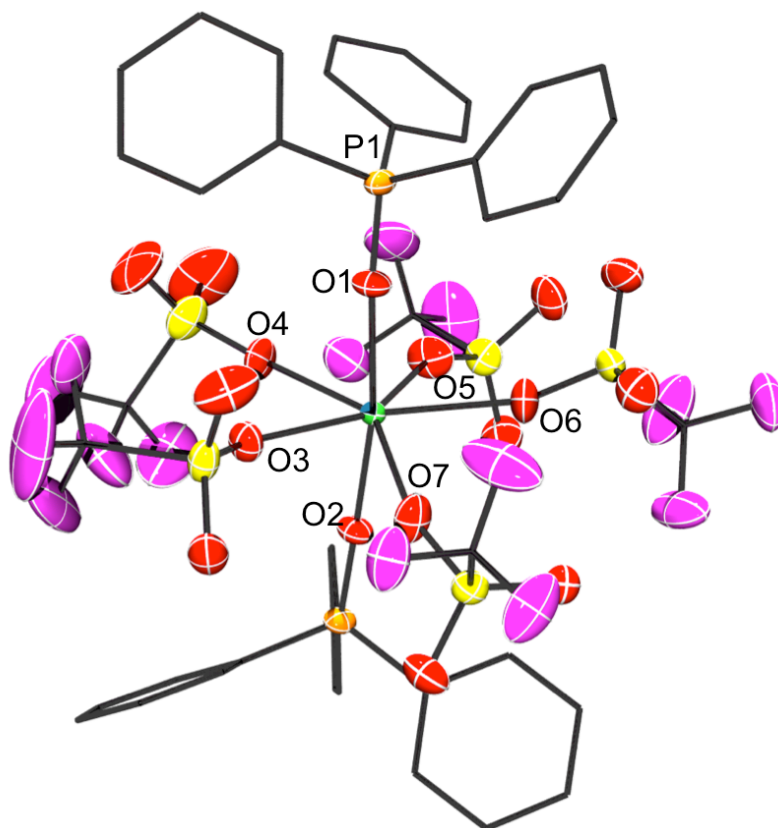
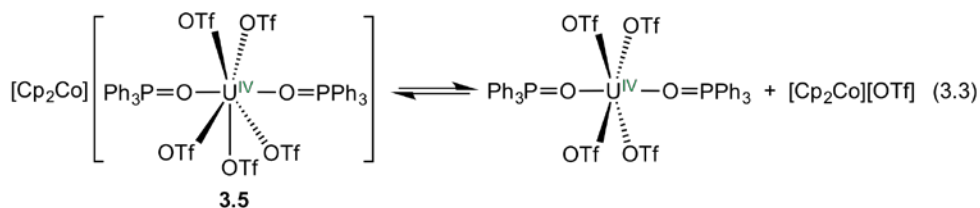


Figure 3.5. Solid-state structure of [Cp₂Co][U^{IV}(OTf)₅(TPPO)₂] (**3.5**) with 50% probability ellipsoids of the heteroatoms. All hydrogen atoms and the cobaltocenium cation have been removed for clarity.

The ¹H NMR spectrum of **3.5** at room temperature consists of three broad resonances at 31.66, 12.04, and 11.16 ppm, assignable to the *o*-, *m*-, and *p*-phenyl

protons of the TPPO ligand, respectively. In addition, this spectrum also features a sharp resonance at 5.70 ppm, which is assignable to the $[\text{Cp}_2\text{Co}]^+$ counterion.⁴⁹ Surprisingly, the room temperature $^{19}\text{F}\{^1\text{H}\}$ NMR spectrum of **3.5** features two very broad resonances at -79.06 and -101.02 ppm. We tentatively, assign the former resonance to an outer sphere OTf anion, while the latter resonance is likely due to a uranium-coordinated OTf ligand. To explain this result, we suggest that complex **3.5** undergoes partial $[\text{OTf}]^-$ dissociation in solution, to form a mixture of **3.5**, $\text{U}^{\text{IV}}(\text{OTf})_4(\text{TPPO})_2$ and $[\text{Cp}_2\text{Co}][\text{OTf}]$ (eq 3.3). Finally, the near-IR spectrum for **3.5** is similar to those of other U(IV) complexes,^{9,10,50,51} supporting the presence of an $5f^2$ ion.

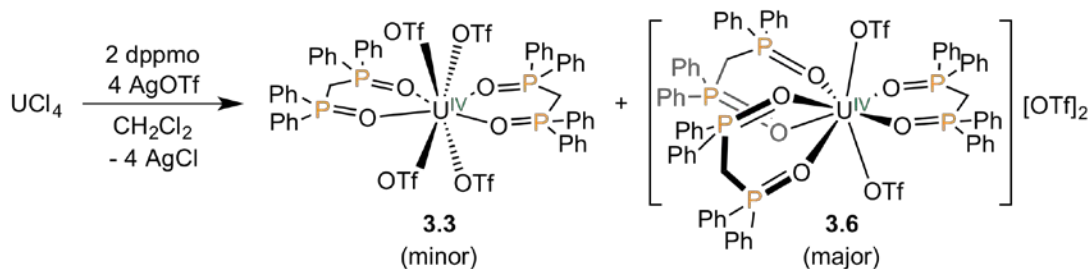


3.2.3 Synthesis of U(IV) Triflate Complexes from U(IV)Cl₄

3.2.3.1 Synthesis and Characterization of $[\text{U}^{\text{IV}}(\text{OTf})_2(\text{dppmo})_3][\text{OTf}]_2$ (**3.6**)

As part of these investigations, we endeavored to synthesize complex **3.3** from an alternative route. Thus, the addition of 2 equiv of dppmo to UCl_4 in CH_2Cl_2 , followed by addition of 4 equiv of AgOTf (as a solid), results in formation of a green solution after 24 h, from which a pale green solid can be isolated. Analysis of the solid by ^1H and $^{19}\text{F}\{^1\text{H}\}$ NMR spectroscopies, revealed a mixture of complex **3.3** and a new paramagnetic uranium containing product in about a 1:2.7 ratio. Pale green plate crystals of just the new uranium-containing product, $[\text{U}^{\text{IV}}(\text{OTf})_2(\text{dppmo})_3][\text{OTf}]_2$ (**3.6**),

were isolated from the mother liquor in 27% yield (Scheme 3.6). We hypothesized that formation of complex **3.6** was favored over complex **3.3**, due to the order of reagent addition (i.e. dppmo is added first). However, attempts to reverse the order of operations by first isolating the U(IV) complex, $U^{IV}(OTf)_4(solv)_x$, before dppmo addition, were unsuccessful.



Scheme 3.6. Synthesis of complex **3.6**.

Complex **3.6** crystallizes in the triclinic space group $P-1$, as the dichloromethane solvate, $3.6 \cdot 4CH_2Cl_2$, with two independent molecules in the asymmetric unit (Figure 3.6). The uranium ion in complex **3.6** is coordinated by three dppmo ligands and two η^1 -OTf ligands. Complex **3.6** features a square antiprism geometry (CSM = 0.28),¹⁸ wherein the two square faces are defined by O1, O3, O4, and O7, and O2, O5, O6, and O8, respectively. The average U-O_{OTf} bond length (av. U-O = 2.41 Å) is comparable to complexes **3.1**, **3.3**, and **3.5**. The average U-O_{dppmo} bond length (av. U-O = 2.35 Å) is comparable to complex **3.3** (av. U-O = 2.31 Å).

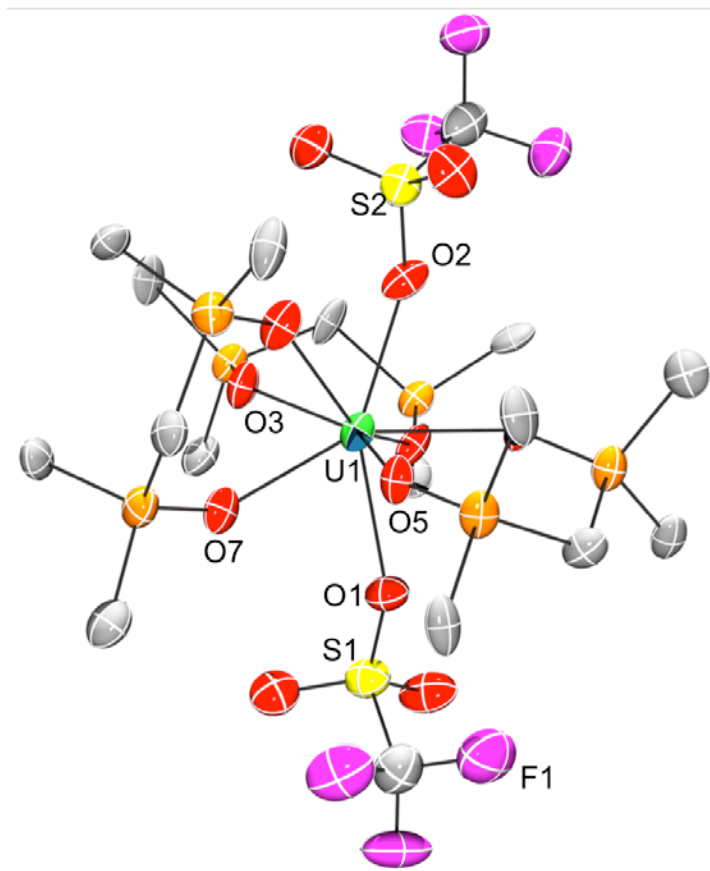


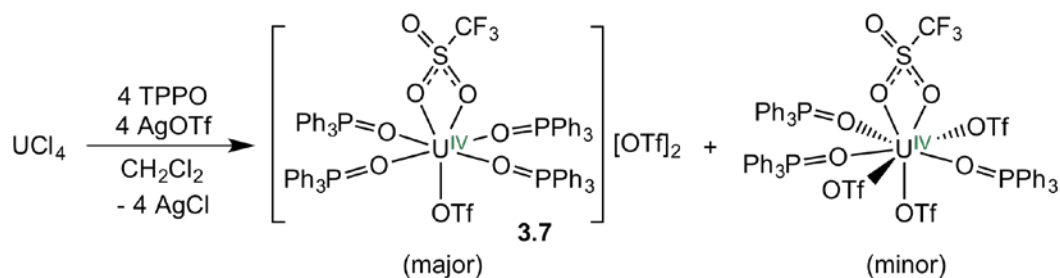
Figure 3.6. Solid-state structure of $[\text{U}^{\text{IV}}(\text{OTf})_2(\text{dppmo})_3][\text{OTf}]_2 \cdot 4\text{CH}_2\text{Cl}_2$ (**3.6**·4 CH_2Cl_2) with 50% probability ellipsoids. Complex **3.6** crystallizes with two independent molecules in the asymmetric unit; only one is pictured here. Solvate molecules, hydrogen atoms, and the triflate counterions, have been removed for clarity. In addition, only the ipso carbons of the dppmo phenyl rings are shown for clarity. Selected bond lengths (Å) and angles (°): U1-O1 = 2.42(1), U1-O2 = 2.40(1), U1-O3 = 2.37(1), U1-O4 = 2.364(9), U1-O5 = 2.36(1), U1-O6 = 2.332(9), U1-O7 = 2.36(1), U1-O8 = 2.31(1), O1-U1-O2 = 145.9(3).

The ^1H NMR spectrum of complex **3.6** in CD_2Cl_2 features three broad singlet resonances at 11.07, 8.15, and 7.85 correspond to the to the *o*-, *p*-, and *m*-phenyl

protons of the dppmo ligands. Interestingly, the CH₂ resonance on the backbone of the dppmo ligands is presumably too broad to be observed. The ¹⁹F{¹H} NMR spectrum of **3.6** in CD₂Cl₂ features two resonances at -77.93 and -96.59 ppm, corresponding to the outer sphere triflates and inner sphere triflates, respectively.

3.2.3.2 Synthesis, Characterization and Reactivity of [U^{IV}(OTf)₂(TPPO)₄][OTf]₂ (**3.7**)

We also made an effort to synthesize a U(IV) triflate complex from the U(IV) starting material, UCl₄, using the TPPO ligand. The reaction of UCl₄ with 4 equiv of TPPO and 4 equiv of AgOTf in dichloromethane results in formation of a teal solution, from which the U(IV) complex, [U^{IV}(OTf)₂(TPPO)₄][OTf]₂ (**3.7**), can be isolated as pale green block crystals in a 72% yield (Scheme 3.7). There is also a small amount of the U(IV) complex, U^{IV}(OTf)₄(TPPO)₃, formed during this reaction. The impurity, U^{IV}(OTf)₄(TPPO)₃, has been previously synthesized by Ephritikhine and co-workers,⁴⁴ and was identified by its ¹H resonances (see below). It is important to note that recrystallization of the mixture of **3.7** and U^{IV}(OTf)₄(TPPO)₃ with excess TPPO results in the formation of **3.7** without the U^{IV}(OTf)₄(TPPO)₃ impurity, however, the excess TPPO cannot be removed.



Scheme 3.7. Synthesis of complex **3.7**.

Complex **3.7** crystallizes in the monoclinic space group $P2_1/n$, as the dichloromethane solvate, **3.7**·CH₂Cl₂ (Figure 3.7). Complex **3.7** features two inner-sphere OTf ligands, where one is bound in an η^2 -fashion. The geometry about the seven-coordinate uranium center could be described as a pentagonal bipyramid (CSM = 2.30),¹⁸ or a capped trigonal prism (CSM = 2.39). The U-O_{OTf} bond distance of the η^1 -OTf ligand is 2.298(2) Å, which is comparable to complex **3.5**, and other U(IV)-O_{OTf} bond distances,³²⁻³⁴ but slightly shorter than the U-O_{OTf} bond lengths in the complex, U^{IV}(OTf)₄(TPPO)₃ (av. U-O = 2.40 Å).⁴⁴ The U-O_{OTf} bond distances of the η^2 -OTf ligand (2.553(2) and 2.527(2) Å) are significantly longer, and closer to the U-O_{OTf} distances of the η^2 -OTf ligand in complex, U^{IV}(OTf)₄(TPPO)₃ (2.563(3) and 2.593(3) Å),⁴⁴ and complex **3.1** (2.614(9) and 2.622(8) Å). In addition, the average U-O_{TPPO} bond length (av. U-O = 2.23 Å) is comparable to the U-O_{TPPO} distances in complex **3.5**.

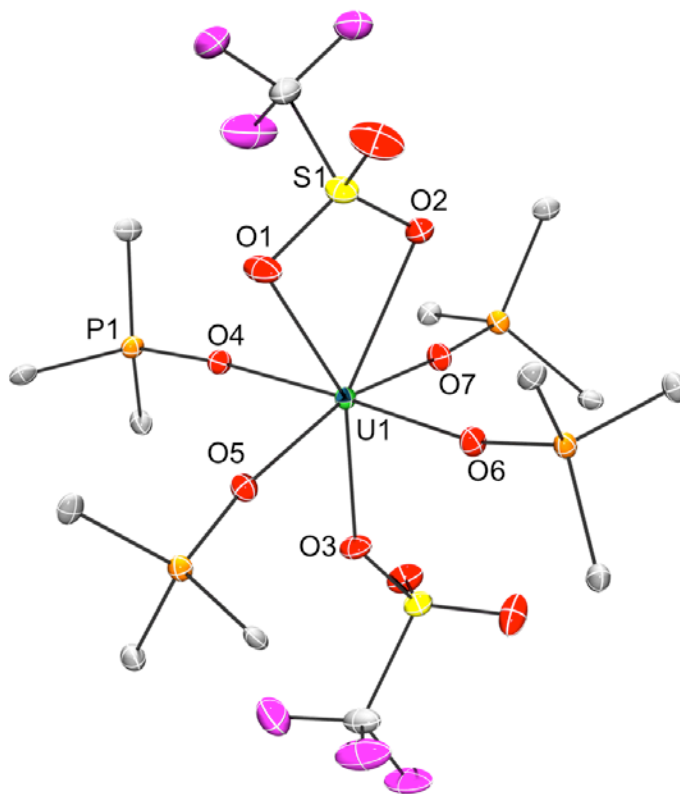
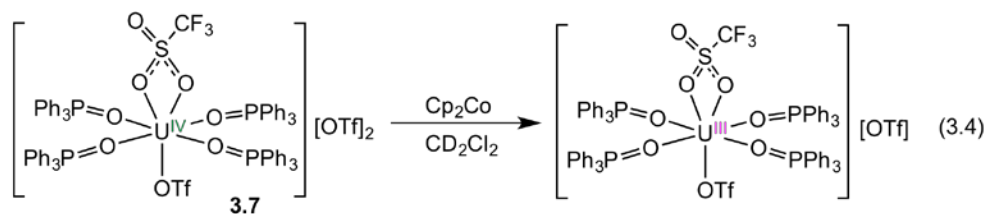


Figure 3.7. Solid-state structure of $[\text{U}^{\text{IV}}(\text{OTf})_2(\text{TPPO})_4][\text{OTf}]_2 \cdot \text{CH}_2\text{Cl}_2$ (**3.7**· CH_2Cl_2) with 50% probability ellipsoids of the heteroatoms. All hydrogen atoms, and the triflate counterions have been removed for clarity. In addition, only the ipso carbons of the TPPO phenyl rings are shown for clarity. Selected bond lengths (\AA) and angles ($^\circ$): U1-O1 = 2.553(2), U1-O2 = 2.527(2), U1-O3 = 2.298(2), U1-O4 = 2.219(2), U1-O5 = 2.240(2), U1-O6 = 2.215(2), U1-O7 = 2.244(2), O1-U1-O3 = 152.58(6), O2-U1-O3 = 151.69(6).

The ^1H NMR spectrum of complex **3.7** in CD_2Cl_2 reveals three paramagnetically shifted resonances at 11.29, 8.41, and 8.15 ppm, which correspond to the *o*-, *p*-, and *m*-phenyl protons of the TPPO ligands. There are also some small resonances at 26.55, 11.00, 10.47, 6.28, and -2.25, which are assignable to the complex, $\text{U}^{\text{IV}}(\text{OTf})_4(\text{TPPO})_3$.⁴⁴

The $^{19}\text{F}\{^1\text{H}\}$ NMR spectrum of **3.7** in CD_2Cl_2 features two resonances at -78.37 and -95.82 ppm, corresponding to the outer sphere triflates and inner sphere triflates, respectively. Only one inner sphere triflate resonance, at room temperature, indicates that the η^1 - and η^2 -OTf ligands exhibit the same chemical environment in solution. The $^{31}\text{P}\{^1\text{H}\}$ NMR spectrum in CD_2Cl_2 only exhibits one resonance at 33.88 ppm.



We also explored the reactivity of **3.7** with Cp_2Co (eq 3.4). Thus, the reaction of **3.7** and 1 equiv of Cp_2Co in CD_2Cl_2 was followed by ^1H and $^{19}\text{F}\{^1\text{H}\}$ NMR spectroscopies. After 10 min, the solution is an intense cherry red color, and the ^1H NMR spectrum reveals the formation of the expected U(III) complex, $[\text{U}^{\text{III}}(\text{OTf})_2(\text{TPPO})_4][\text{OTf}]$, as evidenced by three resonances at 12.58, 8.46, and 8.05 ppm,⁵⁹ as well as $[\text{Cp}_2\text{Co}][\text{OTf}]$, with a broad singlet resonance at -13.88 ppm. The U(III) complex, $[\text{U}^{\text{III}}(\text{OTf})_2(\text{TPPO})_4][\text{OTf}]$, has been previously synthesized by Ephritikhine and co-workers.⁵⁹

3.3 Summary

In summary, reaction of $[\text{UO}_2(\text{dppmo})_2(\text{OTf})][\text{OTf}]$ with 2 equiv of Ph_3SiH and 2 equiv of $\text{B}(\text{C}_6\text{F}_5)_3$ at 105 °C for 72 h, results in the formation of $[\text{U}^{\text{IV}}(\text{OSiPh}_3)(\text{dppmo})_2(\text{OTf})_2][\text{OTf}]$ (**3.1**) and $\text{B}(\text{C}_6\text{F}_5)_3$ decomposition products. Since $\text{B}(\text{C}_6\text{F}_5)_3$ is not

stable under these reaction conditions, we decided that $B(C_6F_5)_3$ will not be a useful catalyst for uranyl reductive silylation (Scheme 3.3). Thus, we focused our efforts on a different reducing agent, Cp_2Co .

The reaction of $[UO_2(dppmo)_2(OTf)][OTf]$ with 4 equiv of Ph_3SiOTf and 2 equiv of Cp_2Co , generates the U(IV) complex, $U^{IV}(OTf)_4(dppmo)_2$ (**3.3**). Also formed in this reaction is $Ph_3SiOSiPh_3$, which is the product of oxo ligand silylation. We were able to isolate two U(IV) silyloxy intermediates from the reaction mixture, complex **3.1** and $[U^{IV}(OSiPh_3)_2(dppmo)_2(OTf)][OTf]$ (**3.4**), which gives insight into the reaction mechanism for the formation of **3.3**, i.e. the reaction is proceeding step-wise through silyloxy intermediates. Similarly, reaction of $[UO_2(TPPO)_4][OTf]_2$ with 6 equiv of Me_3SiOTf and 2 equiv Cp_2Co , generates the U(IV) complex, $[Cp_2Co][U^{IV}(OTf)_5(TPPO)_2]$ (**3.5**), along with $Me_3SiOSiMe_3$. The formation of complexes **3.3** and **3.5** represent rare examples of uranyl oxo ligand substitution, as well as novel examples of one-pot reductions of uranyl to U(IV), at ambient temperatures and pressures. Interestingly, neither Ph_3SiOTf nor Me_3SiOTf alone are capable of reductively silylating $[UO_2(dppmo)_2(OTf)][OTf]$ or $[UO_2(TPPO)_4][OTf]_2$. Instead, these reagents required the aid of an external reductant, namely, Cp_2Co . This synergistic relationship between Cp_2Co and R_3SiOTf makes it possible to perform reductive silylation on more challenging uranyl substrates, such as cationic uranyl complexes, further expanding the scope of the reductive silylation reaction.

3.4 Experimental Section

3.4.1 General Procedures. All reactions and subsequent manipulations were performed under anaerobic and anhydrous conditions under an atmosphere of nitrogen. Hexanes, toluene, THF and Et₂O were dried using a Vacuum Atmospheres DRI-SOLV solvent purification system. CH₂Cl₂, CD₂Cl₂, pyr, and TCE-*d*₂ were dried over activated 3 Å molecular sieves for 24 h before use. UO₂Cl₂(THF)₂,⁶⁰ dppmo,⁶¹ and Ph₃SiOTf,²⁶ were synthesized according to previously reported procedures. Cp₂Co was purchased from Acros Organics and recrystallized from concentrated Et₂O before use. All other reagents were purchased from commercial suppliers and used as received.

NMR spectra were recorded on a Varian UNITY INOVA 400 spectrometer or an Agilent Technologies 400-MR DD2 spectrometer. ¹H NMR spectra were referenced to external SiMe₄ using the residual protio solvent peaks as internal standards. The chemical shifts of the ¹⁹F{¹H} and ³¹P{¹H} spectra were referenced indirectly with the ¹H resonance of SiMe₄ at 0 ppm, according to IUPAC standard.^{62,63} ²⁹Si{¹H} NMR spectra were referenced to external SiMe₄ in C₆D₆. Raman and IR spectra were recorded on a Mattson Genesis FTIR/Raman spectrometer. IR samples were recorded as KBr pellets, while Raman samples were recorded in an NMR tube as neat solids. UV-vis/NIR experiments were performed on a UV-3600 Shimadzu spectrophotometer. Elemental analyses were performed by the Microanalytical Laboratory at UC Berkeley.

3.4.2 Synthesis of [UO₂(dppmo)₂(OTf)][OTf]. The preparation described below was modified from the published procedure for [UO₂(dppmo)₂(TPPO)][OTf]₂.⁶⁴ To a stirring, yellow dichloromethane (3 mL) slurry of UO₂Cl₂(THF)₂ (102.8 mg, 0.212

mmol), was added dropwise a colorless dichloromethane (3 mL) solution of dppmo (175.7 mg, 0.422 mmol). Solid AgOTf (110.2 mg, 0.429 mmol) was then quickly added to the reaction mixture. The reaction mixture was allowed to stir for 24 h at 25 °C, which resulted in formation of a yellow solution concomitant with the deposition of a white precipitate. This solution was filtered through a Celite column supported on glass wool (0.5 cm × 2 cm), which afforded a clear yellow filtrate and a large white plug. The filtrate was concentrated *in vacuo* and layered with diethyl ether (2 mL). Storage of this solution at -25 °C for 24 h resulted in deposition of a pale yellow powder (218.2 mg, 74% yield). Spectral data collected for this material matched those previously reported for this complex, [UO₂(dppmo)₂(OTf)[OTf].¹⁷

3.4.3 Synthesis of [UO₂(TPPO)₄][OTf]₂. This complex was prepared according to a modified literature procedure.⁶⁴ To a stirring, yellow dichloromethane (3 mL) slurry of UO₂Cl₂(THF)₂ (224.0 mg, 0.462 mmol), was added dropwise a colorless dichloromethane (4 mL) solution of TPPO (512.8 mg, 1.843 mmol). Solid AgOTf (275.6 mg, 1.073 mmol) was then quickly added to the reaction mixture. After 3 h, the resulting cloudy yellow solution was filtered through a Celite column supported on glass wool (0.5 cm × 2 cm), which afforded a clear yellow filtrate and a large tan plug. All the volatiles were removed *in vacuo*, which produced a yellow foam. This material was extracted into dichloromethane (8 mL), and filtered through a Celite column supported on glass wool (0.5 cm × 2 cm), which afforded a clear yellow filtrate and a small pale orange plug. The filtrate was then concentrated *in vacuo* and layered with diethyl ether (5 mL). Storage of this solution at -25 °C for 24 h resulted in deposition of a yellow crystalline solid (570.3 mg, 73% yield). Spectral data of this material matched

those previously reported for this complex.⁶⁴ Raman (cm^{-1}): 3064(s), 1587(m), 1572(sh w), 1186(w), 1147(w), 1005(m), 1001(s), 839(m, U=O ν_{sym}), 750(w), 685(w), 615(w), 310(w), 253(m).

3.4.4 Synthesis of $[\text{U}^{\text{IV}}(\text{OSiPh}_3)(\text{dppmo})_2(\text{OTf})_2][\text{OTf}]$ (3.1). A reaction flask was charged with a yellow toluene (10 mL) solution containing $[\text{UO}_2(\text{dppmo})_2(\text{OTf})][\text{OTf}]$ (117.9 mg, 0.085 mmol), Ph_3SiH (44.7 mg, 0.172 mmol), and $\text{B}(\text{C}_6\text{F}_5)_3$ (86.9 mg, 0.170 mmol). The flask was sealed and heated at 105 °C for 3.5 d, which resulted in the formation of a slightly cloudy sea foam green solution. All the volatiles were removed *in vacuo*, and the sea foam green oil was washed with hexanes (3×8 mL). Extraction into dichloromethane (4 mL) begets a cloudy sea foam green solution, which was filtered through a Celite column supported on glass wool (0.5 cm \times 2 cm), concentrated *in vacuo* (2 mL), and layered with hexanes (3 mL). Storage at -25 °C for 24 h, resulted in formation of a sea foam green crystalline solid (24.1 mg, 16% yield). Anal. Calcd for $\text{UO}_{14}\text{P}_4\text{S}_3\text{SiF}_9\text{C}_{71}\text{H}_{59}$: C, 47.55; H, 3.32. Found: C, 50.83; H, 3.42; N, <0.2. ^1H NMR (CD_2Cl_2 , 25 °C, 400 MHz): δ 38.48 (s, 6H, Ph_3Si ortho CH), 12.69 (s, 6H, Ph_3Si meta CH), 11.82 (t, 3H, Ph_3Si para CH), 6.36 (s, 8H, dppmo para CH), 5.90 (s, 16H, dppmo CH), -1.61 (br s, 16H, dppmo CH), -12.79 (br s, 4H, dppmo γ - CH_2). Analysis of this sample by $^{19}\text{F}\{^1\text{H}\}$ NMR spectroscopy revealed the solid contained a fluorinated-phenyl containing side product, indicated by three resonances at -133.62, -163.73, and -166.67 ppm.

3.4.5 Synthesis of 3.1 using Cp_2Co . A 20 mL scintillation vial was charged with a pale yellow solution of $[\text{UO}_2(\text{dppmo})_2(\text{OTf})][\text{OTf}]$ (125.1 mg, 0.090 mmol) in dichloromethane (2 mL). A light brown dichloromethane (2 mL) solution of Ph_3SiOTf (148.1 mg, 0.363 mmol) and Cp_2Co (31.9 mg, 0.175 mmol) was then added dropwise,

which resulted in a color change to dark yellow-green. The reaction mixture was allowed to stand at room temperature for 15 h, whereupon the solution became slightly cloudy. The reaction mixture was filtered through a Celite column supported on glass wool (0.5 cm × 2 cm), concentrated *in vacuo*, and layered with diethyl ether (3 mL). Storage of this solution for 24 h at -25 °C resulted in the deposition of a yellow-green solid (123 mg). The solid was dissolved in dichloromethane (3 mL), and filtered through a Celite column supported on glass wool (0.5 cm × 2 cm). The filtrate was then concentrated *in vacuo*, and layered with diethyl ether (2 mL). Storage of this solution for 24 h at -25 °C resulted in the deposition of a crystalline mixture, which consisted of sea foam green blocks and yellow needles (total mass of 33 mg). The sea foam green blocks were characterized by X-ray crystallography, revealing the presence of $[U^{IV}(\text{OSiPh}_3)(\text{dppmo})_2(\text{OTf})_2][\text{OTf}]$ (**2**). The presence of $[\text{Cp}_2\text{Co}][\text{OTf}]$ was confirmed by a unit cell determination of a yellow needle: $a = 16.35 \text{ \AA}$, $b = 13.13 \text{ \AA}$, $c = 17.62 \text{ \AA}$; $\alpha = 90^\circ$, $\beta = 105.94^\circ$, $\gamma = 90^\circ$, which matches the unit cell reported for $[\text{Cp}_2\text{Co}][\text{OTf}]$.⁶⁵ The ^1H NMR spectrum revealed the presence of both **2** and $[\text{Cp}_2\text{Co}][\text{OTf}]$ in a 2:1 ratio, respectively. ^1H NMR (CD_2Cl_2 , 25 °C, 400 MHz): δ 37.86 (s, 6H, Ph_3Si ortho CH), 12.57 (s, 6H, Ph_3Si meta CH), 11.72 (s, 3H, Ph_3Si para CH), 6.36 (br s, 8H, dppmo para CH), 5.90 (br s, 16H, dppmo meta CH), 5.73 (s, $[\text{Cp}_2\text{Co}]^+$), -1.80 (br s, 16H, dppmo ortho CH), -12.53 (br s, 4H, dppmo γ - CH_2). $^{19}\text{F}\{^1\text{H}\}$ NMR (CD_2Cl_2 , 25 °C, 376 MHz): δ -80.36 (br s, $[\text{OTf}]^-$).

3.4.6 Synthesis of $[\text{Na}(\text{12-crown-4})_2][\text{HB}(\text{C}_6\text{F}_5)_3]$ (3.2**).** To a stirring white suspension of NaBH_4 (9.1 mg, 0.240 mmol) in THF (1 mL), was added a THF (2 mL) solution of $\text{B}(\text{C}_6\text{F}_5)_3$ (107.7 mg, 0.210 mmol) dropwise. Then, 12-crown-4 (68 μL , 0.421

mmol) was added, resulting in noticeable bubbles forming at the solid's surface. The suspension was stirred for 24 h, whereupon the slightly cloudy solution was filtered through a Celite column supported on glass wool (0.5 cm × 2 cm). All volatiles were removed *in vacuo*, which resulted in the formation of a white powder. The powder was then extracted into diethyl ether (8 mL), and filtered again through a Celite column supported on glass wool (0.5 cm × 2 cm). All volatiles were removed *in vacuo*, which produced a white crystalline solid (46.0 mg, 25% yield). ^1H NMR (MeCN- d_3 , 25 °C, 400 MHz): δ 3.62 (s, 12-crown-4). The $[\text{HB}(\text{C}_6\text{F}_5)_3]^-$ proton resonance was not observed. $^{11}\text{B}\{^1\text{H}\}$ NMR (MeCN- d_3 , 25 °C, 320 MHz): δ -25.48 (d, $J_{\text{HB}} = 229$ Hz, $[\text{HB}(\text{C}_6\text{F}_5)_3]^-$). $^{19}\text{F}\{^1\text{H}\}$ NMR: (MeCN- d_3 , 25 °C, 376 MHz): δ -134.69 (s, 6F, ortho CF), -164.91 (t, $J_{\text{FF}} = 20$ Hz, 3F, para CF), -165.76 (t, $J_{\text{FF}} = 19$ Hz, 6F, meta CF).

3.4.7 Synthesis of $\text{U}^{\text{IV}}(\text{OTf})_4(\text{dppmo})_2$ (3.3). To a stirring, pale yellow dichloromethane (2 mL) solution of $[\text{UO}_2(\text{dppmo})_2(\text{OTf})][\text{OTf}]$ (40.4 mg, 0.029 mmol), was added dropwise a dichloromethane (1.5 mL) solution of Ph_3SiOTf (47.2 mg, 0.116 mmol) and Cp_2Co (10.6 mg, 0.058 mmol). This resulted in an immediate color change to green. This solution was allowed to stir for 24 h at 25 °C, which resulted in the deposition of a green precipitate. The mixture was concentrated *in vacuo* and stored at -25 °C for 24 h, which resulted in the further deposition of solid. Isolation of the green powder, followed by dissolution in dichloromethane (4 mL), resulted in formation of a cloudy green solution. This solution was filtered through a Celite column supported on glass wool (0.5 cm × 2 cm), concentrated *in vacuo*, and layered with hexanes (2 mL). Storage of this solution at -25 °C for 24 h, resulted in the deposition of a green crystalline solid, which was isolated by decanting off the supernatant (48.3 mg, 83%

yield). X-ray quality crystals of **3.3**, as a 1:1 co-crystal with [Cp₂Co][OTf], were grown out of a toluene solution layered with hexanes. Anal. Calcd for UO₁₉P₄S₅F₁₅CoC₆₅H₅₂: C, 38.97; H, 2.62. Found: C, 39.36; H, 2.58. ¹H NMR (CD₂Cl₂, 25 °C, 400 MHz): δ 32.75 (br s, 4H, γ-CH₂), 15.25 (br s, 16H, ortho CH), 8.89 (s, 8H, para CH), 8.67 (s, 16H, meta CH), 5.70 (s, 10H, [Cp₂Co]⁺). ¹⁹F{¹H} NMR (CD₂Cl₂, 25 °C, 376 MHz): δ -77.90 (br s, outer sphere [OTf]⁻), -97.14 (br s, inner sphere [OTf]⁻). UV-vis/NIR (CH₂Cl₂, 4.44 × 10⁻³ M, L·mol⁻¹·cm⁻¹): 398 (ε = 332), 542 (ε = 20), 620 (ε = 30), 636 (ε = 31), 658 (ε = 43), 774 (ε = 9), 828 (ε = 11), 1008 (sh, ε = 14), 1062 (sh, ε = 25), 1112 (ε = 53), 1408 (ε = 16), 1522 (ε = 14), 1636 (ε = 9), 2024 (ε = 3). IR (KBr pellet, cm⁻¹): 1591(w), 1487(w), 1441(m), 1417(w), 1331(m), 1277(s), 1255(s), 1234(s), 1221(s sh), 1203(vs), 1163(s sh), 1126(vs), 1074(s sh), 1068(s), 1028(s), 1011(s), 997(s), 864(w), 793(m), 741(m), 690(m), 636(s), 577(w), 569(w), 507(m), 461(w).

3.4.8 Synthesis of [U^{IV}(OSiPh₃)₂(dppmo)₂(pyr)][OTf]₂ (3.4-pyr). To a stirring light yellow solution of [UO₂(dppmo)₂(OTf)][OTf] (83.9 mg, 0.061 mmol) in dichloromethane (2 mL), was added a light brown solution of Ph₃SiOTf (49.6 mg, 0.121 mmol) and Cp₂Co (21.4 mg, 0.118 mmol) in dichloromethane (2 mL) dropwise. This resulted in an immediate darkening of the yellow color, and the reaction was allowed to stir at room temperature for 2h. The dark yellow solution was filtered through a Celite column supported on glass wool (0.5 cm × 2 cm). The dark yellow filtrate was concentrated *in vacuo*, and layered with diethyl ether (2 mL). Storage at -25 °C for 24 h, afforded a light green solid, which appeared to be a mixture of complex **3.1**, [U^{IV}(OSiPh₃)₂(dppmo)₂(OTf)][OTf] (**3.4**), and [Cp₂Co][OTf] in a 2:1:3 ratio, by ¹H NMR spectroscopy. ¹H NMR (CD₂Cl₂, 25 °C, 400 MHz): δ 48.03 (br s, 24H, **3.4**, Ph₃Si ortho

CH), 31.71 (s, 6H, **3.1**, Ph₃Si ortho CH), 14.85 (br s, 24H, **3.4**, Ph₃Si meta CH), 13.61 (br s, 12H, **3.4**, Ph₃Si para CH), 12.53 (s, 6H, **3.1**, Ph₃Si meta CH), 11.69 (s, 3H, **3.1**, Ph₃Si para CH), 6.33 (br s, 4H, **3.1**, dppmo para CH), 5.88 (br s, 8H, **3.1**, dppmo meta CH), 5.63 (s, 60H, [Cp₂Co]⁺ CH), 3.20 (br s, 32H, **3.4**, dppmo meta CH), -2.13 (br s, 8H, **3.1**, dppmo ortho CH), -11.81 (br s, 16H, **3.4**, dppmo para CH), -12.61 (br s, 2H, **3.1**, dppmo γ -CH), -17.28 (br s, 32H, **3.4**, dppmo ortho CH). The γ -CH resonance of complex **3.4** could not be identified, probably due to paramagnetic broadening. From this mixture, a few X-ray quality pale green, plate crystals of [U^{IV}(OSiPh₃)₂(dppmo)₂(pyr)][OTf]₂ (**3.4-pyr**) were grown from a pyridine (2 mL) solution layered with diethyl ether (1 mL) and stored at -25 °C for 24 h. Unfortunately, we were unable to completely separate **3.4-pyr** from complex **3.1** and [Cp₂Co][OTf], in order to complete its characterization. ¹H NMR (CD₂Cl₂, 25 °C, 400 MHz): δ 48.01 (br s, 12H, Ph₃Si ortho CH), 14.90 (br s, 12H, Ph₃Si meta CH), 13.61 (br s, 6H, Ph₃Si para CH), 4.00 (br s, 4H, dppmo γ -CH₂), 3.17 (br s, 16H, dppmo meta CH), -11.81 (br s, 8H, dppmo para CH), -17.31 (br s, 16H, dppmo ortho CH). The coordinated pyridine resonances were not observed, possibly due to overlap with the uncoordinated pyridine solvent resonances. ¹⁹F{¹H} NMR (CD₂Cl₂, 25 °C, 376 MHz): δ -81.21 (br s, 9F, [OTf]⁻ CF), -113.72 (br s, 3F, OTF CF).

3.4.9 Synthesis of [Cp₂Co][U^{IV}(OTf)₅(TPPO)₂] (3.5). To a cold (-25 °C) stirring yellow solution of [UO₂(TPPO)₄][OTf]₂ (83.3 mg, 0.050 mmol) in dichloromethane (3 mL), was added cold (-25 °C) Me₃SiOTf (54 μ L, 0.299 mmol) via syringe, followed by a light brown solution (-25 °C) of Cp₂Co (20.2 mg, 0.111 mmol) in dichloromethane (1 mL). This resulted in a rapid color change to yellow-green, concomitant with the deposition of a small amount of dark grey solid. The reaction mixture was allowed to

stir at room temperature for 19h, whereupon it was filtered through a Celite column supported on glass wool (0.5 cm × 2 cm), which afforded a yellow-green filtrate and a small dark grey plug. The filtrate was concentrated *in vacuo*, and layered with diethyl ether (2 mL). Storage of this solution at -25 °C for 24 h resulted in the deposition of green blocks, which were isolated by decanting off the supernatant (65.6 mg, 76% yield). Anal. Calcd for $\text{UO}_{17}\text{P}_2\text{S}_5\text{F}_{15}\text{CoC}_{51}\text{H}_{40}$: C, 35.43; H, 2.33. Found: C, 35.38; H, 2.13. ^1H NMR (CD_2Cl_2 , 25 °C, 400 MHz): δ 31.66 (br s, 12H, ortho CH), 12.04 (br s, 12H, meta CH), 11.16 (br s, 6H, para CH), 5.70 (s, 10H, $[\text{Cp}_2\text{Co}]^+$). $^{19}\text{F}\{^1\text{H}\}$ NMR (CD_2Cl_2 , 25 °C, 376 MHz): δ -79.06 (br s, outer sphere $[\text{OTf}]^-$), -101.02 (br s, inner sphere $[\text{OTf}]^-$). UV-vis/NIR (CH_2Cl_2 , 3.57×10^{-3} M, $\text{L}\cdot\text{mol}^{-1}\cdot\text{cm}^{-1}$): 400 ($\epsilon = 299$), 634 ($\epsilon = 22$), 906 (sh, $\epsilon = 7$), 1054 ($\epsilon = 26$), 1272 ($\epsilon = 10$), 1378 ($\epsilon = 6$), 1476 ($\epsilon = 7$), 1994 ($\epsilon = 9$). IR (KBr pellet, cm^{-1}): 1591(w), 1487(w), 1439(m), 1417(w), 1344(br m), 1319(sh m), 1259(m), 1236(s), 1203(vs), 1182(sh s), 1163(sh m), 1122(s), 1065(w), 1034(s), 1014(s), 991(vs), 865(w), 800(br w), 756(w), 750(w), 729(m), 690(m), 630(s), 584(w), 569(w), 540(s), 511(w), 507(w), 459(w).

3.4.10 Synthesis of 3.5 using Ph_3SiOTf . To a stirring yellow solution of $[\text{UO}_2(\text{TPPO})_4][\text{OTf}]_2$ (42.0 mg, 0.025 mmol) in dichloromethane (2 mL), was added a light brown dichloromethane (2 mL) solution of Ph_3SiOTf (47.2 mg, 0.116 mmol) and Cp_2Co (10.6 mg, 0.058 mmol) dropwise, which immediately resulted in the formation of a dark yellow solution. The reaction was allowed to stir at room temperature for 16.5 h, before the solution was filtered through a Celite column supported on glass wool (0.5 cm x 2 cm), which afforded a yellow-green filtrate and a small dark grey plug. The filtrate was concentrated *in vacuo*, and layered with diethyl ether (2 mL). Storage

at -25 °C for 3 h, resulted in the deposition of green block crystals, which were isolated by decanting off the supernatant (24.6 mg, 57% yield). The identity of the crystals were confirmed by a unit cell comparison: $a = 16.54 \text{ \AA}$, $b = 20.79 \text{ \AA}$, $c = 18.00 \text{ \AA}$; $\alpha = 90^\circ$, $\beta = 90.10^\circ$, $\gamma = 90^\circ$, which matches the unit cell for **3.5**. $^1\text{H NMR}$ (CD_2Cl_2 , 25 °C, 400 MHz): δ 31.95 (br s, 12H, TPPO ortho CH), 12.06 (br s, 12H, TPPO meta CH), 11.17 (br s, 6H, TPPO para CH), 5.63 (s, 10H, $[\text{Cp}_2\text{Co}]^+$ CH). $^{19}\text{F}\{^1\text{H}\}$ NMR (CD_2Cl_2 , 25 °C, 376 MHz): δ -79.01 (br s, 3F, $[\text{OTf}]^-$ CF), -100.73 (br s, 12F, OTf CF).

3.4.11 Synthesis of $[\text{U}^{\text{IV}}(\text{OTf})_2(\text{dppmo})_3][\text{OTf}]_2$ (3.6**).** To a stirred green slurry of UCl_4 (80.9 mg, 0.213 mmol) in dichloromethane (3 mL), was added a colorless solution of dppmo (181.9 mg, 0.437 mmol) in dichloromethane (4 mL), dropwise, followed by the addition of AgOTf (233.4 mg, 0.908 mmol), as a solid. This resulted in no visible change. The reaction mixture was allowed to stir at room temperature for 17h, whereupon the solution changed to a sea-foam green color, concomitant with the deposition of a white precipitate. The mixture was filtered through a Celite column supported on glass wool (0.5 cm \times 2 cm), which afforded a sea-foam green filtrate and a white plug. The filtrate was concentrated *in vacuo*, and layered with diethyl ether (~2 mL). Storage of this solution at -25 °C for 24 h resulted in the deposition of a green oil, which was dried *in vacuo* to afford a green solid. The $^1\text{H NMR}$ spectrum of this green solid in CD_2Cl_2 revealed the mixture to contain **3.3** and **3.6** in a 1:2.7 ratio. $^1\text{H NMR}$ (CD_2Cl_2 , 25 °C, 400 MHz): δ 38.56 (br s, 4H, **3.3**, $\gamma\text{-CH}_2$), 15.30 (br s, 8H, **3.3**, dppmo ortho CH), 12.05 (br s, 8H, **3.6**, $\gamma\text{-CH}_2$), 11.05 (br s, 32H, **3.6**, dppmo ortho CH), 8.86 (s, 4H, **3.3**, dppmo para CH), 8.67 (s, 8H, **3.3**, dppmo meta CH), 8.17 (s, 16H, **3.6**, dppmo para CH), 7.93 (s, 32H, **3.6**, dppmo meta CH). The pale green mother liquor was

concentrated *in vacuo* and stored at -25 °C for 24 h, which resulted in the deposition of a pale green plate crystals of **3.6** (101.3 mg, 27% yield). ¹H NMR (CD₂Cl₂, 25 °C, 400 MHz): δ 11.07 (br s, 24H, dppmo ortho CH), 8.15 (s, 12H, dppmo para CH), 7.85 (s, 24H, dppmo meta CH). The γ-CH₂ resonance is likely overlapping with the dppmo ortho CH resonance. ¹⁹F{¹H} NMR (CD₂Cl₂, 25 °C, 376 MHz): δ -77.93 (br s, 6F, outer sphere [OTf]⁻), -96.59 (br s, 6F, inner sphere [OTf]⁻).

3.4.12 Synthesis of [U^{IV}(OTf)₂(TPPO)₄][OTf]₂ (3.7). To a stirred green slurry of UCl₄ (161.2 mg, 0.424 mmol) in dichloromethane (3 mL), was added dropwise a colorless solution of TPPO (473.1 mg, 1.700 mmol) in dichloromethane (3 mL), which resulted in no visible change. The mixture was allowed to stir for 3 minutes at room temperature, before AgOTf (436.0 mg, 1.697 mmol) was added as a solid. Within a few minutes, the reaction mixture appeared teal in color. The reaction mixture was stirred at room temperature for 1.5 h, whereupon the solution is an intense teal color, and a fluffy white precipitate formed. The mixture was filtered through a Celite column supported on glass wool (0.5 cm × 2 cm). The resulting teal filtrate was concentrated *in vacuo*, and layered with Et₂O (1 mL). Storage of this solution at -25 °C for 72 h only resulted in a floating light-colored cloudy solid. The mixture was filtered through a Celite column supported on glass wool (0.5 cm × 2 cm). All the volatiles were removed *in vacuo*, and the teal oil was washed with Et₂O (~1 mL), followed by toluene (~1 mL). The teal solid was extracted into dichloromethane (3 mL), and filtered through a Celite column supported on glass wool (0.5 cm × 2 cm). The resulting teal filtrate was concentrated *in vacuo*, and layered with Et₂O (1 mL). Storage of this solution at -25 °C for 24 h resulted in the deposition of pale green blocks, which were isolated by decanting off the

supernatant (339.4 mg, 72% yield). ^1H NMR (CD_2Cl_2 , 25 °C, 400 MHz): δ 11.29 (t, $J_{\text{HH}} = 9$ Hz, 24H, *ortho*-CH), 8.41 (t, $J_{\text{HH}} = 8$ Hz, 12H, *para*-CH), 8.15 (br t, $J_{\text{HH}} = 7$ Hz, 24H, *meta*-CH). $^{19}\text{F}\{^1\text{H}\}$ NMR (CD_2Cl_2 , 25 °C, 376 MHz): δ -78.44 (br s, outer sphere $[\text{OTf}]^-$), -95.80 (br s, inner sphere $[\text{OTf}]^-$). $^{31}\text{P}\{^1\text{H}\}$ NMR (CD_2Cl_2 , 25 °C, 376 MHz): δ 33.88 (br s, OPPh_3).

3.4.13 NMR-Scale Reaction of Ph_3SiOTf with Cp_2Co . A colorless CD_2Cl_2 solution (1 mL) containing Ph_3SiOTf (12.6 mg, 0.031 mmol) was sealed in a J. Young NMR tube, and the ^1H and $^{19}\text{F}\{^1\text{H}\}$ NMR spectra were recorded. Then a light brown CD_2Cl_2 solution (0.5 mL) of Cp_2Co (6.1 mg, 0.032 mmol) was added dropwise, resulting in a light brown solution. The tube was sealed, and the ^1H and $^{19}\text{F}\{^1\text{H}\}$ NMR spectra were recorded after standing at room temperature for 30 min. These spectra revealed mostly unreacted Ph_3SiOTf and Cp_2Co , however, a few new small resonances are also observed at 7.68, 7.54, and 4.80 ppm, suggesting that a slow reaction may be occurring.

3.4.14 NMR-Scale Reaction of $[\text{UO}_2(\text{dppmo})_2(\text{OTf})][\text{OTf}]$ with Cp_2Co . A light brown CD_2Cl_2 solution (1 mL) containing Cp_2Co (9.4 mg, 0.052 mmol) was sealed in a J. Young NMR tube, and the ^1H , $^{19}\text{F}\{^1\text{H}\}$, and $^{31}\text{P}\{^1\text{H}\}$ NMR spectra were recorded. Then, a pale yellow CD_2Cl_2 solution (0.5 mL) of $[\text{UO}_2(\text{dppmo})_2(\text{OTf})][\text{OTf}]$ (36.3 mg, 0.026 mmol) was added dropwise, which resulted in a yellow brown solution. The tube was sealed, and the ^1H , $^{19}\text{F}\{^1\text{H}\}$ and $^{31}\text{P}\{^1\text{H}\}$ NMR spectra were recorded after standing at room temperature for 10 min. Spectra were also recorded after 1h, 2h, 4h, and 22h. These spectra revealed the formation of $[\text{Cp}_2\text{Co}][\text{OTf}]$, free dppmo, and an unidentified paramagnetic uranium-containing product.

3.4.15 NMR-Scale Reaction of $[\text{UO}_2(\text{dppmo})_2(\text{OTf})][\text{OTf}]$ with Ph_3SiOTf . A pale yellow CD_2Cl_2 solution (1 mL) containing $[\text{UO}_2(\text{dppmo})_2(\text{OTf})][\text{OTf}]$ (21.4 mg, 0.015

mmol) was sealed in a J. Young NMR tube, and the ^1H , $^{19}\text{F}\{^1\text{H}\}$, and $^{31}\text{P}\{^1\text{H}\}$ NMR spectra were recorded. Then, a colorless CD_2Cl_2 solution (0.5 mL) of Ph_3SiOTf (13.1 mg, 0.032 mmol) was added dropwise. This resulted in no visible change to the solution. The tube was sealed, and the ^1H , $^{19}\text{F}\{^1\text{H}\}$ and $^{31}\text{P}\{^1\text{H}\}$ NMR spectra were recorded after 20 min. These spectra only revealed the presence of unreacted $[\text{UO}_2(\text{dppmo})_2(\text{OTf})][\text{OTf}]$ and Ph_3SiOTf .

3.4.16 NMR-Scale Reaction of $[\text{UO}_2(\text{TPPO})_4][\text{OTf}]_2$ with Cp_2Co . A light brown CD_2Cl_2 solution (1 mL) containing Cp_2Co (4.1 mg, 0.022 mmol) was sealed in a J. Young NMR tube, and the ^1H NMR spectrum was recorded. Then, a pale yellow CD_2Cl_2 solution (0.5 mL) of $[\text{UO}_2(\text{TPPO})_4][\text{OTf}]_2$ (18.8 mg, 0.011 mmol) was added dropwise, which resulted in the formation of a dark yellow-brown solution. The tube was sealed, and the ^1H , $^{19}\text{F}\{^1\text{H}\}$ and $^{31}\text{P}\{^1\text{H}\}$ NMR spectra were recorded after standing at room temperature for 10 min. These spectra revealed the formation of $[\text{Cp}_2\text{Co}][\text{OTf}]$, and several minor unidentified paramagnetic uranium-containing products.

3.4.17 NMR-Scale Reaction of $[\text{UO}_2(\text{TPPO})_4][\text{OTf}]_2$ with Me_3SiOTf . A pale yellow CD_2Cl_2 solution (1 mL) containing $[\text{UO}_2(\text{TPPO})_4][\text{OTf}]_2$ (37.1 mg, 0.022 mmol) was sealed in a J. Young NMR tube, and the ^1H , $^{19}\text{F}\{^1\text{H}\}$, and $^{31}\text{P}\{^1\text{H}\}$ NMR spectra were recorded. Then, cold ($-25\text{ }^\circ\text{C}$) Me_3SiOTf (16 μL , 0.088 mmol) in CD_2Cl_2 (0.5 mL) was added dropwise via syringe. This resulted in no visible change to the solution. The tube was sealed, and the ^1H , $^{19}\text{F}\{^1\text{H}\}$, and $^{31}\text{P}\{^1\text{H}\}$ NMR spectra were recorded after 10 min. These spectra revealed the presence of $[\text{Ph}_3\text{POSiMe}_3][\text{OTf}]$,^{54,55} and $\text{UO}_2(\text{OTf})_2(\text{TPPO})_2$.

3.4.18 NMR-Scale Reaction of Me_3SiOTf with Cp_2Co . A light brown CD_2Cl_2 solution (1 mL) containing Cp_2Co (10.6 mg, 0.058 mmol) was sealed in a J. Young NMR tube, and

the ^1H spectrum was recorded. Then cold ($-25\text{ }^\circ\text{C}$) Me_3SiOTf ($11\ \mu\text{L}$, $0.061\ \text{mmol}$) was added via syringe, which resulted in no visible change. The tube was sealed, and the ^1H and $^{19}\text{F}\{^1\text{H}\}$ NMR spectra were recorded after standing at room temperature for 20 min. These spectra revealed only unreacted Me_3SiOTf and Cp_2Co .

3.4.19 X-ray Crystallography. Data for **3.1**, **3.3**, **3.4-pyr**, **3.5**, **3.6**, and **3.7** were collected on a Bruker 3-axis platform diffractometer equipped with a SMART-1000 CCD detector using a graphite monochromator with a Mo $\text{K}\alpha$ X-ray source ($\lambda = 0.71073\ \text{\AA}$). The crystals were mounted on a glass fiber under Paratone-N oil and all data were collected at $100(2)\ \text{K}$ using an Oxford nitrogen gas cryostream system. A hemisphere of data was collected using ω scans with 0.3° frame widths. Frame exposures of 10, 30, 10, 10, and 5 seconds were used for complexes **3.1**, **3.3**, **3.4-pyr**, **3.5** and **3.6**, respectively, while frame exposures of 5 and 10 seconds were used for complex **3.7**. Data collection and cell parameter determinations were conducted using the SMART program.⁶⁶ Integration of the data frames and final cell parameter refinement were performed using SAINT software.⁶⁷ Absorption correction of the data was carried out using the multi-scan method SADABS.⁶⁸ Subsequent calculations were carried out using SHELXTL.⁶⁹ Structure determinations were done using direct or Patterson methods and difference Fourier techniques. All hydrogen atom positions were idealized, and rode on the atom of attachment. Hydrogen atoms were not assigned to the disordered carbon atoms. Structure solution, refinement, graphics, and creation of publication materials were performed using SHELXTL.⁶⁹

For complex **3.1**, the diethyl ether solvate molecule exhibited mild positional disorder. The EADP, DFIX and FLAT commands were used to constrain its orientation. Disordered atoms were not refined anisotropically. In addition, a few carbon atoms and one oxygen atom of a dppmo ligand were constrained with the EADP command. Complex **3.2** exhibits positional disorder of one hexane solvate molecule. This positional disorder was addressed by modeling the molecule in two positions, in a 50:50 ratio. The EADP, DFIX, and FLAT commands were used to constrain both positions of the hexane molecule. Complex **3.2** also features a disordered toluene solvate molecule with half occupancy, which overlaps with one position of the hexane solvate. The EADP, DFIX, and FLAT commands were used to constrain the orientation of the toluene molecule. Disordered carbon atoms were not refined anisotropically. In addition, one of the dppmo phenyl rings exhibited mild positional disorder and was constrained using the EADP, DFIX, and FLAT commands. The OTf carbon atoms, two carbon atoms on the $[\text{Cp}_2\text{Co}]^+$, and a few other dppmo carbon atoms were also constrained with the EADP command. Finally, one dppmo C-C bond distance was restrained by the DFIX command in complex **3.5**. A summary of relevant crystallographic data for **3.1**, **3.3**, **3.4-pyr**, **3.5**, **3.6**, and **3.7** is presented in Tables 3.3-3.4.

Table 3.3. X-ray Crystallographic Information for **3.1**, **3.3** and **3.4-pyr**

	3.1 ·3CH ₂ Cl ₂ ·C ₄ H ₁₀ O	[3.3] [Cp ₂ Co][OTf] ·1.5C ₇ H ₈ ·C ₆ H ₁₄	3.4-pyr ·2C ₅ H ₅ N·C ₄ H ₁₀ O
empirical formula	UCl ₆ O ₁₅ P ₄ S ₃ SiF ₉ C ₇₈ H ₆₅	UO ₁₉ P ₄ S ₅ F ₁₅ CoC ₈₂ H ₆₀	UO ₁₃ P ₄ S ₂ Si ₂ F ₆ N ₃ C ₁₀₇ H ⁹⁹
Crystal habit, color	block, sea-green	block, yellow-green	plate, pale green
crystal size (mm)	0.40 × 0.20 × 0.20	0.35 × 0.25 × 0.25	0.10 × 0.30 × 0.50
crystal system	monoclinic	triclinic	monoclinic
space group	<i>P</i> 2 ₁ / <i>n</i>	<i>P</i> -1	<i>P</i> 2 ₁ / <i>c</i>
vol (Å ³)	8559(3)	4658(2)	10095(2)
a (Å)	17.810(3)	15.665(5)	25.230(4)
b (Å)	18.573(3)	15.876(5)	16.169(2)
c (Å)	25.953(4)	19.073(6)	27.244(3)
α (deg)	90	90.641(7)	90
β (deg)	94.423(4)	91.942(6)	114.731(3)
γ (deg)	90	100.661(6)	90
Z	4	2	4
fw (g/mol)	2112.18	2215.44	2231.10
density (calcd) (Mg/m ³)	1.639	1.580	1.468
abs coeff (mm ⁻¹)	2.327	2.189	1.811
F ₀₀₀	4200	2196	4528.0
Total no. reflections	90417	25154	84814
Unique reflections	17225	15158	25189
final R indices [I > 2σ(I)]	R ₁ = 0.0729 wR ₂ = 0.1806	R ₁ = 0.1029 wR ₂ = 0.2215	R ₁ = 0.0389 wR ₂ = 0.1260
largest diff peak and hole (e ⁻ Å ⁻³)	3.364 and -2.335	2.483 and -3.034	1.222 and -0.816
GOF	1.037	0.929	0.834

Table 3.4. X-ray Crystallographic Information for **3.5**, **3.6** and **3.7**

	3.5	3.6 ·4CH ₂ Cl ₂	3.7 ·CH ₂ Cl ₂
empirical formula	UO ₁₇ P ₂ S ₅ F ₁₅ CoC ₅₁ H ₄₀	UO ₁₈ P ₆ S ₄ F ₁₂ Cl ₈ C ₈₃ H ₇₄	UO ₁₆ P ₄ S ₄ F ₁₂ Cl ₂ C ₇₇ H ₆₂
Crystal habit, color	plate, yellow-green	plate, pale-green	block, pale-green
crystal size (mm)	0.10 × 0.20 × 0.50	0.40 × 0.20 × 0.05	0.10 × 0.05 × 0.05
crystal system	monoclinic	triclinic	monoclinic
space group	<i>P</i> 2 ₁ / <i>c</i>	<i>P</i> -1	<i>P</i> 2 ₁ / <i>n</i>
vol (Å ³)	6043(1)	10327(1)	8073.7(5)
a (Å)	16.464(2)	15.625(1)	14.6620(5)
b (Å)	20.580(3)	24.056(2)	25.1744(9)
c (Å)	17.835(2)	28.083(2)	21.9983(8)
α (deg)	90	90	90
β (deg)	90.708(3)	78.063(5)	96.106(1)
γ (deg)	90	90	90
Z	4	4	4
fw (g/mol)	1729.03	2423.11	2032.32
density (calcd) (Mg/m ³)	1.901	1.559	1.672
abs coeff (mm ⁻¹)	3.292	2.034	2.353
F ₀₀₀	3384	4824	4040
Total no. reflections	39529	40377	20067
Unique reflections	12364	18027	14758
final R indices [I > 2σ(I)]	R ₁ = 0.0456 wR ₂ = 0.0978	R ₁ = 0.1107 wR ₂ = 0.2422	R ₁ = 0.0307 wR ₂ = 0.0474
largest diff peak and hole (e ⁻ Å ⁻³)	1.489 and -0.850	3.557 and -1.605	1.188 and -0.884
GOF	1.028	1.122	1.176

3.5 References

- (1) Arnold, P. L.; Patel, D.; Wilson, C.; Love, J. B. *Nature* **2008**, *451*, 315.
- (2) Arnold, P. L.; Love, J. B.; Patel, D. *Coord. Chem. Rev.* **2009**, *253*, 1973
- (3) Yahia, A.; Arnold, P. L.; Love, J. B.; Maron, L. *Chem. Commun.* **2009**, 2402.
- (4) Yahia, A.; Arnold, P. L.; Love, J. B.; Maron, L. *Chem. Eur. J.* **2010**, *16*, 4881.
- (5) Arnold, P. L.; Hollis, E.; Nichol, G. S.; Love, J. B.; Griveau, J.-C.; Caciuffo, R.; Magnani, N.; Maron, L.; Castro, L.; Yahia, A.; Odoh, S. O.; Schreckenbach, G. *J. Am. Chem. Soc.* **2013**, *135*, 3841.
- (6) Jones, G. M.; Arnold, P. L.; Love, J. B. *Chem. Eur. J.* **2013**, *19*, 10287.
- (7) Arnold, P. L.; Pecharman, A.-F.; Hollis, E.; Yahia, A.; Maron, L.; Parsons, S.; Love, J. B. *Nat. Chem.* **2010**, *2*, 1056.
- (8) Schnaars, D. D.; Wu, G.; Hayton, T. W. *J. Am. Chem. Soc.* **2009**, *131*, 17532.
- (9) Schnaars, D. D.; Wu, G.; Hayton, T. W. *Inorg. Chem.* **2011**, *50*, 4695.
- (10) Schnaars, D. D.; Wu, G.; Hayton, T. W. *Inorg. Chem.* **2011**, *50*, 9642.
- (11) Pedrick, E. A.; Wu, G.; Kaltsoyannis, N.; Hayton, T. W. *Chem. Sci.* **2014**, *5*, 3204.
- (12) Berthet, J.-C.; Siffredi, G.; Thuéry, P.; Ephritikhine, M. *Eur. J. Inorg. Chem.* **2007**, *2007*, 4017.
- (13) Brown, J. L.; Wu, G.; Hayton, T. W. *J. Am. Chem. Soc.* **2010**, *132*, 7248
- (14) Bagnall, K. W.; du Preez, J. G. H. *Chem. Commun.* **1973**, 820.
- (15) Brown, J. L.; Mokhtarzadeh, C. C.; Lever, J. M.; Wu, G.; Hayton, T. W. *Inorg. Chem.* **2011**, *50*, 5105.
- (16) Fortier, S.; Hayton, T. W. *Coord. Chem. Rev.* **2010**, *254*, 197.
- (17) Cornet, S. M.; May, I.; Redmond, M. P.; Selvage, A. J.; Sharrad, C. A.; Rosnel, O. *Polyhedron* **2009**, *28*, 363.
- (18) Casanova, D.; Alemany, P.; Bofill, J. M.; Alvarez, S. *Chem. Eur. J.* **2003**, *9*, 1281.
- (19) Porchia, M.; Brianese, N.; Casellato, U.; Ossola, F.; Rossetto, G.; Zanella, P. *J. Chem. Soc. Dalton Trans.* **1989**, 677
- (20) Liedtke, R.; Scheidt, F.; Ren, J.; Schirmer, B.; Cardenas, A. J. P.; Daniliuc, C. G.; Eckert, H.; Warren, T. H.; Grimme, S.; Kehr, G.; Erker, G. *J. Am. Chem. Soc.* **2014**, *136*, 9014.
- (21) Walker, D. A.; Woodman, T. J.; Schormann, M.; Hughes, D. L.; Bochmann, M. *Organometallics* **2003**, *22*, 797
- (22) Whittell, G. R.; Balmond, E. I.; Robertson, A. P. M.; Patra, S. K.; Haddow, M. F.; Manners, I. *Eur. J. Inorg. Chem.* **2010**, *2010*, 3967.
- (23) Millot, N.; Santini, Catherine C.; Fenet, B.; Basset, Jean M. *Eur. J. Inorg. Chem.* **2002**, *2002*, 3328.
- (24) Bavarian, N.; Baird, M. C. *Organometallics* **2005**, *24*, 2889.
- (25) Alcarazo, M.; Gomez, C.; Holle, S.; Goddard, R. *Angew. Chem. Int. Ed.* **2010**, *49*, 5788.
- (26) Asadi, A.; Avent, A. G.; Eaborn, C.; Hill, M. S.; Hitchcock, P. B.; Meehan, M. M.; Smith, J. D. *Organometallics* **2002**, *21*, 2183.
- (27) Lickiss, P. D.; Lucas, R. J. *Organomet. Chem.* **1996**, *510*, 167.

- (28) Kläring, P.; Jungton, A.-K.; Braun, T.; Müller, C. *Eur. J. Inorg. Chem.* **2012**, 2012, 1430.
- (29) Kraft, B. M.; Jones, W. D. *J. Organomet. Chem.* **2002**, 658, 132.
- (30) Massey, A. G.; Park, A. J. *J. Organomet. Chem.* **1966**, 5, 218.
- (31) Lehmann, M.; Schulz, A.; Villinger, A. *Angew. Chem. Int. Ed.* **2009**, 48, 7444.
- (32) Berthet, J.-C.; Nierlich, M.; Ephritikhine, M. *C. R. Chimie* **2002**, 5, 81.
- (33) Natrajan, L.; Mazzanti, M.; Bezombes, J. P.; Pecaut, J. *Inorg. Chem.* **2005**, 44, 6115.
- (34) Maynadié, J.; Berthet, J.-C.; Thuéry, P.; Ephritikhine, M. *Organometallics* **2006**, 25, 5603.
- (35) Schnaars, D. D.; Wu, G.; Hayton, T. W. *Dalton Trans.* **2008**, 6121.
- (36) Jilek, R. E.; Tomson, N. C.; Shook, R. L.; Scott, B. L.; Boncella, J. M. *Inorg. Chem.* **2014**, 53, 9818.
- (37) Charpin, P.; Lance, M.; Soulie, E.; Vigner, D.; Marquet-Ellis, H. *Acta Crystallogr. Sec. C* **1985**, 41, 1723.
- (38) Bombieri, G.; Brown, D.; Graziani, R. *J. Chem. Soc. Dalton Trans.* **1975**, 1873.
- (39) Prakash, J.; Rohde, G. T.; Meier, K. K.; Jasniewski, A. J.; Van Heuvelen, K. M.; Münck, E.; Que, L. *J. Am. Chem. Soc.* **2015**, 137, 3478.
- (40) Mandai, T.; Masu, H.; Johansson, P. *Dalton Trans.* **2015**, 44, 11259.
- (41) Fukuzumi, S.; Morimoto, Y.; Kotani, H.; Naumov, P.; Lee, Y.-M.; Nam, W. *Nat. Chem.* **2010**, 2, 756.
- (42) Linti, G.; Seifert, A. *Z. Anorg. Allg. Chem.* **2008**, 634, 1312.
- (43) Logemann, C.; Klüner, T.; Wickleder, M. *S. Z. Anorg. Allg. Chem.* **2013**, 639, 485.
- (44) Berthet, Jean C.; Nierlich, M.; Ephritikhine, M. *Eur. J. Inorg. Chem.* **2002**, 2002, 850.
- (45) Redshaw, C.; Wilkinson, G.; Hussain-Bates, B.; Hursthouse, M. B. *J. Chem. Soc., Dalton Trans.* **1992**, 1803.
- (46) Busetto, L.; Zanotti, V.; Bordoni, S.; Carlucci, L.; Albano, V. G.; Braga, D. *J. Chem. Soc., Dalton Trans.* **1992**, 1105.
- (47) Rawji, G. H.; Lynch, V. M. *Acta Cryst.* **1992**, C48, 1667.
- (48) Kuate, A. C. T.; Sameni, S.; Freytag, M.; Jones, P. G.; Tamm, M. *Angew. Chem.* **2013**, 52, 8638.
- (49) Andrews, C. G.; Macdonald, C. L. B. *J. Organomet. Chem.* **2005**, 690, 5090.
- (50) Cohen, D.; Carnall, W. T. *J. Phys. Chem.* **1960**, 64, 1933
- (51) Monreal, M. J.; Diaconescu, P. L. *Organometallics* **2008**, 27, 1702.
- (52) Harris, R. K.; Pritchard, T. N.; Smith, E. G. *J. Chem. Soc., Faraday Trans. 1* **1989**, 85, 1853.
- (53) Kurfürst, M.; Blechta, V.; Schraml, J. *Mag. Reson. Chem.* **2011**, 49, 492.
- (54) Pell, T. P.; Couchman, S. A.; Ibrahim, S.; Wilson, D. J. D.; Smith, B. J.; Barnard, P. J.; Dutton, J. L. *Inorg. Chem.* **2012**, 51, 13034.
- (55) Kuroboshi, M.; Yano, T.; Kamenoue, S.; Kawakubo, H.; Tanaka, H. *Tetrahedron* **2011**, 67, 5825.
- (56) Bassindale, A. R.; Stout, T. *Tetrahedron Lett.* **1985**, 26, 3403.

- (57) Torapava, N.; Persson, I.; Eriksson, L.; Lundberg, D. *Inorg. Chem.* **2009**, *48*, 11712.
- (58) Babai, A.; Pitula, S.; Mudring, A.-V. *Eur. J. Inorg. Chem.* **2010**, *2010*, 4933.
- (59) Berthet, J.-C.; Lance, M.; Nierlich, M.; Ephritikhine, M. *Eur. J. Inorg. Chem.* **1999**, 2005.
- (60) Wilkerson, M. P.; Burns, C. J.; Paine, R. T.; Scott, B. L. *Inorg. Chem.* **1999**, *38*, 4156.
- (61) Sutton, A. D.; John, G. H.; Sarsfield, M. J.; Renshaw, J. C.; May, I.; Martin, L. R.; Selvage, A. J.; Collison, D.; Helliwell, M. *Inorg. Chem.* **2004**, *43*, 5480.
- (62) Harris, R. K.; Becker, E. D.; Cabral De Menezes, S. M.; Goodfellow, R.; Granger, P. *Pure Appl. Chem.* **2001**, *73*, 1795.
- (63) Harris, R. K.; Becker, E. D.; Cabral De Menezes, S. M.; Granger, P.; Hoffman, R. E.; Zilm, K. W. *Pure Appl. Chem.* **2008**, *80*, 59.
- (64) Kannan, S.; Moody, M. A.; Barnes, C. L.; Duval, P. B. *Inorg. Chem.* **2006**, *45*, 9206.
- (65) Mountain, A. R. E.; Kaltsoyannis, N. *Dalton Trans.* **2013**, *42*, 13477.
- (66) SMART, Apex II, Version 2.1; Bruker AXS Inc.: Madison, WI, 2005.
- (67) SAINT, Software User's Guide, Version 7.34a; Bruker AXS Inc.: Madison, WI, 2005.
- (68) Sheldrick, G. M. *SADABS*, University of Gottingen: Germany, 2005.
- (69) *SHELXTL PC*, Version 6.12; Bruker AXS Inc.: Madison, WI, 2005.

Chapter 4. Reductive Silylation of the Uranyl Ion with R₃SiOTf (R = Ph, Me)

4.1. Introduction	113
4.2. Results and Discussion	115
4.2.1. Synthesis and Characterization of U(OSiPh ₃) ₂ (dbm) ₂ (OTf) (4.1) and [U(OSiPh ₃) ₂ (^{Ar} acnac) ₂][OTf] (4.2)	115
4.2.2. Reactions with Me ₃ SiOTf	120
4.2.3. Synthesis and Characterization of UO ₂ (dbm ^{Me}) ₂ (THF) (4.3)	121
4.2.4. Synthesis and Characterization of U(OSiPh ₃) ₂ (dbm ^{Me}) ₂ (OTf) (4.4)	123
4.2.5. Synthesis and Characterization of UO ₂ (dbm) ₂ (DMPO) (4.5)	126
4.3. Summary	129
4.4. Experimental Section	131
4.4.1. General Procedures	131
4.4.2. Synthesis of U(OSiPh ₃) ₂ (dbm) ₂ (OTf) (4.1)	131
4.4.3. Synthesis of 4.1 with 1 equiv Ph ₃ SiOTf	132
4.4.4. Reaction of 4.1 with Me ₃ SiOTf	133
4.4.5. Synthesis of [U(OSiPh ₃) ₂ (^{Ar} acnac) ₂][OTf] (4.2)	133
4.4.6. Synthesis of H(dbm ^{Me})	134
4.4.7. Synthesis of UO ₂ (dbm ^{Me}) ₂ (THF) (4.3)	135
4.4.8. Synthesis of U(OSiPh ₃) ₂ (dbm ^{Me}) ₂ (OTf) (4.4)	136
4.4.9. Synthesis of UO ₂ (dbm) ₂ (DMPO) (4.5)	136
4.4.10. Synthesis of 4.1 from 4.5	137
4.4.11. X-Ray Crystallography	138
4.5. Acknowledgements	140

4.1 Introduction

Reductive silylation is a promising means of chemically modifying the uranyl ion (Section 1.2),¹⁻⁷ and is compatible with a variety of co-ligand types, including a polypyrrolic “Pacman” macrocycle,^{2,5,7-11} β -diketonates and β -ketoiminates,^{3,4,12-14} phosphine oxides,¹⁵ and even halides.¹ In contrast, however, the scope of silylating reagents that are able to effect reductive silylation is not as well established. In particular, it is not clear what roles the leaving group or the incoming silyl group play in promoting Si-O bond formation and U⁶⁺ reduction. The identity of both is potentially important, a fact which is illustrated by several examples. For instance, the reductive silylation of UO₂(Aracnac)₂ (Aracnac = ArNC(Ph)CHC(Ph)O, Ar = 3,5-^tBu₂C₆H₃) with Me₃SiI is enabled by the accessible I₂/I⁻ redox potential (Figure 4.1a),³ which allows I⁻ to function as the reductant in the transformation. Similarly, reductive silylation of UO₂(THF)(H₂L) (L = polypyrrolic macrocycle) with PhCH₂SiMe₃ is no doubt enabled by the relative stability of the benzyl radical (Figure 4.1b).² In another example, we demonstrated that the reductive silylation of UO₂(Aracnac)₂ with R₃SiH (R = Et, Ph) only proceeded in the presence of a Lewis acid activator, namely B(C₆F₅)₃, which was required to increase the electrophilicity of the Si center by abstraction of the hydride ligand (Figure 4.1c).^{12,13} In chapter 3, we demonstrated that R₃SiOTf (R = Ph, Me) promotes the reductive silylation of the cationic uranyl complexes, [UO₂(dppmo)₂(OTf)][OTf] (dppmo = Ph₂P(O)CH₂P(O)Ph₂) and [UO₂(TPPO)₄][OTf]₂

(TPPO = Ph₃PO), without a Lewis acid activator, however, the presence of a strong reductant, Cp₂Co, is required to generate the U(IV) complexes, U(OTf)₄(dppmo)₂ (**3.3**) and [Cp₂Co][U(OTf)₅(TPPO)₂] (**3.5**), respectively.¹⁵ These reactions proceed without the addition of a Lewis acid activator, because triflate is a better leaving group than a hydride ligand.

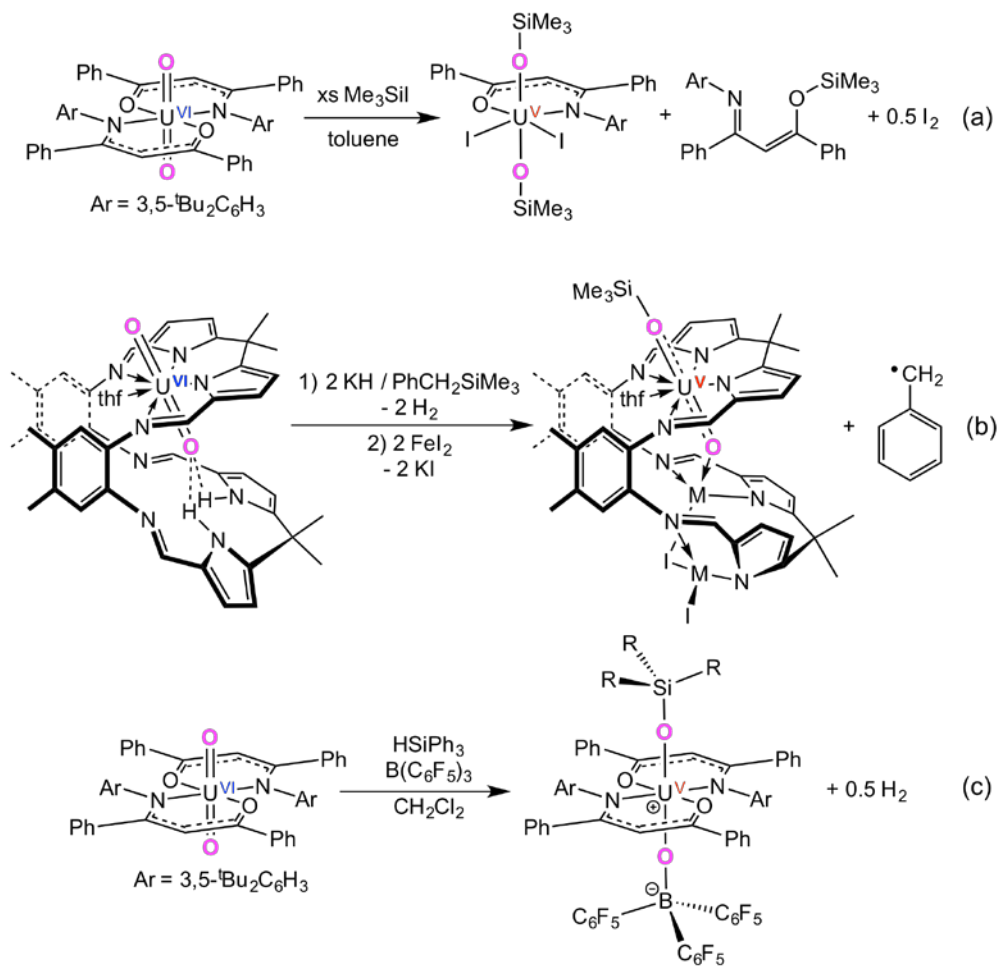


Figure 4.1. Examples of reductive silylation of the uranyl ion with various silylating reagents. **a)** reproduced from reference 3. **b)** reproduced from reference 2. **c)** reproduced from reference 12.

Intrigued by the use of R_3SiOTf ($R = Ph, Me$) as silylating reagents in organic and main group synthesis,¹⁶⁻¹⁸ as well as their ability to silylate the cationic uranyl complexes, $[UO_2(dppmo)_2(OTf)][OTf]$ and $[UO_2(TPPO)_4][OTf]_2$, we wanted to investigate the ability of the silyl triflates, R_3SiOTf ($R = Ph, Me$), to effect the reductive silylation of a series of uranyl β -diketonate and β -ketoiminate complexes. The enhanced electrophilicity of the Si center in Ph_3SiOTf , relative to that of R_3SiH ($R = Et, Ph$), suggests that it should not require the addition of a Lewis acid activator.¹²⁻¹⁴

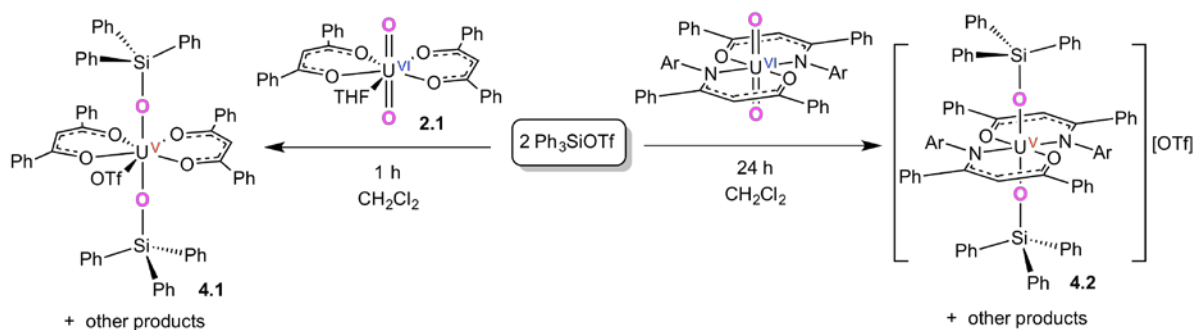
4.2 Results and Discussion

4.2.1 Synthesis and Characterization of $U(OSiPh_3)_2(dbm)_2(OTf)$ (**4.1**) and $[U(OSiPh_3)_2(Aracnac)_2][OTf]$ (**4.2**)

Addition of 2 equiv of Ph_3SiOTf to $UO_2(dbm)_2(THF)$, in CH_2Cl_2 , results in the formation of a dark red solution over the course of 1.5 h. From this solution, the U(V) bis-silyloxy, $U(OSiPh_3)_2(dbm)_2(OTf)$ (**4.1**), can be isolated as red crystalline material in 61% yield (Scheme 4.1). Similarly, addition of 2 equiv of Ph_3SiOTf to $UO_2(Aracnac)_2$, in CH_2Cl_2 , results in the formation of a dark red-brown solution, from which $[U(OSiPh_3)_2(Aracnac)_2][OTf]$ (**4.2**) can be isolated as dark red crystalline solid in 57% yield (Scheme 4.1). Complexes **4.1** and **4.2** are derived from the $1e^-$ reduction of the U center, concomitant with silylation of both oxo ligands, however, the identity of the reducing agent involved in these transformations is not immediately apparent. In fact, the formation of **4.1** and **4.2** was rather unexpected, since addition of 2 equiv of Ph_3SiOTf alone to $[UO_2(dppmo)_2(OTf)][OTf]$, resulted in no reaction (Section 3.2.1.2),

however, this is consistent with our hypothesis that the oxo ligands in $\text{UO}_2(\text{dbm})_2(\text{THF})$ or $\text{UO}_2(\text{Aracnac})_2$ are more nucleophilic than those in $[\text{UO}_2(\text{dppmo})_2(\text{OTf})][\text{OTf}]$.

It is also important to note that the formation of complexes **4.1** and **4.2** proceed in higher yields if 2 equiv of Ph_3SiOTf are added to the reaction mixtures. Addition of 1 equiv of Ph_3SiOTf to $\text{UO}_2(\text{dbm})_2(\text{THF})$ results in formation of complex **4.1** in only 33% yield.



Scheme 4.1. Synthesis of complexes **4.1** and **4.2**.

Complex **4.1** crystallizes in the monoclinic space group $P2_1/c$, while complex **4.2** crystallizes in the triclinic space group $P-1$ as a THF solvate, **4.2**·THF. Their solid-state molecular structures are shown in Figure 4.2. Complex **4.1** exhibits a pentagonal bipyramidal geometry about the uranium center, wherein two oxo-derived triphenylsilyl alkoxide ligands occupy the axial coordination sites, while two dbm ligands and one triflate ligand occupy the five equatorial coordination sites. In contrast, the cation in

complex **4.2** features an octahedral coordination geometry about the uranium center, wherein two oxo-derived triphenylsilyl alkoxide ligands occupy the axial coordination sites, while two ^{Ar}acnac ligands occupy the four equatorial sites. The monocationic charge of this fragment is balanced by the presence of an outer sphere triflate anion. The different geometry of **4.2** vs. **4.1** can be rationalized by the greater steric bulk of the ^{Ar}acnac ligand, which forces the [OTf]⁻ counterion out of the uranium coordination sphere in complex **4.2**. The U-O_{Si} bond lengths in **4.1** are 2.005(2) and 2.018(2) Å, while for **4.2**, the U-O_{Si} bond length is 2.044(2) Å (Table 4.1). These values are consistent with a significant reduction in the U-O bond order upon silylation, and are comparable to other recently reported U(V)-silyloxide U-O bond distances.^{2,3,12-14} For example, U(OB{C₆F₅}₃)(OSiPh₃)(dbm)₂(THF) (**2.2**) features a U-O bond length of 2.024(2) Å,¹⁴ and [U(OSiEt₃)₂(^{Ar}acnac)₂][HB(C₆F₅)₃] features a U-O bond length of 2.011(4) Å.¹³ The U-O_{dbm} bond lengths in **4.1** (av. U-O = 2.25 Å) are slightly shorter than those observed for uranyl dibenzoylmethanate complexes,^{14,19-22} which is consistent with the absence of uranyl character in the molecule. However, the U-O_{triflate} distance in **4.1** (2.349(2) Å) is similar to those exhibited by uranyl triflate complexes.^{3,23,24} Finally, the U-N and U-O_{acnac} bond lengths in **4.2** are 2.380(2) and 2.153(2) Å, respectively, and are comparable to those observed for related U(V) silyloxide complexes, such as U(OB{C₆F₅}₃)(OSiPh₃)(^{Ar}acnac)₂.¹²

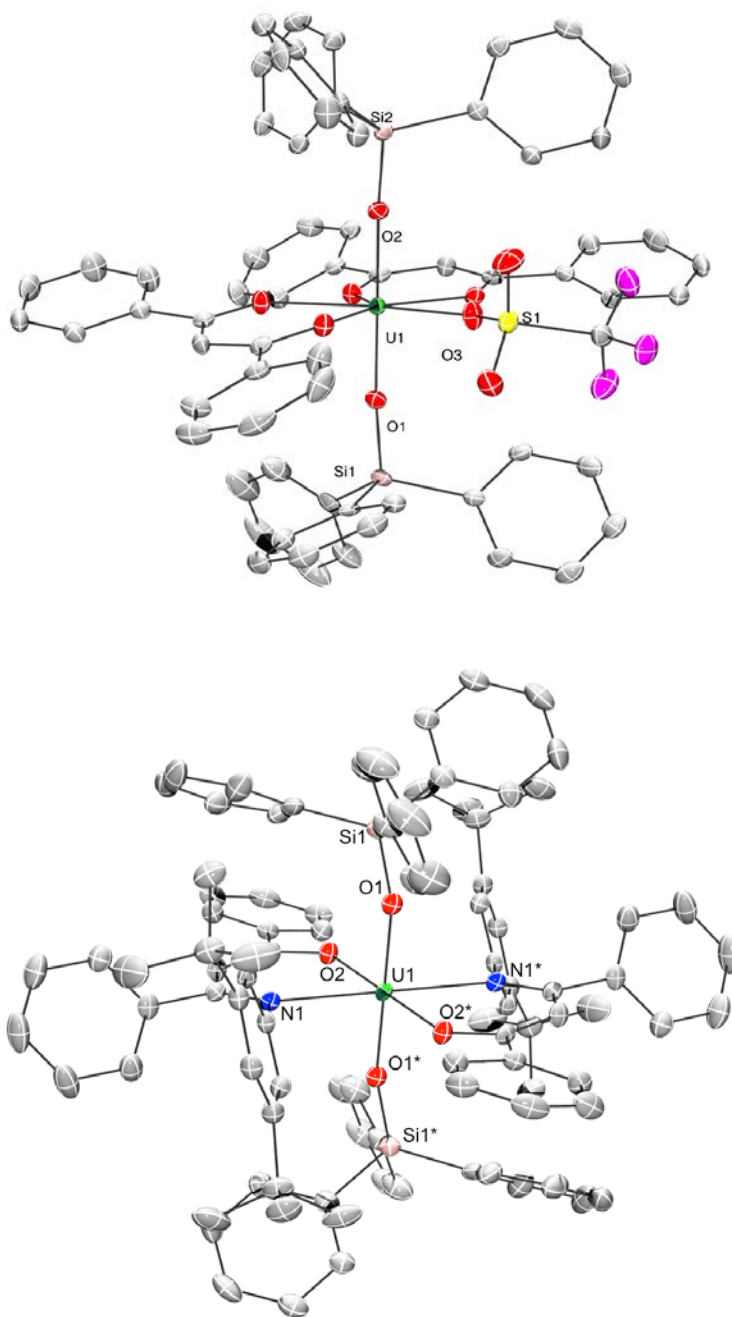


Figure 4.2. Solid-state structures of $\text{U}(\text{OSiPh}_3)_2(\text{dbm})_2(\text{OTf})$ (**4.1**) (top) and $[\text{U}(\text{OSiPh}_3)_2(\text{Aracnac})_2][\text{OTf}] \cdot \text{THF}$ (**4.2**·THF) (bottom) with 50% probability ellipsoids. For **4.1**, all hydrogens have been removed for clarity. For **4.2**, all hydrogens, the THF solvate, and the triflate counterion have been removed for clarity.

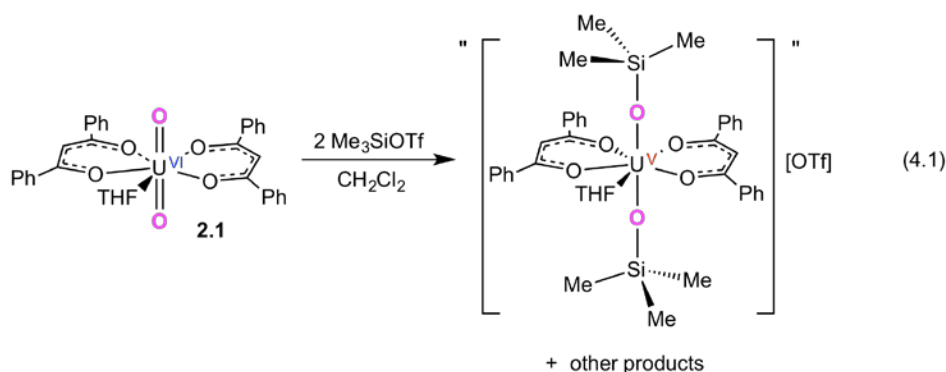
Table 4.1. Selected Bond Lengths (Å) and Angles (deg) for Complexes **4.1**, **4.2**, and **4.4**.

	4.1	4.2	4.4
U-O _{Si1}	2.005(2)	2.044(2)	2.007(5)
U-O _{Si2}	2.018(2)		2.016(4)
U-O _{eq}	2.246(2)	2.153(2)	2.238(5)
	2.259(3)		2.247(4)
	2.261(2)		2.265(4)
	2.267(2)		2.276(4)
U-O _{triflate}	2.349(2)		2.359(4)
U-N		2.380(2)	
O-Si1	1.669(2)	1.664(2)	1.666(5)
O-Si2	1.668(2)		1.655(5)
O-U-O	178.81(8)	180.0	177.8(2)
U-O-Si1	169.0(1)	164.8(1)	164.3(3)
U-O-Si2	176.1(1)		168.1(3)

The ¹H NMR spectrum of **4.1** in CD₂Cl₂ features two broad resonances at 11.09 and 7.57 ppm, which are present in a 12:18 ratio, respectively, and which correspond to the three proton environments of the Ph₃Si groups. Additionally, each dbm ligand features two magnetically inequivalent phenyl environments, a consequence of [OTf]⁻ coordination to the equatorial plane. The ¹H NMR spectrum of **4.2** in CD₂Cl₂ features three broad resonances, at 9.78, -0.43 and -0.98 ppm, which correspond to the three proton environments of the Ph₃Si groups. In addition, the presence of the ^{Aracnac} ligand is confirmed by the observation of a broad singlet at -0.53 ppm, which is assignable to the *t*Bu groups of the ^{Aracnac} moiety. The ¹⁹F{¹H} NMR spectra of **4.1** and **4.2** each consist of a single resonance at -81.28 and -78.99 ppm, respectively, corresponding to the fluorine atoms of the [OTf]⁻ group. The ²⁹Si{¹H} NMR spectrum of **4.1** consists of a broad resonance at 102.2 ppm, which is similar to the chemical shifts reported for related U(V) silyloxides.²⁵ The ²⁹Si resonance for complex **4.2** was not observed. Finally,

the near-IR spectra for **4.1** and **4.2** are similar to those of other U(V) complexes,^{3,12-14,26-28} supporting the presence of a 5f¹ ion in each complex. Interestingly, the extinction coefficients for the f-f transitions of **4.2** are much weaker than those observed for **4.1**, consistent with the presence of an inversion center in the former.^{29,30}

4.2.2 Reactions with Me₃SiOTf



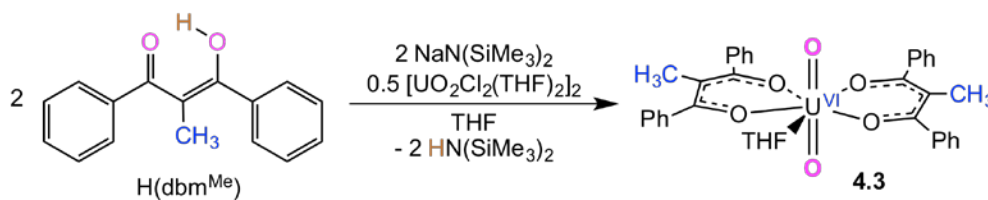
We also wanted to explore the ability of Me₃SiOTf to effect the reductive silylation of the uranyl β-diketonate complex, UO₂(dbm)₂(THF) (**2.1**). Thus, reaction of **2.1** with 2 equiv of Me₃SiOTf, in CH₂Cl₂, results in the formation of a dark red-brown solution, from which a red crystalline solid can be isolated, which we have tentatively assigned as the U(V) bis-silyloxy complex, [U(OSiMe₃)₂(dbm)₂(THF)][OTf] (eq 4.1). The formation of a reduced uranyl complex was unexpected, because the reaction of UO₂(^{Ar}acnac)₂ with Me₃SiOTf only resulted in the ligand protonation product, UO₂(OTf)₂(H{^{Ar}acnac})₂.³ This difference in reactivity is most easily explained by the basicity of the ^{Ar}acnac ligand vs. dbm, as the ^{Ar}acnac ligand is more easily protonated; however, the oxo ligands in UO₂(^{Ar}acnac)₂ are more sterically protected and harder to silylate, which could also account for the difference.

Although the solid-state molecular structure of $[\text{U}(\text{OSiMe}_3)_2(\text{dbm})_2(\text{THF})][\text{OTf}]$ was not obtained, we have tentatively confirmed its formation using ^1H and ^{19}F NMR spectroscopies. The ^1H NMR spectrum of the isolated red solid, from the reaction of **2.1** with 2 equiv of Me_3SiOTf , in CD_2Cl_2 (Figure A.5), features six broad paramagnetically shifted resonances, indicative of a reduced uranyl complex. The resonances at 8.43, 8.09 and 7.17 ppm, which are present in a 4:1:2 ratio, respectively, likely correspond to the *o*-phenyl, γ -CH, and *p*-phenyl proton environments of the dbm ligands. Additionally, there is a broad resonance at 7.58 ppm, likely corresponding to both the *m*-phenyl dbm proton environment and Me_3Si groups proton environment. This spectrum also features two broadened resonances at 4.53 and 2.02, indicating there is a THF solvate molecule attached to the uranium center. The $^{19}\text{F}\{^1\text{H}\}$ NMR spectrum of the isolated red solid, from the reaction of **2.1** with 2 equiv of Me_3SiOTf , in CD_2Cl_2 (Figure A.6), consists of a single resonance at -76.13 ppm, likely corresponding to the fluorine atoms of an outer-sphere $[\text{OTf}]^-$ group, as it is significantly downfield shifted from that of **4.1** (-81.28 ppm), and really similar to complex **4.2** (-78.99 ppm).

4.2.3. Synthesis and Characterization of $\text{UO}_2(\text{dbm}^{\text{Me}})_2(\text{THF})$ (**4.3**).

To expand the library of supporting ligands for uranyl reductive silylation, the utility of dbm^{Me} ($\text{dbm}^{\text{Me}} = \text{OC}(\text{Ph})\text{CCH}_3\text{C}(\text{Ph})\text{O}$) was also probed. $\text{H}(\text{dbm}^{\text{Me}})$ can be synthesized from the reaction of $\text{H}(\text{dbm})$ and CH_3I , in the presence of K_2CO_3 .³¹ We hypothesize that the electron donating methyl substituents will allow $\text{H}(\text{dbm}^{\text{Me}})$ to exhibit intermediate electron donation properties between the $^{\text{Aracnac}}$ and dbm co-

ligands. Similar to complex **2.1**, reaction of 4 equiv of Na(dbm^{Me}), generated *in situ*, with [UO₂Cl₂(THF)₂]₂ results in formation of a red-orange solution, from which UO₂(dbm^{Me})₂(THF) (**4.3**) can be isolated as a red-orange powder in 33% yield (Scheme 4.2). This complex features a singlet at 2.28 ppm in its ¹H NMR spectrum (CD₂Cl₂), which is assignable to the γ-C(CH₃) groups of the dbm ligands. In addition, broad singlets at 4.68 and 2.19 ppm, confirm the presence of THF in the uranyl coordination sphere.



Scheme 4.2. Synthesis of UO₂(dbm^{Me})₂(THF) (**4.3**).

We evaluated the strength of the U=O bonds in complex **4.3** relative to the previously characterized β-ketoiminate complex, UO₂(^{Ar}acnac)₂, and β-diketonate complex, UO₂(dbm)₂(THF) (**2.1**). Complex **4.3** features a U=O ν_{sym} mode of 827 cm⁻¹ in its Raman spectrum (Figure 4.3). For comparison, the U=O ν_{sym} modes for UO₂(^{Ar}acnac)₂ and **2.1** were determined to be 812 cm⁻¹,⁴ and 823 cm⁻¹,¹⁴ respectively. Surprisingly, this reveals that the U=O bonds in **4.3** exhibit comparable strength to **2.1**, within error, and shows that the effect of methyl substituents of the dbm^{Me} ligand are negligible.

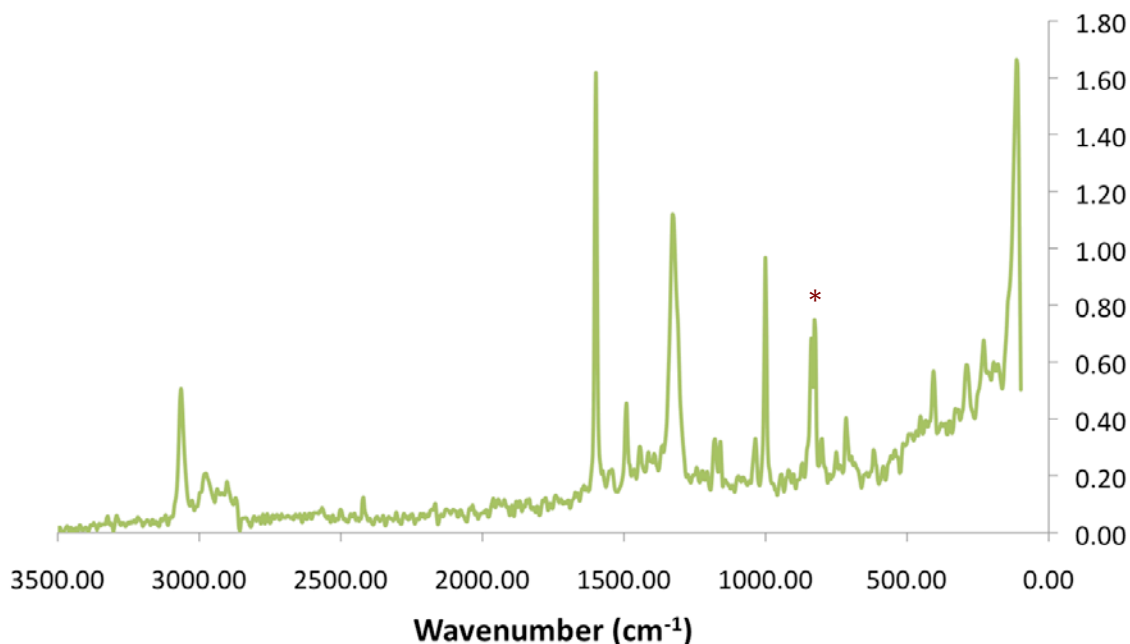
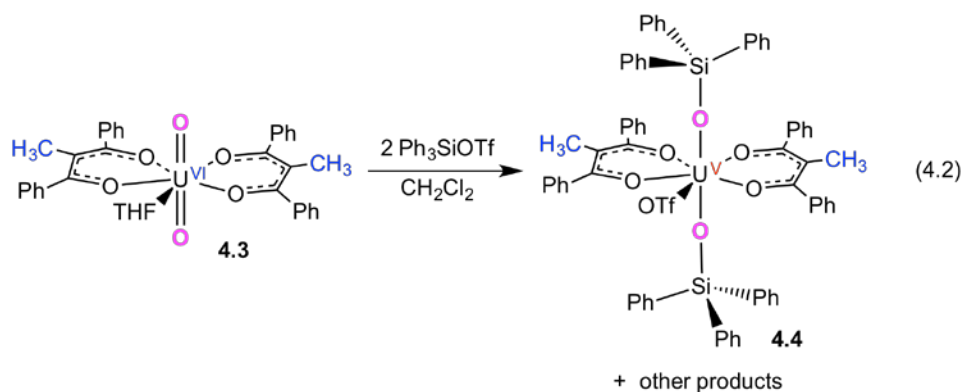


Figure 4.3. Solid-state Raman spectrum of **4.3**. U=O ν_{sym} stretch is observed at 827 cm^{-1} (*).

4.2.4. Synthesis and Characterization of $\text{U}(\text{OSiPh}_3)_2(\text{dbm}^{\text{Me}})_2(\text{OTf})$ (**4.4**).

Upon establishing the relative donor strength of dbm^{Me} , we subjected **4.3** to our Ph_3SiOTf reductive silylation protocol. Similarly to complex **4.1**, addition of 2 equiv of Ph_3SiOTf to **4.3**, in CH_2Cl_2 , results in the formation of a dark red-brown solution over 24 h, from which the U(V) bis-silyloxide, $\text{U}(\text{OSiPh}_3)_2(\text{dbm}^{\text{Me}})_2(\text{OTf})$ (**4.4**), can be isolated as red crystalline material in 40% yield (eq 4.2).



Complex **4.4** crystallizes in the monoclinic space group $P2_1/n$, and its solid-state molecular structure is shown in Figure 4.4. Complex **4.4** exhibits a pentagonal bipyramidal geometry about the uranium center, as determined from the inter-ligand bond angles. For example, complex **4.4** exhibits an O_{Si} -U- O_{Si} bond angle of $177.8(2)^\circ$, while the O_{eq} -U- O_{ax} bond angles range from $86.1(2)$ to $96.1(2)^\circ$.³²⁻³⁴ The U- O_{Si} bond lengths are $2.007(5)$ and $2.016(4)$ Å (Table 4.1), and are comparable to those observed in complexes **2.2**, **2.3**, **2.6**, **4.1** and **4.2**, as well as those previously reported for other U(V)-silyloxides.^{2,3,12,13} The U- O_{dbmMe} bond lengths in **4.4** (av. U-O = 2.26 Å) are similar to the U- O_{dbm} bond lengths in **4.1** (av. U-O = 2.25 Å), which demonstrates the similarity of the dbm and dbm^{Me} co-ligands. The U- $O_{triflate}$ distance in **4.4** ($2.359(4)$ Å) is also similar to **4.1** ($2.349(2)$ Å), as well as those exhibited by uranyl triflate complexes.^{3,23,24}

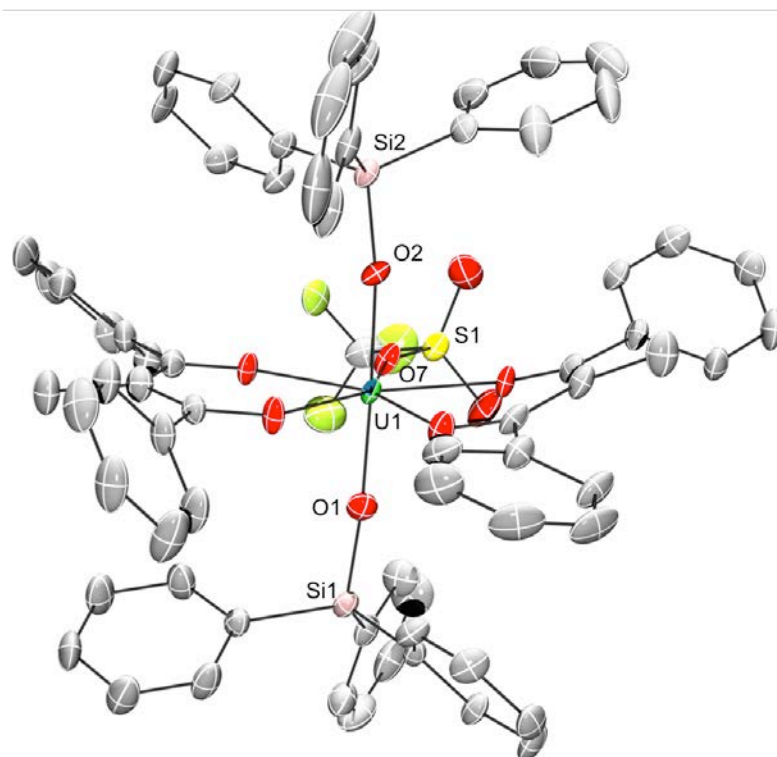


Figure 4.4. Solid-state structure of $\text{U}(\text{OSiPh}_3)_2(\text{dbm}^{\text{Me}})_2(\text{OTf})$ (**4.4**) with 50% probability ellipsoids. All hydrogens have been removed for clarity.

The ^1H NMR spectrum of **4.4** in CD_2Cl_2 features two broad resonances at 10.97 and 7.68 ppm, which are present in a 12:18 ratio, respectively, and which correspond to the three proton environments of the Ph_3Si groups. Additionally, similar to **4.1**, each dbm ligand features two magnetically inequivalent phenyl environments, a consequence of $[\text{OTf}]^-$ coordination to the equatorial plane. This spectrum also features one resonance at 1.98 ppm, assignable to the γ -methyl proton environment of the dbm^{Me} ligands. The $^{19}\text{F}\{^1\text{H}\}$ NMR spectrum of **4.4** consists of a single broad resonance at -81.26 ppm, corresponding to the fluorine atoms of the $[\text{OTf}]^-$ group.

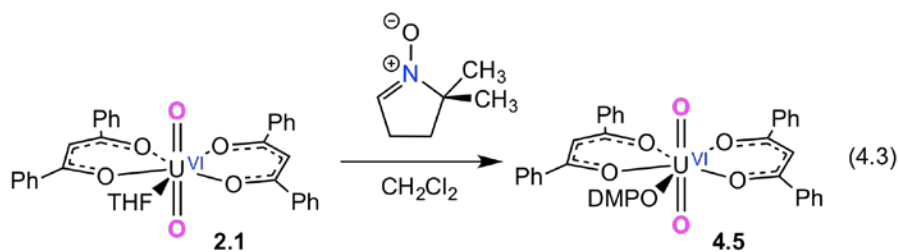
4.2.5. Synthesis and Characterization of $\text{UO}_2(\text{dbm})_2(\text{DMPO})$ (4.5).

Interestingly, complexes **4.1**, **4.2**, and **4.4** require 2 equiv of Ph_3SiOTf for their formation, but only 1 equiv of OTf is incorporated into the final product. Moreover, the identity of the reducing agent involved in the transformation is not immediately apparent. To determine the fate of the missing OTf group we monitored the formation of **4.1** by $^{19}\text{F}\{^1\text{H}\}$ NMR spectroscopy in CD_2Cl_2 . The *in situ* $^{19}\text{F}\{^1\text{H}\}$ NMR spectrum of the reaction mixture reveals the formation complex **4.1**, as revealed by a singlet at -81.24 ppm, along with the presence of unreacted Ph_3SiOTf , as revealed by a sharp singlet at -76.97 ppm. In addition, two other triflate environments are observed at -76.41 and -77.68 ppm, which we have been unable to assign. We also monitored the formation of **4.1** by ^1H NMR spectroscopy in toluene- d_8 . The *in situ* ^1H NMR spectrum of the reaction mixture reveals the formation of complex **4.1** and unreacted Ph_3SiOTf , along with small amounts of $\text{H}(\text{dbm})$ and unidentified products characterized by resonances at 8.22, 7.90, 6.93 and 6.85 ppm.⁴⁸ These data suggest that, perhaps, the dbm ligand is sacrificially oxidized to generate the U(V) center observed in the final product. The resulting dbm radical then undergoes further reactivity, such as abstracting a hydrogen atom from the solvent. To test this hypothesis we recorded a ^2H NMR spectrum of the reaction mixture in CH_2Cl_2 . However, this spectrum does not reveal ^2H incorporation into complex **4.1**, $\text{H}(\text{dbm})$, or the unidentified products.

To explain these observations, we propose that reductive silylation with Ph_3SiOTf results in the generation of a radical, perhaps a triflate radical or dbm radical, which subsequently reacts with the other components of the reaction mixture, and

forms other OTf environments observed in the *in situ* $^{19}\text{F}\{^1\text{H}\}$ spectrum. Importantly, this hypothesis would account for the $1e^-$ reduction of the uranium center to U(V) and the fact that the second triflate moiety is not incorporated into the product. A triflate radical is anticipated to be a highly reactive species, which has only been proposed as an intermediate in a few instances. For example, it is likely formed upon photolysis of a 1,8-naphthalimide photoacid,^{35,36} whereupon it undergoes a rapid H-atom abstraction to generate triflic acid. Similarly, methane sulfonate radicals, $\text{CH}_3\text{SO}_3\cdot$, are proposed intermediates in methane sulfonation.³⁷⁻³⁹ Importantly, $\text{CH}_3\text{SO}_3\cdot$ is thought to be capable of hydrogen atom abstraction from methane,³⁷⁻³⁹ which is further evidence in support of its high reactivity. As a result, it is not clear if its proposed intermediacy in the formation of **4.1**, **4.2**, and **4.4** is reasonable. Thus, we endeavored to test for the presence of any radical species in the reductive silylation reaction by employment of a hydrogen atom donor.

The reaction of either $\text{UO}_2(\text{dbm})_2(\text{THF})$ or $\text{UO}_2(\text{Aracnac})_2$ with 2 equiv Ph_3SiOTf , in the presence of 10 equiv of 1,4-cyclohexadiene, a commonly used hydrogen atom donor due to its weak C-H bonds,⁴⁰ was followed by ^1H NMR spectroscopy in CD_2Cl_2 , which revealed in the formation of complex **4.1** and **4.2**, respectively; however, the formation of anthracene or bianthracene was not observed. Accordingly, we turned our attention to 5,5-dimethyl-1-pyrroline-*N*-oxide (DMPO), due to its ability to trap a variety of oxygen-centered radicals.⁴¹⁻⁴⁵ Conveniently, we found that DMPO can easily displace THF in $\text{UO}_2(\text{dbm})_2(\text{THF})$, forming a uranyl DMPO complex, $\text{UO}_2(\text{dbm})_2(\text{DMPO})$ (**4.5**), which can be isolated as orange blocks in 84% yield (eq 4.3).



The ^1H NMR spectrum of **4.5** in CD_2Cl_2 exhibits four peaks at 7.73, 2.69, 2.31, and 1.90 ppm, assignable to the four proton environments of the coordinated DMPO ligand. These resonances are shifted slightly downfield from those observed for free DMPO (e.g., 6.66, 2.53, 2.10, and 1.36 ppm in CD_2Cl_2). This spectrum also reveals the presence of two magnetically inequivalent phenyl environments, as evidenced by the two characteristic *o*-proton resonances at 8.59 and 8.40 ppm. This suggests that, unlike the THF solvate in complex **2.1**, the DMPO ligand does not undergo rapid exchange in solution. The different *m*- and *p*-proton resonances are overlapping in one large multiplet at 7.66 ppm. There is also a resonance at 7.30 ppm, assignable to the one γ -proton environment. Complex **4.5** crystallizes in the monoclinic space group $P2_1/n$; however, the crystals were badly twinned and only a preliminary structure could be obtained. Nonetheless, the X-ray data did confirm its formulation as a DMPO complex (Figure A.7).

The direct incorporation of DMPO into the uranyl coordination sphere should ensure the close proximity of the spin trap to the site of radical generation, thus ensuring a high probability that any radicals formed will be intercepted before they can undergo other, unwanted reactivity. However, it is important to demonstrate that **4.5** also undergoes analogous reductive silylation chemistry with Ph_3SiOTf . As a result,

addition of 2 equiv of Ph₃SiOTf to **4.5**, forms a deep red-brown solution which was allowed to stir for 24 h. After work-up, complex **4.1** can be isolated as red brown crystals in 38% yield (eq 4.4), verifying the reaction proceeds in a similar manner in the presence of DMPO. Although, it should be noted that with DMPO in the uranium coordination sphere the reaction proceeds at a slower rate. Once it was clear the reaction of **4.5** with Ph₃SiOTf was still generating complex **4.1**, we monitored the reaction of **4.5** with 2 equiv of Ph₃SiOTf in CH₂Cl₂ by EPR spectroscopy. The *in situ* EPR spectra revealed no resonances, suggesting all of the reaction components are EPR silent. To our dismay, these experiments cannot be used to confirm or deny the formation a radical by-product in the reaction of **4.5** with 2 equiv of Ph₃SiOTf.

4.3 Summary

In summary, reaction of UO₂(dbm)₂(THF) (**2.1**) or UO₂(^{Ar}acnac)₂ with 2 equiv of Ph₃SiOTf, results in isolation of the reductive silylation products, U(OSiPh₃)₂(dbm)₂(OTf) (**4.1**), and [U(OSiPh₃)₂(^{Ar}acnac)₂][OTf] (**4.2**), respectively. Similarly, reaction of UO₂(dbm^{Me})₂(THF) (**4.3**) with 2 equiv of Ph₃SiOTf, results in the isolation of the reductive silylation product, U(OSiPh₃)₂(dbm)₂(OTf) (**4.4**), demonstrating that complex **4.3** and **2.1** undergo analogous reductive silylation chemistry with Ph₃SiOTf. This suggests that the U=O activation exhibited by the co-ligands is comparable.

Interestingly, we previously reported that the reaction of UO₂(^{Ar}acnac)₂ with Me₃SiOTf did not result in reductive silylation. Instead, this reaction only resulted in formation of the product of ligand protonation, namely UO₂(OTf)₂(H{^{Ar}acnac})₂.³ In contrast, it appears that reaction of **2.1** with 2 equiv of Me₃SiOTf, results in the

formation of a reduced uranyl complex. The varying reactivity exhibited by Ph_3SiOTf vs. Me_3SiOTf is significant because it reveals the importance of the $\text{R}_3\text{Si-}$ group in determining the outcome of the reductive silylation reaction.

Most notably, we have demonstrated that Ph_3SiOTf , unlike Ph_3SiH , is capable of effecting the reductive silylation of uranyl without the addition of an exogenous Lewis acid activator. This observation can be rationalized by the increased electrophilicity of the Si center in Ph_3SiOTf vs. Ph_3SiH , as evidenced by the ^{29}Si NMR resonance of Ph_3SiOTf (3.6 ppm),⁴⁹ which is downfield of that observed for Ph_3SiH (-21.1 ppm),⁵⁰ consistent with its greater silylium character.⁵¹

4.4 Experimental Section

4.4.1. General Procedures. All reactions and subsequent manipulations were performed under anaerobic and anhydrous conditions under an atmosphere of nitrogen. Hexanes and diethyl ether were dried using a Vacuum Atmospheres DRI-SOLV solvent purification system. THF was distilled twice, first from calcium hydride and then from sodium benzophenone ketyl, and stored over 3Å molecular sieves for 24 h prior to use. CH₂Cl₂, CD₂Cl₂, toluene-*d*₈ and C₆D₆ were dried over activated 3 Å molecular sieves for 24 h before use. UO₂(Aracnac)₂,⁵² UO₂(dbm)₂(THF),¹⁴ and Ph₃SiOTf,⁴⁹ were synthesized according to previously reported procedures. All other reagents were purchased from commercial suppliers and used as received.

NMR spectra were recorded on a Varian UNITY INOVA 400 spectrometer or an Agilent Technologies 400-MR DD2 spectrometer. ¹H NMR spectra were referenced to external SiMe₄ using the residual protio solvent peaks as internal standards. The chemical shifts of the ¹⁹F{¹H} spectra were referenced indirectly with the ¹H resonance of SiMe₄ at 0 ppm, according to IUPAC standard.^{53,54} ²⁹Si{¹H} NMR spectra were referenced to external SiMe₄ in C₆D₆. Raman and IR spectra were recorded on a Mattson Genesis FTIR/Raman spectrometer. IR samples were recorded as KBr pellets, while Raman samples were recorded in an NMR tube as neat solids. UV-vis/NIR experiments were performed on a UV-3600 Shimadzu spectrophotometer. Elemental analyses were performed by the Microanalytical Laboratory at UC Berkeley.

4.4.2. Synthesis of U(OSiPh₃)₂(dbm)₂(OTf) (4.1). To an orange dichloromethane (3 mL) solution of UO₂(dbm)₂(THF) (57.9 mg, 0.073 mmol) was added dropwise a

solution of Ph₃SiOTf (58.9 mg, 0.144 mmol) in dichloromethane (2 mL), which resulted in formation of a dark red-brown solution. The solution was stirred for 1.5 h, whereupon the solution was filtered through a Celite column supported on glass wool (0.5 cm × 2 cm). The filtrate was concentrated *in vacuo*, layered with hexanes (2 mL), and stored at -25 °C for 24 h. This resulted in the deposition of a dark red crystalline material, which was isolated by decanting off the supernatant (62.3 mg, 61% yield). Anal. Calcd for UO₉Si₂SF₃C₆₇H₅₂: C, 58.13; H, 3.79. Found: C, 57.88; H, 3.67. ¹H NMR (CD₂Cl₂, 25 °C, 400 MHz): δ 11.09 (br s, 12H, Ph₃Si ortho CH), 7.57 (br s, 18H, Ph₃Si meta and para CH), 7.29 (br s, 2H, dbm para CH), 6.32 (br s, 4H, dbm ortho CH), 5.94 (br s, 4H, dbm ortho CH), 5.09 (br s, 4H, dbm meta CH), 3.87 (br s, 4H, dbm meta CH). One dbm para CH resonance was not observed due to overlapping peaks at ~7.4 ppm. The γ-CH was also not observed, possibly due to broadening. ¹⁹F{¹H} NMR (CD₂Cl₂, 25 °C, 376 MHz): δ -81.28 (br s, OTf). ²⁹Si{¹H} NMR (CD₂Cl₂, 25 °C, 79 MHz): δ 102.2 (br s, Ph₃Si). UV-vis/NIR (CH₂Cl₂, 3.83 × 10⁻³ M, L·mol⁻¹·cm⁻¹): 916 (ε = 13), 1082 (ε = 24), 1394(sh, ε = 25), 1454 (ε = 41), 1612 (ε = 36), 1670 (sh, ε = 19). IR (KBr pellet, cm⁻¹): 1585(sh vw), 1587(w), 1524(sh s), 1512(s), 1489(m), 1479(m), 1458(w), 1437(m), 1429(m), 1348(sh w), 1333(m), 1319(m), 1296(m), 1288(m), 1236(m), 1200(m), 1178(m), 1157(w), 1105(vs), 1068(m), 1007(m), 964(m), 939(w), 872(w), 837(s), 786(vw), 762(w), 744(vw), 712(m), 698(m), 683(m), 631(m), 617(vw), 600(vw), 530(m), 513(m), 505(sh m).

4.4.3. Synthesis of 4.1 with 1 equiv of Ph₃SiOTf. To an orange dichloromethane (2 mL) solution of UO₂(dbm)₂(THF) (40.3 mg, 0.051 mmol) was added dropwise a solution of Ph₃SiOTf (20.2 mg, 0.049 mmol) in dichloromethane (1 mL). This resulted

in rapid formation of a dark red-brown solution. The solution was stirred for 1.5 h, whereupon the solution was filtered through a Celite column supported on glass wool (0.5 cm × 2 cm). The filtrate was concentrated *in vacuo*, layered with hexanes (5 mL), and stored at -25 °C for 24 h. This resulted in the deposition of a dark red crystalline material (23.4 mg, 33% yield), which was subsequently identified as complex **4.1** by ¹H NMR spectroscopy.

4.4.4. Reaction of 4.1 and Me₃SiOTf. To a stirring light orange solution of UO₂(dbm)₂(THF) (48.6 mg, 0.061 mmol) in dichloromethane (6 mL), was added Me₃SiOTf (22 μL, 0.123 mmol) via micro syringe, which resulted in an immediate color change to dark red-brown. The solution was stirred for 1.5 h, whereupon it was filtered through a Celite column supported on glass wool (0.5 cm × 2 cm). The red-brown filtrate was concentrated *in vacuo*, layered with hexanes (2 mL), and stored at -25 °C for 24 h. This resulted in the deposition of a dark red crystalline material, which was isolated by decanting off the supernatant (23.6 mg). The yield is 35%, if the formula, [U(OSiMe₃)₂(dbm)₂(THF)][OTf], is assumed. ¹H NMR (CD₂Cl₂, 25 °C, 400 MHz): δ 8.43 (br s, 8H, dbm ortho CH), 8.09 (br s, 2H, dbm γ-CH), 7.58 (br s, 17H, dbm meta CH and CH₃), 7.17 (br s, 4H, dbm para CH), 4.53 (br s, 4H, THF), 2.02 (br s, 4H, THF). ¹⁹F{¹H} NMR (CD₂Cl₂, 25 °C, 376 MHz): δ -76.13 (br s, OTf).

4.4.5. Synthesis of [U(OSiPh₃)₂(^{Ar}acnac)₂][OTf] (Ar = 3,5-^tBu₂C₆H₃) (4.2). To a red dichloromethane (2 mL) solution of UO₂(^{Ar}acnac)₂ (101.2 mg, 0.093 mmol) was added dropwise a solution of Ph₃SiOTf (76.4 mg, 0.187 mmol) in dichloromethane (2 mL). This resulted in the formation of a slightly darker red solution. The solution was stirred for 24 h, whereupon the volatiles were removed *in vacuo*. The tacky red oil was washed

with hexanes (3 mL), before being extracted into diethyl ether (4 mL). The solution was filtered through a Celite column supported on glass wool (0.5 cm × 2 cm), concentrated *in vacuo*, and stored at -25 °C for 24 h. This resulted in the deposition of a dark red crystalline material, which was isolated by decanting off the supernatant (93.1 mg, 57% yield). X-ray quality crystals were grown from a solution of THF layered with hexanes and stored at 25 °C for 24 h. Anal. Calcd for UO₇N₂Si₂SF₃C₉₅H₉₄: C, 64.87; H, 5.39; N, 1.59. Found: C, 64.46; H, 5.82; N, 1.49. ¹H NMR (CD₂Cl₂, 25 °C, 400 MHz): δ 9.78 (br s, 6H, Ph₃Si para CH), 9.14 (br s, 2H, Ar para CH or ^{Ar}acnac γ-CH), 7.75 (m, 4H, acnac CH), 7.46 (m, 4H, acnac CH), 7.33 (m, 4H, acnac CH), 6.84 (m, 4H, acnac CH), 6.63 (br s, 2H, acnac CH), 6.03 (br s, 2H, acnac CH), 5.73 (br s, 2H, Ar para CH or ^{Ar}acnac γ-CH), -0.43 (s, 12H, Ph₃Si meta CH), -0.53 (s, 36H, CH₃), -0.98 (s, 12H, Ph₃Si ortho CH), -1.83 (br s, 4H, Ar ortho CH). ¹⁹F{¹H} NMR (CD₂Cl₂, 25 °C, 376 MHz): δ -78.99 (br s, OTf). UV-vis/NIR (CH₂Cl₂, 4.10 × 10⁻³ M, L·mol⁻¹·cm⁻¹): 1082 (ε = 4), 1382 (sh, ε = 2), 1456 (ε = 6), 1664 (ε = 4). IR (KBr pellet, cm⁻¹): 1585(m), 1558(s), 1541(m), 1477(m), 1462(vs), 1429(m), 1352(m), 1336(m), 1333(m), 1290(m), 1281(sh m), 1246(m), 1234(m), 1200(s), 1115(s), 1105(sh m), 1063(w), 1028(sh m), 1022(m), 1001(sh w), 962(w), 953(sh vw), 845(sh w), 824(vs), 770(vw), 744(vw), 712(m), 698(s), 636(m), 582(vw), 513(s), 442(sh w), 424(m).

4.4.6. Synthesis of H(dbm^{Me}). The preparation described below was modified from the published procedure for H(dbm^{Me}).³¹ To a stirring colorless solution of dbm (5.0121 g, 0.022 mol) in THF (7 mL), was added a white slurry of K₂CO₃ (4.6239 g, 0.033 mol) in THF (10 mL), followed by CH₃I (1.41 mL, 0.023 mol), which resulted in no observable change. The white slurry was refluxed at 75 °C for 5 h, whereupon the

solution is a dark orange color, concomitant with a small amount of white solid. Once the reaction mixture was cooled to room temperature, deionized water (~ 40 mL) was added to quench the reaction, which resulted in a colorless aqueous layer, and an orange-brown THF layer. The organic layer was extracted using a separatory funnel, and the aqueous layer was washed with dichloromethane (3 × 10 mL). The dichloromethane washes were combined with the organic layer. The orange-brown organic fraction was dried with sodium sulphate, whereupon it was filtered, using filter paper and a Buchner funnel. All the volatiles were removed from the orange-brown filtrate *in vacuo*, and the resulting orange-brown solid was washed with hexanes (2 × 10 mL). The dark orange solid was dried *in vacuo* (4.5793 g, 86% yield). Spectral data collected for this material matched those previously reported for H(dbm^{Me}).³¹

4.4.7. Synthesis of UO₂(dbm^{Me})₂(THF) (4.3). To a stirring THF (3 mL) solution of [UO₂Cl₂(THF)₂]₂ (427.3 mg, 0.440 mmol), was added dropwise a solution of dbm^{Me} (368.8 mg, 1.539 mmol) and NaN(SiMe₃)₂ (286.3 mg, 1.559 mmol) in THF (3 mL). This resulted in formation of a dark red-orange solution. This solution was stirred for 24 h, whereupon the solution was filtered through a Celite column supported on glass wool (0.5 cm × 2 cm) to remove NaCl. The solution was then concentrated *in vacuo*, layered with hexanes (3 mL), and stored at -25 °C for 24 h, which resulted in the deposition of an red-orange powder. The solid was then extracted into dichloromethane (6 mL), and filtered through a Celite column supported on glass wool (0.5 cm × 2 cm). The filtrate was then concentrated *in vacuo*, layered with hexanes (3 mL), and stored at -25 °C for 24 h, which resulted in the deposition of an red-orange powder (208.9 mg, 33% yield). ¹H NMR (CD₂Cl₂, 25 °C, 400 MHz): δ 7.95 (br s, 8H, ortho CH), 7.62 (br s, 4H, para CH),

7.54 (br s, 8H, meta CH), 4.68 (br s, 4H, THF), 2.28 (s, 6H, CH₃), 2.19 (br s, 4H, THF). IR (KBr pellet, cm⁻¹): 1599(w), 1581(m), 1541(vs), 1495(m), 1468(m), 1444(w), 1417(s), 1328(sh m), 1315(m), 1306(m), 1275(m), 1205(w), 1175(w), 1101(w), 1074(w), 1020(sh w), 1009(m), 926(m), 906(m), 868(w), 800(w), 773(w), 748(m), 714(m), 694(m), 609(w), 557(w), 532(w). Raman (cm⁻¹): 3064(w), 2968(w), 1599(s), 1491(w), 1325(s), 1162(w), 1159(w), 1036(w), 1001(s), 839(m), 827(m, U=O ν_{sym}), 715(w), 407(w), 283(w).

4.4.8. Synthesis of U(OSiPh₃)₂(dbm^{Me})₂(OTf) (4.4). To a red-orange dichloromethane (1 mL) solution of UO₂(dbm^{Me})₂(THF) (24.3 mg, 0.030 mmol) was added dropwise a colorless solution of Ph₃SiOTf (25.2 mg, 0.062 mmol) in dichloromethane (1 mL), which resulted in formation of a dark red-brown solution. The solution was stirred for 24 h, whereupon the solution was filtered through a Celite column supported on glass wool (0.5 cm × 2 cm). The filtrate was concentrated *in vacuo*, layered with hexanes (1 mL), and stored at -25 °C for 24 h. This resulted in the deposition of a dark red crystalline material, which was isolated by decanting off the supernatant (16.8 mg, 40% yield). ¹H NMR (CD₂Cl₂, 25 °C, 400 MHz): δ 10.97 (br s, 12H, Ph₃Si ortho CH), 8.82 (s, 4H, dbm^{Me} ortho CH), 7.83 (s, 4H, dbm^{Me} ortho CH), 7.68 (br s, 18H, Ph₃Si meta and para CH), 6.34 (br s, 4H, dbm^{Me} meta CH), 5.83 (br s, 4H, dbm^{Me} meta CH), 5.53 (br s, 2H, dbm^{Me} para CH), 3.78 (br s, 2H, dbm^{Me} para CH), 1.98 (s, 6H, dbm^{Me} CH₃). ¹⁹F{¹H} NMR (CD₂Cl₂, 25 °C, 376 MHz): δ -81.26 (br s, OTf).

4.4.9. Synthesis of UO₂(dbm)₂(DMPO) (4.5). To an orange dichloromethane (3 mL) solution of UO₂(dbm)₂THF (138.3 mg, 0.175 mmol) was added a colorless solution of DMPO (20.1 mg, 0.178 mmol) in dichloromethane (1 mL) dropwise, which resulted in

the formation of a slightly more intense orange solution. The solution was allowed to stir at room temperature for 20 min, before it was filtered through a Celite column supported on glass wool (0.5 cm × 2 cm). The filtrate was then concentrated *in vacuo*, layered with hexanes (2 mL), and stored at -25 °C for 24 h, which afforded a dark orange crystals (121.5 mg, 84% yield). Anal. Calcd for UO₇NC₃₆H₃₃: C, 52.11; H, 4.01; N, 1.69. Found: C, 52.18; H, 3.91; N, 1.78. ¹H NMR (CD₂Cl₂, 25 °C, 500 MHz): δ 8.59 (m, 4H, ortho CH), 8.40 (m, 4H, ortho CH), 7.73 (s, 1H, DMPO CH), 7.66-7.53 (m, 12H, CH), 7.27 (s, 2H, γ-CH), 2.72 (t of d, *J*_{HH} = 14.8 Hz, *J*_{HH} = 2.5 Hz, 2H, DMPO CH₂), 2.31 (t, *J*_{HH} = 15.0 Hz, 2H, DMPO CH₂), 1.90 (s, 6H, CH₃). IR (KBr pellet, cm⁻¹): 1612(sh w), 1591(m), 1537(vs), 1524(vs), 1477(m), 1452(m), 1441(w), 1371(s), 1350(sh m), 1311(m), 1300(sh w), 1290(sh w), 1221(w), 1190(sh w), 1178(vw), 1148(vw), 1142(w), 1067(w), 1024(w), 939(w), 902(s), 785(w), 750(m), 716(w), 681(sh w), 685(m), 609(vw), 606(w), 596(sh vw), 513(w).

4.4.10. Synthesis of 4.1 from 4.5. To a stirring orange solution of complex **4.5** (53.8 mg, 0.065 mmol) in dichloromethane (3 mL), was added a colorless solution of Ph₃SiOTf (52.0 mg, 0.127 mmol) in dichloromethane (2 mL) dropwise, which resulted in an immediate color change to dark red. The reaction mixture was allowed to stir for 24h at room temperature, whereupon the dark red solution was filtered through a Celite column supported on glass wool (0.5 cm × 2 cm). The filtrate was then concentrated *in vacuo*, layered with Et₂O (2 mL), and stored at -25 °C for 24 h, which afforded a dark red crystals (34.3 mg, 38% yield), which was subsequently identified as complex **4.1** by ¹H NMR spectroscopy.

4.4.11. X-ray Crystallography. Data for **4.1**, **4.2** and **4.4** were collected on a Bruker KAPPA APEX II diffractometer equipped with an APEX II CCD detector using a TRIUMPH monochromater with a Mo K α X-ray source ($\lambda = 0.71073 \text{ \AA}$). The crystals were mounted on a cryoloop under Paratone-N oil and all data were collected at 100(2) K using an Oxford nitrogen gas cryostream system. A hemisphere of data was collected using ω scans with 0.5° frame widths. Frame exposures of 10 s were used for both complexes **4.1** and **4.2**, while frame exposures of 10 and 15 s were used for complex **4.4**. Data collection and cell parameter determination were conducted using the SMART program.⁵⁵ Integration of the data frames and final cell parameter refinement were performed using SAINT software.⁵⁶ Absorption correction of the data was carried out using the multi-scan method SADABS.⁵⁷ Subsequent calculations were carried out using SHELXTL.⁵⁸ Structure determination was done using direct or Patterson methods and difference Fourier techniques. All hydrogen atom positions were idealized, and rode on the atom of attachment. Structure solution, refinement, graphics, and creation of publication materials were performed using SHELXTL.⁵⁸ A summary of relevant crystallographic data for **4.1**, **4.2** and **4.4** is presented in Table 4.2.

The OTf counter ion in **4.2** possesses positional disorder, wherein the SO₃ and CF₃ groups are mutually disordered in a 50:50 ratio. This disorder was modeled by assigning C52 and S1 over the same two positions with 0.5 occupancies. The disorder in F1 and O5, F2 and O6, and F3 and O7 was modeled in the same way.

Table 4.2. X-Ray Crystallographic Data for Complexes **4.1**, **4.2** and **4.4**.

	4.1	4.2·THF	4.4
empirical formula	UO ₉ F ₃ SSi ₂ C ₆₇ H ₅₂	UO ₈ N ₂ F ₃ SSi ₂ C ₉₉ H ₁₀₂	UO ₉ F ₃ SSi ₂ C ₆₉ H ₅₆
Crystal habit, color	plate, red-orange	block, red	block, red
crystal size (mm)	0.30 × 0.20 × 0.20	0.15 × 0.15 × 0.05	0.25 × 0.25 × 0.10
crystal system	monoclinic	triclinic	monoclinic
space group	<i>P</i> 2 ₁ / <i>c</i>	<i>P</i> -1	<i>P</i> 2 ₁ / <i>n</i>
vol (Å ³)	5776.5(2)	2377.60(8)	6159.1(6)
a (Å)	12.507(2)	13.2871(2)	13.5134(7)
b (Å)	19.719(3)	14.1711(3)	20.766(1)
c (Å)	23.422(4)	15.2003(3)	22.408(1)
α (deg)	90	63.915(1)	90
β (deg)	89.692(3)	73.800(1)	101.617(2)
γ (deg)	90	69.232(1)	90
Z	4	1	4
fw (g/mol)	1384.36	1831.10	1412.41
density (calcd) (Mg/m ³)	1.592	1.279	1.523
abs coeff (mm ⁻¹)	2.957	1.813	2.775
F ₀₀₀	2756	937	2820
Total no. reflections	47674	18712	12541
Unique reflections	13845	10088	9120
final R indices [<i>I</i> > 2σ(<i>I</i>)]	R ₁ = 0.0348 wR ₂ = 0.0520	R ₁ = 0.0315 wR ₂ = 0.0914	R ₁ = 0.0505 wR ₂ = 0.1030
largest diff peak and hole (e ⁻ Å ⁻³)	0.743 and -0.638	1.665 and -0.989	3.914 and -1.497
GOF	1.118	1.081	0.923

4.5 Acknowledgements

I would like to thank my undergraduate, Jessica Tuck, for the synthesis and characterization of complex **4.3**.

4.6 References

- (1) Berthet, J.-C.; Siffredi, G.; Thuéry, P.; Ephritikhine, M. *Eur. J. Inorg. Chem.* **2007**, 4017.
- (2) Arnold, P. L.; Patel, D.; Wilson, C.; Love, J. B. *Nature* **2008**, *451*, 315.
- (3) Brown, J. L.; Wu, G.; Hayton, T. W. *J. Am. Chem. Soc.* **2010**, *132*, 7248
- (4) Brown, J. L.; Mokhtarzadeh, C. C.; Lever, J. M.; Wu, G.; Hayton, T. W. *Inorg. Chem.* **2011**, *50*, 5105.
- (5) Arnold, P. L.; Jones, G. M.; Odoh, S. O.; Schreckenbach, G.; Magnani, N.; Love, J. B. *Nat. Chem.* **2012**, *4*, 221.
- (6) Wu, W.-M.; Carley, J.; Gentry, T.; Ginder-Vogel, M. A.; Fienen, M.; Mehlhorn, T.; Yan, H.; Carroll, S.; Pace, M. N.; Nyman, J.; Luo, J.; Gentile, M. E.; Fields, M. W.; Hickey, R. F.; Gu, B.; Watson, D.; Cirpka, O. A.; Zhou, J.; Fendorf, S.; Kitanidis, P. K.; Jardine, P. M.; Criddle, C. S. *Environ. Sci. Technol.* **2006**, *40*, 3986.
- (7) Arnold, P. L.; Love, J. B.; Patel, D. *Coord. Chem. Rev.* **2009**, *253*, 1973
- (8) Yahia, A.; Arnold, P. L.; Love, J. B.; Maron, L. *Chem. Commun.* **2009**, 2402.
- (9) Yahia, A.; Arnold, P. L.; Love, J. B.; Maron, L. *Chem. Eur. J.* **2010**, *16*, 4881.
- (10) Jones, G. M.; Arnold, P. L.; Love, J. B. *Chem. Eur. J.* **2013**, *19*, 10287.
- (11) Arnold, P. L.; Hollis, E.; Nichol, G. S.; Love, J. B.; Griveau, J.-C.; Caciuffo, R.; Magnani, N.; Maron, L.; Castro, L.; Yahia, A.; Odoh, S. O.; Schreckenbach, G. *J. Am. Chem. Soc.* **2013**, *135*, 3841.
- (12) Schnaars, D. D.; Wu, G.; Hayton, T. W. *Inorg. Chem.* **2011**, *50*, 4695.
- (13) Schnaars, D. D.; Wu, G.; Hayton, T. W. *Inorg. Chem.* **2011**, *50*, 9642.
- (14) Pedrick, E. A.; Wu, G.; Kaltsoyannis, N.; Hayton, T. W. *Chem. Sci.* **2014**, *5*, 3204.
- (15) Pedrick, E. A.; Wu, G.; Hayton, T. W. *Inorg. Chem.* **2015**, *54*, 7038.
- (16) Bräckow, J.; Wanner, K. T. *Tetrahedron* **2006**, *62*, 2395.
- (17) Hoesl, C. E.; Maurus, M.; Pabel, J.; Polborn, K.; Wanner, K. T. *Tetrahedron* **2002**, *58*, 6757.
- (18) Heift, D.; Benko, Z.; Grutzmacher, H. *Dalton Trans.* **2014**, *43*, 5920.
- (19) Kannan, S.; Rajalakshmi, N.; Chetty, K. V.; Venugopal, V.; Drew, M. G. B. *Polyhedron* **2004**, *23*, 1527.

- (20) Alagar, M.; Rajagopal, K.; Krishnakumar, R. V.; Subha Nandhini, M.; Kannan, S.; Natarajan, S. *Acta Crystallogr. Sec. E* **2003**, *E59*, m524.
- (21) Hayton, T. W.; Wu, G. *Inorg. Chem.* **2008**, *47*, 7415
- (22) Zhu, L.; Yuan, D.; Li, B.; Li, H. *J. Coord. Chem.* **2010**, *63*, 3006.
- (23) Tourneux, J.-C.; Berthet, J.-C.; Cantat, T.; Thuery, P.; Mezailles, N.; Ephritikhine, M. *J. Am. Chem. Soc.* **2011**, *133*, 6162.
- (24) Berthet, J.-C.; Nierlich, M.; Ephritikhine, M. *Dalton Trans.* **2004**, 2814.
- (25) Windorff, C. J.; Evans, W. J. *Organometallics* **2014**, *33*, 3786.
- (26) Schnaars, D. D.; Wu, G.; Hayton, T. W. *J. Am. Chem. Soc.* **2009**, *131*, 17532.
- (27) Graves, C. R.; Vaughn, A. E.; Schelter, E. J.; Scott, B. L.; Thompson, J. D.; Morris, D. E.; Kiplinger, J. L. *Inorg. Chem.* **2008**, *47*, 11879.
- (28) Ryan, J. L. *J. Inorg. Nucl. Chem.* **1971**, *33*, 153.
- (29) Cooper, O. J.; Mills, D. P.; McMaster, J.; Moro, F.; Davies, E. S.; Lewis, W.; Blake, A. J.; Liddle, S. T. *Angew. Chem. Int. Ed.* **2011**, *50*, 2383.
- (30) Drago, R. S. *Physical Methods for Chemists*; 2 ed.; Saunders College Publishing, 1992.
- (31) Choudhary, A.; Baumstark, A. L. *Synthesis* **1989**, *9*, 688.
- (32) Wester, D.; Palenik, G. J. *J. Am. Chem. Soc.* **1973**, *95*, 6505.
- (33) La Pierre, H. S.; Meyer, K. *Inorg. Chem.* **2013**, *52*, 529.
- (34) Jiang, J.; Sarsfield, M. J.; Renshaw, J. C.; Livens, F. R.; Collison, D.; Charnock, J. M.; Helliwell, M.; Eccles, H. *Inorg. Chem.* **2002**, *41*, 2799.
- (35) Malval, J.-P.; Suzuki, S.; Morlet-Savary, F.; Allonas, X.; Fouassier, J.-P.; Takahara, S.; Yamaoka, T. *J. Phys. Chem. A* **2008**, *112*, 3879.
- (36) Malval, J.-P.; Morlet-Savary, F.; Allonas, X.; Fouassier, J.-P.; Suzuki, S.; Takahara, S.; Yamaoka, T. *Chem. Phys. Lett.* **2007**, *443*, 323.
- (37) Lobree, L. J.; Bell, A. T. *Ind. Eng. Chem. Res.* **2001**, *40*, 736.
- (38) Mukhopadhyay, S.; Bell, A. T. *Ind. Eng. Chem. Res.* **2002**, *41*, 5901.
- (39) Basickes, N.; Hogan, T. E.; Sen, A. *J. Am. Chem. Soc.* **1996**, *118*, 13111.
- (40) Warren, J. J.; Tronic, T. A.; Mayer, J. M. *Chem. Rev.* **2010**, *110*, 6961.
- (41) Buettner, G. R. *Free Radical Bio. Med.* **1987**, *3*, 259.
- (42) Zhao, H.; Joseph, J.; Zhang, H.; Karoui, H.; Kalyanaraman, B. *Free Radical Bio. Med.* **2001**, *31*, 599.
- (43) Khusnutdinova, J. R.; Rath, N. P.; Mirica, L. M. *J. Am. Chem. Soc.* **2011**, *134*, 2414.
- (44) Tang, F.; Zhang, Y.; Rath, N. P.; Mirica, L. M. *Organometallics* **2012**, *31*, 6690.
- (45) Kao, D.; Chaintreau, A.; Lepoittevin, J.-P.; Giménez-Arnau, E. *J. Org. Chem.* **2011**, *76*, 6188.
- (46) Janzen, E. G.; Liu, J. I.-P. *J. Mag. Resonance* **1973**, *9*, 510.
- (47) Makino, K.; Hagi, A.; Ide, H.; Murakami, A.; Nishi, M. *Can. J. Chem.* **1992**, *70*, 2818.
- (48) Vandenberg, H. W.; Evans, D. H. *J. Am. Chem. Soc.* **1974**, *96*, 4296.
- (49) Asadi, A.; Avent, A. G.; Eaborn, C.; Hill, M. S.; Hitchcock, P. B.; Meehan, M. M.; Smith, J. D. *Organometallics* **2002**, *21*, 2183.
- (50) Harris, R. K.; Pritchard, T. N.; Smith, E. G. *J. Chem. Soc., Faraday Trans. 1* **1989**, *85*, 1853.

- (51) Reed, C. A. *Acc. Chem. Res.* **1998**, *31*, 325.
- (52) Hayton, T. W.; Wu, G. *Inorg. Chem.* **2009**, *48*, 3065.
- (53) Harris, R. K.; Becker, E. D.; Cabral De Menezes, S. M.; Goodfellow, R.; Granger, P. *Pure Appl. Chem.* **2001**, *73*, 1795.
- (54) Harris, R. K.; Becker, E. D.; Cabral De Menezes, S. M.; Granger, P.; Hoffman, R. E.; Zilm, K. W. *Pure Appl. Chem.* **2008**, *80*, 59.
- (55) *SMART*, Apex II, Version 2.1; Bruker AXS Inc.: Madison, WI, 2005.
- (56) *SAINTE*, Software User's Guide, Version 7.34a; Bruker AXS Inc.: Madison, WI, 2005.
- (57) Sheldrick, G. M. *SADABS*, University of Gottingen: Germany, 2005.
- (58) *SHELXTL PC*, Version 6.12; Bruker AXS Inc.: Madison, WI, 2005.

Chapter 5. Coordination of a Tetra(aza)macrocycle to the Uranyl Ion

5.1. Introduction	145
5.2. Results and Discussion	148
5.2.1. Synthesis and Characterization of $\text{UO}_2(\text{tmtaaH})(\text{N}(\text{SiMe}_3)_2)(\text{THF})$ (5.1) and $\text{UO}_2(\text{tmtaaH})_2$ (5.2)	148
5.2.2. Synthesis and Characterization of the β -diketimate pyrazolium macrocycle (<i>Z</i> -isomer: 5.3 ; <i>E</i> -isomer: 5.4)	153
5.2.3. Synthesis and Characterization of $[\text{Li}]_2[\text{Li}(\text{THF})_3\text{Cl}]_2[\text{UO}_2\text{Cl}_2\{\text{tmtaa}\}_2\text{UO}_2\text{Cl}_2]$ (5.5).....	157
5.2.4. Synthesis and Characterization of $[\text{Li}(\text{THF})]_2[\text{UO}_2(\text{N}(\text{SiMe}_3)_2)_2(\text{tmtaa})]$ (5.6).....	160
5.3. Summary	163
5.4. Experimental Section	165
5.4.1. General Procedures	165
5.4.2. Raman Spectroscopy.....	165
5.4.3. Synthesis of Li_2tmtaa	166
5.4.4. Synthesis of $\text{UO}_2(\text{tmtaaH})(\text{N}(\text{SiMe}_3)_2)(\text{THF})$ (5.1).....	166
5.4.5. Synthesis of $\text{UO}_2(\text{tmtaaH})_2$ (5.2)	167
5.4.6. Synthesis of the β -diketimate pyrazolium macrocycle (<i>Z</i> -isomer: 5.3)	168
5.4.7. Synthesis of the β -diketimate pyrazolium macrocycle (<i>E</i> -isomer: 5.4)	170
5.4.8. Synthesis of $[\text{Li}]_2[\text{Li}(\text{THF})_3\text{Cl}]_2[\text{UO}_2\text{Cl}_2\{\text{tmtaa}\}_2\text{UO}_2\text{Cl}_2]$ (5.5).....	170

5.4.9. Synthesis of $[\text{Li}(\text{THF})]_2[\text{UO}_2(\text{N}(\text{SiMe}_3)_2)_2(\text{tmtaa})]$ (5.6).....	171
5.4.10. X-Ray Crystallography	171
5.5. Acknowledgements	176
5.6. References	176

5.1 Introduction

The uranyl ion ($trans\text{-UO}_2^{2+}$) is well known to be kinetically inert and thermodynamically robust.^{1,2} This stability is reflected in its reactivity, but also in its electrochemical properties. Despite containing the high valent U^{6+} ion, uranyl is a rather poor oxidant. For example, the standard U(VI)/U(V) redox potential for $UO_2^{2+}(aq)$ is -0.35 V (vs. Fc/Fc^+) (Figure 1.3).³ This is much higher than the classic U(VI) coordination complex, UF_6 , which is a really good oxidant, and features a U(VI)/U(V) redox potential of 2.38 V (vs. Fc/Fc^+).⁴ Although the coordination of anionic donor co-ligands to uranyl is known to lower this potential, it has also been shown that the U(VI)/U(V) redox potential can be effected by disruption of the $O=U=O$ bonding framework within uranyl. For example, our group previously demonstrated that coordination of $B(C_6F_5)_3$ to the oxo ligand in $UO_2(Aracnac)_2$ ($Aracnac = ArNC(Ph)CHC(Ph)O$; $Ar = 3,5\text{-}^t\text{Bu}_2C_6H_3$) results in a 700 mV shift of the U(VI)/U(V) couple to more oxidizing potentials.⁵ Similarly, Schelter and co-workers observed a shift of similar magnitude in $[K(\text{toluene})]_2[UO_2(NPh(3,5\text{-(CF}_3)_2C_6H_3))_4]$ vs. $[K(16\text{-crown-6})]_2[UO_2(NPh(3,5\text{-(CF}_3)_2C_6H_3))_4]$, due to coordination of the potassium cations to the uranyl oxo ligands in the former complex.⁶ These shifts in the U(VI)/U(V) redox potentials can be explained by a weakening of the U-O bonds from a reduction in electron donation from the oxo ligands to the U^{6+} ion.

The $trans/cis$ isomerization of uranyl is also expected to affect the U(VI)/U(V) redox potential. While a cis -uranyl complex has yet to be isolated, there is evidence to suggest that $cis\text{-UO}_2^{2+}$ is a substantially better oxidant than $trans\text{-UO}_2^{2+}$. For example,

an attempt to synthesize *cis*-Cp'₂UO₂ (Cp' = 1,2,4-*t*Bu₃C₅H₂) by reaction of Cp'₂UCl₂ with KC₈ and pyridine-*N*-oxide, in pyridine, resulted in formation of the U(V) oxo cluster, Cp'₄(bipy)₂U₆O₁₃, along with formation of Cp'H and (Cp')₂ (Scheme 1.4).⁷ In this example, it was argued that *cis*-Cp'₂UO₂ was initially formed, but quickly decomposed via homolytic Cp'-U cleavage. Similarly, reaction of Cp*₂UI(THF) with KC₈ and pyridine-*N*-oxide generates (Cp*)₂, also via an unstable *cis*-Cp*₂UO₂ intermediate (Scheme 1.4).⁸ In another example, Clark and co-workers demonstrated that reaction of a tripodal ligand, [Li]₃[N(CH₂CH₂NSi^{*i*}BuMe₂)₃], with the *trans*-uranyl complex, [K(18-crown-6)]₂[*trans*-UO₂Cl₄], affords a mixed-valent U(V/VI) oxo-imido dimer, [K(18-crown-6)(Et₂O)][UO(μ₂-NCH₂CH₂N(CH₂CH₂NSi^{*i*}BuMe₂)₂)]₂ (Scheme 1.5),⁹ formed through abstraction of a silyl group from the tripodal ligand and U=O cleavage. All these examples can be rationalized by arguing that *trans/cis* isomerization disrupts the O-U-O bonding framework, thereby making the U⁶⁺ ion a much better oxidant. In this regard, the isolation and characterization of a *cis*-uranyl complex could provide unique insights into the nature of the U=O bonds within the uranyl fragment, especially with respect to f orbital involvement in the U-O bonds¹ and the Inverse Trans Influence (ITI).¹⁰⁻¹³

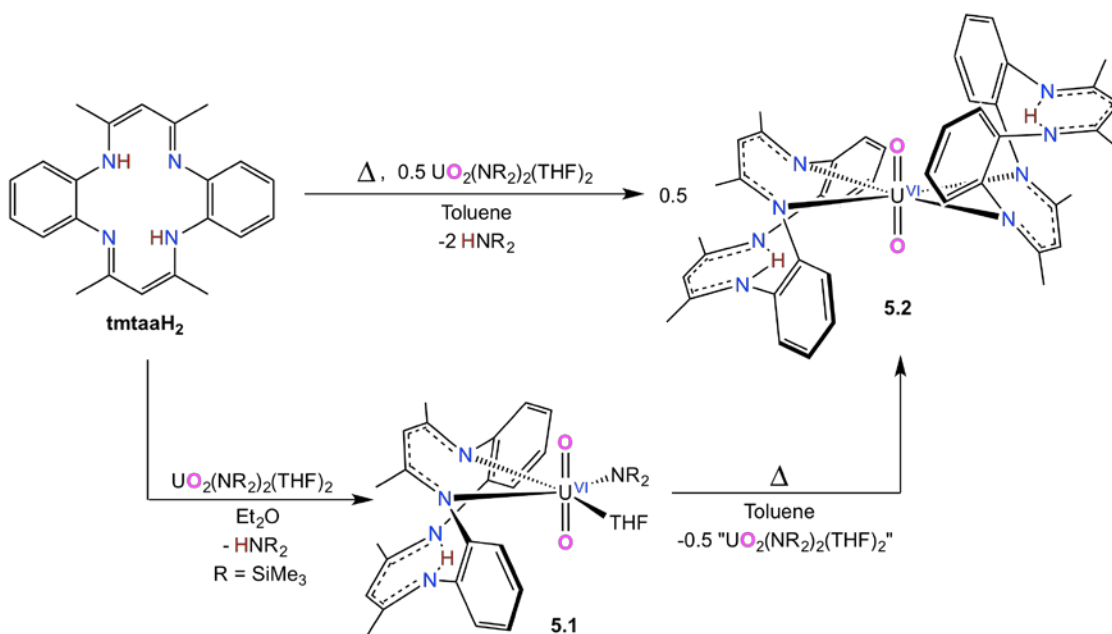
Drawing inspiration from the results of Clark and co-workers, we sought to coordinate a polydentate ligand, specifically a macrocyclic ligand, to the uranyl fragment to effect a *trans* to *cis* isomerization of the oxo ligands. One ligand that would be well suited for this purpose is the 14-membered tetra(aza)macrocyclic ligand, (tmtaa)²⁻ (tmtaaH₂ = dibenzotetramethyltetraaza[14]annulene). Many transition metal complexes of the (tmtaa)²⁻ ligand are known, including *cis*-TiCl₂(tmtaa),¹⁴ *cis*-

Zr(Bn)₂(tmtaa),¹⁵ *cis*-Ru(CN^tBu)₂(tmtaa),¹⁶ and Rh(HCO)(tmtaa).¹⁷ The case of *cis*-Zr(Bn)₂(tmtaa) is particularly informative, as the Zr ion cannot fit within the binding pocket of the tmtaa ligand, which results in the enforcement of a *cis* arrangement of the two benzyl ligands. The example is particularly illustrative because Zr⁴⁺ (0.72 Å) has a similar ionic radius to U⁶⁺ (0.73 Å), which suggests that tmtaa can only bind to one hemisphere of the U⁶⁺ ion, enforcing a *cis* stereochemistry of the two oxo ligands.¹⁸ In this chapter, we report our attempts to ligate (tmtaa)²⁻ to the *trans*-uranyl ion in order to promote a *trans/cis* oxo isomerization. However, we do not observe the formation of a *cis*-uranyl complex. Instead, we observe the formation of oxidized tmtaa products and several *trans*-uranyl tmtaa complexes, where only two nitrogen atoms of the tmtaa ligands are coordinated to the uranium centers. This demonstrates that the tmtaa ligand was more flexible than anticipated, and too easily oxidized.

5.2 Results and Discussion

5.2.1. Synthesis and Characterization of $\text{UO}_2(\text{tmtaaH})(\text{N}(\text{SiMe}_3)_2)(\text{THF})$ (**5.1**) and $\text{UO}_2(\text{tmtaaH})_2$ (**5.2**)

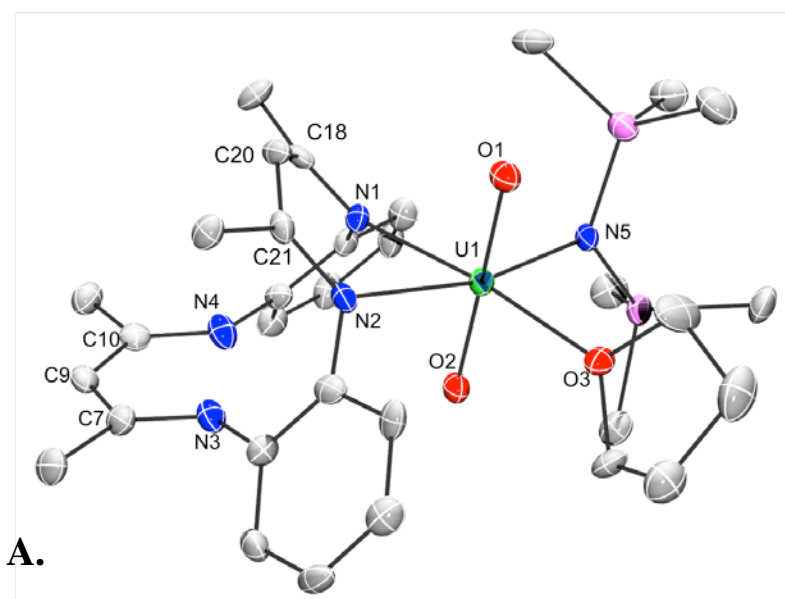
Addition of 1 equiv of tmtaaH_2 (tmtaa = dibenzotetramethyltetraaza-[14]annulene) to $\text{UO}_2(\text{N}(\text{SiMe}_3)_2)_2(\text{THF})_2$ in Et_2O , results in formation of a dark red-orange solution, from which $\text{UO}_2(\text{tmtaaH})(\text{N}(\text{SiMe}_3)_2)(\text{THF})$ (**5.1**) can be isolated as dark red crystals in 83% yield (Scheme 5.1). In this reaction only two nitrogens of the tmtaaH ligand are coordinated to the uranium center, while one of the amide ligands is still attached. In an attempt to drive the protonolysis reaction to completion, and coordinate the other two nitrogen atoms of the tmtaa ligand to the metal, a mixture of tmtaaH_2 and $\text{UO}_2(\text{N}(\text{SiMe}_3)_2)_2(\text{THF})_2$ was gently heated. The ^1H NMR spectra of these solutions reveal the formation of a new uranium-containing product, $\text{UO}_2(\text{tmtaaH})_2$ (**5.2**), in a 1:2 ratio with complex **5.1**. This demonstrates that complex **5.1** undergoes ligand exchange to form **5.2**, instead of forming the desired complex, *cis*- $\text{UO}_2(\text{tmtaa})$. In order to synthesize complex **5.2** purposely, 2 equiv of tmtaaH_2 and 1 equiv of $\text{UO}_2(\text{N}(\text{SiMe}_3)_2)_2(\text{THF})_2$ are heated to 85°C for 18 h, from which **5.2** is isolated as red-orange crystals in 67% yield (Scheme 5.1).



Scheme 5.1. Synthesis of complexes **5.1** and **5.2**.

Complexes **5.1** and **5.2** crystallize in the triclinic space group *P*-1 (Figure 5.1), where both exhibit octahedral geometries about the uranium centers. The oxo ligands of both complexes exhibit metrical parameters typical of the uranyl(VI) moiety with nearly linear O-U-O angles (173.7° for **5.1** and 180° for **5.2**),¹⁹⁻²¹ indicating coordination of the tmtaaH ligands have not perturbed the UO₂²⁺ fragment (Table 5.1). The tmtaaH ligands in **5.1** and **5.2** only coordinate to the uranium centers with two nitrogen atoms, while the other two nitrogen atoms still coordinate a proton. The U-N_{tmtaaH} bond lengths in **5.1** (2.387 and 2.417 Å) are similar to the U-N_{tmtaaH} bond lengths in **5.2** (2.37(1) and 2.40(1) Å), which are comparable to the U-N bond lengths in uranyl β-diketimate complexes, such as [UO₂(Ar₂nacnac)Cl]₂ (Ar₂nacnac = (2,6-*i*Pr₂C₆H₃)NC(Me)CHC(Me)N(2,6-*i*Pr₂C₆H₃)) (av. U-N = 2.40 Å),¹⁹ UO₂(Ar₂nacnac)(acac) (U-N = 2.419(5) and 2.409(5) Å),²² UO₂(Ar₂nacnac)(dbm) (U-N = 2.402(5) and 2.388(5)

Å),²² $\text{UO}_2(\text{Ar}_2\text{nacnac})(\text{pyr})_2$ (U-N = 2.484(7) and 2.515(7) Å),²³ and $[\text{Li}(\text{MeIm})][\text{UO}(\mu\text{-O})(\text{Ar}_2\text{nacnac})(\mu\text{-}N,C\text{-C}_4\text{H}_5\text{N}_2)_2]$ (U-N = 2.446(5) and 2.459(5) Å).²⁴ Both complexes **5.1** and **5.2** also do not exhibit alternation in the N-C and C-C bond lengths (Scheme 5.2). The binding mode of the *tmtaaH* ligand in **5.1** and **5.2** is similar to that observed in the transition metal complex, *cis*- $\text{MoO}_2(\text{acac})(\text{tmtaaH})$.²⁵ Ideally, all four nitrogen atoms of the *tmtaaH* ligand in **5.1** would have coordinated to the uranium center to generate significant steric pressure on the UO_2^{2+} fragment, but the *tmtaaH*²⁻ macrocycle appears to be surprisingly flexible.



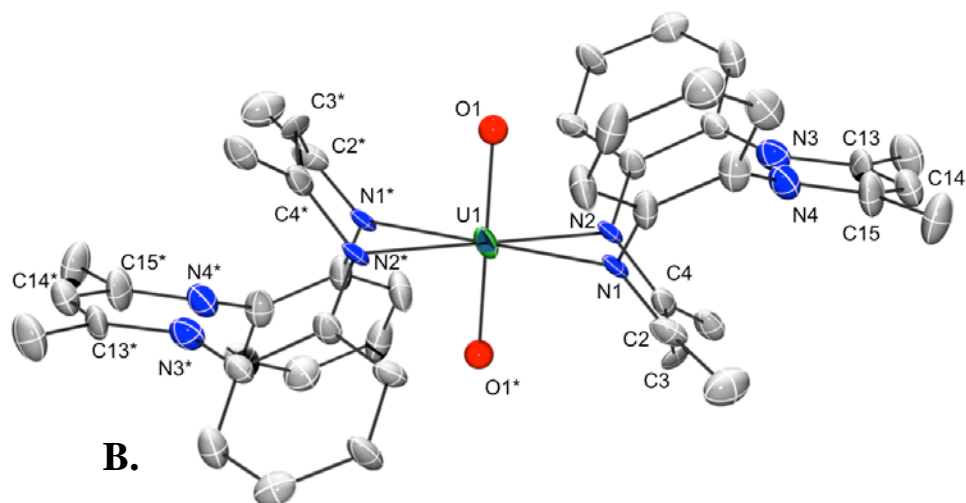
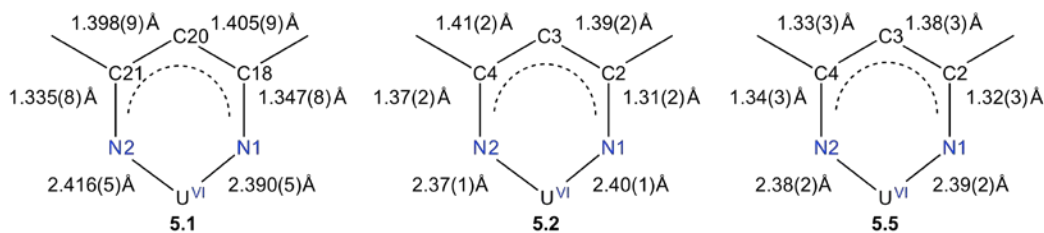


Figure 5.1. Solid-state structures of **A)** $\text{UO}_2(\text{tmtaaH})(\text{N}(\text{SiMe}_3)_2)(\text{THF})$ (**5.1**) and **B)** $\text{UO}_2(\text{tmtaaH})_2$ (**5.2**), with 50% probability ellipsoids. All hydrogen atoms have been omitted for clarity. Complex **5.1** crystallizes with two independent molecules in the asymmetric unit, only one is shown here.

Table 5.1. Selected bond lengths (\AA) and angles (deg) for complexes **5.1**, **5.2**, **5.5**, and **5.6**.

	5.1	5.2	5.5	5.6
U=O	av. 1.788 av. 1.794	1.734(8)	1.74(2) 1.77(2)	1.74(2) 1.77(2)
U-N _{tmtaa}	av. 2.387 av. 2.417	2.37(1) 2.40(1)	2.38(2) 2.39(2)	2.51(2)
U-N _{amide}	av. 2.307	-	-	2.29(1)
O-Li	-	-	2.01(4)	2.03(3)
C _v -C _v	-	-	1.53(4)	-
O-U-O	av. 173.7	179.999(1)	175.3(6)	175.2(7)
U-O-Li	-	-	138(2)	133(1)



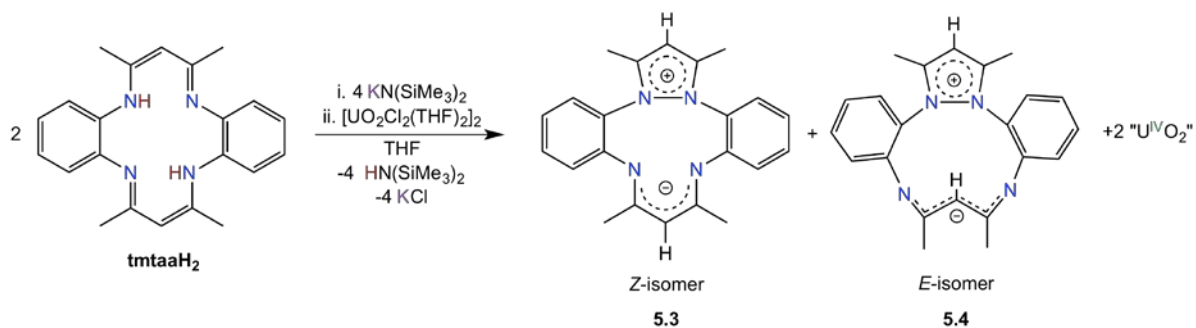
Scheme 5.2. Bond length comparison for complexes **5.1**, **5.2**, and **5.5**.

The ^1H NMR spectrum of **5.1** in C_6D_6 exhibits one NH resonance at 13.13 ppm, and seven aryl resonances at 8.20, 7.33, 7.27, 6.99, 6.95, 6.86, and 6.72 ppm. The eighth aryl resonance appears to be overlapping with the resonance at 6.95 ppm. As expected, there are also two resonances assignable to the γ -CH protons at 4.90 and 4.63 ppm, and three resonances assignable to the CH_3 groups of the tmtaaH ligand at 1.88, 1.85, and 1.80 in a 1:1:2 ratio, respectively, indicating complex **5.1** maintains its solid-state structure in solution. Interestingly, the spectrum also displays two resonances at 0.75 and 0.46 ppm assignable to the two SiMe_3 groups, which suggests the rotation of the two SiMe_3 groups about the $\text{U-N}_{\text{amide}}$ bond is hindered in solution. The ^1H NMR spectrum of **5.2** in C_6D_6 is very similar to complex **5.1**, with one characteristic NH resonance at 13.58 ppm, and four aryl resonances at 8.21, 7.24, 6.93, and 6.77 ppm. While the ^1H NMR spectrum of **5.2** also exhibits two γ -CH proton resonances at 4.99 and 4.69 ppm in a 1:1 ratio, which is expected based on the solid-state structure, surprisingly, there is only one CH_3 resonance at 1.90 ppm. Complexes **5.1** and **5.2** also exhibit identical $\text{U}=\text{O}$ ν_{sym} stretches of 805 cm^{-1} in their Raman spectra, which are comparable to other uranyl complexes with multiple amide co-ligands, such as

$[\text{UO}_2(\text{N}(\text{SiMe}_3)_2)_3]^-$ (805 cm^{-1}),²⁶ and $\text{UO}_2(\text{NCN})_2(\text{THF})$ [$\text{NCN} = \text{Me}_3\text{Si}(\text{N})\text{CPh}(\text{N})\text{SiMe}_3$] (803 cm^{-1}).²⁷

5.2.2. Synthesis and Characterization of the β -diketiminato pyrazolium macrocycle (*Z*-isomer: **5.3**; *E*-isomer: **5.4**)

Subsequently, we wanted to explore the reactivity of $\text{K}_2(\text{tmtaa})$ with $[\text{UO}_2\text{Cl}_2(\text{THF})_2]_2$, as we hypothesized that the formation of KCl should be a better driving force than the formation of $\text{HN}(\text{SiMe}_3)_2$. First, the $\text{K}_2(\text{tmtaa})$ is prepared *in situ* by addition of 4 equiv of $\text{KN}(\text{SiMe}_3)_2$ to 2 equiv of tmtaaH_2 in THF. This mixture is then added to $[\text{UO}_2\text{Cl}_2(\text{THF})_2]_2$ in THF, which results in a red-brown slurry, from which the β -diketiminato pyrazolium macrocycle (*Z*-isomer: **5.3**; *E*-isomer: **5.4**), which can be isolated as a mixture of the *E* and *Z* isomers in 12% yield (Scheme 5.3). Compounds **5.3** and **5.4** are isolated in roughly a 10:1 ratio, respectively. Although no uranium containing products can be observed in the *in situ* ^1H NMR spectra, the isolated yields of **5.3** and **5.4** are very low. Investigations to determine the identities of the other products are still ongoing.



Scheme 5.3. Synthesis of compounds **5.3** and **5.4**.

Compound **5.3** crystallizes in the monoclinic space group $P2_1/n$, while compound **5.4** crystallizes in the monoclinic space group $P2_1/c$, as the THF solvate **5.4**·C₄H₈O (Figure 5.2). Compounds **5.3** and **5.4** are both zwitterions; compound **5.3** is the *Z*-isomer and compound **5.4** is the *E*-isomer, where both exhibit the same pyrazolium cation ring with similar N-N bond lengths (**5.3**: 1.380(2) Å; **5.4**: 1.396(2) Å). The C-C bond lengths and C-N bond lengths of the pyrazolium cationic fragments in **5.3** and **5.4** (avg. C-C: 1.38 Å; avg. C-N: 1.35 Å) are very similar to other structurally characterized pyrazolium cations.²⁸⁻³² For example, the organic compound, (pyrazolinonyl)(hydroxypyrazolylium)methanepersulfate, exhibits two pyrazolium cations with an avg. N-N bond length of 1.38 Å, an avg. C-N bond length of 1.37 Å, and an avg. C-C bond length of 1.40 Å.²⁸ The positive charges in **5.3** and **5.4** are balanced by a negative charge localized on the other γ -carbon. Compound **5.3** exhibits N-C bond lengths in the anionic fragment of 1.339(2) and 1.301(2) Å, which are slightly shorter compared to the pyrazolium cation fragment, and C-C bond lengths of 1.389(2) and 1.439(2) Å, which are slightly longer in comparison to the pyrazolium cation fragment. The same trend is demonstrated in the anionic fragment of compound **5.4** (C-N: 1.323(3) and 1.328(2) Å; C-C: 1.404(3) and 1.403(3) Å). The anionic fragment in **5.3** is structurally similar to the β -diketiminato lithium salt, 1,5-diphenyl-1,5-diaazapentadienyl lithium, which is the *Z*-isomer, and has C-N bond lengths of 1.326(3) and 1.322(3) Å, and C-C bond lengths of 1.394(4) and 1.387(4) Å.³³ The anionic fragment in **5.4** is most structurally similar to the anionic β -diketiminato ligand in the complex, [K(L^{But})(THF)₃] (L^{But}H = [HC{C(^tBu)NDipp}{C(^tBu)NHDipp}]), which is the *E*-

isomer, and exhibits C-N bond lengths of 1.321(5) and 1.340(5) Å and C-C bond lengths of 1.417(5) and 1.420(5) Å.³⁴ Compound **5.4** exhibits C_s symmetry, as there is a mirror plane that intersects the C3 and C14 γ -carbon atoms, while compound **5.3** exhibits C_1 symmetry. All the other metrical parameters are comparable.

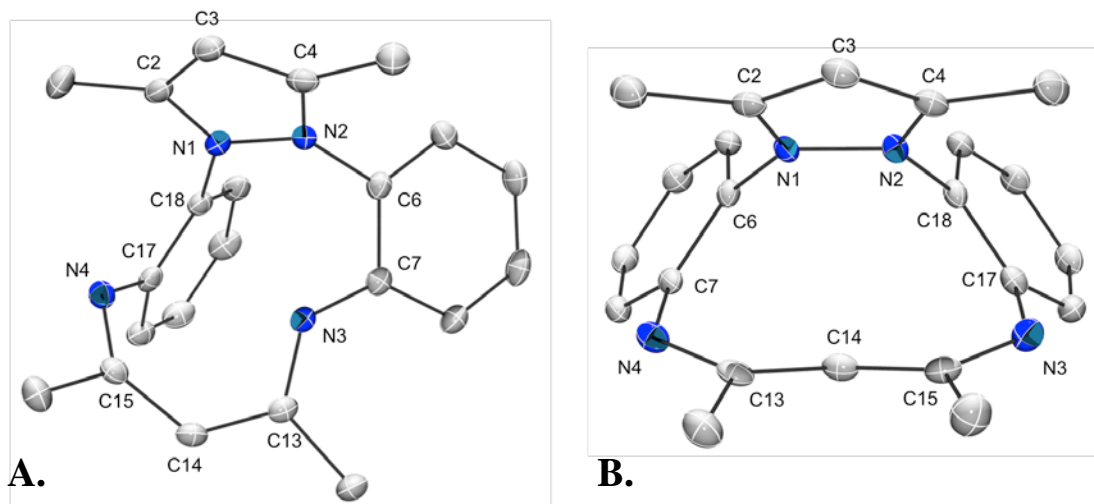


Figure 5.2. Solid-state structures of **A)** $C_{22}H_{22}N_4$ (**5.3**) and **B)** $C_{22}H_{22}N_4 \cdot C_4H_8O$ (**5.4**· C_4H_8O), with 50% probability ellipsoids. All hydrogen atoms have been removed for clarity. Selected bond lengths (Å) for **5.3**: N1-N2 = 1.380(2), N1-C2 = 1.352(2), C2-C3 = 1.378(2), C3-C4 = 1.388(2), N2-C4 = 1.345(2), N3-C13 = 1.339(2), C13-C14 = 1.389(2), C14-C15 = 1.439(2), C15-N4 = 1.301(2). For **5.4**: N1-N2 = 1.396(2), N1-C2 = 1.346(2), C2-C3 = 1.388(3), C3-C4 = 1.376(3), N2-C4 = 1.347(2), N3-C15 = 1.323(3), C15-C14 = 1.404(3), C14-C13 = 1.403(3), C13-N4 = 1.328(2).

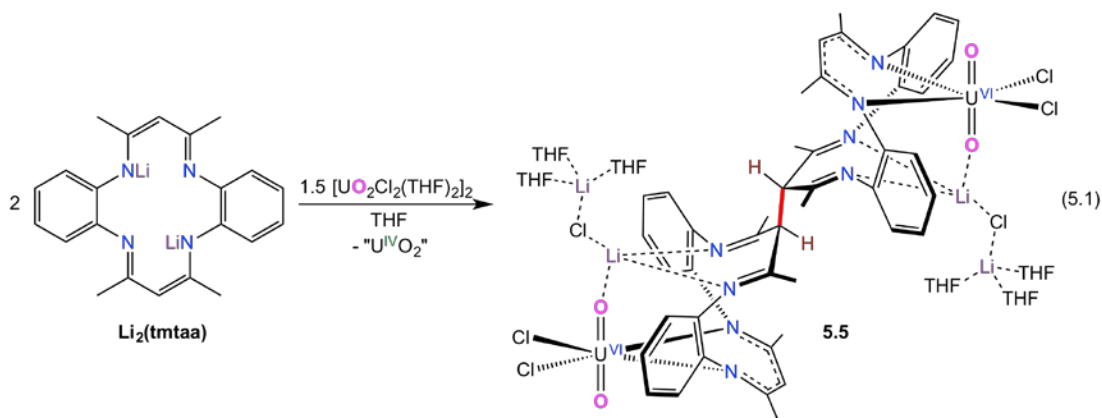
Compound **5.3** exhibits two γ -CH resonances at 5.27 and 4.99 ppm in its 1H NMR spectrum in C_6D_6 . The C_1 symmetry exhibited in the solid-state structure appears to be maintained in solution, as there are also 8 aryl proton resonances ranging from

7.26 to 6.33 ppm, as well as four methyl proton resonances at 2.31, 2.27, 2.06, and 1.48 ppm. Compound **5.4** also appears to maintain the C_s symmetry exhibited in its solid-state structure in solution, as there are only four aryl proton resonances at 7.23, 6.96, 6.86, and 6.52 ppm, and two methyl proton resonances at 2.26 and 1.87 ppm observed in its ^1H NMR spectrum in C_6D_6 (Figure A.8). In addition, compound **5.4** also exhibits two γ -CH resonances at 5.14 and 4.51 ppm. A $^{13}\text{C}\{^1\text{H}\}$ NMR spectrum was recorded of a sample containing mostly complex **5.4** in C_6D_6 (Figure A.9). Compound **5.4** exhibits two γ -carbon resonances at 106.97 and 88.77 ppm, six aryl carbon resonances at 154.01, 133.12, 131.70, 121.92 and 117.37 ppm (the sixth resonance is hidden by the benzene resonance), as well as two methyl carbon resonances at 25.73 and 12.89 ppm, which supports that the C_s symmetry is maintained in solution. There are also two NCCH_3 carbon resonances observed at 161.48 and 147.73 ppm.

In the reaction to form compounds **5.3** and **5.4**, we hypothesize that a *cis*-uranyl tmtaa complex, *cis*- $\text{UO}_2(\text{tmtaa})$, is transiently generated, however, it is unstable and undergoes decomposition, in which the uranium center becomes reduced by $2e^-$, presumably generating $\text{U}^{\text{IV}}\text{O}_2$, while simultaneously oxidizing the tmtaa ligand by $2e^-$. Notably, *trans*-uranyl is typically a poor oxidant, but when the O-U-O moiety is no longer linear, the $6p_z$ uranium AO cannot participate in the σ -bonding framework,^{1,35} which weakens the U-O bonds, and allows the U(VI) center to become more oxidizing. This reactivity is similar to the previous attempts to make *cis*- $\text{Cp}'_2\text{UO}_2$ ($\text{Cp}' = \text{Cp}^*$ or 1,2,4- $\text{C}_5\text{H}_2\text{tBu}_3$) (Scheme 1.4),^{7,8} in which the reactions resulted in ligand oxidation and the formation of unwanted “uranium oxides”.

5.2.3. Synthesis and Characterization of $[\text{Li}]_2[\text{Li}(\text{THF})_3\text{Cl}]_2[\text{UO}_2\text{Cl}_2\{\text{tmtaa}\}_2\text{UO}_2\text{Cl}_2]$ (5.5)

The reactivity of $\text{Li}_2(\text{tmtaa})$ with $[\text{UO}_2\text{Cl}_2(\text{THF})_2]_2$ was also explored. Addition of 2 equiv of $\text{Li}_2(\text{tmtaa})$ to $[\text{UO}_2\text{Cl}_2(\text{THF})_2]_2$ in THF results in a red-brown solution, from which $[\text{Li}]_2[\text{Li}(\text{THF})_3\text{Cl}]_2[\text{UO}_2\text{Cl}_2\{\text{tmtaa}\}_2\text{UO}_2\text{Cl}_2]$ (**5.5**) can be isolated as red-brown crystals in 42% yield (based on the stoichiometry in eq 5.1). Complex **5.5** contains the $\{\text{tmtaa}\}_2^{2-}$ dimer, which is a $1e^-$ oxidation product of the $[\text{tmtaa}]^{2-}$ ligand, and was probably formed by the coupling of two initially formed π radicals.³⁶



Complex **5.5** crystallizes in the triclinic space group $P-1$, as the THF solvate, $\mathbf{5.5} \cdot \text{C}_4\text{H}_8\text{O}$ (Figure 5.3). Its solid-state structure shows that complex **5.5** is composed of two $[\text{UO}_2\text{Cl}_2(\text{tmtaa})]$ units linked via a carbon single bond bridge ($\text{C14}-\text{C14}^* = 1.53(4)$ Å), which exhibit octahedral geometries about the uranium atoms. One lithium atom for each $[\text{UO}_2\text{Cl}_2(\text{tmtaa})]$ unit interacts with one uranyl oxo ligand. Complex **5.5** also features two co-crystallized $[\text{Li}(\text{THF})_3][\text{Cl}]$ units. The oxo ligands of complex **5.5** exhibit metrical parameters typical of the uranyl(VI) moiety with short $\text{U}=\text{O}$ bond lengths of $1.74(2)$ and $1.77(2)$ Å and a nearly linear $\text{O}-\text{U}-\text{O}$ angle ($175.3(6)^\circ$) (Table 5.1). For each $[\text{UO}_2\text{Cl}_2(\text{tmtaa})]$ unit, the tmtaa ligand has two nitrogen atoms bound to

the U center and two nitrogen atoms interacting with a Li cation. This binding mode, which is reminiscent of the polypyrolic macrocyclic ligand employed by the Arnold group to direct uranyl-oxo functionalization,^{37,38} creates two metal coordination pockets, and helps direct Li cation coordination to one of the uranyl oxos in complex **5.5**. The binding mode is also similar to the transition metal complex, *cis*-MoO₂(acac)(tmtaaH), where only two N atoms of the tmtaaH ligand are coordinated to the metal center.²⁵ The Li1-O2 distance in **5.5** is 2.01(4) Å, which is in the normal range of U^{VI}=O---Li interactions.^{6,38-42} For example, the complex, [Li(12-crown-4)]₂[UO₂Cl₄], exhibits a Li-O distance of 1.89(2) Å,⁴⁰ and the uranyl alkyl complex, [Li(DME)_{1.5}]₂[U(μ-O)₂(CH₂SiMe₃)₄], which is stabilized by “ate” complex formation, exhibits two Li-O distances of 2.00(1) and 2.02(1) Å.⁴¹ The Li1-O2 distance in **5.5** is significantly shorter than the U^{VI}=O---K interactions exhibited by [K(toluene)]₂[UO₂(NPh(3,5-(CF₃)₂C₆H₃))₄] (K-O = 2.589(2) and 2.615(3) Å), however, this difference is consistent with the difference in ionic radii of K⁺ vs. Li⁺.⁶ The U-N_{tmtaa} bond lengths (2.38(2) and 2.39(2) Å) in complex **5.5** are comparable to the U-N bond lengths in **5.1** and **5.2**, as well as the U-N bond lengths in typical uranyl β-diketimate complexes.^{19,23,24} In addition, **5.5** does not exhibit alternation in the N-C and C-C bond lengths of the β-diketimate portion of the {tmtaa}₂²⁻ ligand attached to the U centers (Scheme 5.2).

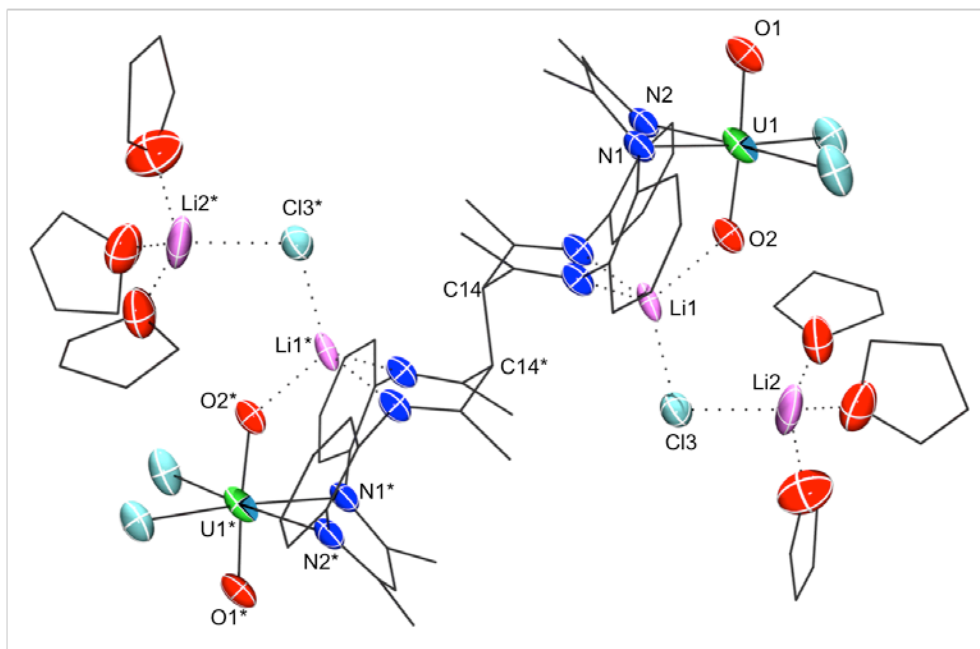


Figure 5.3. Solid-state structure of $[\text{Li}]_2[\text{Li}(\text{THF})_3\text{Cl}]_2[\text{UO}_2\text{Cl}_2\{\text{tmtaa}\}_2\text{UO}_2\text{Cl}_2]\cdot\text{C}_4\text{H}_8\text{O}$ ($5.5\cdot\text{C}_4\text{H}_8\text{O}$), with 30% probability ellipsoids for the heteroatoms. All hydrogen atoms and the THF solvate have been removed for clarity.

Complex **5.5** is insoluble in non-polar solvents and Et_2O , and only exhibits partial solubility in THF. However, complex **5.5** is completely soluble in pyridine. The ^1H NMR spectrum of **5.5** in $\text{pyr-}d_5$ exhibits distinct singlets at 4.85 and 4.81 ppm, which correspond to the two different γ -CH environments, along with 2 sharp singlets at 2.25 and 1.99 ppm, which correspond to two different methyl environments. The remaining methyl resonances could not be assigned. There are two THF resonances at 3.66 and 1.61 ppm, which integrate to three equivalents of THF, as predicted by the solid-state structure. The $^7\text{Li}\{^1\text{H}\}$ NMR spectrum in $\text{pyr-}d_5$ exhibits two sharp resonances at 3.60 and 2.67 ppm in a 4:1 ratio, respectively, indicating that in solution the Li cations are probably not in the same configuration as the solid-state structure suggests. This is not

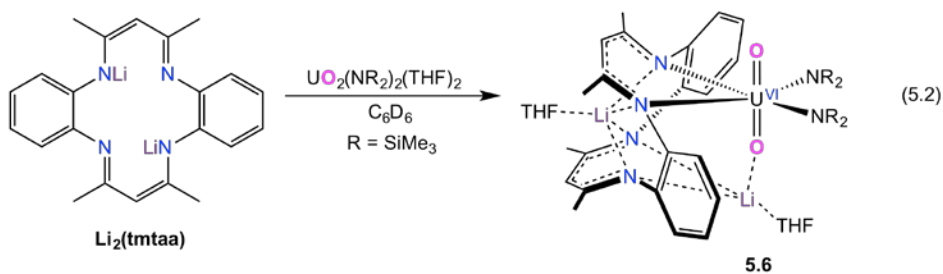
surprising, considering the donor strength of pyridine could disrupt the Li-O interactions.

Similarly to compounds **5.3** and **5.4**, to explain the formation of **5.5**, we hypothesize that a *cis*-uranyl tmtaa complex, is transiently generated, but rapidly decomposes to form the 1e⁻ oxidation product, [tmtaa]⁻, which couples to form the {tmtaa}₂²⁻ dimer, along with unobserved low-valent uranium oxides. The difference in reactivity between the potassium and lithium salts of the tmtaa ligand can potentially be explained by “ate” complex formation, which stabilizes the unobserved *cis*-uranyl intermediate, in the case of the Li example. The dimerization of tmtaa has been observed previously during the electropolymerization of Ni(II) tmtaa complexes.³⁶ Reactivity at the γ -carbon position of the tmtaa ligand in several transition metal complexes has also been documented.^{16,43} For instance, addition of CO to the ruthenium carbene complex, Ru(PhCCOOMe)(tmtaa), causes the carbene to attack the γ -carbon of the tmtaa ligand and rearrange to generate a bridging C=C-O unit between the Ru and the tmtaa γ -carbon.¹⁶

5.2.4. Synthesis and Characterization of [Li(THF)]₂[UO₂(N(SiMe₃)₂)₂(tmtaa)] (5.6)

In an effort to stabilize the highly-oxidizing intermediate formed upon reaction of tmtaa with uranyl, we explored the reaction of Li₂tmtaa with UO₂(N(SiMe₃)₂)₂(THF)₂. In particular, we hypothesized that the electron donating amide co-ligands on the uranyl starting material would help to stabilize the

unobserved intermediate formed in eq 5.1. Importantly, the strongly donating amides should make the uranium center less oxidizing, and therefore stop the unwanted oxidation of the tmtaa ligand. Thus, an NMR-scale reaction of $\text{UO}_2(\text{N}(\text{SiMe}_3)_2)_2(\text{THF})_2$ with 1 equiv of $\text{Li}_2(\text{tmtaa})$, in C_6D_6 , results in an immediate color change to red and the formation of a new product, indicated by ^1H and ^7Li NMR spectroscopies. Allowing the NMR tube to sit at room temperature for 3 h, results in the formation of red block crystals. The identity of the crystals was determined to be $[\text{Li}(\text{THF})]_2[\text{UO}_2(\text{N}(\text{SiMe}_3)_2)_2(\text{tmtaa})]$ (**5.6**) by X-ray crystallography. Gratifyingly, the amide co-ligands did hinder the unwanted reduction of the tmtaa ligand, however, a *cis*-uranyl complex was not isolated, probably due to the unique flexibility of the tmtaa ligand only allowing 2 nitrogen atoms to coordinate the uranium center, while the other 2 nitrogen atoms are free to interact with a lithium cation.



Complex **5.6** crystallizes in the orthorhombic space group $Pnma$, as the C_6D_6 solvate, $\mathbf{5.6} \cdot 2\text{C}_6\text{D}_6$ (Figure 5.4). Similarly to complex **5.5**, the tmtaa ligand is bound to the U center by only two nitrogen atoms, and the other two nitrogens are interacting with an inner-sphere Li cation. This binding mode creates two metal coordination pockets, and helps direct Li cation coordination to one of the uranyl oxos in complex

5.6, which is similar to complex **5.5** and is also reminiscent of the polypyrolic macrocyclic ligand, employed by the Arnold group.^{37,38} In contrast to complex **5.5**, complex **5.6** exhibits a second Li cation, which interacts with all four nitrogen atoms, and sits just out of the plane created by these four tmtaa nitrogen atoms. The U-N_{tmtaa} bond length in **5.6** (2.51(2) Å) is slightly longer than the U-N_{tmtaa} bond lengths in **5.5** (2.39(2), U1-N2 = 2.38(2) Å), which can be explained by the more electron donating nature of the amide vs. chloride co-ligands (Table 5.1). However, the U-N_{tmtaa} bond length in **5.6** is still within the typical range of U-N bond lengths in uranyl β-diketimate complexes.^{19,22-24} The oxo ligands of complex **5.6** exhibit metrical parameters typical of the uranyl(VI) moiety with short U=O bond lengths of 1.74(2) and 1.77(2) Å, and a nearly linear O-U-O angle (175.2(7)°). The Li1-O2 distance in **5.6** is 2.03(3) Å, which is in the normal range of U^{VI}=O---Li interactions,^{6,38-42} and comparable to complex **5.5**.

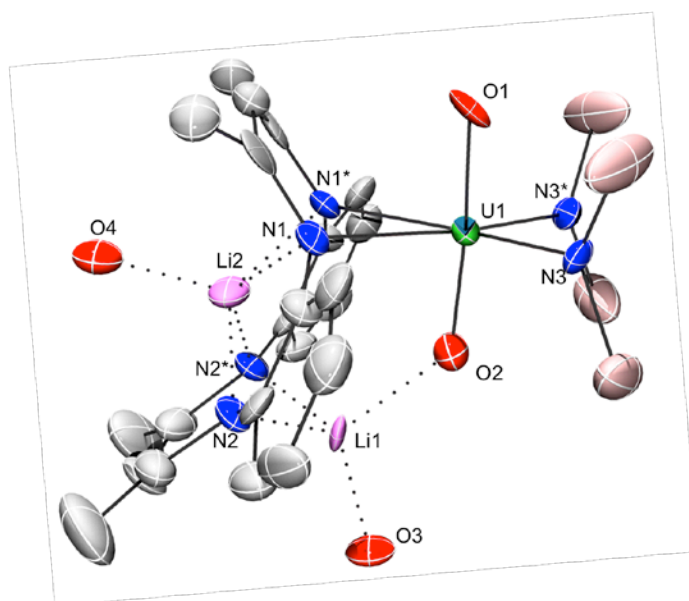


Figure 5.4. Solid-state structure of $[\text{Li}(\text{THF})]_2[\text{UO}_2(\text{N}(\text{SiMe}_3)_2)_2(\text{tmtaa})] \cdot 2\text{C}_6\text{D}_6$ (**5.6**· $2\text{C}_6\text{D}_6$), with 50% probability ellipsoids. All hydrogen atoms, THF carbon atoms, SiMe_3 carbon atoms, and the benzene solvates have been removed for clarity.

The ^1H NMR spectrum of complex **5.6** in C_6D_6 , consistent with its solid-state structure, exhibits four tmtaa aryl proton resonances at 7.87, 7.24, 7.04, and 6.79 ppm, two tmtaa γ -proton resonances at 4.77 and 4.32 ppm, two tmtaa methyl proton resonances at 1.95 and 1.82 ppm, and two resonances at 0.78 and 0.33 ppm, assignable to the proton environments of the SiMe_3 groups (Figure A.10). Similar to complex **5.1**, the rotation of the four SiMe_3 groups about the $\text{U-N}_{\text{amide}}$ is hindered in solution. In addition, complex **5.6** also exhibits two broad resonances at 3.35 and 1.28 ppm, which are assignable to the two proton environments of the THF solvates. The $^7\text{Li}\{^1\text{H}\}$ NMR spectrum of **5.6** in C_6D_6 features two lithium resonances at 1.87 and -0.47 ppm in a 1:1 ratio (Figure A.11). This indicates that complex **5.6** retains its solid-state structure in solution.

5.3 Summary

Reaction of $\text{UO}_2(\text{N}(\text{SiMe}_3)_2)_2(\text{THF})_2$ with 1 or 2 equiv of tmtaaH_2 , results in formation of $\text{UO}_2(\text{tmtaaH})(\text{N}(\text{SiMe}_3)_2)(\text{THF})$ (**5.1**) and $\text{UO}_2(\text{tmtaaH})_2$ (**5.2**), respectively, where only two nitrogen atoms of the tmtaaH ligands are coordinated to the uranium center. Additionally, reaction of $[\text{UO}_2\text{Cl}_2(\text{THF})_2]_2$ with 2 equiv of

$K_2(\text{tmtaa})$, results in the formation of the $2e^-$ oxidation products, the β -diketiminato pyrazolium macrocycles (*Z*-isomer: **5.3**; *E*-isomer: **5.4**), and some unobserved low-valent uranium oxides. Similarly, reaction of $[\text{UO}_2\text{Cl}_2(\text{THF})_2]_2$ with 2 equiv of $\text{Li}_2(\text{tmtaa})$ results in the formation of the $1e^-$ oxidation product, $[\text{Li}]_2[\text{Li}(\text{THF})_3\text{Cl}]_2[\text{UO}_2\text{Cl}_2\{\text{tmtaa}\}_2\text{UO}_2\text{Cl}_2]$ (**5.5**), along with some unobserved low-valent uranium oxides. We propose that the difference in reactivity between the potassium and lithium salts of the tmtaa ligand is due to the ability of Li cations to form “ate” complexes, which could somewhat stabilize a *cis*-uranyl intermediate.

All attempts to synthesize the desired *cis*- $\text{UO}_2(\text{tmtaa})$ complex were thwarted by coordination of only two nitrogen atoms of the tmtaa ligand to the uranium center or unwanted ligand oxidation. In an attempt to hinder the oxidation of the tmtaa ligand in the reaction to form **5.5**, more electron donating amide co-ligands were implemented to stabilize the unobserved intermediate, by making the uranium center less oxidizing. Thus, reaction of $\text{UO}_2(\text{N}(\text{SiMe}_3)_2)_2(\text{THF})_2$ with 1 equiv of $\text{Li}_2(\text{tmtaa})$ results in the formation of $[\text{Li}(\text{THF})]_2[\text{UO}_2(\text{N}(\text{SiMe}_3)_2)_2(\text{tmtaa})]$ (**5.6**). The amide co-ligands did hinder the unwanted reduction of the tmtaa ligand, however, a *cis*-uranyl complex was not isolated. This is likely caused by the large binding pocket of the tmtaa ligand only allowing two nitrogen atoms to coordinate the uranium center. This work suggests that the tmtaa ligand is easily oxidized and too flexible, for the purposes of using it to force a *trans/cis* isomerization of the uranyl moiety. In the future, more robust, rigid, and smaller macrocyclic ligands will need to be investigated.

5.4 Experimental

5.4.1 General Procedures. All reactions and subsequent manipulations were performed under anaerobic and anhydrous conditions under an atmosphere of nitrogen. Hexanes, Et₂O, THF, and toluene were dried using a Vacuum Atmospheres DRI-SOLV solvent purification system, and stored over 3 Å molecular sieves for 24 h prior to use. C₆D₆, CH₂Cl₂, CD₂Cl₂ and pyr-*d*₅ were dried over activated 3 Å molecular sieves for 24 h before use. [UO₂Cl₂(THF)₂]₂,²⁰ UO₂(N(SiMe₃)₂(THF)₂),⁴⁴ and tmtaaH₂,⁴⁵ were prepared according to literature procedures. All other reagents were purchased from commercial suppliers and used as received.

NMR spectra were recorded on a Varian UNITY INOVA 400 MHz spectrometer or a Varian unity INOVA 500 MHz spectrometer. ¹H and ¹³C{¹H} NMR spectra are referenced to external SiMe₄ using the residual protio solvent peaks as internal standards (¹H NMR experiments) or the characteristic resonances of the solvent nuclei (¹³C NMR experiments). ⁷Li{¹H} NMR spectra were referenced indirectly with the ¹H resonance of SiMe₄ at 0 ppm, according to IUPAC standard.^{46,47} IR spectra were recorded on a Mattson Genesis FTIR/Raman spectrometer with a NXR FT Raman Module. IR samples were recorded as KBr pellets. Mass spectra were collected by the Mass Spectrometry Facility at the University of California, Santa Barbara, using a field desorption (FD) ion source with a Waters GCT Premier high-resolution Time-of-flight mass spectrometer. Elemental analyses were performed by the Microanalytical Laboratory at UC Berkeley.

5.4.2 Raman Spectroscopy. Raman spectra were recorded on a LabRam Aramis microRaman system (Horiba Jobin Yvon) equipped with 1200 grooves/mm

holographic gratings, and Peltier-cooled CCD camera. The 633 nm output of a Melles Griot He-Ne laser was used to excite the spectra, which were collected in a back scattering geometry using a confocal Raman Microscope (high stability BX40) equipped with Olympus objectives (MPlan 50x). Sample preparation was performed inside the glovebox: Pure crystalline solid samples were placed between a glass microscope slide and coverslip, sealed with a bead of silicone grease, and removed from the glovebox for spectral acquisition.

5.4.3 Synthesis of $\text{Li}_2(\text{tmtaa})$. The preparation described below was modified from the published procedure for $\text{Li}_2(\text{tmtaa})$.⁴⁸ To a stirring dark yellow slurry of tmtaaH_2 (200.2 mg, 0.581 mmol) in Et_2O (8 mL), was added a 2.5 M solution of $n\text{BuLi}$ (0.47 mL, 1.175 mmol) in hexanes, diluted with 1 mL of Et_2O , very slowly dropwise, resulting in an immediate change to a dark red solution. The solution was allowed to stir at room temperature for ~ 3 min, before the solution was filtered through a Celite column supported on glass wool (0.5 cm \times 2 cm). The resulting red filtrate was concentrated *in vacuo* (ca. 3 mL), which resulted in the deposition of red crystals (87.3 mg). The volume of the red supernatant was further reduced *in vacuo* (ca. 1.5 mL), and stored at -25°C for 24 h, which resulted in the deposition of red crystals (76.8 mg, 79% yield). Spectral data of this material matched those previously reported for this complex.⁴⁸

5.4.4 Synthesis of $\text{UO}_2(\text{tmtaaH})(\text{N}(\text{SiMe}_3)_2)(\text{THF})$ (5.1). To a stirred bright orange Et_2O (2 mL) solution of $\text{UO}_2(\text{N}(\text{SiMe}_3)_2)_2(\text{THF})_2$ (68.0 mg, 0.0925 mmol) was added a dark yellow solution of tmtaaH_2 (31.8 mg, 0.0923 mmol) in Et_2O (4 mL) dropwise, which resulted in an immediate color change to dark red-orange. The solution was

allowed to stir for 15 h at room temperature, whereupon no visible change was observed. The dark red solution was filtered twice through a Celite column supported on glass wool (0.5 cm × 2 cm), which produced a small orange plug. The clear red filtrate was concentrated *in vacuo* (ca. 2 mL). Storage at -25°C for 24 h resulted in the deposition of dark red crystals (151.3 mg, 83% yield). Anal. Calcd C₃₂H₄₉N₅O₃Si₂U₁: C, 45.43; H, 5.84; N, 8.28. Found: C, 45.70; H, 5.79; N, 8.02. ¹H NMR (C₆D₆, 25 °C, 400 MHz): δ 13.13 (s, 1H, NH), 8.20 (d, *J*_{HH} = 8 Hz, 1H, aryl CH), 7.33 (t, *J*_{HH} = 8 Hz, 1H, aryl CH), 7.27 (d, *J*_{HH} = 7 Hz, 1H, aryl CH), 6.99 (t, *J*_{HH} = 7 Hz, 1H, aryl CH), 6.95 (t, *J*_{HH} = 8 Hz, 2H, aryl CH), 6.86 (d, *J*_{HH} = 7 Hz, 1H, aryl CH), 6.72 (d, *J*_{HH} = 8 Hz, 1H, aryl CH), 4.90 (s, 1H, γ-CH), 4.63 (s, 1H, γ-CH), 4.18 (br m, 4H, THF), 1.88 (s, 3H, CH₃), 1.85 (s, 3H, CH₃), 1.80 (d, *J*_{HH} = 6 Hz, 6H, CH₃), 1.48 (br t, *J*_{HH} = 6 Hz, 4H, THF), 0.75 (s, 9H, SiMe₃), 0.46 (s, 9H, SiMe₃). IR (KBr pellet, cm⁻¹): 1620(s), 1595(m), 1547(s), 1508(m), 1466(s), 1444(sh m), 1437(m), 1381(s), 1365(s), 1288(m), 1271(m), 1257(sh m), 1252(m), 1240(m), 1196(sh w), 1186(m), 1157(w), 1105(w), 1068(w), 1039(w), 1014(m), 928(s), 891(m), 883(m), 875(m), 868(m), 845(sh s), 835(s), 793(m), 773(w), 742(s), 692(w), 667(w), 661(w), 650(w), 640(w), 611(w), 575(w), 559(w), 536(w), 532(w), 511(w), 482(w), 474(w), 457(w), 424(w), 410(w). Raman (neat solid, cm⁻¹): 1581(m), 1577(m), 1539(vs), 1501(s), 1494(s), 1486(s), 1467(m), 1437(m), 1340(m), 1325(m), 1278(m), 1267(m), 1220(m), 1023(w), 1011(w), 929(w), 863(w), 830(m), 805(m, U=O ν_{sym}), 746(w), 653(w), 597(w), 541(w), 471(w), 379(w), 321(w), 186(m), 136(m), 95(m).

5.4.5 Synthesis of UO₂(tmtaaH)₂ (5.2). To a stirred orange solution of UO₂(N(SiMe₃)₂)₂(THF)₂ (136.6 mg, 0.186 mmol) in toluene (3 mL) was added a green-

yellow solution of tmtaaH₂ (128.0 mg, 0.372 mmol) in toluene (4 mL) dropwise, which yielded an immediate color change to red-brown. The reaction mixture was sealed under vacuum in a bomb flask, whereupon it was heated at 85°C for 18 h, which resulted in a red-brown solution concomitant with a red-orange powder. The solution was decanted away from the red-orange powder, and washed quickly with Et₂O (2 mL) (118.9 mg, 67% yield). X-ray quality crystals of **2** were grown out of neat toluene. Anal. Calcd C₄₄H₄₆N₈O₂U₁: C, 55.23; H, 4.58; N, 11.71. Found: C, 55.62; H, 4.56; N, 11.63. ¹H NMR (C₆D₆, 25 °C, 400 MHz): δ 13.58 (s, 2H, NH), 8.21 (d, *J*_{HH} = 8 Hz, 4H, aryl CH), 7.24 (t, *J*_{HH} = 7 Hz, 4H, aryl CH), 6.93 (t, *J*_{HH} = 8 Hz, 4H, aryl CH), 6.77 (t, *J*_{HH} = 8 Hz, 4H, aryl CH), 4.99 (s, 2H, γ-CH), 4.69 (s, 2H, γ-CH), 1.90 (d, 24H, CH₃). IR (KBr pellet, cm⁻¹): 1618(m), 1593(w), 1560(sh m), 1545(s), 1512(m), 1464(m), 1446(w), 1435(w), 1380(m), 1362(s), 1290(w), 1263(w), 1225(w), 1192(sh vw), 1178(w), 1153(w), 1107(m), 1045(w), 1018(m), 1003(w), 941(sh vw), 920(m), 906(vs), 868(sh w), 862(m), 852(sh w), 829(m), 808(m), 793(m), 752(m), 742(s), 729(s), 688(w), 667(w), 648(w), 606(w), 573(m), 559(w), 538(m), 523(w), 503(w), 484(w), 471(m), 459(w), 434(w), 420(w), 411(w), 403(w). Raman (neat solid, cm⁻¹): 1581(s), 1536(s), 1502(s), 1464(s), 1430(m), 1325(s), 1286(s), 1223(m), 1148(m), 1032(w), 925(w), 834(m), 805(m, U=O ν_{sym}), 734(w), 653(w), 593(w), 554(m), 463(w), 361(w), 326(w), 223(w), 191(w), 113(m).

5.4.6 Synthesis of the β-diketimate pyrazolium macrocycle (Z-isomer: 5.3). To a stirred dark yellow slurry of tmtaaH₂ (82.6 mg, 0.240 mmol) in THF (1 mL), was added a colorless solution of KN(SiMe₃)₂ (96.6 mg, 0.484 mmol) in THF (1 mL) dropwise, which resulted in a red-brown solution. The solution was allowed to stir at room

temperature for 5 minutes, whereupon it was added to a stirring yellow slurry of $[\text{UO}_2\text{Cl}_2(\text{THF})_2]_2$ (117.4 mg, 0.121 mmol) in THF (1.5 mL) dropwise. This resulted in an immediate change to a dark red-brown solution, concomitant with the formation of a brown suspended solid. The mixture was allowed to stir at room temperature for 40 min. All of the volatiles were removed *in vacuo*, and the resulting red-brown solid was triturated with Et_2O (1 mL). The red-brown solid was extracted into Et_2O (5 mL), and filtered through a Celite column supported on glass wool (0.5 cm \times 2 cm), which generated a brown plug and an orange filtrate. The orange filtrate was concentrated *in vacuo* (ca. 1 mL). Storage at -25°C for 24 h resulted in the deposition of orange crystals (10.2 mg, 12% yield). The identity of the orange crystals were determined to be a mix of compounds **5.3** and **5.4** in a 10:1 ratio based on the ^1H NMR spectrum. Anal. Calcd $\text{C}_{22}\text{H}_{22}\text{N}_4$: C, 77.16; H, 6.48; N, 16.36. Found: C, 76.83; H, 6.38; N, 15.99. ^1H NMR (C_6D_6 , 25°C , 400 MHz): δ 7.05 (t, $J_{\text{HH}} = 8$ Hz, 1H, aryl CH), 7.01 (d, $J_{\text{HH}} = 9$ Hz, 1H, aryl CH), 6.97 (d, $J_{\text{HH}} = 8$ Hz, 1H, aryl CH), 6.73 (d, $J_{\text{HH}} = 9$ Hz, 1H, aryl CH), 6.70 (d, $J_{\text{HH}} = 8$ Hz, 1H, aryl CH), 6.61 (d, $J_{\text{HH}} = 8$ Hz, 1H, aryl CH), 6.42 (t, $J_{\text{HH}} = 7$ Hz, 1H, aryl CH), 6.33 (t, $J_{\text{HH}} = 7$ Hz, 1H, aryl CH), 5.27 (s, 1H, γ -CH), 4.99 (s, 1H, γ -CH), 2.31 (s, 3H, CH_3), 2.27 (s, 3H, CH_3), 2.06 (s, 3H, CH_3), 1.48 (s, 3H, CH_3). ESI-MS: m/z 343.18 $[\text{M}-\text{H}]^+$. IR (KBr pellet, cm^{-1}): 1589(sh m), 1581(m), 1549(m), 1516(m), 1468(m), 1460(m), 1444(sh m), 1410(sh s), 1396(vs), 1385(sh m), 1367(m), 1309(sh w), 1299(m), 1272(sh w), 1265(m), 1207(m), 1173(w), 1155(w), 1103(w), 1029(w), 1024(w), 1007(m), 928(w), 850(w), 827(w), 810(m), 802(m), 771(w), 742(sh m), 744(s), 733(m), 719(s), 677(m), 627(m), 602(w), 543(w), 490(m).

5.4.7 Synthesis of the β -diketiminato pyrazolium macrocycle (*E*-isomer: 5.4). For preparation see experimental details for compound 5.3. X-ray quality crystals of 5.4 were obtained from recrystallizing a mixture of 5.3 and 5.4 from a concentrated Et₂O/THF solution in a 5:1 ratio. ¹H NMR (C₆D₆, 25 °C, 400 MHz): δ 7.23 (d, $J_{\text{HH}} = 7$ Hz, 2H, aryl CH), 6.96 (t, $J_{\text{HH}} = 6$ Hz, 2H, aryl CH), 6.86 (d, $J_{\text{HH}} = 6$ Hz, 2H, aryl CH), 6.52 (t, $J_{\text{HH}} = 5$ Hz, 2H, aryl CH), 5.14 (s, 1H, γ -CH), 4.51 (s, 1H, γ -CH), 2.26 (s, 6H, CH₃), 1.87 (s, 6H, CH₃). ¹³C{¹H} NMR (C₆D₆, 25 °C, 126 MHz): δ 161.48 (s, 2C, NCCH₃), 154.01 (s, 2C, NC_{aryl}), 147.73 (s, 2C, NCCH₃), 133.12 (s, 2C, aryl CH), 131.70 (s, 2C, aryl CH), 121.92 (s, 2C, NC_{aryl}), 117.37 (s, 2C, aryl CH), 106.97 (s, 1C, γ -CH), 88.77 (s, 1C, γ -CH), 25.73 (s, 2C, CH₃), 12.89 (s, 2C, CH₃). One aryl CH resonance is not observed due to overlap with the benzene resonance.

5.4.8 Synthesis of [Li]₂[Li(THF)₃Cl]₂[UO₂Cl₂{tmtaa}₂UO₂Cl₂] (5.5). To a cold (-25°C) stirred yellow slurry of [UO₂Cl₂(THF)₂]₂ (66.2 mg, 0.068 mmol) in THF (1.5 mL), was added a cold (-25°C) red solution of Li₂(tmtaa) (49.2 mg, 0.138 mmol) in THF (1 mL) dropwise, which resulted in an immediate change to a dark red-brown solution. The solution was allowed to stir for ~ 1 min at room temperature, whereupon the red-brown solution was filtered through a Celite column supported on glass wool (0.5 cm × 2 cm). The red-brown filtrate was concentrated *in vacuo*, and layered with Et₂O (1.5 mL). Storage at -25°C for 48 h, resulted in the deposition of red-brown crystals (36.2 mg, 28% yield based on the starting materials, or 42% yield based on the stoichiometry in eq 5.1). Anal. Calcd C₆₈H₉₂Cl₆Li₄N₈O₁₀U₂: C, 43.03; H, 4.89; N, 5.90. Anal. Calcd C₆₀H₇₆Cl₆Li₄N₈O₈U₂: C, 41.09; H, 4.37; N, 6.39. Found: C, 40.99; H, 3.96; N, 6.22. ¹H NMR (pyr-*d*₅, 25 °C, 400 MHz): δ 7.17 (br s, 2H, aryl CH), 7.09 (t, 4H, aryl CH), 7.01 (br s, 2H,

aryl CH), 6.97 (d, 4H, aryl CH), 6.90 (br s, 2H, aryl CH), 6.87 (br d, 2H, aryl CH), 4.85 (s, 2H, γ -CH), 4.81 (s, 2H, γ -CH), 2.25 (s, 3H, CH₃), 1.99 (s, 3H, CH₃). ⁷Li{¹H} NMR (THF-*d*₈, 25 °C, 155 MHz): δ 1.93 (s, LiCl). ⁷Li{¹H} NMR (pyr-*d*₅, 25 °C, 155 MHz): δ 3.60 (s, 4Li), 2.67 (s, 1Li). IR (KBr pellet, cm⁻¹): 1660(m), 1645(sh w), 1618(sh w), 1591(w), 1535(sh w), 1518(m), 1473(s), 1441(m), 1373(sh s), 1362(vs), 1273(w), 1259(w), 1182(m), 1107(w), 1059(sh w), 1039(m), 1014(sh w), 928(sh w), 897(s), 818(sh w), 800(m), 787(sh w), 743(w), 740(w).

5.4.9 Synthesis of [Li(THF)]₂[UO₂(N(SiMe₃)₂)₂(tmtaa)] (5.6). To an orange solution of UO₂(N(SiMe₃)₂)₂(THF)₂ (7.6 mg, 0.010 mmol) in C₆D₆ (1 mL), in an NMR tube, was added a red solution of Li₂(tmtaa)₂ (3.6 mg, 0.010 mmol) in C₆D₆ (0.5 mL) dropwise, which resulted in a slightly darker red solution. The solution was allowed to stand at room temperature for 3 h, whereupon red block crystals formed, whose identity was confirmed using X-ray crystallography. ¹H NMR (C₆D₆, 25 °C, 400 MHz): δ 7.87 (d, $J_{\text{HH}} = 8$ Hz, 2H, aryl CH), 7.24 (t, $J_{\text{HH}} = 8$ Hz, 2H, aryl CH), 7.04 (t, $J_{\text{HH}} = 8$ Hz, 2H, aryl CH), 6.79 (d, $J_{\text{HH}} = 8$ Hz, 2H, aryl CH), 4.77 (s, 1H, γ -CH), 4.32 (s, 1H, γ -CH), 3.35 (br s, 8H, THF), 1.95 (s, 6H, CH₃), 1.82 (s, 6H, CH₃), 1.28 (br s, 8H, THF), 0.78 (s, 18H, SiMe₃), 0.33 (s, 18H, SiMe₃). ⁷Li{¹H} NMR (C₆D₆, 25 °C, 155 MHz): δ 1.87 (s, 1Li), -0.47 (s, 1Li).

5.4.10 X-ray Crystallography. The solid-state molecular structures of complexes **5.1**, **5.2**, and **5.6**, and compounds **5.3** and **5.4**, were determined similarly with exceptions noted in the following paragraph. Crystals were mounted on a cryoloop under Paratone-N oil. Data collection was carried out on a Bruker KAPPA APEX II diffractometer equipped with an APEX II CCD detector using a TRIUMPH

monochromator with a Mo K α X-ray source ($\lambda = 0.71073 \text{ \AA}$). Data for **5.1** - **5.4** and **5.6** were collected at 100(2) K, using an Oxford nitrogen gas cryostream system. A hemisphere of data was collected using ω scans with 0.5° frame widths. Frame exposures of 5, 10, 10 and 20 seconds were used for **5.1**, **5.3**, **5.4**, and **5.6** respectively, while frame exposures of 10 and 20 seconds were used for complex **5.2**. Data for **5.5** were collected on a Bruker Proteum2 diffractometer equipped with a PLATINUM CCD detector using multilayer optics with a CuK α X-ray source ($\lambda = 1.4178 \text{ \AA}$). The crystals of **5.5** were mounted on a cryoloop under Paratone-N oil, and all data were collected at 100(2) K using an Oxford nitrogen gas cryostream system. A hemisphere of data was collected using ω and ϕ scans with 0.5° frame widths. Frame exposures of 30 and 60 seconds were used for **5.5**. Data collection and cell parameter determination for complexes **5.1** - **5.6** were conducted using the SMART program.⁴⁹ Integration of the data frames and final cell parameter refinement were performed using SAINT software.⁵⁰ Absorption correction of the data was carried out using the multi-scan method SADABS.⁵¹ Subsequent calculations were carried out using SHELXTL.⁵² Structure determination was done using direct or Patterson methods and difference Fourier techniques. All hydrogen atom positions were idealized, and rode on the atom of attachment. However, hydrogen atoms were not assigned to the disordered carbon atoms. Structure solution, refinement, graphics, and creation of publication materials were performed using SHELXTL.⁵²

Complex **5.2** contains an oxo ligand in the main residue that exhibits mild disorder. Since no other positions were identified in the difference map, the disorder was addressed by not refining the atom anisotropically. Complex **5.5** contains a THF

solvent molecule that exhibits positional disorder. The positional disorder was addressed by modeling the molecule in two orientations in a 50:50 ratio. Disordered atoms were not refined anisotropically and were constrained with the EADP and DFIX commands. Hydrogen atoms were not assigned to these carbon atoms. Additionally, complex **5.5** exhibits some mild disorder of the other THF solvates. The disorder was addressed with the EADP command. Complex **5.6** exhibits mild disorder of the two SiMe₃ groups. The disordered carbon atoms were not refined anisotropically and were constrained with the EADP and SADI commands. Additionally, one of these carbon atoms exhibits positional disorder. The positional disorder was addressed by modeling the atom in two orientations in a 50:50 ratio. A summary of crystallographic data for **5.1-5.6** is presented in Tables 5.2-5.3.

Table 5.2. X-ray Crystallographic Information for **5.1**, **5.2**, and **5.5**.

	5.1	5.2	5.5·C₄H₈O
empirical formula	UN ₅ O ₃ Si ₂ C ₃₂ H ₄₉	UN ₈ O ₂ C ₄₄ H ₄₆	UCl ₃ Li ₂ N ₄ O ₆ C ₃₈ H ₅₄
Crystal habit, color	block, red	block, red-orange	shard, red-brown
crystal size (mm)	0.4 × 0.3 × 0.2	0.3 × 0.2 × 0.2	0.2 × 0.1 × 0.05
crystal system	triclinic	triclinic	triclinic
space group	<i>P</i> -1	<i>P</i> -1	<i>P</i> -1
vol (Å ³)	3576(2)	990(2)	2074.0(2)
a (Å)	12.614(4)	8.568(8)	10.6754(7)
b (Å)	17.491(5)	9.760(8)	13.6529(9)
c (Å)	17.517(5)	11.88(1)	14.8458(9)
α (deg)	93.119(4)	91.84(2)	81.566(5)
β (deg)	103.060(4)	94.46(2)	77.776(4)
γ (deg)	106.749(4)	90.84(2)	80.959(5)
Z	4	1	2
fw (g/mol)	845.97	956.92	1021.11
density (calcd) (Mg/m ³)	1.572	1.605	1.635
abs coeff (mm ⁻¹)	4.644	4.148	13.182
F ₀₀₀	1680	474	1014
Total no. reflections	17762	3959	3477
Unique reflections	11513	3035	2552
final R indices [I > 2σ(I)]	R ₁ = 0.0460 wR ₂ = 0.0950	R ₁ = 0.0903 wR ₂ = 0.1954	R ₁ = 0.0728 wR ₂ = 0.1725
largest diff peak and hole (e ⁻ Å ⁻³)	3.014 and -2.262	4.722 and -4.512	2.609 and -0.709
GOF	0.896	1.107	1.097

Table 5.3. X-ray Crystallographic Information for **5.3**, **5.4** and **5.6**.

	5.3	5.4 ·C ₄ H ₈ O	5.6 ·2C ₆ D ₆
empirical formula	N ₄ C ₂₂ H ₂₂	N ₄ OC ₂₆ H ₃₀	ULi ₂ N ₆ O ₄ Si ₄ C ₅₄ H ₅₆ D ₁₂
Crystal habit, color	block, orange	hexagon, orange	block, red
crystal size (mm)	0.1 × 0.1 × 0.05	0.1 × 0.1 × 0.05	0.2 × 0.1 × 0.05
crystal system	monoclinic	monoclinic	orthorhombic
space group	<i>P</i> 2 ₁ / <i>n</i>	<i>P</i> 2 ₁ / <i>c</i>	<i>Pnma</i>
vol (Å ³)	1799.6(3)	2186.0(2)	5838(2)
a (Å)	12.281(1)	8.9736(4)	24.581(3)
b (Å)	10.405(1)	12.4407(6)	19.479(3)
c (Å)	14.842(1)	19.6623(8)	12.193(2)
α (deg)	90	90	90
β (deg)	108.383(6)	95.202(3)	90
γ (deg)	90	90	90
Z	4	4	4
fw (g/mol)	342.44	414.54	1229.41
density (calcd) (Mg/m ³)	1.264	1.260	1.399
abs coeff (mm ⁻¹)	0.077	0.078	2.909
F ₀₀₀	728	888	2480
Total no. reflections	4485	3027	5154
Unique reflections	3179	2336	2164
final R indices [I > 2σ(I)]	R ₁ = 0.0474 wR ₂ = 0.1266	R ₁ = 0.0373 wR ₂ = 0.0850	R ₁ = 0.0906 wR ₂ = 0.2033
largest diff peak and hole (e ⁻ Å ⁻³)	0.322 and -0.274	0.231 and -0.246	2.187 and -1.263
GOF	0.837	0.999	0.942

5.5 Acknowledgements

I would like to thank my undergraduate, Megan Wakefield, for the synthesis of the tmtaaH_2 ligand, as well as the synthesis and characterization of complexes **5.1** and **5.2**.

5.6 References

- (1) Denning, R. G. *J. Phys. Chem. A* **2007**, *111*, 4125.
- (2) Cotton, S. *Lanthanide and Actinide Chemistry*; John Wiley & Sons, Ltd.: West Sussex, England, 2006.
- (3) Morris, D. E. *Inorg. Chem.* **2002**, *41*, 3542.
- (4) Moock, K.; Turowsky, L.; Seppelt, K. *J. Fluorine Chem.* **1987**, *37*, 253.
- (5) Hayton, T. W.; Wu, G. *Inorg. Chem.* **2009**, *48*, 3065.
- (6) Lewis, A. J.; Yin, H.; Carroll, P. J.; Schelter, E. J. *Dalton Trans.* **2014**, *43*, 10844.
- (7) Duval, P. B.; Burns, C. J.; Clark, D. L.; Morris, D. E.; Scott, B. L.; Thompson, J. D.; Werkema, E. L.; Jia, L.; Andersen, R. A. *Angew. Chem. Int. Ed.* **2001**, *40*, 3357.
- (8) Cantat, T.; Graves, C. R.; Scott, B. L.; Kiplinger, J. L. *Angew. Chem. Int. Ed.* **2009**, *48*, 3681.
- (9) Duval, P. B.; Burns, C. J.; Buschmann, W. E.; Clark, D. L.; Morris, D. E.; Scott, B. L. *Inorg. Chem.* **2001**, *40*, 5491.
- (10) La Pierre, H. S.; Meyer, K. *Inorg. Chem.* **2013**, *52*, 529.
- (11) Kovács, A.; Konings, R. J. M. *Chem. Phys. Chem.* **2006**, *7*, 455.
- (12) Lam, O. P.; Franke, S. M.; Nakai, H.; Heinemann, F. W.; Hieringer, W.; Meyer, K. *Inorg. Chem.* **2012**, *51*, 6190.
- (13) Pedrick, E. A.; Wu, G.; Kaltsoyannis, N.; Hayton, T. W. *Chem. Sci.* **2014**, *5*, 3204.
- (14) Goedken, V. L.; Ladd, J. A. *J. Chem. Soc., Chem. Commun.* **1982**, 142.
- (15) Giannini, L.; Solari, E.; De Angelis, S.; Ward, T. R.; Floriani, C.; Chiesi-Villa, A.; Rizzoli, C. *J. Am. Chem. Soc.* **1995**, *117*, 5801.
- (16) Klose, A.; Solari, E.; Hesschenbrouck, J.; Floriani, C.; Re, N.; Geremia, S.; Randaccio, L. *Organometallics* **1999**, *18*, 360.
- (17) Imler, G. H.; Zdilla, M. J.; Wayland, B. B. *J. Am. Chem. Soc.* **2014**, *136*, 5856.

- (18) Shriver, D. F.; Atkins, P. W.; Overton, T. L.; Rourke, J. P.; Weller, M. T.; Armstrong, F. A. *Inorganic Chemistry*; W. H. Freeman: New York, 2006.
- (19) Hayton, T. W.; Wu, G. *J. Am. Chem. Soc.* **2008**, *130*, 2005.
- (20) Wilkerson, M. P.; Burns, C. J.; Paine, R. T.; Scott, B. L. *Inorg. Chem.* **1999**, *38*, 4156.
- (21) Copping, R.; Jeon, B.; Pemmaraju, C. D.; Wang, S.; Teat, S. J.; Janousch, M.; Tyliczszak, T.; Canning, A.; Grønbech-Jensen, N.; Prendergast, D.; Shuh, D. K. *Inorg. Chem.* **2014**, *53*, 2506.
- (22) Hayton, T. W.; Wu, G. *Inorg. Chem.* **2008**, *47*, 7415
- (23) Schettini, M. F.; Wu, G.; Hayton, T. W. *Inorg. Chem.* **2009**, *48*, 11799.
- (24) Schettini, M. F.; Wu, G.; Hayton, T. W. *Chem. Commun.* **2012**, *48*, 1484.
- (25) Lee, S.; Floriani, C.; Chiesi-Villa, A.; Guastini, C. *J. Chem. Soc., Dalton Trans.* **1989**, 145.
- (26) Burns, C. J.; Clark, D. L.; Donohoe, R. J.; Duval, P. B.; Scott, B. L.; Tait, C. D. *Inorg. Chem.* **2000**, *39*, 5464.
- (27) Sarsfield, M. J.; Helliwell, M. *J. Am. Chem. Soc.* **2004**, *126*, 1036.
- (28) Burschka, C.; Akgün, E.; Pindur, U. *Z. Naturforsch., B. Chem. Sci.* **1983**, *38*, 373.
- (29) Han, Y.; Yuan, D.; Teng, Q.; Huynh, H. V. *Organometallics* **2011**, *30*, 1224.
- (30) Esteruelas, M. A.; Gómez, A. V.; López, A. M.; Oñate, E. *Organometallics* **1998**, *17*, 3567.
- (31) Han, Y.; Huynh, H. V. *Chem. Commun.* **2007**, 1089.
- (32) Bertolasi, V.; Mantovani, N.; Marvelli, L.; Rossi, R.; Bianchini, C.; de los Rios, I.; Peruzzini, M.; Akbayeva, D. N. *Inorg. Chim. Acta* **2003**, *344*, 207.
- (33) Mair, F. S.; Scully, D.; Edwards, A. J.; Raithby, P. R.; Snaith, R. *Polyhedron* **1995**, *14*, 2397.
- (34) Wooles, A. J.; Lewis, W.; Blake, A. J.; Liddle, S. T. *Organometallics* **2013**, *32*, 5058.
- (35) Kaltsoyannis, N. *Inorg. Chem.* **2000**, *39*, 6009.
- (36) Deronzier, A.; Marques, M.-J. *Electrochim. Acta* **1994**, *39*, 1377.
- (37) Arnold, P. L.; Patel, D.; Wilson, C.; Love, J. B. *Nature* **2008**, *451*, 315.
- (38) Arnold, P. L.; Pecharman, A.-F.; Hollis, E.; Yahia, A.; Maron, L.; Parsons, S.; Love, J. B. *Nat. Chem.* **2010**, *2*, 1056.
- (39) Seaman, L. A.; Schnaars, D. D.; Wu, G.; Hayton, T. W. *Dalton Trans.* **2010**, 39, 6635.
- (40) Danis, J. A.; Lin, M. R.; Scott, B. L.; Eichhorn, B. W.; Runde, W. H. *Inorg. Chem.* **2001**, *40*, 3389.
- (41) Seaman, L. A.; Hrobárik, P.; Schettini, M. F.; Fortier, S.; Kaupp, M.; Hayton, T. W. *Angew. Chem. Int. Ed.* **2013**, *52*, 3259.
- (42) Thuéry, P.; Masci, B. *Dalton Trans.* **2003**, 2411.
- (43) Cutler, A. R.; Alleyne, C. S.; Dolphin, D. *Inorg. Chem.* **1985**, *24*, 2276.
- (44) Barnhart, D. M.; Burns, C. J.; Sauer, N. N.; Watkin, J. G. *Inorg. Chem.* **1995**, *34*, 4079.
- (45) Niewahner, J. H.; Walters, K. A.; Wagner, A. *J. Chem. Educ.* **2007**, *84*, 477.
- (46) Harris, R. K.; Becker, E. D.; Cabral De Menezes, S. M.; Goodfellow, R.; Granger, P. *Pure Appl. Chem.* **2001**, *73*, 1795.

- (47) Harris, R. K.; Becker, E. D.; Cabral De Menezes, S. M.; Granger, P.; Hoffman, R. E.; Zilm, K. W. *Pure Appl. Chem.* **2008**, *80*, 59.
- (48) Black, D. G.; Swenson, D. C.; Jordan, R. F.; Rogers, R. D. *Organometallics* **1995**, *14*, 3539.
- (49) *SMART*, Apex II, Version 2.1; Bruker AXS Inc.: Madison, WI, 2005.
- (50) *SAINTE*, Software User's Guide, Version 7.34a; Bruker AXS Inc.: Madison, WI, 2005.
- (51) Sheldrick, G. M. *SADABS*, University of Gottingen: Germany, 2005.
- (52) *SHELXTL PC*, Version 6.12; Bruker AXS Inc.: Madison, WI, 2005.

Chapter 6. Perturbation of the O-U-O Angle in Uranyl by Coordination to a 12-membered Macrocycle

6.1. Introduction	180
6.2. Results and Discussion	182
6.2.1. Synthesis and Characterization of $\text{UO}_2\text{Cl}_2(\text{HN4})$ (6.1) and $\text{UO}_2\text{Cl}_2(\text{MeN4})$ (6.2)	182
6.2.2. Synthesis and Characterization of $\text{UO}_2(\text{OTf})_2(\text{HN4})$ (6.3) and $[\text{UO}_2(\text{OTf})(\text{THF})(\text{MeN4})][\text{OTf}]$ (6.4).....	187
6.2.3. Raman $\text{U}=\text{O}$ ν_{sym} Stretch Comparison.....	189
6.2.4. Solution Phase Behavior of Complexes 6.1 - 6.4	192
6.3. Summary	194
6.4. Experimental Section	196
6.4.1. General Procedures	196
6.4.2. Raman Spectroscopy.....	196
6.4.3. Characterization of $[\text{UO}_2\text{Cl}_2(\text{THF})_2]_2$	197
6.4.4. Characterization of $\text{UO}_2(\text{OTf})_2(\text{THF})_3$	197
6.4.5. Synthesis of $\text{UO}_2\text{Cl}_2(\text{HN4})$ (6.1)	197
6.4.6. Synthesis of $\text{UO}_2\text{Cl}_2(\text{MeN4})$ (6.2)	198
6.4.7. Synthesis of $\text{UO}_2(\text{OTf})_2(\text{HN4})$ (6.3)	199
6.4.8. Synthesis of $[\text{UO}_2(\text{OTf})(\text{THF})(\text{MeN4})][\text{OTf}]$ (6.4).....	200
6.4.9. X-Ray Crystallography	201
6.5. Acknowledgements	205
6.6. References	205

6.1 Introduction

The uranyl (UO_2^{2+}) ion is known to exhibit a strictly linear O-U-O bond angle,¹ which rarely deviates past 170° . Multiple attempts have been made to generate a *cis*-uranyl complex,²⁻⁹ employing two major strategies, however none have been successful. The first strategy is to introduce oxo ligands to a uranium precursor complex, where the geometry is predisposed for *cis* coordination.^{2,3} The second strategy is to generate a *cis*-uranyl complex, by ligating a bulky, multidentate ligand to a *trans*-uranyl moiety, in order to effect a *trans* to *cis* isomerization.⁴⁻⁶ However, most attempts have failed due to either ligand oxidation or ligand decomposition (discussion in Section 1.4).²⁻⁴ Inspired by the second strategy, we sought to coordinate a polydentate macrocyclic ligand to the uranyl fragment to effect a *trans* to *cis* isomerization of the oxo ligands.

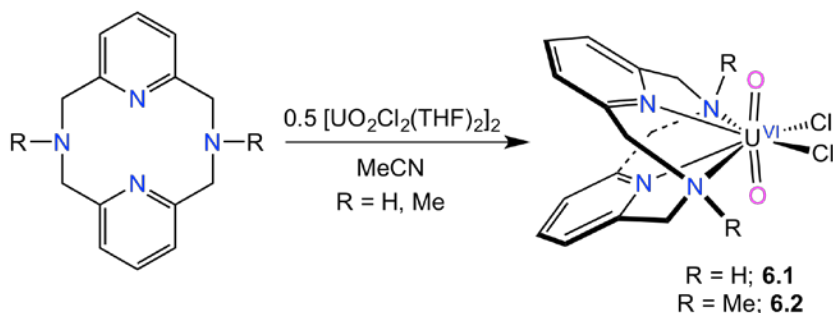
Several researchers have previously explored the coordination of macrocycles to the uranyl ion. For example, Sessler and co-workers have demonstrated that the uranyl ion can fit within the binding pocket of the 20-membered pentaphyrin ligand.¹⁰ With this large binding pocket there is no steric pressure placed upon the two oxo ligands, and, as a result, the *trans* configuration is observed experimentally.¹⁰⁻¹² Similarly, Sessler and co-workers also demonstrated that the uranyl ion fits within the binding pocket of the 18-membered alaskaphyrin ligand.¹³ In contrast, there are no known uranyl porphyrin complexes, likely because the uranyl ion cannot be accommodated by the binding pocket of the smaller 16-membered porphyrin core.¹¹ These observations suggest that coordination of uranyl to a small (≤ 16 member ring

size) macrocycle could effect the desired *trans/cis* isomerization. In Chapter 5, our group demonstrated that reaction of the anionic 14-membered macrocycle, [tmtaa]²⁻ (tmtaaH₂ = dibenzotetramethyltetraaza[14]annulene), with *trans*-uranyl precursors, resulted in the formation of the four tmtaa uranyl complexes, UO₂(tmtaaH)(N(SiMe₃)₂)(THF) (5.1), UO₂(tmtaaH)₂ (5.2), [Li]₂[Li(THF)₃Cl]₂[UO₂Cl₂{tmtaa}₂UO₂Cl₂] (5.5), and [Li(THF)]₂[UO₂(N(SiMe₃)₂)₂(tmtaa)] (5.6), where only two nitrogen atoms of the tmtaa ligands coordinate to the uranium centers, effectively leaving the O-U-O fragments unperturbed. This showcases that the tmtaa ligand is too flexible, and we hypothesize that more rigid and smaller macrocycles should be investigated. Tetradentate macrocycles will apply better steric pressure to the O-U-O fragment, and could result in O-U-O deformation. Accordingly, in collaboration with the Mirica group at Washington University in St. Louis, we sought to explore the reactivity of the uranyl ion with the 12-membered macrocyclic ligands, ^HN4 (^HN4 = 2,11-diaza[3,3](2,6) pyridinophane) and ^{Me}N4 (^{Me}N4 = *N,N'*-dimethyl-2,11-diaza[3,3](2,6) pyridinophane), which were synthesized by Jason W. Schultz in the Mirica group. These ^HN4 and ^{Me}N4 ligands were recently shown to act as tetradentate ligands for transition metal ions, while leaving two open coordination sites in a *cis* arrangement.¹⁴⁻¹⁶

6.2 Results and Discussion

6.2.1 Synthesis and Characterization of $\text{UO}_2\text{Cl}_2(\text{HN4})$ (**6.1**) and $\text{UO}_2\text{Cl}_2(\text{MeN4})$ (**6.2**)

Addition of 2 equiv of HN4 to $[\text{UO}_2\text{Cl}_2(\text{THF})_2]_2$, in MeCN, results in the formation of a yellow-orange slurry, from which $\text{UO}_2\text{Cl}_2(\text{HN4})$ (**6.1**) can be isolated as a yellow crystalline solid in 66% yield (Scheme 6.1). Similarly, addition of 2 equiv of MeN4 to $[\text{UO}_2\text{Cl}_2(\text{THF})_2]_2$, in MeCN, results in the formation of an orange-yellow slurry, from which $\text{UO}_2\text{Cl}_2(\text{MeN4})$ (**6.2**) can be isolated as a yellow-orange powder in 73% yield (Scheme 6.1).



Scheme 6.1. Synthesis of complexes **6.1** and **6.2**.

Complex **6.1** crystallizes in the monoclinic space group $P2_1/m$ as the MeCN solvate, **6.1**·2MeCN (Figure 6.1), while complex **6.2** crystallizes in the orthorhombic space group $Cmcm$ as the MeCN solvate, **6.2**·2MeCN (Figure 6.1). Complex **6.2** is also isolable in a second crystal modification (**6.2a**) with no co-crystallized MeCN solvate, which occupies the orthorhombic space group $Pbcn$ (See Below). All four nitrogen atoms of the macrocyclic ligands are coordinated to the U centers in complexes **6.1** and **6.2**, generating 8-coordinate species. According to the continuous shape measure developed by Alvarez and co-workers,¹⁷ the geometries about the uranium centers in

6.1 and **6.2** could be described as either a triangular dodecahedron (**6.1**: CSM = 3.47; **6.2**: CSM = 3.79), or a snub diphendoid J84 (**6.1**: CSM = 3.44; **6.2**: CSM = 3.24). The O-U-O angles in **6.1** and **6.2** are 164.1(3)° and 168.2(3)°, respectively (Table 6.1). These O-U-O angles are amongst the smallest reported for the uranyl fragment, and are comparable to those observed for Cp*UO₂(*t*Bu-MesPDI^{Me}) (O-U-O = 167.4(4)°),¹⁸ [NEt₄]₂[UO₂(η⁵-Cp*)(CN)₃] (O-U-O = 168.40(9)°),¹⁹ UO₂(SCS)(py)₂ (SCS = C(PPh₂S)₂; O-U-O = 168.5(1)°),²⁰ [UO₂(BIPM^{TMS})(DMAP)₂] (BIPM^{TMS} = C(PPh₂NSiMe₃)₂; DMAP = 4-(dimethylamino)pyridine; O-U-O = 167.16(9)°),²¹ [UO₂(O-2,6-*t*Bu₂C₆H₃)₂(THF)₂] (O-U-O = 167.8(4)°),²² and [UO₂(κ²-NO₃)₂(ⁿPrbtp)] (ⁿPrbtp = 2,6-bis(5,6-di-*n*-propyl-1,2,4-triazin-3-yl)pyridine; O-U-O = 166.2(1)°).²³ We suggest that the deviation from linearity in complexes **6.1** and **6.2**, in particular, is due to an unfavorable steric interaction between the oxo ligands and the macrocycle backbone. In this regard, the smaller O-U-O angle in **6.1** vs. **6.2** may be due to the shorter U-N_R (R = H, Me) and U-N_{pyr} bond lengths in the former, which is a result of the smaller steric profile of ^HN4 vs. ^{Me}N4. A difference in M-N_R bond distances between ^HN4 and ^{Me}N4 can also be seen in [FeCl₂(^HN4)][Cl] (Fe-N = 2.189(1) Å),²⁴ and [FeCl₂(^{Me}N4)][FeCl₄] (Fe-N = 2.237(2) and 2.219(2) Å).²⁵ The U-O bond lengths in **6.1** (1.776(5) and 1.785(5) Å) and **6.2** (1.779(6) Å), in contrast to the O-U-O angles, are similar to those exhibited by *trans*-uranyl.²³ Interestingly, the N_{pyr}-M-N_{pyr} angles in **6.1** (58.5(2)°) and **6.2** (56.2(2)°) are much smaller than those observed in other ^HN4 and ^{Me}N4 complexes,²⁶⁻²⁸ such as [Fe(^HN4)Cl₂][Cl] (84.95(7)°),²⁴ [FeCl₂(^{Me}N4)][FeCl₄] (78.05(8)°),²⁵ OsCl₂(^{Me}N4) (82.4(3)°),²⁹ and MnCl₂(^{Me}N4) (73.5(1)°).³⁰ This difference can be rationalized by greater steric constraints placed upon the ^RN4 ligands by the uranyl fragment in

complexes **6.1** and **6.2**, which are also reflected in the odd coordination geometries about the uranium centers.

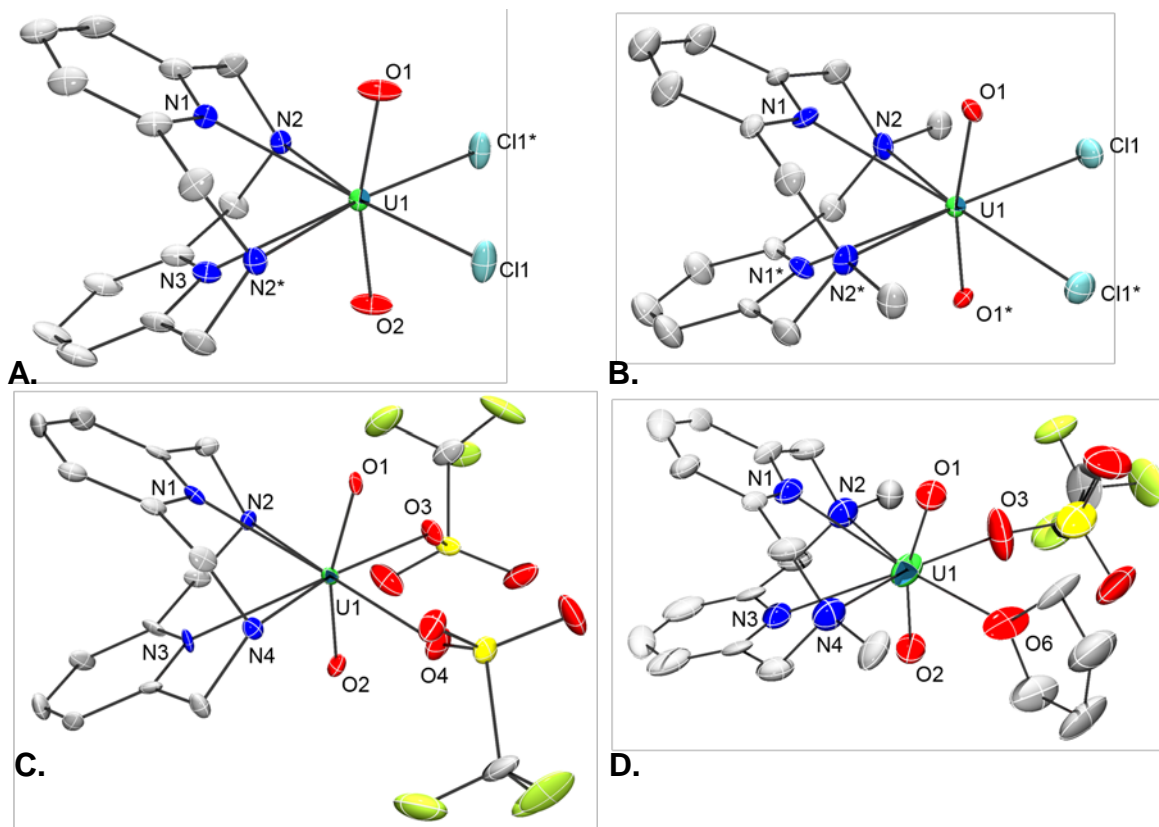


Figure 6.1. Solid-state structures of **6.1-6.4**, with 50% probability ellipsoids. **A)** Solid-state structure of $\text{UO}_2\text{Cl}_2(\text{HN4})\cdot 2\text{MeCN}$ (**6.1**·2MeCN). **B)** Solid-state structure of $\text{UO}_2\text{Cl}_2(\text{MeN4})\cdot 2\text{MeCN}$ (**6.2**·2MeCN). **C)** Solid-state structure of $\text{UO}_2(\text{OTf})_2(\text{HN4})$ (**6.3**). **D)** Solid-state structure of $[\text{UO}_2(\text{OTf})(\text{THF})(\text{MeN4})][\text{OTf}]\cdot 0.5\text{C}_4\text{H}_8\text{O}$ (**6.4**·0.5C₄H₈O). Complex **4** crystallizes with two independent molecules in the asymmetric unit. Only one is shown for clarity. Counterions, solvate molecules, and all hydrogen atoms have been omitted for clarity for complexes **6.1 – 6.4**.

Table 6.1. Selected bond lengths (Å) and angles (deg) for complexes **6.1-6.4**.

	6.1	6.2	6.2a	6.3	6.4
U=O	1.776(5) 1.785(5)	1.779(6)	1.769(4)	1.759(6) 1.781(6)	1.76(1) 1.77(1)
U-N _{pyr}	2.639(6) 2.674(7)	2.732(5)	2.693(5)	2.626(7) 2.635(7)	2.68(1) 2.73(1)
U-N _R	2.601(5)	2.727(6)	2.728(5)	2.580(7) 2.597(7)	2.63(1) 2.67(1)
U-Cl	2.735(1)	2.686(2)	2.677(2)	-	-
U-O _{OTf}	-	-	-	2.397(6) 2.409(6)	2.34(1)
O-U-O	164.1(3)	168.2(3)	168.3(3)	162.8(3)	161.7(5)
N _{pyr} -U-N _{pyr}	58.5(2)	56.2(2)	57.3(2)	59.4(2)	57.8(3)
Difference in O-U-O and N _{pyr} -U- N _{pyr} planes	0	10.99(9)°	27.1(5)°	9.8(9)°	9.2(6)°
Distance of the N _{pyr} atom from the equatorial plane	av. 1.298 Å	1.288(5) Å	1.083(5) Å	av. 1.302 Å	av. 1.305 Å

An interesting aspect of these structures is the displacement of the N atoms of the two ^RN₄ pyridine rings from the uranyl equatorial plane (defined by U1, N2, N2*, Cl1 and Cl1* in **6.1** and U1, N2, and N2* in **6.2**). In particular, the N_{pyr} atoms are displaced from the uranyl equatorial plane by 1.298 Å and 1.288(5) Å in **6.1** and **6.2**, respectively (Table 6.1). Deviations of multiple donor atoms from the equatorial plane of the UO₂²⁺ ion are very rare, and only a handful of examples are known.^{23,31-35} For instance, the nitrogen atoms in [UO₂(terpy)₂][OTf]₂ (terpy = 2,6-bis(2-pyridyl)pyridine) and [UO₂(phen)₃][OTf]₂ (phen = 1,10-phenanthroline), feature maximum displacements from the uranyl equatorial plane of 0.49 and 0.71 Å,

respectively.^{33,36} Similarly, an N atom in the recently reported $\text{UO}_2\text{Cl}_2(\text{H}_2\text{BBP})$ (H_2BBP = 2,6-bis(2-benzimidazolyl)pyridine) is displaced from the uranyl equatorial plane by 0.74 Å.³¹ The most striking example of donor atom displacement from the equatorial plane is that exhibited by $[\text{NEt}_4]_2[\text{UO}_2(\eta^5\text{-Cp}^*)(\text{CN})_3]$. In this example, the maximum displacement of one of the carbon atoms on the cyclopentadienyl ring is 1.494(6) Å.¹⁹

Another interesting aspect of the structures of **6.2** and **6.2a**, in particular, is the difference between the planes defined by the O-U-O and $\text{N}_{\text{pyr}}\text{-U-N}_{\text{pyr}}$ atoms (Figure 6.2). This difference is $10.99(9)^\circ$ and $27.1(5)^\circ$ in **6.2** and **6.2a**, respectively. As a consequence, the geometry about the uranium center in **2a** is best described as a square antiprism (CSM = 3.38).¹⁷ Presumably, the change in R_4N ligand orientation upon moving from complex **6.2** to complex **6.2a** allows the uranyl fragment to avoid the large perturbation of the O-U-O fragment. Although, it is important to note that the O-U-O bond angles in **6.2** and **6.2a** are basically identical, despite this difference between the O-U-O and $\text{N}_{\text{pyr}}\text{-U-N}_{\text{pyr}}$ planes.

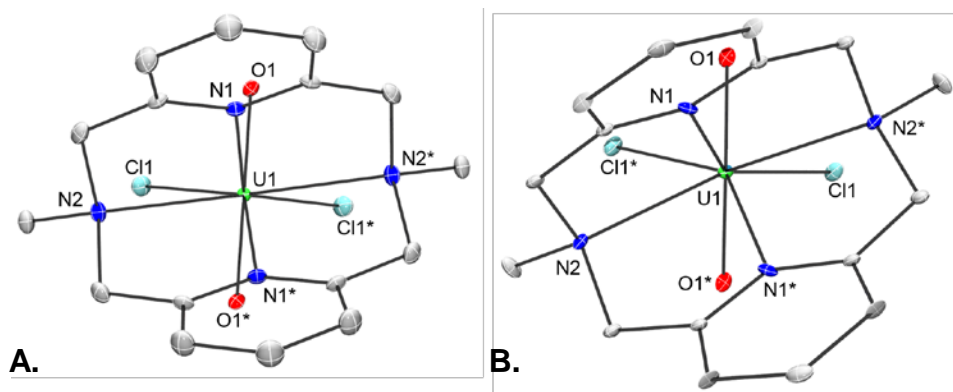
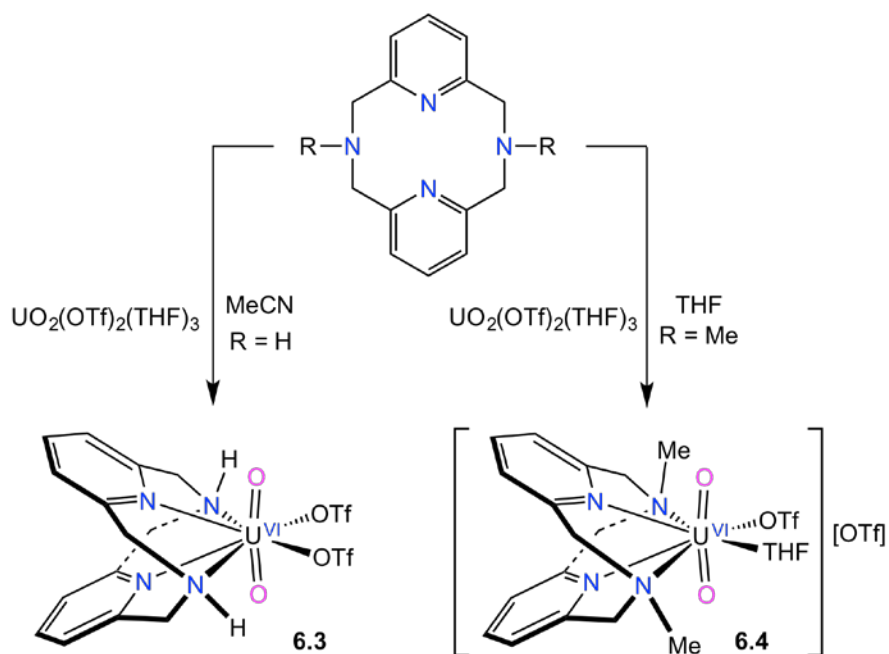


Figure 6.2. Solid-state structures of (A) **6.2** and (B) **6.2a**, with 50% probability ellipsoids, highlighting the difference between the O-U-O and $\text{N}_{\text{pyr}}\text{-U-N}_{\text{pyr}}$ planes. All hydrogens and the MeCN solvates in **6.2** have been removed for clarity.

6.2.2 Synthesis and Characterization of $\text{UO}_2(\text{OTf})_2(\text{HN4})$ (6.3) and $[\text{UO}_2(\text{OTf})(\text{THF})(\text{MeN4})][\text{OTf}]$ (6.4)

In an effort to strengthen (and shorten) the U-N bonds, and thereby decrease the O-U-O angle even further, we explored the substitution of the chloride ligands in **6.1** and **6.2** with weaker electron donating pseudo-halide ligands. Thus, addition of 1 equiv of HN4 to $\text{UO}_2(\text{OTf})_2(\text{THF})_3$ in MeCN, results in formation of an orange solution, from which $\text{UO}_2(\text{OTf})_2(\text{HN4})$ (**6.3**) can be isolated in a 76% yield as an orange powder (Scheme 6.2). Similarly, addition of 1 equiv of MeN4 to $\text{UO}_2(\text{OTf})_2(\text{THF})_3$ in THF, results in formation of $[\text{UO}_2(\text{OTf})(\text{THF})(\text{MeN4})][\text{OTf}]$ (**6.4**), which can be isolated as an orange powder in a 73% yield (Scheme 6.2). We also attempted the reaction of MeN4 and $\text{UO}_2(\text{OTf})_2(\text{THF})_3$ in MeCN. However, X-ray quality crystals could not be grown from this solvent.



Scheme 6.2. Synthesis of complexes **6.3** and **6.4**.

Complex **6.3** crystallizes in the orthorhombic space group $Pna2_1$, while complex **6.4** crystallizes in the triclinic space group $P-1$ as a THF solvate, $4 \cdot 0.5C_4H_8O$ (Figure 6.1). As with complexes **6.1** and **6.2**, all four nitrogen atoms of the macrocyclic ligand are coordinated to the U centers in **6.3** and **6.4**. Complex **6.3** also features two [OTf]⁻ ligands within its inner coordination sphere, while complex **6.4** features a THF ligand and an [OTf]⁻ ligand within its inner coordination sphere. Similar to **6.1** and **6.2**, the geometries about the uranium centers in **6.3** and **6.4** could be described as either a triangular dodecahedron (**6.3**: CSM = 2.37; **6.4**: CSM = 2.49),¹⁷ or a snub diphenoid J84 (**6.3**: CSM = 2.80; **6.4**: CSM = 2.58). Gratifyingly, the O-U-O bond angles in **6.3** (162.8(3)°) and **6.4** (161.7(5)°) are smaller than those observed in **6.1** and **6.2** (Table 6.1), and, more significantly, are smaller than any O-U-O angles reported previously.¹⁹⁻

²³ These smaller angles are likely due to the exchange of chloride for the poorly electron donating [OTf]⁻ ligands, which strengthens the U-N interactions. That said, the U-N_R and U-N_{pyr} distances in **6.3** and **6.4** are not significantly shorter than those observed in **6.1** and **6.2**. In contrast, the U-N bond lengths in complexes **6.1** – **6.4** (ca. 2.66 Å) are significantly longer than the U-N bond lengths in the tmtaa uranyl complexes UO₂(tmtaaH)(N(SiMe₃)₂)(THF) (**5.1**) (tmtaaH₂ = dibenzotetramethyltetraaza[14]annulene), UO₂(tmtaaH)₂ (**5.2**), [Li]₂[Li(THF)₃Cl]₂[UO₂Cl₂{tmtaa}₂UO₂Cl₂] (**5.5**), and [Li(THF)]₂⁻ [UO₂(N(SiMe₃)₂)₂(tmtaa)] (**5.6**) (ca. 2.41 Å), indicating the anionic [tmtaa]²⁻ ligand does have a stronger interaction with the uranium metal center than the neutral ^HN₄ and ^{Me}N₄ ligands. Similar to **6.1** and **6.2**, both complexes **6.3** and **6.4** exhibit U=O distances that are typical of the uranyl fragment (**6.3**: 1.759(6) and 1.781(6) Å, **6.4**: 1.76(1) and 1.77(1) Å).³⁷ Both structures exhibit displacement of

the N atoms of the two ^RN4 pyridine rings from the uranyl equatorial plane (defined by the atoms U, N2, N4, O3 and O4 in **6.3** and U, N2, N4, O3 and O6 in **6.4**). In particular, the N_{pyr} atoms are displaced from the equatorial plane by 1.302 Å and 1.305 Å in **6.3** and **6.4** (Table 6.1). These deviations are comparable to the deviations observed in **6.1** and **6.2**. The other metrical parameters in **6.3** and **6.4**, including the N_{pyr}-U-N_{pyr} angles, are comparable to those observed in **6.1** and **6.2**.

6.2.3 Raman U=O ν_{sym} Stretch Comparison

In an effort to better understand the effect of coordinating the ^RN4 macrocycles to the uranyl fragment, since the differences between the O-U-O bond angles of complexes **6.1** – **6.4** are rather small (only a total difference of 7°), we turned to Raman spectroscopy. This technique has proven to be useful for probing the relative strengths of the U=O bond in the uranyl fragment.³⁸ Raman spectroscopic data for complexes **6.1** – **6.4** are shown in Table 6.2. Complexes **6.1** and **6.2** exhibit U=O ν_{sym} modes at 813 and 815 cm⁻¹, respectively, in their Raman spectra. Interestingly, these values are on the lower end of the U=O ν_{sym} modes measured previously for the uranyl ion, and are similar to those observed for uranyl complexes with anionic, electron rich ligands, such as [UO₂(CO₃)₃]⁴⁻ and UO₂(^{Ar}acnac)₂ (^{Ar}acnac = ArNC(Ph)CHC(Ph)O; Ar = 3,5-^tBu₂C₆H₃).^{39,40} For further comparison, the U=O ν_{sym} mode in [UO₂Cl₂(THF)₂]₂ was found to be 20 cm⁻¹ higher, at 835 cm⁻¹. Both of these observations suggest that coordination of the macrocycle ligand to the uranyl ion does weaken the U-O bond to some extent. Complexes **6.3** and **6.4** exhibit U=O ν_{sym} modes at 833 and 831 cm⁻¹,

respectively (Figure 6.3; Table 6.2), in their Raman spectra. For comparison, the U=O ν_{sym} mode in $\text{UO}_2(\text{OTf})_2(\text{THF})_3$ is observed at 842 cm^{-1} , an increase of ca. 10 cm^{-1} vs. the values observed for **6.3** and **6.4**. Again, this difference can be interpreted as evidence that the U=O bonds in the uranyl moiety are weakened upon coordination of the $^{\text{RN4}}$ macrocycle. That said, it is unlikely that the decrease in the U=O ν_{sym} mode observed upon coordination of $^{\text{RN4}}$ to $[\text{UO}_2\text{Cl}_2(\text{THF})_2]_2$ or $\text{UO}_2(\text{OTf})_2(\text{THF})_3$ is due to the bending of the O-U-O fragment. Instead, this decrease is probably due to coordination of a relatively good tetradentate donor to the uranyl moiety. In particular, it should be noted that complexes **6.1** and **6.2**, which feature larger O-U-O angles than **6.3** and **6.4**, actually exhibit weaker U=O bonds (as indicated by their lower U=O ν_{sym} modes). Their weaker U=O bonds can be rationalized by the stronger donor strength of Cl^- vs. OTf^- , highlighting the fact that the identity of the equatorial ligands has a greater effect on the U=O ν_{sym} frequency than does a change in O-U-O angle, at least when the changes in the O-U-O angles are small. It is also important to note that the three perturbed uranyl complexes, $\text{Cp}^*\text{UO}_2(^t\text{Bu-MesPDI}^{\text{Me}})$ (O-U-O = $167.4(4)^\circ$),¹⁸ $\text{UO}_2(\text{O-2,6-}^t\text{Bu}_2\text{C}_6\text{H}_3)_2(\text{THF})_2$ (O-U-O = $167.8(4)^\circ$),³⁸ and complex **6.2** (O-U-O = $168.2(3)^\circ$), with very similar O-U-O angles, exhibit vastly different U=O ν_{sym} stretches of 789, 808, and 815 cm^{-1} , respectively. This is definitely a consequence of the donating strength of the various co-ligands.

Table 6.2. Comparison of the U=O ν_{sym} Stretch for a Series of Uranyl Complexes.

Complex	U=O ν_{sym} stretch (cm ⁻¹)	Ref.
[UO ₂ (OCH(^t Pr) ₂) ₂] ₄	713	41
[Na(THF)UO ₂ (NCN) ₂] ₂ (μ_2 -O) [NCN = Me ₃ Si(N)CPh(N)SiMe ₃]	757	42
[Na(THF) ₂ PhCN][UO ₂ (NCN) ₃]	773	42
[UO ₂ (OH) ₄] ²⁻	784	43
Cp*UO ₂ (^{Mes} PDI ^{Me}) (^{Mes} PDI ^{Me} = 2,6-((Mes)N=CMe) ₂ C ₅ H ₃ N)	788	18
Cp*UO ₂ (^t Bu- ^{Mes} PDI ^{Me}) (^t Bu- ^{Mes} PDI ^{Me} = 2,6-((Mes)N=CMe) ₂ - <i>p</i> -C(CH ₃) ₃ C ₅ H ₂ N)	789	18
UO ₂ [OCH(^t Bu)Ph] ₂ (THF) ₂	796	41
[UO ₂ (N{SiMe ₃ }) ₂] ₄ ²⁻	801	44
UO ₂ (NCN) ₂ (THF)	803	45
UO ₂ (O-2,6- ^t Bu ₂ C ₆ H ₃) ₂ (THF) ₂	804	22
UO ₂ (OCHPh) ₂ (THF) ₂	804	41
[UO ₂ (N{SiMe ₃ }) ₃] ⁻	805	44
UO ₂ (tmtaaH)(N(SiMe ₃) ₂)(THF) (5.1)	805	Ch. 5
UO ₂ (tmtaaH) ₂ (5.2)	805	Ch. 5
UO ₂ (O-2,6-Ph ₂ C ₆ H ₃) ₂ (THF) ₂	808	38
[UO ₂ (CO ₃) ₃] ⁴⁻	812	39
UO ₂ (^{Ar} acnac) ₂ (^{Ar} acnac = ArNC(Ph)CHC(Ph)O)	812	40
UO ₂ Cl ₂ (^H N4) (6.1)	813	Ch. 6
UO ₂ Cl ₂ (^{Me} N4) (6.2)	815	Ch. 6
UO ₂ (NCN) ₂	818	42
UO ₂ (N{SiMe ₃ }) ₂ (THF)	819	44
UO ₂ (NCS) ₂ (Me-N-Sal) ₃ (H ₂ O) ₂ (Me-N-Sal = <i>p</i> -CH ₃ -salicylideneaniline)	822	46
UO ₂ (^t Buacnac) ₂ (THF) (^t Buacnac = ^t BuNC(Ph)CHC(Ph)O)	823	40
UO ₂ (dbm) ₂ (THF) (2.1)	823	Ch. 2
UO ₂ (dbm ^{Me}) ₂ THF (4.3)	827	Ch. 4
UO ₂ (sal- <i>p</i> -phdn)(H ₂ O) (sal- <i>p</i> -phdn = <i>N,N'</i> - <i>p</i> -phenylene-bis(salicylideneiminato))	830	47
[UO ₂ (OTf)(THF)(^{Me} N4)][OTf] (6.4)	831	Ch. 6
UO ₂ (OTf) ₂ (^H N4) (6.3)	833	Ch. 6
[UO ₂ Cl ₂ (THF) ₂] ₂	835 (834, 840)	Ch. 6 (^{42,45})
[UO ₂ Cl(O-2,6-Me ₂ C ₆ H ₃)(THF) ₂] ₂	835	22
[UO ₂ (TPPO) ₄][OTf] ₂	839	48
[UO ₂ (O-2,6-Cl ₂ C ₆ H ₃) ₂ (THF) ₂] ₂	839	22
UO ₂ (OTf) ₂ (THF) ₃	842	Ch. 6
[UO ₂ (OAc) ₃] ⁻	843	39
[UO ₂ (dppmo) ₂ OTf][OTf]	849	49
[UO ₂ Cl ₄] ²⁻	854	39
[UO ₂ (H ₂ O) ₅] ²⁺	870	39

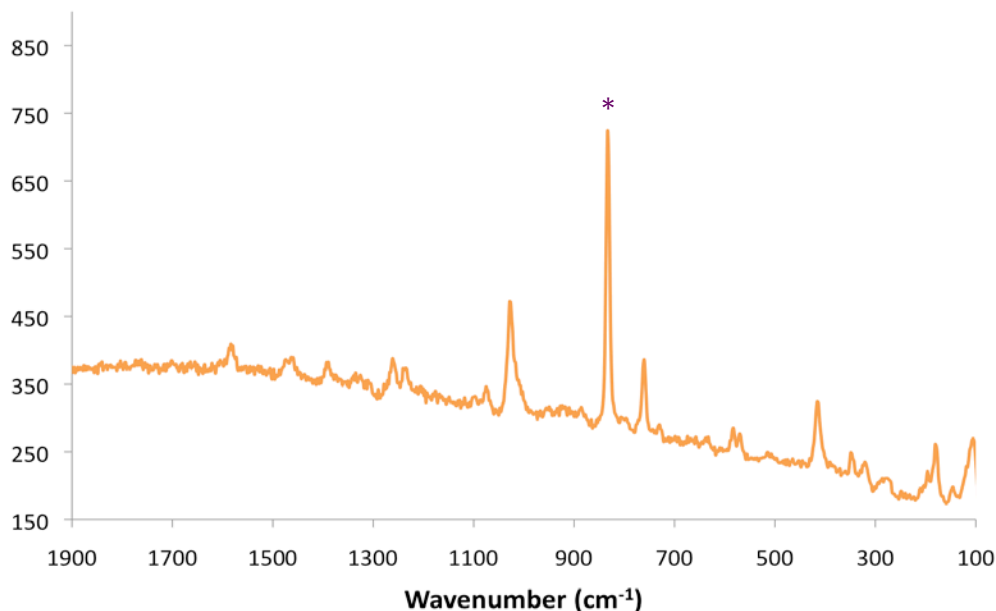


Figure 6.3. Solid-state Raman spectrum of **6.3**. U=O ν_{sym} stretch is observed at 833 cm^{-1} (*).

6.2.4 Solution Phase Behavior of Complexes 6.1 - 6.4

Finally, we explored the chemical properties and solution phase behavior of complexes **6.1** – **6.4**. Complexes **6.1** – **6.3** are insoluble in non-polar solvents, aromatic solvents, and Et₂O and THF, and only sparingly soluble in CH₂Cl₂ and MeCN. In contrast, complex **6.4** is slightly soluble in THF, and very soluble in CH₂Cl₂ and MeCN. The ¹H NMR spectrum of **6.1** in CD₂Cl₂ features diastereotopic methylene environments at 5.23 ppm and 4.82 ppm for the ^HN₄ ligand, consistent with its ligation to a metal center.⁵⁰⁻⁵² Similarly, the ¹H NMR spectrum of **6.2** in CD₂Cl₂ exhibits diastereotopic methylene resonances at 4.85 and 4.29 ppm for the ^{Me}N₄ ligand (Figure 6.4). Also observed in this spectrum is a singlet at 3.57 ppm, which is assignable to the two

methyl substituents. The ^1H NMR spectrum of **6.3** in CD_2Cl_2 features diastereotopic methylene environments at 5.19 ppm and 4.91 ppm for the $^{\text{H}}\text{N}_4$ ligand.⁵⁰ In addition, this spectrum also features a broad resonance at 5.76 ppm, which we have assigned to the NH substituent. The $^{19}\text{F}\{^1\text{H}\}$ NMR spectrum of **6.3** exhibits a singlet -77.41 ppm. As observed for **6.3**, the ^1H NMR spectrum of **6.4** in CD_2Cl_2 exhibits diastereotopic methylene resonances at 4.87 and 4.53 ppm. The spectrum also features a CH_3 resonance at 3.59 ppm and two broad singlets at 3.73 and 1.84 ppm, which are assignable to the THF ligand. The $^{19}\text{F}\{^1\text{H}\}$ NMR spectrum of **6.4** in CD_2Cl_2 only exhibits a single resonance at -77.56 ppm, suggesting that the inner- and outer-sphere $[\text{OTf}]^-$ moieties undergo rapid exchange in solution.

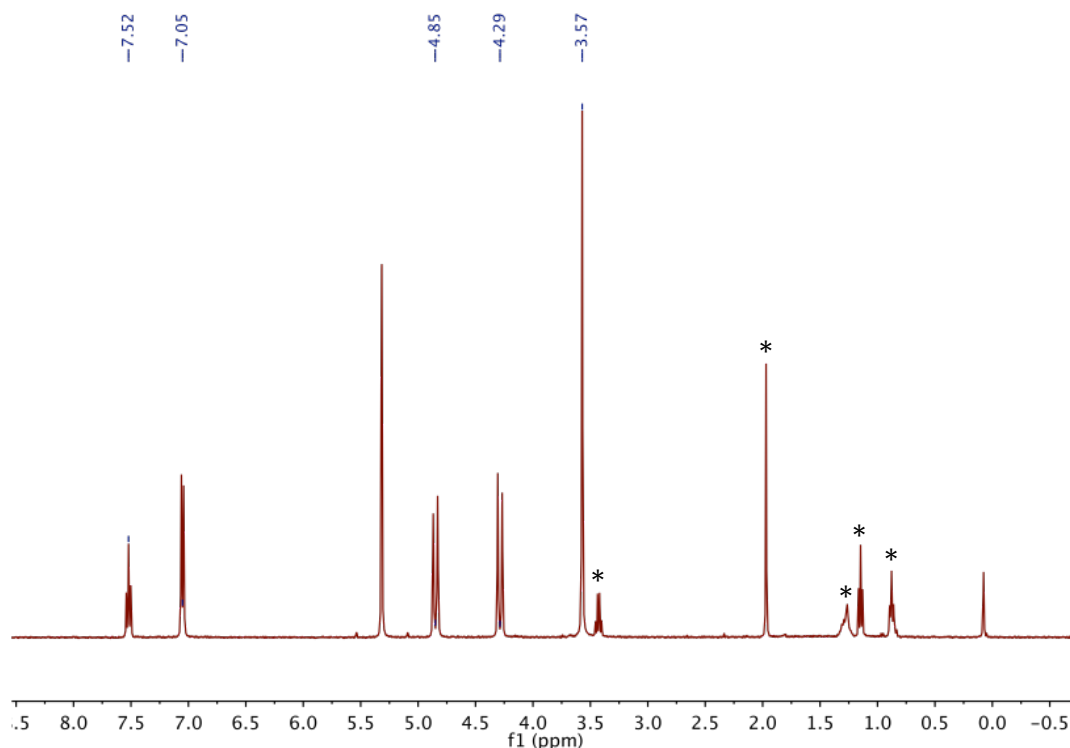
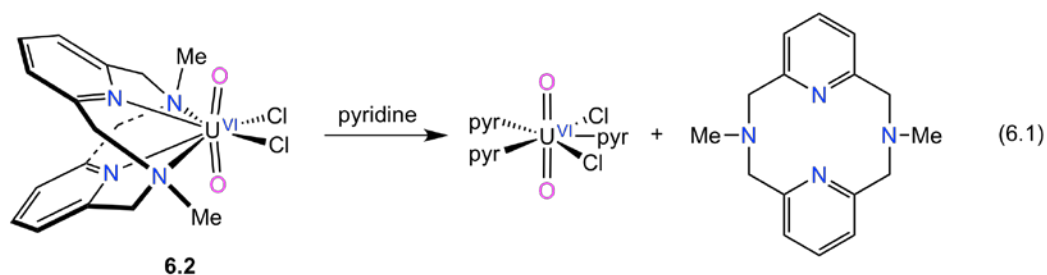


Figure 6.4. ^1H NMR spectrum of complex **6.2** in CD_2Cl_2 . Asterisks indicate the presence of MeCN, Et_2O , and hexanes.



Complexes **6.1** – **6.4** are also very soluble in pyridine. However, dissolution of complex **6.2** in pyridine- d_5 results in displacement of the macrocycle from the uranyl coordination sphere, according to ^1H NMR spectroscopy, along with probable formation of $\text{UO}_2(\text{py})_3(\text{Cl})_2$ (eq 6.1).⁵³ This observation is significant because it suggests that uranyl-macrocycle interaction in **6.2** is relatively weak; no doubt because of the mismatch between the uranyl ion and the $^{\text{Me}}\text{N}_4$ macrocycle binding pocket. Dissolution of **6.1**, **6.3**, or **6.4** in pyridine does not result in macrocycle dissociation, likely because of the smaller steric profile of $^{\text{H}}\text{N}_4$ (in the case of **6.1** and **6.3**) or the positive charge of the complex (in the case of **6.4**). Both effects are anticipated to strengthen the uranyl-macrocycle bonds.

6.3 Summary

The four 8-coordinate perturbed uranyl complexes, $\text{UO}_2\text{Cl}_2(\text{R}\text{N}_4)$ ($\text{R} = \text{H}$; **6.1**; Me, **6.2**), $\text{UO}_2(\text{OTf})_2(^{\text{H}}\text{N}_4)$ (**6.3**), and $[\text{UO}_2(\text{OTf})(\text{THF})(^{\text{Me}}\text{N}_4)][\text{OTf}]$ (**6.4**), can be synthesized by ligation of the 12-membered macrocyclic ligands $^{\text{H}}\text{N}_4$ and $^{\text{Me}}\text{N}_4$ to the uranyl ion. Complexes **6.3** and **6.4** exhibit the smallest O-U-O bond angles yet reported, although all four complexes feature O-U-O angles that are 168° or smaller. These small O-U-O

angles are a result of steric repulsion between the oxo ligands of the uranyl fragment and the macrocycle backbone, which is a consequence of the small binding pocket of the RN_4 ligand. Perhaps more importantly, our results reveal that coordination of a small macrocycle to the uranyl ion is a viable strategy for the perturbation of the O-U-O angle. Although these complexes are clearly not *cis*-uranyl complexes, they do give a lot of insight into how to potentially isolate a *cis*-uranyl complex in the future. As evidenced by the relatively small $\text{N}_{\text{pyr}}\text{-U-N}_{\text{pyr}}$ angles of complexes **6.1** – **6.4**, the macrocyclic ligands still feature significant flexibility. Also, dissolution of **6.2** in pyridine, will displace the macrocyclic ligand, indicating they are not strongly bound to the metal centers. Future studies will need to focus on macrocycles with even greater rigidity, such as the “cross-bridged” cyclam ligands,^{54,55} and focus on anionic macrocycle ligands, which result in shorter uranyl-macrocycle bonds on account of the greater electrostatic attraction to UO_2^{2+} , as evidenced by the difference in U-N bond lengths between complexes **6.1** – **6.4** (ca. 2.67 Å) and the tmtaa uranyl complexes **5.1**, **5.2**, **5.5**, and **5.6** (ca. 2.41 Å).

6.4 Experimental

6.4.1 General Procedures. All reactions and subsequent manipulations were performed under anaerobic and anhydrous conditions under an atmosphere of nitrogen. Et₂O, THF and toluene were dried by passage over activated molecular sieves using a Vacuum Atmospheres solvent purification system. CH₂Cl₂, CD₂Cl₂, MeCN, MeCN-*d*₃ and pyr-*d*₅ were dried over activated 3Å molecular sieves for 24 h before use. [UO₂Cl₂(THF)₂]₂,³⁷ UO₂(OTf)₂(THF)₃,⁵⁶ HN₄,⁵⁷ and MeN₄,⁵⁸ were prepared according to literature procedures. All other reagents were purchased from commercial suppliers and used as received.

NMR spectra were recorded on a Varian UNITY INOVA 400 spectrometer or a Varian UNITY INOVA 500 spectrometer. ¹H NMR spectra were referenced to external SiMe₄ using the residual protio solvent peaks as internal standards. The chemical shifts of ¹⁹F{¹H} were referenced indirectly with the ¹H resonance of SiMe₄ at 0 ppm, according to IUPAC standard.^{59,60} IR spectra were recorded on a Mattson Genesis FTIR/Raman spectrometer. UV-vis/NIR experiments were performed on a UV-3600 Shimadzu spectrophotometer. Elemental analyses were performed by the Microanalytical Laboratory at UC Berkeley.

6.4.2 Raman Spectroscopy. Raman spectra were recorded on a LabRam Aramis microRaman system (Horiba Jobin Yvon) equipped with 1200 grooves/mm holographic gratings, and Peltier-cooled CCD camera. The 633 nm output of a Melles Griot He-Ne laser was used to excite the sample, and spectra were collected in a back scattering geometry using a confocal Raman Microscope (high stability BX40) equipped with Olympus objectives (MPlan 50x). Sample preparation was performed

inside the glovebox: Pure crystalline solid samples were placed between a glass microscope slide and coverslip, sealed with a bead of silicone grease, and removed from the glovebox for spectral acquisition.

6.4.3 Characterization of $[\text{UO}_2\text{Cl}_2(\text{THF})_2]_2$. This complex was prepared according to the published procedure.³⁷ Raman (neat solid, cm^{-1}): 1491 (w), 1463 (w), 1460 (w), 1367 (w), 1248 (w), 1231 (w), 1046 (w), 922 (m), 884 (vs), 835 (vs, U=O ν_{sym}), 238 (m), 192 (m), 176 (m).

6.4.4 Characterization of $\text{UO}_2(\text{OTf})_2(\text{THF})_3$. This complex was prepared according to the published procedure.⁵⁶ Raman (neat solid, cm^{-1}): 1448 (w), 1332 (w), 1233 (m), 1162 (w), 1029 (sh w), 1016 (m), 999 (sh w), 915 (m), 878 (m), 843 (s, U=O ν_{sym}), 758 (m), 580 (w), 564 (w), 346 (w), 343 (w), 317 (m), 177 (m).

6.4.5 Synthesis of $\text{UO}_2\text{Cl}_2(\text{HN4})$ (6.1**).** To a stirring yellow solution of $[\text{UO}_2\text{Cl}_2(\text{THF})_2]_2$ (30.6 mg, 0.032 mmol) in MeCN (2 mL), was added dropwise an off-white slurry of HN4 (15.0 mg, 0.062 mmol) in MeCN (1 mL). This resulted in an immediate color change to dark yellow, concomitant with the deposition of yellow solid. The mixture was then allowed to stir at room temperature for 1 h, whereupon the slurry was heated to ca. 70 °C. After 5 min at 70 °C, most of the solid had dissolved, and the yellow-orange slurry was quickly filtered through a Celite column (2 cm × 0.5 cm) supported on glass wool. Storage of the yellow filtrate at -25 °C for 24 h resulted in the deposition of a yellow crystalline solid (24.1 mg, 66% yield). X-ray quality crystals of **6.1** were grown from a hot, concentrated MeCN solution that was allowed to cool slowly to room temperature. Anal. Calcd for $\text{UCl}_2\text{N}_4\text{O}_2\text{C}_{14}\text{H}_{16}$: C, 28.93; H, 2.77; N, 9.64. Found: C, 29.25; H, 2.42; N, 9.91. ^1H NMR (CD_2Cl_2 , 25 °C, 500 MHz): δ 7.57 (t, $J_{\text{HH}} = 8$ Hz, 2H, aryl CH), 7.17 (d, $J_{\text{HH}} =$

8 Hz, 4H, aryl CH), 5.23 (dd, $J_{\text{HH}} = 6$ Hz, $J_{\text{HH}} = 16$ Hz, 4H, CH₂), 4.82 (d, $J_{\text{HH}} = 16$ Hz, 4H, CH₂). The NH resonance was not observed. ¹H NMR (pyr-*d*₅, 25 °C, 400 MHz): δ 7.39 (t, $J_{\text{HH}} = 8$ Hz, 2H, aryl CH), 7.05 (d, $J_{\text{HH}} = 8$ Hz, 4H, aryl CH), 6.47 (t, $J_{\text{HH}} = 6$ Hz, 2H, NH), 5.33 (dd, $J_{\text{HH}} = 6$ Hz, $J_{\text{HH}} = 16$ Hz, 4H, CH₂), 4.82 (d, $J_{\text{HH}} = 16$ Hz, 4H, CH₂). IR (KBr pellet, cm⁻¹): 1606 (sh m), 1599 (s), 1583 (m), 1470 (m), 1443 (s), 1423 (sh m), 1379 (m), 1373 (sh w), 1311 (m), 1290 (w), 1255 (w), 1209 (w), 1155 (m), 1088 (m), 1061 (s), 1041 (s), 1010 (sh m), 997 (s), 949 (w), 910 (s), 903 (vs), 889 (vs), 816 (s), 791 (s), 752 (m), 706 (w), 671 (w), 636 (vs), 480 (w). Raman (neat solid, cm⁻¹): 1582 (w), 1395 (w), 1260 (w), 1099 (w), 1015 (m), 910 (w), 813 (vs, U=O ν_{sym}), 760 (w), 709 (w), 520 (w), 424 (w), 196 (m).

6.4.6 Synthesis of UO₂Cl₂(^{Me}N4) (6.2). To a stirring yellow solution of [UO₂Cl₂(THF)₂]₂ (48.5 mg, 0.050 mmol) in MeCN (1 mL), was added dropwise a colorless solution of ^{Me}N4 (24.3 mg, 0.091 mmol) in MeCN (1 mL). This resulted in an immediate color change to orange-yellow, concomitant with the deposition of an orange-yellow precipitate. This orange-yellow slurry was allowed to stir at room temperature for 10 min, whereupon the orange-yellow solid was isolated by decanting off the supernatant. The solid was washed with Et₂O (1 mL), and then dried *in vacuo* (41.8 mg, 73% yield). X-ray quality crystals of **6.2** were grown from a concentrated MeCN solution layered with an equal volume of Et₂O, and which was stored at -25 °C for 24 h. Anal. Calcd for UCl₂N₄O₂C₁₆H₂₀: C, 31.54; H, 3.31; N, 9.20. Found: C, 31.17; H, 2.58; N, 10.35. ¹H NMR (CD₂Cl₂, 25 °C, 400 MHz): δ 7.52 (t, $J_{\text{HH}} = 8$ Hz, 2H, aryl CH), 7.05 (d, $J_{\text{HH}} = 8$ Hz, 4H, aryl CH), 4.85 (d, $J_{\text{HH}} = 15$ Hz, 4H, CH₂), 4.29 (d, $J_{\text{HH}} = 15$ Hz, 4H, CH₂), 3.57 (s, 6H, CH₃). IR (KBr pellet, cm⁻¹): 1597 (m), 1578 (w), 1468 (m), 1452 (sh m),

1446 (s), 1427 (sh w), 1385 (m), 1367 (w), 1309 (w), 1263 (w), 1254 (w), 1232 (w), 1219 (m), 1182 (w), 1165 (m), 1093 (sh w), 1088 (m), 1082 (m), 1014 (s), 980 (w), 951 (w), 895 (vs), 885 (sh m), 812 (sh w), 802 (s), 762 (m), 727 (w), 636 (w), 538 (w), 471 (w), 455 (w). Raman (neat solid, cm^{-1}): 1580 (w), 1465 (w), 1454 (w), 1386 (w), 1258 (w), 1085 (w), 1015 (m), 815 (s, $\text{U}=\text{O}$ ν_{sym}), 769 (w), 730 (w), 403 (m), 396 (m), 284 (m), 240 (m), 199 (m), 152 (m), 118 (vs).

6.4.7 Synthesis of $\text{UO}_2(\text{OTf})_2(\text{H}^{\text{N}}\text{4})$ (6.3). To a stirring yellow solution of $\text{UO}_2(\text{OTf})_2(\text{THF})_3$ (49.5 mg, 0.063 mmol) in MeCN (1 mL), was added dropwise an off-white slurry of $\text{H}^{\text{N}}\text{4}$ (14.6 mg, 0.061 mmol) in MeCN (1 mL). This resulted in an immediate color change to orange. The orange solution was allowed to stir at room temperature for 10 min, whereupon it was filtered through a Celite column (2 cm \times 0.5 cm) supported on glass wool. The resulting orange filtrate was concentrated *in vacuo* to ca. 1 mL, and layered with Et_2O (3 mL). Storage of this solution at -25 $^\circ\text{C}$ for 24 h resulted in the deposition of orange powder (38.6 mg, 76% yield). X-ray quality crystals were grown from a MeCN solution layered with an equal volume of Et_2O , which was stored at -25 $^\circ\text{C}$ for 24 h. Anal. Calcd for $\text{UF}_6\text{N}_4\text{O}_8\text{S}_2\text{C}_{16}\text{H}_{16}$: C, 23.77; H, 1.99; N, 6.93. Found: C, 24.19; H, 1.21; N, 7.09. ^1H NMR (CD_2Cl_2 , 25 $^\circ\text{C}$, 400 MHz): δ 7.66 (t, $J_{\text{HH}} = 8$ Hz, 2H, aryl CH), 7.29 (d, $J_{\text{HH}} = 8$ Hz, 4H, aryl CH), 5.76 (br s, 2H, NH), 5.19 (dd, $J_{\text{HH}} = 5$ Hz, $J_{\text{HH}} = 16$ Hz 4H, CH_2), 4.91 (d, $J_{\text{HH}} = 16$ Hz, 4H, CH_2). ^1H NMR (pyr- d_5 , 25 $^\circ\text{C}$, 400 MHz): δ 7.59 (br t, $J_{\text{HH}} = 9$ Hz, 2H, aryl CH), 7.28 (d, $J_{\text{HH}} = 7$ Hz, 4H, aryl CH), 6.17 (br s, 2H, NH), 5.23 (br d, $J_{\text{HH}} = 14$ Hz 4H, CH_2), 4.96 (d, $J_{\text{HH}} = 16$ Hz, 4H, CH_2). $^{19}\text{F}\{^1\text{H}\}$ NMR (CD_2Cl_2 , 25 $^\circ\text{C}$, 376 MHz): δ -77.41. $^{19}\text{F}\{^1\text{H}\}$ NMR (pyr- d_5 , 25 $^\circ\text{C}$, 376 MHz): δ -77.29. IR (KBr pellet, cm^{-1}): 1610 (sh w), 1603 (w), 1585 (w), 1475 (w), 1450 (m), 1325 (s), 1309 (sh m),

1296 (m), 1252 (sh m), 1232 (s), 1203 (s), 1198 (s), 1178 (s), 1171 (sh m), 1088 (w), 1068 (w), 1057 (m), 1026 (m), 1009 (vs), 950 (w), 942 (sh w), 903 (s), 825 (w), 802 (m), 796 (w), 756 (w), 633 (vs), 579 (w), 571 (w), 515 (m). Raman (neat solid, cm^{-1}): 1587 (w), 1474 (w), 1393 (w), 1264 (w), 1243 (w), 1079 (w), 1028 (m), 833 (s, U=O ν_{sym}), 762 (m), 585 (w), 574 (w), 415 (m), 349 (w), 325 (w), 181 (w).

6.4.8 Synthesis of $[\text{UO}_2(\text{OTf})(\text{THF})(\text{Me}_4\text{N})][\text{OTf}]$ (6.4**).** To a stirring yellow solution of $\text{UO}_2(\text{OTf})_2(\text{THF})_3$ (67.1 mg, 0.086 mmol) in THF (1.5 mL), was added dropwise a colorless solution of Me_4N (22.0 mg, 0.082 mmol) in THF (1 mL). This resulted in the immediate color change to orange. The mixture was allowed to stir at room temperature for 10 min, whereupon it was filtered through a Celite column (2 cm \times 0.5 cm) supported on glass wool. The resulting orange filtrate was then layered with Et_2O (1 mL). Storage of this solution at $-25\text{ }^\circ\text{C}$ for 24 h resulted in the deposition an orange powder, which was isolated by decanting off the supernatant (56.8 mg, 73% yield). X-ray quality crystals were grown in a 2 vial system, whereby a THF solution (3 mL) of **6.4** was transferred to a 4 mL scintillation vial that was placed inside a 20 mL scintillation vial. Et_2O (2 mL) was then added to the outer vial. Storage of this 2 vial system at $-25\text{ }^\circ\text{C}$ for 24 h afforded orange X-ray quality crystals. Anal. Calcd for $\text{UF}_6\text{N}_4\text{O}_9\text{S}_2\text{C}_{22}\text{H}_{28}$: C, 29.08; H, 3.11; N, 6.17. Found: C, 29.50; H, 3.07; N, 5.89. ^1H NMR (CD_2Cl_2 , $25\text{ }^\circ\text{C}$, 400 MHz): δ 7.67 (t, $J_{\text{HH}} = 8\text{ Hz}$, 2H, aryl CH), 7.23 (d, $J_{\text{HH}} = 8\text{ Hz}$, 4H, aryl CH), 4.87 (d, $J_{\text{HH}} = 15\text{ Hz}$, 4H, CH_2), 4.53 (d, $J_{\text{HH}} = 15\text{ Hz}$, 4H, CH_2), 3.73 (br s, 4H, THF), 3.59 (br s, 6H, CH_3), 1.84 (br s, 4H, THF). ^1H NMR (pyr- d_5 , $25\text{ }^\circ\text{C}$, 400 MHz): δ 7.59 (br s, 2H, aryl CH), 7.22 (br s, 4H, aryl CH), 4.94 (d, $J_{\text{HH}} = 15\text{ Hz}$, 4H, CH_2), 4.78 (d, $J_{\text{HH}} = 16\text{ Hz}$, 4H, CH_2), 3.66 (br s, 4H, THF), 2.93 (br s, 6H, CH_3), 1.62 (br s, 4H, THF). $^{19}\text{F}\{^1\text{H}\}$ NMR

(CD₂Cl₂, 25 °C, 376 MHz): δ -77.57. ¹⁹F{¹H} NMR (pyr-*d*₅, 25 °C, 376 MHz): δ -77.41. IR (KBr pellet, cm⁻¹): 3049 (w), 3006 (sh w), 2980 (m), 2962 (sh m), 2943 (sh m), 2877 (w), 2873 (w), 2806 (sh vw), 1603 (m), 1583 (m), 1470 (sh m), 1462 (m), 1452 (sh m), 1390 (w), 1362 (sh w), 1327 (s), 1265 (s), 1255 (s), 1234 (s), 1223 (m), 1205 (s), 1173 (sh m), 1155 (s), 1080 (sh w), 1068 (w), 1065 (w), 1030 (s), 1012 (s), 957 (w), 912 (m), 883 (m), 866 (m), 854 (m), 812 (m), 768 (m), 756 (w), 729 (w), 636 (vs), 580 (sh w), 573 (m), 526 (w), 517 (m), 471 (w). Raman (neat solid, cm⁻¹): 1608 (w), 1585 (w), 1465 (w), 1391 (w), 1262 (m), 1237 (w), 1227 (w), 1079 (w), 1030 (m), 1028 (m), 924 (w), 831 (s, U=0 v_{sym}), 766 (w), 764 (w), 574 (w), 418 (m), 347 (w), 187 (w), 116 (m).

6.4.9 X-ray Crystallography. The solid-state molecular structures of complexes **6.1** – **6.4** were determined similarly with exceptions noted in the following paragraph. Crystals were mounted on a cryoloop under Paratone-N oil. Data collection was carried out on a Bruker KAPPA APEX II diffractometer equipped with an APEX II CCD detector using a TRIUMPH monochromator with a Mo K α X-ray source ($\alpha = 0.71073 \text{ \AA}$). Data for **6.1** – **6.4** were collected at 100(2) K, using an Oxford nitrogen gas cryostream system. A hemisphere of data was collected using ω scans with 0.5° frame widths. Frame exposures of 5, 10, 15, 5, and 45 seconds were used for complexes **6.1**, **6.2**, **6.2a**, **6.3**, and **6.4**, respectively. Data collection and cell parameter determination were conducted using the SMART program.⁶¹ Integration of the data frames and final cell parameter refinement were performed using SAINT software.⁶² Absorption correction of the data was carried out using the multi-scan method SADABS.⁶³ Subsequent calculations were carried out using SHELXTL.⁶⁴ Structure determination was done

using direct or Patterson methods and difference Fourier techniques. All hydrogen atom positions were idealized, and rode on the atom of attachment. However, hydrogen atoms were not assigned to the disordered carbon atoms. Structure solution, refinement, graphics, and creation of publication materials were performed using SHELXTL.⁶⁴

Complex **6.1** contains a MeCN solvent molecule that exhibits mild positional disorder about the methyl carbon atom. The positional disorder was addressed by modeling the CH₃ group in two orientations in a 50:50 ratio. Hydrogen atoms were not assigned to this carbon atom. Complex **6.1** was also mildly twined. The twinning was subsequently revealed by using the program CELL_NOW.⁶⁵ Complex **6.2** contains two oxo ligands and two chloride ligands in the main residue that exhibit positional disorder. The positional disorder was addressed by modeling the affected atoms in two orientations in a 50:50 ratio. Additionally, complex **6.2** exhibits some mild positional disorder of the two MeCN solvent molecules. Hydrogen atoms were not assigned to these carbon atoms. Complex **6.4** exhibits positional disorder of one OTf moiety in the main residue. This disorder was addressed by modeling the OTf moiety in two orientations in a 50:50 ratio. The atoms of the OTf moiety were not refined anisotropically. Complex **6.4** also contains a THF solvent molecule that exhibited positional disorder, which was address by modeling the molecule in two orientations in a 50:50 ratio. Disordered atoms were not refined anisotropically and were constrained with the EADP, DFIX, and FLAT commands. Hydrogen atoms were not assigned to these carbon atoms. A summary of relevant crystallographic data for **6.1** – **6.4** is presented in Tables 6.3-6.4.

Table 6.3. X-ray Crystallographic Information for **6.1** – **6.2a**.

	6.1·2MeCN	6.2·2MeCN	6.2a
empirical formula	UCl ₂ N ₆ O ₂ C ₁₈ H ₂₂	UCl ₂ N ₆ O ₂ C ₂₀ H ₂₆	UCl ₂ N ₄ O ₂ C ₁₆ H ₂₀
Crystal habit, color	block, yellow orange	shard, light yellow	block, orange
crystal size (mm)	0.15 × 0.15 × 0.05	0.1 × 0.05 × 0.025	0.1 × 0.1 × 0.05
crystal system	monoclinic	orthorhombic	orthorhombic
space group	<i>P</i> 2 ₁ / <i>m</i>	<i>Cmcm</i>	<i>Pbcn</i>
vol (Å ³)	1146.9(1)	2334(2)	1864.1(8)
a (Å)	8.3513(5)	16.085(7)	9.434(2)
b (Å)	15.0623(9)	10.152(4)	14.676(3)
c (Å)	9.9039(6)	14.291(6)	13.464(4)
α (deg)	90	90	90
β (deg)	112.981(3)	90	90
γ (deg)	90	90	90
Z	2	4	4
fw (g/mol)	660.32	691.40	609.29
density (calcd) (Mg/m ³)	1.912	1.968	2.171
abs coeff (mm ⁻¹)	7.334	7.213	9.011
F ₀₀₀	622	1320	1144
Total no. reflections	2451	1285	1902
Unique reflections	2279	1149	1177
final R indices [<i>I</i> > 2σ(<i>I</i>)]	R ₁ = 0.0286 wR ₂ = 0.0764	R ₁ = 0.0360 wR ₂ = 0.0609	R ₁ = 0.0304 wR ₂ = 0.0510
largest diff peak and hole (e ⁻ Å ⁻³)	3.015 and -1.765	1.386 and -0.822	0.896 and -0.971
GOF	1.107	1.052	0.949

Table 6.4. X-ray Crystallographic Information for **6.3** and **6.4**.

	6.3	6.4·0.5C₄H₈O
empirical formula	UF ₆ N ₄ O ₈ S ₂ C ₁₆ H ₁₆	UF ₆ N ₄ O _{9.5} S ₂ C ₂₄ H ₃₂
Crystal habit, color	block, orange	rod, brown
crystal size (mm)	0.10 × 0.10 × 0.05	0.1 × 0.05 × 0.04
crystal system	orthorhombic	triclinic
space group	<i>Pna</i> 2 ₁	<i>P</i> -1
vol (Å ³)	2378.5(2)	3159(5)
a (Å)	11.7508(5)	12.33(1)
b (Å)	18.807(1)	16.38(2)
c (Å)	10.7623(4)	16.61(2)
α (deg)	90	90.59(2)
β (deg)	90	100.23(2)
γ (deg)	90	106.38(2)
Z	4	4
fw (g/mol)	808.48	944.69
density (calcd) (Mg/m ³)	2.258	1.983
abs coeff (mm ⁻¹)	7.098	5.363
F ₀₀₀	1528	1825
Total no. reflections	4744	10655
Unique reflections	3857	3616
final R indices [I > 2σ(I)]	R ₁ = 0.0341 wR ₂ = 0.0759	R ₁ = 0.0612 wR ₂ = 0.0812
largest diff peak and hole (e ⁻ Å ⁻³)	1.771 and -2.114	1.344 and -1.170
GOF	0.930	0.823

6.5 Acknowledgements

I would like to thank Jason W. Schultz, from Liviu M. Mirica's group at Washington University in St. Louis, for the synthesis of the ^HN4 and ^{Me}N4 ligands.

6.6 References

- (1) Denning, R. G. *J. Phys. Chem. A* **2007**, *111*, 4125.
- (2) Cantat, T.; Graves, C. R.; Scott, B. L.; Kiplinger, J. L. *Angew. Chem. Int. Ed.* **2009**, *48*, 3681.
- (3) Duval, P. B.; Burns, C. J.; Clark, D. L.; Morris, D. E.; Scott, B. L.; Thompson, J. D.; Werkema, E. L.; Jia, L.; Andersen, R. A. *Angew. Chem. Int. Ed.* **2001**, *40*, 3357.
- (4) Duval, P. B.; Burns, C. J.; Buschmann, W. E.; Clark, D. L.; Morris, D. E.; Scott, B. L. *Inorg. Chem.* **2001**, *40*, 5491.
- (5) Arnold, P. L.; Jones, G. M.; Odoh, S. O.; Schreckenbach, G.; Magnani, N.; Love, J. B. *Nat. Chem.* **2012**, *4*, 221.
- (6) Jones, G. M.; Arnold, P. L.; Love, J. B. *Angew. Chem. Int. Ed.* **2012**, *51*, 12584.
- (7) Vaughn, A. E.; Barnes, C. L.; Duval, P. B. *Angew. Chem. Int. Ed.* **2007**, *46*, 6622.
- (8) Villiers, C.; Thuéry, P.; Ephritikhine, M. *Angew. Chem. Int. Ed.* **2008**, *47*, 5892.
- (9) Guan, Q. L.; Bai, F. Y.; Xing, Y. H.; Liu, J.; Zhang, H. Z. *Inorg. Chem. Commun.* **2015**, *59*, 36.
- (10) Burrell, A. K.; Hemmi, G.; Lynch, V.; Sessler, J. L. *J. Am. Chem. Soc.* **1991**, *113*, 4690.
- (11) Sessler, J. L.; Vivian, A. E.; Seidel, D.; Burrell, A. K.; Hoehner, M.; Mody, T. D.; Gebauer, A.; Weghorn, S. J.; Lynch, V. *Coord. Chem. Rev.* **2001**, *216–217*, 411.
- (12) Liao, M.-S.; Kar, T.; Scheiner, S. *J. Phys. Chem. A* **2004**, *108*, 3056.
- (13) Sessler, J. L.; Mody, T. D.; Lynch, V. *Inorg. Chem.* **1992**, *31*, 529.
- (14) Khusnutdinova, J. R.; Luo, J.; Rath, N. P.; Mirica, L. M. *Inorg. Chem.* **2013**, *52*, 3920.
- (15) Khusnutdinova, J. R.; Rath, N. P.; Mirica, L. M. *Inorg. Chem.* **2014**, *53*, 13112.
- (16) Zheng, B.; Tang, F.; Luo, J.; Schultz, J. W.; Rath, N. P.; Mirica, L. M. *J. Am. Chem. Soc.* **2014**, *136*, 6499.

- (17) Casanova, D.; Alemany, P.; Bofill, J. M.; Alvarez, S. *Chem. Eur. J.* **2003**, *9*, 1281.
- (18) Kiernicki, J. J.; Cladis, D. P.; Fanwick, P. E.; Zeller, M.; Bart, S. C. *J. Am. Chem. Soc.* **2015**, *137*, 11115.
- (19) Maynadie, J.; Berthet, J.-C.; Thuery, P.; Ephritikhine, M. *Chem. Commun.* **2007**, 486.
- (20) Tourneux, J.-C.; Berthet, J.-C.; Cantat, T.; Thuery, P.; Mezailles, N.; Ephritikhine, M. *J. Am. Chem. Soc.* **2011**, *133*, 6162.
- (21) Lu, E.; Cooper, O. J.; McMaster, J.; Tuna, F.; McInnes, E. J. L.; Lewis, W.; Blake, A. J.; Liddle, S. T. *Angew. Chem. Int. Ed.* **2014**, *53*, 6696.
- (22) Wilkerson, M. P.; Burns, C. J.; Morris, D. E.; Paine, R. T.; Scott, B. L. *Inorg. Chem.* **2002**, *41*, 3110.
- (23) Berthet, J.-C.; Thuéry, P.; Dognon, J.-P.; Guillaneux, D.; Ephritikhine, M. *Inorg. Chem.* **2008**, *47*, 6850.
- (24) Raffard, N.; Carina, R.; Simaan, A. J.; Sainon, J.; Rivière, E.; Tchertanov, L.; Bourcier, S.; Bouchoux, G.; Delroisse, M.; Banse, F.; Girerd, J.-J. *Eur. J. Inorg. Chem.* **2001**, *2001*, 2249.
- (25) Chow, T. W.-S.; Wong, E. L.-M.; Guo, Z.; Liu, Y.; Huang, J.-S.; Che, C.-M. *J. Am. Chem. Soc.* **2010**, *132*, 13229.
- (26) O. Koch, W.; T. Kaiser, J. *Chem. Commun.* **1997**, 2237.
- (27) Koch, W. O.; Barbieri, A.; Grodzicki, M.; Schünemann, V.; Trautwein, A. X.; Krüger, H.-J. *Angew. Chem. Int. Ed.* **1996**, *35*, 422.
- (28) Lee, W.-T.; Muñoz, S. B.; Dickie, D. A.; Smith, J. M. *Angew. Chem. Int. Ed.* **2014**, *53*, 9856.
- (29) Sugimoto, H.; Ashikari, K.; Itoh, S. *Inorg. Chem.* **2013**, *52*, 543.
- (30) Albela, B.; Carina, R.; Policar, C.; Poussereau, S.; Cano, J.; Guilhem, J.; Tchertanov, L.; Blondin, G.; Delroisse, M.; Girerd, J.-J. *Inorg. Chem.* **2005**, *44*, 6959.
- (31) Copping, R.; Jeon, B.; Pemmaraju, C. D.; Wang, S.; Teat, S. J.; Janousch, M.; Tylliszczak, T.; Canning, A.; Grønbech-Jensen, N.; Prendergast, D.; Shuh, D. K. *Inorg. Chem.* **2014**, *53*, 2506.
- (32) Schettini, M. F.; Wu, G.; Hayton, T. W. *Inorg. Chem.* **2009**, *48*, 11799.
- (33) Berthet, J.-C.; Nierlich, M.; Ephritikhine, M. *Dalton Trans.* **2004**, 2814.
- (34) Sarsfield, M. J.; Steele, H.; Helliwell, M.; Teat, S. J. *Dalton Trans.* **2003**, 3443.
- (35) Sarsfield, M. J.; Helliwell, M.; Collison, D. *Chem. Commun.* **2002**, 2264.
- (36) Berthet, J.-C.; Nierlich, M.; Ephritikhine, M. *Chem. Commun.* **2003**, 1660.
- (37) Wilkerson, M. P.; Burns, C. J.; Paine, R. T.; Scott, B. L. *Inorg. Chem.* **1999**, *38*, 4156.
- (38) Fortier, S.; Hayton, T. W. *Coord. Chem. Rev.* **2010**, *254*, 197.
- (39) Nguyen Trung, C.; Begun, G. M.; Palmer, D. A. *Inorg. Chem.* **1992**, *31*, 5280.
- (40) Brown, J. L.; Mokhtarzadeh, C. C.; Lever, J. M.; Wu, G.; Hayton, T. W. *Inorg. Chem.* **2011**, *50*, 5105.
- (41) Wilkerson, M. P.; Burns, C. J.; Dewey, H. J.; Martin, J. M.; Morris, D. E.; Paine, R. T.; Scott, B. L. *Inorg. Chem.* **2000**, *39*, 5277.
- (42) Sarsfield, M. J.; Helliwell, M.; Raftery, J. *Inorg. Chem.* **2004**, *43*, 3170.

- (43) Clark, D. L.; Conradson, S. D.; Donohoe, R. J.; Keogh, D. W.; Morris, D. E.; Palmer, P. D.; Rogers, R. D.; Tait, C. D. *Inorg. Chem.* **1999**, *38*, 1456.
- (44) Burns, C. J.; Clark, D. L.; Donohoe, R. J.; Duval, P. B.; Scott, B. L.; Tait, C. D. *Inorg. Chem.* **2000**, *39*, 5464.
- (45) Sarsfield, M. J.; Helliwell, M. J. *Am. Chem. Soc.* **2004**, *126*, 1036.
- (46) Azeez, W. I.; Abdulla, A. I. *Inorg. Chim. Acta* **1985**, *110*, 15.
- (47) Nour, E. M.; Alnaimi, I. S.; Alem, N. A. *J. Phys. Chem. Solids* **1992**, *53*, 197.
- (48) Pedrick, E. A.; Wu, G.; Hayton, T. W. *Inorg. Chem.* **2015**, *54*, 7038.
- (49) Cornet, S. M.; May, I.; Redmond, M. P.; Selvage, A. J.; Sharrad, C. A.; Rosnel, O. *Polyhedron* **2009**, *28*, 363.
- (50) Khusnutdinova, J. R.; Rath, N. P.; Mirica, L. M. *J. Am. Chem. Soc.* **2010**, *132*, 7303.
- (51) Tang, F.; Zhang, Y.; Rath, N. P.; Mirica, L. M. *Organometallics* **2012**, *31*, 6690.
- (52) Tang, F.; Qu, F.; Khusnutdinova, J. R.; Rath, N. P.; Mirica, L. M. *Dalton Trans.* **2012**, *41*, 14046.
- (53) Berthet, J.-C.; Siffredi, G.; Thuery, P.; Ephritikhine, M. *Dalton Trans.* **2009**, 3478.
- (54) Weisman, G. R.; Wong, E. H.; Hill, D. C.; Rogers, M. E.; Reed, D. P.; Calabrese, J. C. *Chem. Commun.* **1996**, 947.
- (55) Wong, E. H.; Weisman, G. R.; Hill, D. C.; Reed, D. P.; Rogers, M. E.; Condon, J. S.; Fagan, M. A.; Calabrese, J. C.; Lam, K.-C.; Guzei, I. A.; Rheingold, A. L. *J. Am. Chem. Soc.* **2000**, *122*, 10561.
- (56) Oldham, S. M.; Scott, B. L.; Oldham, W. J. *Appl. Organometal. Chem.* **2006**, *20*, 39.
- (57) Alpha, B.; Anklam, E.; Deschenaux, R.; Lehn, J.-M.; Pietraskiewicz, M. *Helv. Chim. Acta* **1988**, *71*, 1042.
- (58) Bottino, F.; Di Grazia, M.; Finocchiaro, P.; Fronczek, F. R.; Mamo, A.; Pappalardo, S. *J. Org. Chem.* **1988**, *53*, 3521.
- (59) Harris, R. K.; Becker, E. D.; Cabral De Menezes, S. M.; Goodfellow, R.; Granger, P. *Pure Appl. Chem.* **2001**, *73*, 1795.
- (60) Harris, R. K.; Becker, E. D.; Cabral De Menezes, S. M.; Granger, P.; Hoffman, R. E.; Zilm, K. W. *Pure Appl. Chem.* **2008**, *80*, 59.
- (61) SMART, Apex II, Version 2.1; Bruker AXS Inc.: Madison, WI, 2005.
- (62) SAINT, Software User's Guide, Version 7.34a; Bruker AXS Inc.: Madison, WI, 2005.
- (63) Sheldrick, G. M. *SADABS*, University of Gottingen: Germany, 2005.
- (64) *SHELXTL PC*, Version 6.12; Bruker AXS Inc.: Madison, WI, 2005.
- (65) Sheldrick, G. M. *CELL_NOW*, Version 2008-4; Bruker AXS Inc.: Madison, WI, 2008.

Chapter 7. Synthesis and Reactivity of a U(IV) Dibenzynes Complex

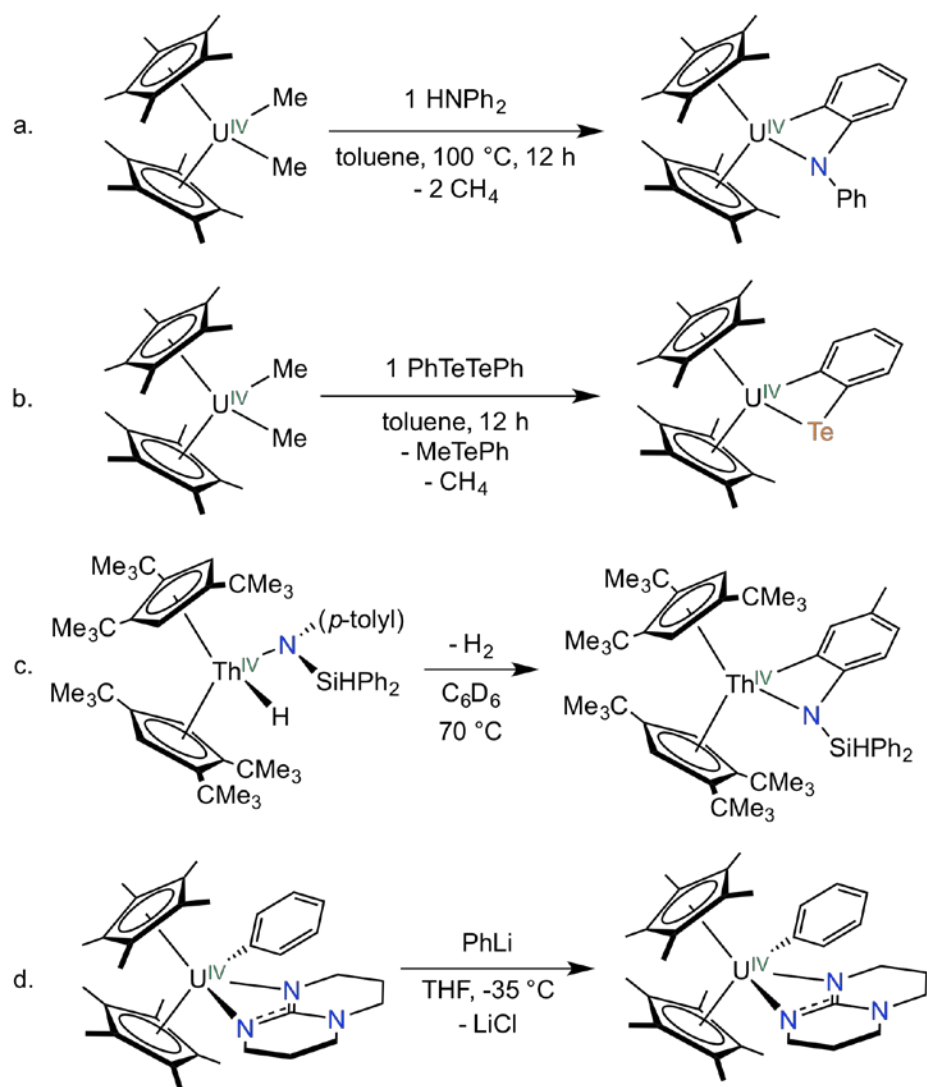
7.1. Introduction	210
7.1.1. Actinide Aryl Complexes.....	210
7.1.2. Metal-Stabilized Benzynes.....	212
7.2. Results and Discussion	218
7.2.1. Synthesis and Characterization of $[\text{Li}]_2[\text{U}(2,3\text{-C}_6\text{H}_3\text{CH}_2\text{NMe}_2)_2(2\text{-C}_6\text{H}_4\text{CH}_2\text{NMe}_2)_2]$ (7.1) and $[\text{Li}][\text{Li}(\text{THF})_2][\text{U}(2,3\text{-C}_6\text{H}_3\text{CH}_2\text{NMe}_2)_2(2\text{-C}_6\text{H}_4\text{CH}_2\text{NMe}_2)_2]$ (7.2).....	218
7.2.2. Synthesis and Characterization of $[\text{Li}][\text{U}(2\text{-C}_6\text{H}_3\text{CH}_2\text{NMe}_2\text{-3-COPh}_2)_2(2\text{-C}_6\text{H}_4\text{CH}_2\text{NMe}_2)]$ (7.3).....	223
7.2.3. Synthesis and Characterization of $[\text{Li}][\text{Li}(\text{Et}_2\text{O})][\text{U}(2,3\text{-C}_6\text{H}_3\text{CH}_2\text{NMe}_2)(2\text{-C}_6\text{H}_3\text{CH}_2\text{NMe}_2\text{-3-C}(\text{Ph})=\text{N})(2\text{-C}_6\text{H}_4\text{CH}_2\text{NMe}_2)_2]$ (7.4)	227
7.2.4. Synthesis and Characterization of $[\text{Li}][\text{Li}(\text{Et}_2\text{O})][\text{U}(2,3\text{-C}_6\text{H}_3\text{CH}_2\text{NMe}_2)(5\text{-C}_6\text{H}_3\text{CH}_2\text{NMe}_2\text{-2-S})(2\text{-C}_6\text{H}_4\text{CH}_2\text{NMe}_2)_2]$ (7.5).....	230
7.2.5. Reactivity of 7.1 with Unsaturated Hydrocarbons.....	232
7.2.6. Synthesis and Characterization of $[\text{Li}(12\text{-crown-4})_2][\text{Li}][\text{U}(2\text{-C}_6\text{H}_3\text{CH}_2\text{NMe}_2\text{-3-(N=N-Ad)})_2(2\text{-C}_6\text{H}_4\text{CH}_2\text{NMe}_2)_2]$ (7.6)	233
7.3. Summary	237
7.4. Experimental Section	239
7.4.1. General Procedures	239
7.4.2. Synthesis of $[\text{Li}]_2[\text{U}(2,3\text{-C}_6\text{H}_3\text{CH}_2\text{NMe}_2)_2(2\text{-C}_6\text{H}_4\text{CH}_2\text{NMe}_2)_2]$ (7.1).....	239
7.4.3. Synthesis of $[\text{Li}][\text{U}(2\text{-C}_6\text{H}_3\text{CH}_2\text{NMe}_2\text{-3-COPh}_2)_2(2\text{-C}_6\text{H}_4\text{CH}_2\text{NMe}_2)]$ (7.3).....	241

7.4.4. Synthesis of [Li][Li(Et ₂ O)][U(2,3-C ₆ H ₃ CH ₂ NMe ₂)(2-C ₆ H ₃ CH ₂ NMe ₂ -3-C(Ph)=N)(2-C ₆ H ₄ CH ₂ NMe ₂) ₂] (7.4).....	242
7.4.5. Synthesis of [Li][Li(Et ₂ O)][U(2,3-C ₆ H ₃ CH ₂ NMe ₂)(5-C ₆ H ₃ CH ₂ NMe ₂ -2-S)(2-C ₆ H ₄ CH ₂ NMe ₂) ₂] (7.5).....	243
7.4.6. Synthesis of [Li(12-crown-4) ₂][Li][U(2-C ₆ H ₃ CH ₂ NMe ₂ -3-(N-N=N-Ad)) ₂ (2-C ₆ H ₄ CH ₂ NMe ₂) ₂] (7.6).....	244
7.4.7. X-Ray Crystallography	245
7.5. Acknowledgements	249
7.6. References	249

7.1 Introduction

7.1.1 Actinide Aryl Complexes

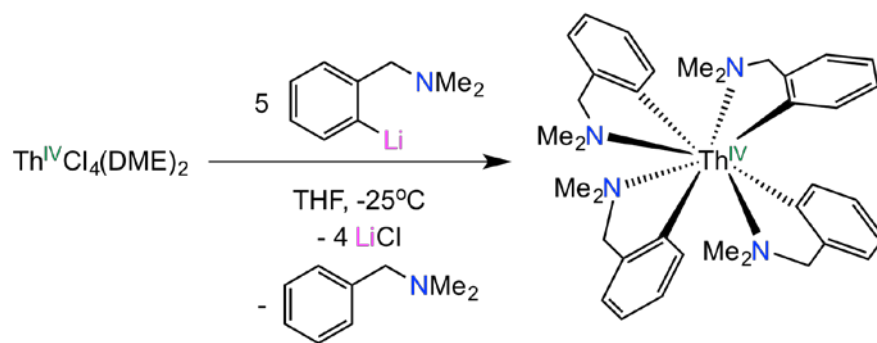
Not much is known about the chemistry of the An-C_{aryl} bond, as only a few actinide aryl complexes have been structurally characterized.¹⁻⁴ Like the majority of alkyl actinide complexes, actinide aryl complexes have been dominated by the use of cyclopentadienyl (Cp) as a supporting ligand, specifically the bis(Cp) framework or “metallocene” framework.^{1,2,5-9} For example, Kiplinger and co-workers demonstrated that reaction of the dimethyl uranium complex, (η⁵-Cp*)₂UMe₂, with 1 equiv of HNPh₂ at 100 °C, led to the isolation of the uranium metallacycle, (η⁵-Cp*)₂[U(*N,C*)-(o-C₆H₄)NPh], which has been structurally characterized (Scheme 7.1a).¹ This product is likely formed by intermolecular C-H activation at the *ortho* position on the phenyl ring. Additionally, Evans and co-workers synthesized a telluride supported aryl complex with the formula, (η⁵-Cp*)₂U(η²-TeC₆H₄) (Scheme 7.1b),² and Zi and co-workers synthesized the thorium metallacycle, [η⁵-1,2,4-(Me₃C)₃C₅H₂]₂Th[η²-*N,C*-{N(*p*-MeC₆H₃)(SiHPh₂)}] (Scheme 7.1c).⁴ Notably, these aryl complexes are supported by chelate-type ligands. The first and only crystallographically characterized “true” uranium phenyl complex, (η⁵-Cp*)₂U(hpp)(C₆H₅), was synthesized by Evans and co-workers by reaction of (η⁵-Cp*)₂U(hpp)(Cl) with PhLi (Scheme 7.1d).³



Scheme 7.1. Synthesis of **a**) $(\eta^5\text{-Cp}^*)_2[\text{U}(\text{N},\text{C})\text{-}(o\text{-C}_6\text{H}_4)\text{NPh}]$, **b**) $(\eta^5\text{-Cp}^*)_2\text{U}(\eta^2\text{-TeC}_6\text{H}_4)$, **c**) $[\eta^5\text{-1,2,4-(Me}_3\text{C)}_3\text{C}_5\text{H}_2]_2\text{Th}[\eta^2\text{-N,C}\{-\text{N}(p\text{-MeC}_6\text{H}_3)(\text{SiHPh}_2)\}]$, and **d**) $(\eta^5\text{-Cp}^*)_2\text{U}(\text{hpp})(\text{C}_6\text{H}_5)$. Scheme reproduced from references 1-4.

There are only a small number of structurally characterized non-metallocene actinide aryl complexes,⁶ such as $[\text{Li}(\text{DME})_3]_2[\text{Th}(\text{C}_6\text{H}_5)_6]$,¹⁰ $[\text{Li}(\text{THF})(12\text{-crown-4})]_2[\text{Th}(\text{C}_6\text{H}_5)_6]$,¹⁰ $\text{Th}(2\text{-C}_6\text{H}_4\text{CH}_2\text{NMe}_2)_4$,¹¹ $[\text{Li}][\text{U}(2,3\text{-C}_6\text{H}_3\text{CH}_2\text{NMe}_2)(2\text{-C}_6\text{H}_4\text{CH}_2\text{NMe}_2)_3]$,¹¹ and $[\text{Li}][\text{Li}(\text{THF})_2][\text{UCl}_2(2,3\text{-C}_6\text{H}_3\text{CH}_2\text{NMe}_2)(2\text{-C}_6\text{H}_4\text{CH}_2\text{NMe}_2)_2]$.¹¹

Our research group has utilized the chelating *N,N*-dimethylbenzylamine ligand to isolate and crystallographically characterize a rare non-metallocene, homoletic thorium aryl complex, $\text{Th}(\text{2-C}_6\text{H}_4\text{CH}_2\text{NMe}_2)_4$, which is synthesized by reaction of $\text{ThCl}_4(\text{DME})_2$ and 5 equiv of $\text{2-Li-C}_6\text{H}_4\text{CH}_2\text{NMe}_2$ (Scheme 7.2).¹¹ This ligand is bidentate and can provide kinetic stabilization of the M-C bond because of a strong σ -donating dimethylamino group.¹²⁻¹⁷ Similarly, the *N,N*-dimethylbenzylamine ligand has also been used to stabilize a series of homoleptic lanthanide(III) aryl complexes, namely $\text{Ln}(\text{2-C}_6\text{H}_4\text{CH}_2\text{NMe}_2)_3$ ($\text{Ln} = \text{Er, Yb, Y, Lu}$),¹² and the U(IV) complex, $\text{UCl}_2(\text{2-C}_6\text{H}_4\text{CH}_2\text{NMe}_2)(\text{Tp}^{\text{Ms}})$,¹⁷ however, the X-ray crystallographic data was of poor quality for this complex.

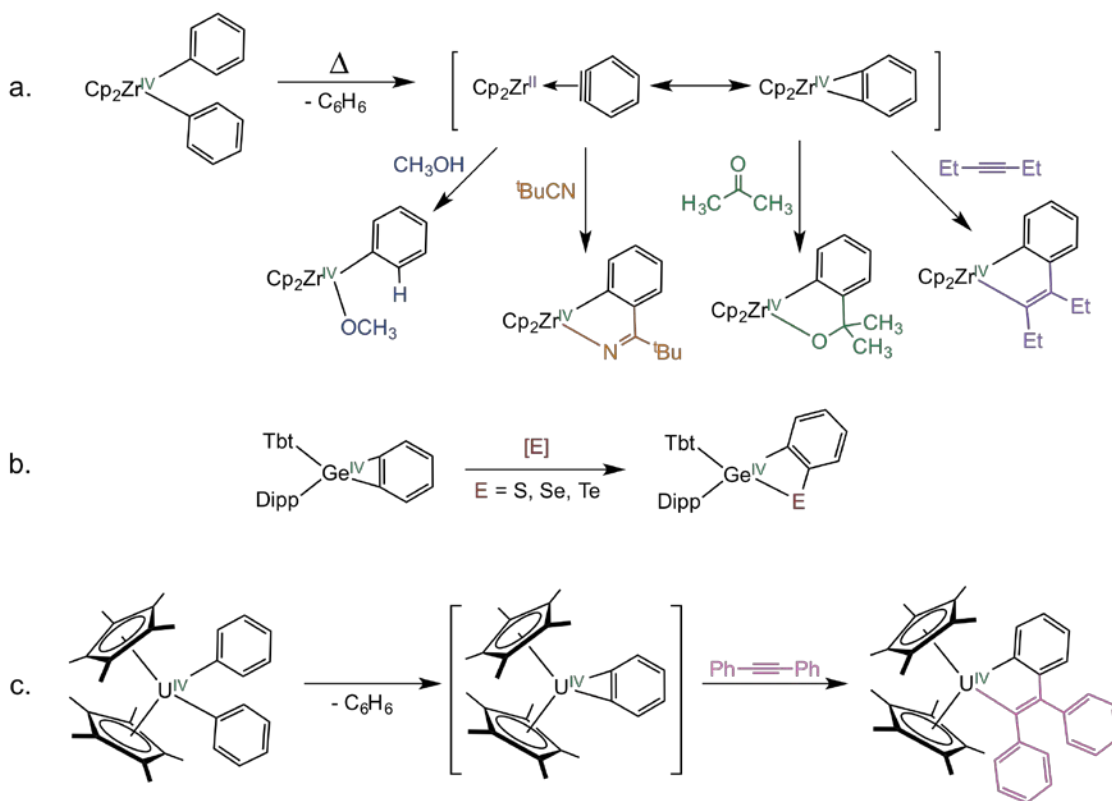


Scheme 7.2. Synthesis of $\text{Th}(\text{2-C}_6\text{H}_4\text{CH}_2\text{NMe}_2)_4$. Scheme adapted from reference 11.

7.1.2 Metal-Stabilized Benzyne

Benzyne are widely used in organic chemistry,¹⁸ as they are highly reactive intermediates that allow for multiple, rapid functionalizations of an aromatic ring in a single step. However, as noted by Tadross and Stoltz, “metal-catalyzed processes are still considered to be underdeveloped”,¹⁸ which points to a need for further work with

metal-stabilized benzyne chemistry. Nonetheless, metal-mediated benzyne reaction strategies are known. Transition metal benzyne reactivity studies first came to light in 1979, when Erker and coworkers found, upon heating, the transition metal complex, $\text{Cp}_2\text{Zr}^{\text{IV}}(\text{C}_6\text{H}_5)_2$, forms the dianionic benzyne complex, $\text{Cp}_2\text{Zr}^{\text{IV}}(\text{C}_6\text{H}_4)$, by loss of benzene (Scheme 7.3a).^{19,20} It is proposed that the dianionic metallacyclopropene form of the complex is in resonance with the neutral aryne π -donor form, which is considered the “true” benzyne form.²¹ Buchwald and coworkers really pioneered this area of study by showing that this same zirconium benzyne complex, $\text{Cp}_2\text{Zr}^{\text{IV}}(\text{C}_6\text{H}_4)$, is able to undergo insertion chemistry by several reagents, namely $t\text{BuCN}$, diethylacetylene, and acetone, to form the insertion products (Scheme 7.3a).²⁰ Since the discovery of the zirconium benzyne complexes, several transition metal aryl complexes have been used to synthesize the corresponding benzyne complexes.²²⁻²⁵ Among these is the germanium benzyne complex, $\text{Ge}^{\text{IV}}(\text{Tbt})(\text{Dipp})(\text{C}_6\text{H}_4)$ (Scheme 7.3b),²⁵ which has been shown to undergo chalcogenide insertion reactivity, when exposed to elemental sulfur, selenium and tellurium to generate $\text{Ge}^{\text{IV}}(\text{Tbt})(\text{Dipp})(\kappa^2\text{-C}_6\text{H}_4\text{E})$ ($\text{E} = \text{S}, \text{Se}, \text{Te}$).²⁵ Interestingly, there are also two transition metal dibenzyne complexes that have been structurally characterized, $[\text{Li}(\text{THF})_3]_2[\text{LiCl}(\text{THF})_2]_2[\text{Li}(\text{THF})_2]_4[\text{Ta}(\eta^2\text{-C}_6\text{H}_4)_2\text{Ph}_4]_2$ and $[\text{Li}(\text{THF})]_4[\text{LiPh}(\text{THF})]-[\text{Nb}(\eta^2\text{-C}_6\text{H}_4)_2\text{Ph}_3]$.²⁴



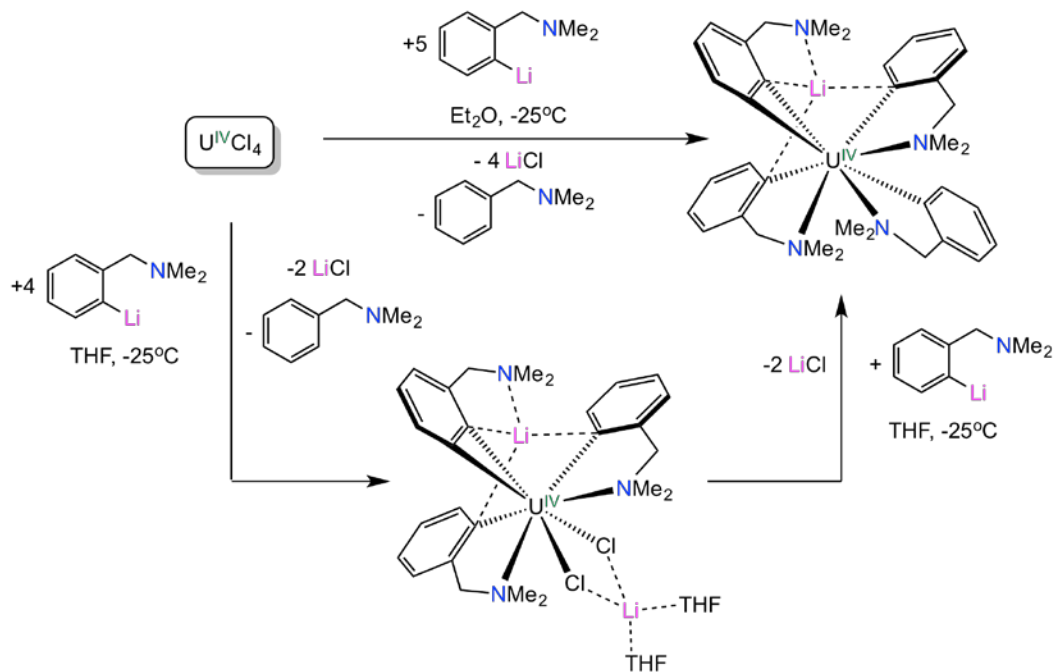
Scheme 7.3. Reactivity of aryl complexes of **a)** zirconium and **b)** germanium and **c)** uranium. Scheme adapted from references 9, 19, 20, and 25.

More recently, the use of metal-stabilized benzyne complexes as intermediates in organic synthesis is becoming more popular.^{19,20,22,23,26,27} Interestingly, the early transition metal benzynes exhibit varying reactivity from the late metal benzynes. This is partly a result of the two resonance forms available to the benzyne ligand.²¹ Early metal benzynes, like $\text{Cp}_2\text{Zr}^{\text{IV}}(\text{C}_6\text{H}_4)$,^{19,20} typically feature the metalla-cyclopropene resonance form, and readily react with electrophiles, such as nitriles, ketones and alkynes, to generate the insertion products.^{20,22-24} In contrast, late metal benzynes, which are often described with the neutral aryne resonance form, can react with nucleophiles, such as CH_3^- ,^{21,28} and can undergo [2 + 2 + 2]-cycloaddition with

alkynes.²⁹⁻³⁴ For example, the total synthesis of Taiwanin C, developed by Mori and coworkers, utilizes a palladium-catalyst to generate a palladium aryne intermediate, which undergoes [2 + 2 + 2]-cycloaddition of the aryne ring.²⁹ The palladium catalyst is used to stabilize the reactive aryne intermediate, and simultaneously guide it towards subsequent reactivity. Additionally, the platinum benzyne complex, (triphos)Pt(Me)(C₆H₄)⁺ (triphos = PhP[CH₂CH₂PPh₂]₂), developed by Gagné and coworkers, has been shown to undergo C-C bond coupling of the methyl and the benzyne ligands within the complex to generate toluene.²¹ Furthermore, the use of the palladium catalyst, Pd(OAc)₂, has been shown to aid in the challenging transformation of acrylamides and arynes into quinolinones, by generating a palladium benzyne intermediate.³⁵ Notably, late metal benzynes can also react with electrophiles,^{23,36-38} generating similar insertion products as those observed for early metal benzynes.

Actinide benzyne reactivity is also still relatively unexplored, however, on account of the high electropositivity of the metal, actinide benzynes should behave like early metal benzynes. Preliminary reactivity studies appear to confirm this hypothesis. For example, Marks and co-workers isolated a uranindene complex, (η⁵-Cp*)₂U(κ²-C(Ph)=C(Ph)C₆H₄), from the reaction of (η⁵-Cp*)₂UPh₂ with diphenylacetylene. They proposed that this transformation proceeds through an unobserved U(IV) benzyne intermediate, (η⁵-Cp*)₂U(η²-C₆H₄), based on elimination of benzene at room temperature (Scheme 7.3c).⁹ Evans and co-workers reported a similar transformation with the same benzyne intermediate.⁷ A previous Hayton group member, Dr. Lani Seaman, reported the syntheses of the first isolable actinide benzyne complexes, [Li][U(2,3-C₆H₃CH₂NMe₂)(2-C₆H₄CH₂NMe₂)₃] and [Li][Li(THF)₂][UCl₂(2,3-

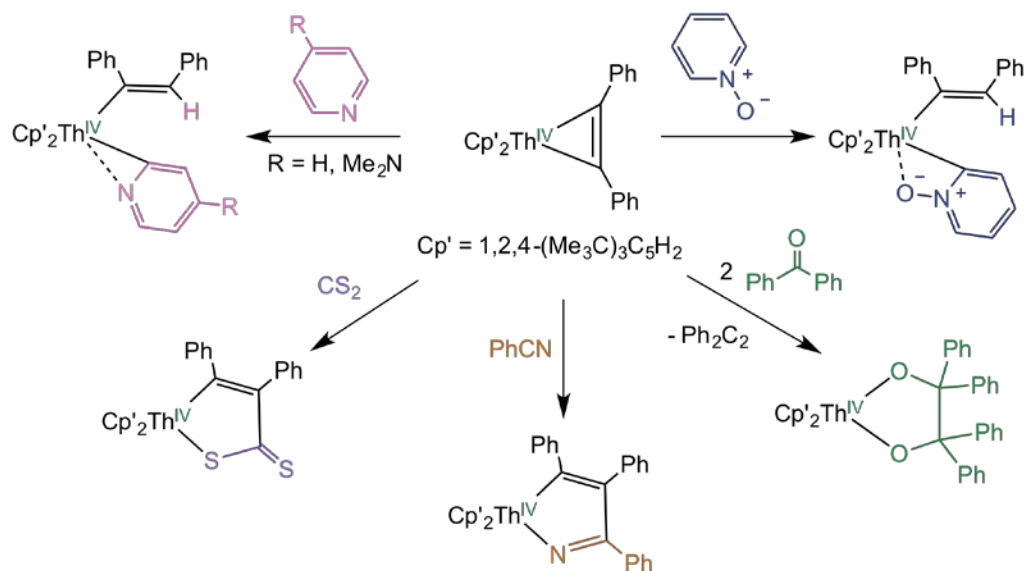
$\text{C}_6\text{H}_3\text{CH}_2\text{NMe}_2)(2\text{-C}_6\text{H}_4\text{CH}_2\text{NMe}_2)_2]$ (Scheme 7.4).¹¹ Both complexes are stabilized through “ate” complex formation, and the chelating *N,N*-dimethylbenzylamine ligands. (The SQUID magnetometry data for $[\text{Li}][\text{U}(2,3\text{-C}_6\text{H}_3\text{CH}_2\text{NMe}_2)(2\text{-C}_6\text{H}_4\text{CH}_2\text{NMe}_2)_3]$ can be seen in Figure A.12).



Scheme 7.4. Synthesis of $[\text{Li}(\text{THF})_2][\text{UCl}_2(2,3\text{-C}_6\text{H}_3\text{CH}_2\text{NMe}_2)(2\text{-C}_6\text{H}_4\text{CH}_2\text{NMe}_2)_2]$ and $[\text{Li}][\text{U}(2,3\text{-C}_6\text{H}_3\text{CH}_2\text{NMe}_2)(2\text{-C}_6\text{H}_4\text{CH}_2\text{NMe}_2)_3]$. Scheme adapted from reference 11.

In a related example, the isolable actinide diphenylacetylene complex, $[\eta^5\text{-1,2,4-(Me}_3\text{C)}_3\text{C}_5\text{H}_2]_2\text{Th}(\eta^2\text{-C}_2\text{Ph}_2)$, reacts with a variety of electrophiles, including CS_2 , benzophenone, benzylnitrile, pyridine, pyridine *N*-oxide, *N,N'*-dicyclohexylcarbodiimide and $\text{CH}_3\text{CONMe}_2$, to give the insertion products (Scheme 7.5).^{39,40} However, it is possible that alternate reactivity manifolds could also be accessible in a uranium benzyne. In particular, uranium has more available oxidation

states in comparison to a Group 4 metal, and a high valent uranium benzyne could behave differently than a Group 4 benzyne.



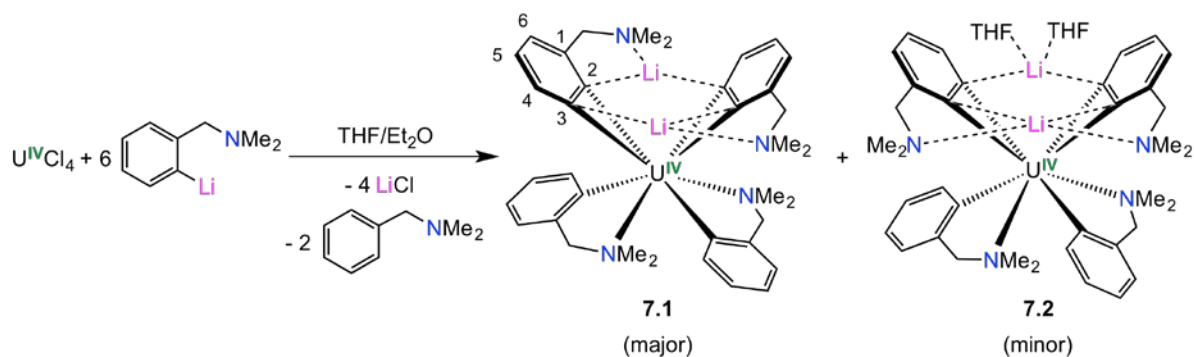
Scheme 7.5. Reactivity of a thorium metalla-cyclopropene complex. Scheme adapted from references 39 and 40.

In this chapter, we report the synthesis and characterization of a thermally stable uranium(IV) dibenzyne complex, and also explore its reactivity with both electrophiles and oxidants. This report represents the first reactivity study of an isolable actinide benzyne complex.

7.2 Results and Discussion

7.2.1. Synthesis and Characterization of $[\text{Li}]_2[\text{U}(2,3\text{-C}_6\text{H}_3\text{CH}_2\text{NMe}_2)_2(2\text{-C}_6\text{H}_4\text{CH}_2\text{NMe}_2)_2]$ (7.1) and $[\text{Li}][\text{Li}(\text{THF})_2][\text{U}(2,3\text{-C}_6\text{H}_3\text{CH}_2\text{NMe}_2)_2(2\text{-C}_6\text{H}_4\text{CH}_2\text{NMe}_2)_2]$ (7.2)

Addition of 6 equiv of 2-Li-C₆H₄CH₂NMe₂ to UCl₄, in a 2:1 mixture of Et₂O:THF at room temperature, results in formation of the U(IV) dibenzynes complex, $[\text{Li}]_2[\text{U}(2,3\text{-C}_6\text{H}_3\text{CH}_2\text{NMe}_2)_2(2\text{-C}_6\text{H}_4\text{CH}_2\text{NMe}_2)_2]$ (7.1), which can be isolated as dark blue crystalline solid in 40% yield after recrystallization from Et₂O (Scheme 7.6). Interestingly, in a few instances, a small number of dark brown crystals of a second product, $[\text{Li}][\text{Li}(\text{THF})_2][\text{U}(2,3\text{-C}_6\text{H}_3\text{CH}_2\text{NMe}_2)_2(2\text{-C}_6\text{H}_4\text{CH}_2\text{NMe}_2)_2]$ (7.2), were also isolated from the reaction mixture. Complex 7.2 is also a dibenzynes complex and only differs from 7.1 by the inclusion of two molecules of THF, which coordinate to one of its Li cations (see below). Importantly, though, complex 7.1 can be formed exclusively if care is taken to remove all of the THF before recrystallization of the reaction mixture. If no THF is present, complex 7.2 is not formed, and even if small amounts of THF are present during crystallization the yield of 7.2 is very low (just a few crystals).

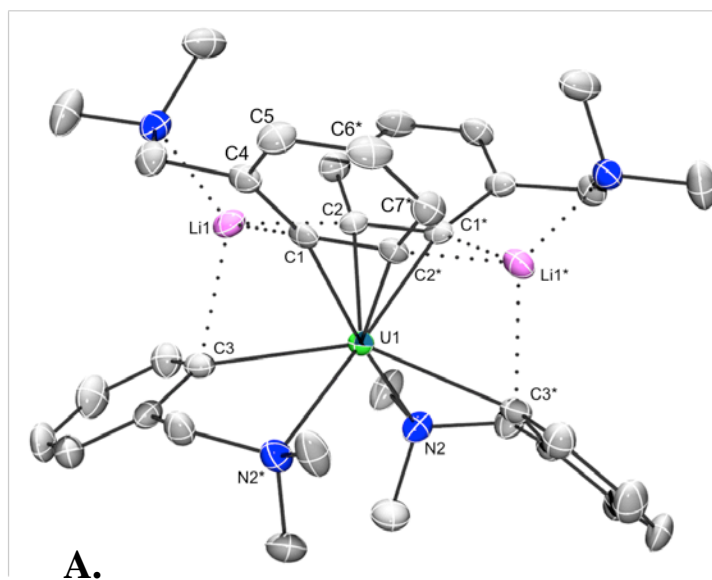


Scheme 7.6. Synthesis of complexes 7.1 and 7.2.

Complex **7.1** crystallizes in the monoclinic space group $C2/c$, while complex **7.2** crystallizes in the monoclinic space group $P2_1/n$ (Figure 7.1). Complex **7.1** features a distorted octahedral coordination geometry about the U center (if the benzyne ligands in **7.1** are considered to be monodentate ligands). Two of the arylamine ligands are bound in a N,C- κ^2 fashion, whereas the other two are bound in a C,C- η^2 fashion, forming two benzyne ligands. The dimethylamino groups of the two benzyne ligands are arranged in a “trans” orientation with respect to each other, and each dimethylamino group is bound to a Li cation. Each Li cation also coordinates to an *ipso*-carbon of an arylamine ligand, the C2 carbon of a benzyne ligand, and the C3 carbon of the other benzyne ligand (see Scheme 7.6 for numbering convention), in an overall tetrahedral geometry. It is likely that these Li-C_{benzyne} interactions play an important role in stabilizing the benzyne ligand. The U-C_{benzyne} bond lengths in **7.1** are 2.409(3) and 2.432(3) Å (Table 7.1), which are comparable to the U-C_{benzyne} distances in the structurally similar U(IV) monobenzyne complex, [Li][U(2,3-C₆H₃CH₂NMe₂)(2-C₆H₄CH₂NMe₂)₃] (2.340(5) and 2.473(5) Å).¹¹ Not surprisingly, the U-C_{aryl} distance in **7.1** (2.609(4) Å) is substantially longer than the U-C_{benzyne} distances, however it is similar to other reported U-C_{aryl} bond lengths.^{2,3,7,8,11} Finally, the C-C bond lengths in the two benzyne rings do not exhibit any alternation, consistent with the expected dianionic metalla-cyclopropene resonance form found in our previously characterized benzyne complexes, as well as the Group 4 and 5 benzyne complexes.^{19,20,24}

Complex **7.2** has a similar coordination geometry about the U center as that found for **7.1** (Figure 7.1); however, the dimethylamino groups of the two benzyne ligands are instead arranged in a “cis” orientation with respect to each other. Both

dimethylamino groups are bound to the same Li cation, which also interacts with each C2 carbon of the benzyne ligands (see Scheme 7.6 for numbering convention), and the *ipso*-carbon of an aryl amine ligand, to generate a distorted square pyramidal coordination geometry. The other Li cation is bound to the two C3 carbons of the benzyne ligands, along with two THF molecules, in an overall tetrahedral arrangement. Interestingly, only two other dibenzyne complexes have been previously structurally characterized, namely, $[\text{Li}(\text{THF})_3]_2[\text{LiCl}(\text{THF})_2]_2[\text{Li}(\text{THF})_2]_4$ - $[\text{Ta}(\eta^2\text{-C}_6\text{H}_4)_2\text{Ph}_4]_2$ and $[\text{Li}(\text{THF})]_4[\text{LiPh}(\text{THF})][\text{Nb}(\eta^2\text{-C}_6\text{H}_4)_2\text{Ph}_3]$.²⁴ However, a few other transition metal dibenzynes have been synthesized but not characterized by X-ray crystallography, including $[\text{Li}(\text{Et}_2\text{O})]_3[\text{W}(p\text{-Tol})_4(\eta^2\text{-C}_6\text{H}_3\text{CH}_3)_2]$.⁴¹⁻⁴⁴



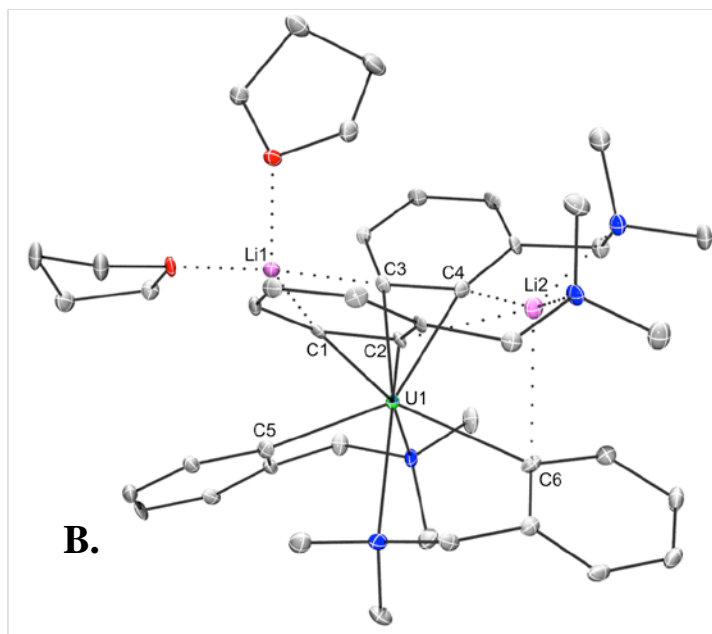


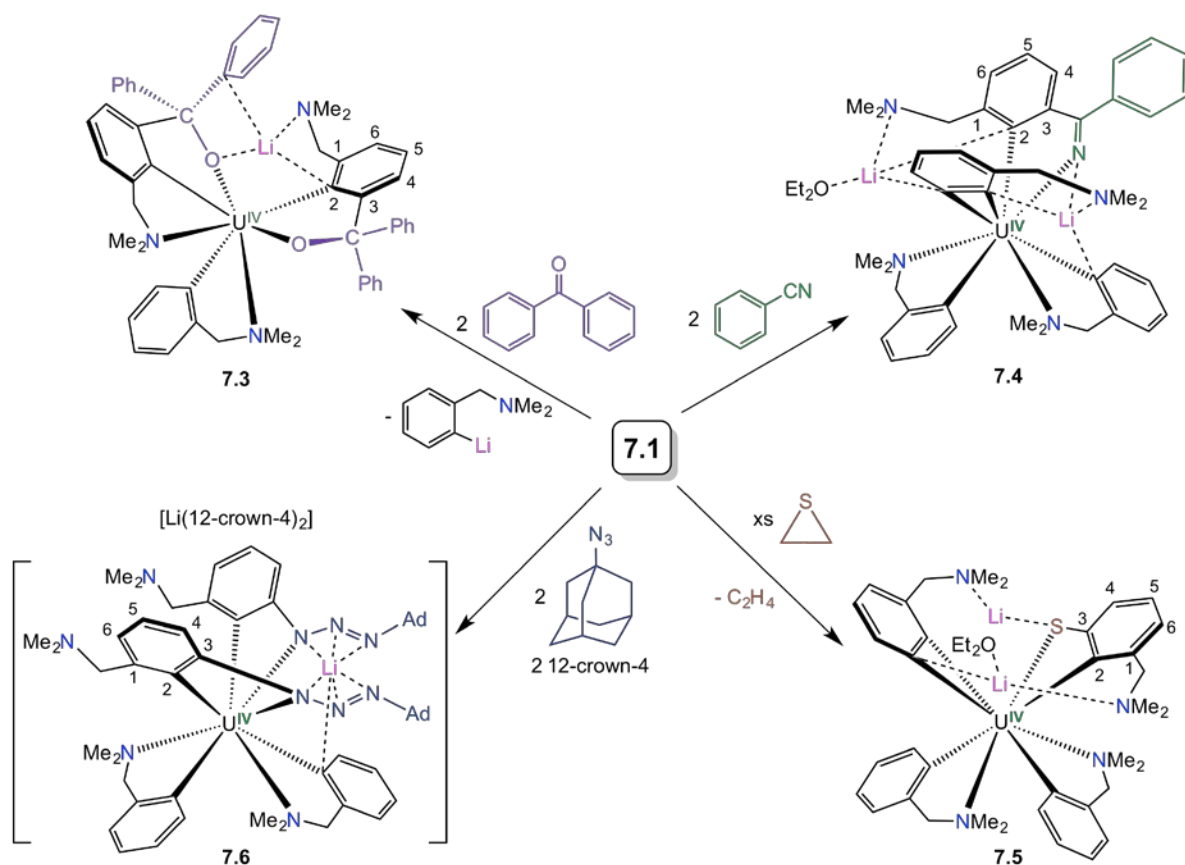
Figure 7.1. Solid-state structures of **(A)** $[\text{Li}]_2[\text{U}(\text{2,3-}\text{C}_6\text{H}_3\text{CH}_2\text{NMe}_2)_2(\text{2-C}_6\text{H}_4\text{CH}_2\text{NMe}_2)_2]$ (**7.1**) and **(B)** $[\text{Li}][\text{Li}(\text{THF})_2][\text{U}(\text{2,3-}\text{C}_6\text{H}_3\text{CH}_2\text{NMe}_2)_2(\text{2-C}_6\text{H}_4\text{CH}_2\text{NMe}_2)_2]$ (**7.2**) with 50% and 30% probability ellipsoids, respectively. All hydrogen atoms have been removed for clarity.

Table 7.1. Selected bond lengths (\AA) for complexes **7.1** and **7.2**.

	7.1	7.2
U-C_{benzyne}	2.409(3)	2.404(6)
	2.432(3)	2.417(6)
		2.427(6)
U-C_{aryl}	2.609(4)	2.455(7)
		2.570(6)
U-N_{amine}	2.697(3)	2.629(6)
		2.745(5)
Li-N	2.042(6)	2.752(5)
		2.17(1)
Li-C_{benzyne}		2.26(1)
	2.234(7)	2.28(1)
	2.298(8)	2.47(1)
		2.47(1)

Complex **7.1** is insoluble in hexane, but quite soluble in Et₂O, THF, and aromatic solvents. It is stable as a solid, and as a C₆D₆ solution, for at least 3 weeks at room temperature. In C₆D₆, complex **7.1** appears blue, and exhibits 15 resonances in its ¹H NMR spectrum, ranging from 75.43 to -42.86 ppm, consistent with the C₂ symmetric structure observed in the solid-state. Additionally, the ⁷Li{¹H} spectrum of **7.1** in C₆D₆ exhibits a distinctive resonance at 48.03 ppm. This large downfield shift is consistent with incorporation of the Li cation into the secondary coordination sphere of the paramagnetic uranium ion, and is consistent with the structure observed by X-ray crystallography. This spectrum also features a second resonance, at 13.53 ppm, which is assignable to an unidentified minor impurity. Interestingly, complex **7.1** appears brown when dissolved in THF-*d*₈, and its ¹H NMR spectrum is substantially more complicated than that observed in C₆D₆. In particular, this spectrum features 28 resonances ranging from 36.79 ppm to -42.32 ppm, consistent with a C₁ symmetric structure. Additionally, the ⁷Li{¹H} spectrum in THF-*d*₈ features two resonances at 7.72 and 2.95 ppm, in a 1:1 ratio. Both of these observations are consistent with the NMR spectra anticipated for complex **2**, and suggest that complex **7.1** converts into **7.2** when dissolved in THF. The profound color changes observed upon changing the Li coordination environments suggest that the Li-C_{benzyne} interactions have a profound effect on the overall electronic structure of the complex. These experiments also identify the U-C_{benzyne} bonds as the probable chromophore for this complex. Finally, the NIR spectrum of **7.1** is similar to those of other U(IV) complexes,^{11,45,46} which is in agreement with the benzyne ligands being in the dianionic resonance form.

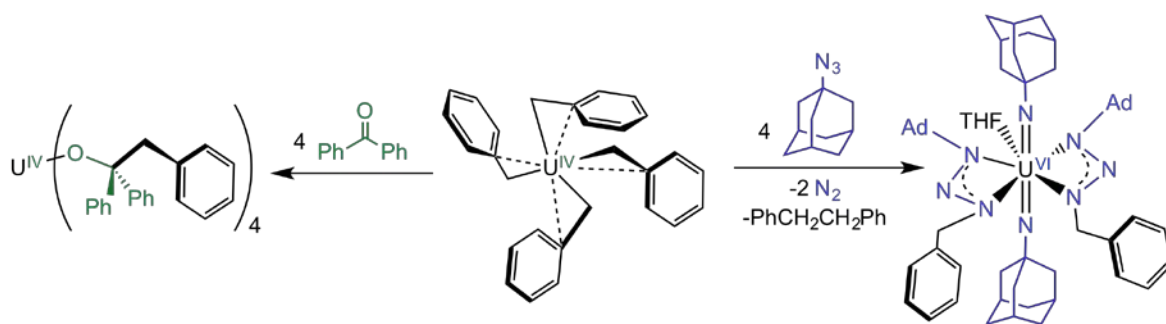
7.2.2. Synthesis and Characterization of $[\text{Li}][\text{U}(\text{2-C}_6\text{H}_3\text{CH}_2\text{NMe}_2\text{-3-COPh}_2)_2(\text{2-C}_6\text{H}_4\text{CH}_2\text{NMe}_2)]$ (7.3)



Scheme 7.7. Reactivity of complex **7.1**. All reactions performed at -25 °C in Et₂O.

In an effort to understand the chemical properties of actinide benzyne complexes, the reactivity of **7.1** with a variety of substrates was explored. Thus, treatment of complex **7.1** with 2 equiv of benzophenone in Et₂O results in an immediate color change from dark blue to red-orange (Scheme 7.7), indicating the formation of $[\text{Li}][\text{U}(\text{2-C}_6\text{H}_3\text{CH}_2\text{NMe}_2\text{-3-COPh}_2)_2(\text{2-C}_6\text{H}_4\text{CH}_2\text{NMe}_2)]$ (**7.3**), which can be isolated as a red-orange solid in 61% yield after work up. Also formed in the reaction is one equiv of 2-Li-C₆H₄CH₂NMe₂, which was confirmed by inspection of the ¹H and

$^7\text{Li}\{^1\text{H}\}$ NMR spectra of the reaction mixture.⁴⁷ Interestingly, reaction of **7.1** with only 1 equiv of benzophenone does not result in a mono-inserted product, but rather complexes **7.1** and **7.3** in a 1:0.2 ratio, respectively, as determined by inspection of the ^1H and $^7\text{Li}\{^1\text{H}\}$ NMR spectra of the reaction mixture. The formation of **7.3** is reminiscent of the reaction of the homoleptic U(IV) tetrabenzyl complex, $\text{U}(\text{CH}_2\text{C}_6\text{H}_5)_4$, with 4 equiv of benzophenone to generate $\text{U}[\text{OC}(\text{C}_6\text{H}_5)_2(\text{CH}_2\text{C}_6\text{H}_5)]_4$ (Scheme 7.8).⁴⁸ Replacement of two reactive U-C bonds with two stronger U-O bonds is the driving force for this reaction. The formation of **7.3** is also similar to the addition of ketones to Group 4 benzynes.^{20,37,38}



Scheme 7.8. Insertion chemistry of tetrabenzyluranium. Scheme adapted from reference 48.

Complex **7.3** crystallizes in the monoclinic space group $P2_1/n$, as the hexanes solvate $\mathbf{7.3} \cdot 0.5\text{C}_6\text{H}_{14}$ (Figure 7.2). Its solid-state structure confirms the insertion of one benzophenone molecule into each benzyne ligand, specifically at the C3 position (see Scheme 7.7 for numbering convention). The stereochemistry of the insertion can be rationalized on the basis of the reduced steric profile of C3 vs. C2, the uranium-bound carbon next to the dimethylamino group. The U-O bond lengths in **7.3** are 2.144(3) and

2.253(3) Å, which are comparable to those observed in other U(IV) alkoxides.⁴⁸⁻⁵¹ The C-O bond distances (1.425(4) and 1.438(5) Å) are indicative of C-O single bonds, demonstrating reduction of the C=O bonds of the benzophenone moiety.^{48,50} Finally, the U-C_{aryl} bond lengths in **7.3** range from 2.453(4) to 2.651(4) Å, and are similar to those in complexes **7.1** and **7.2**.

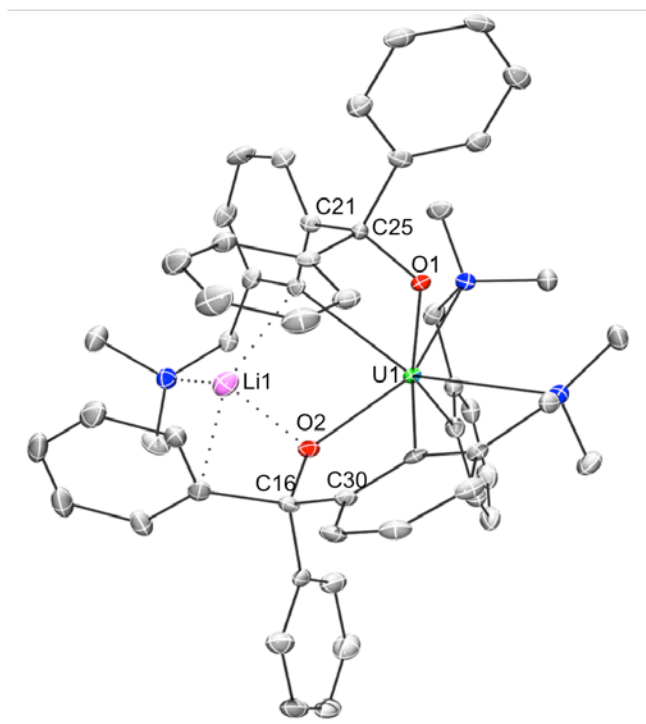


Figure 7.2. Solid-state structure of [Li][U(2-C₆H₃CH₂NMe₂-3-COPh)₂(2-C₆H₄CH₂NMe₂)]·0.5C₆H₁₄ (**7.3**·0.5C₆H₁₄) with 50% probability ellipsoids. All hydrogen atoms and the hexane solvate have been removed for clarity. Selected bond lengths (Å) and angles (deg): U1-O1 = 2.144(3), U1-O2 = 2.253(3), U1-C2 = 2.453(4), U1-C4 = 2.651(4), U1-C24 = 2.557(4), U1-N1 = 2.909(3), U1-N2 = 2.734(4), C21-C25 = 1.526(6), C16-C30 = 1.523(6), C25-O1 = 1.425(4), C16-O2 = 1.438(5), O1-U1-O2 = 120.6(1).

The ^1H NMR spectrum of **7.3** in C_6D_6 consists of 32 paramagnetically shifted resonances ranging from 63.73 to -64.81 ppm, consistent with the C_1 symmetric structure observed in the solid state (Figure 7.3). The $^7\text{Li}\{^1\text{H}\}$ NMR spectrum displays a single, paramagnetically shifted resonance at -117.68 ppm. Finally, the NIR spectrum of **7.3** is similar to those of other U(IV) complexes, confirming that no uranium redox chemistry has occurred upon insertion.^{11,45,52,53}

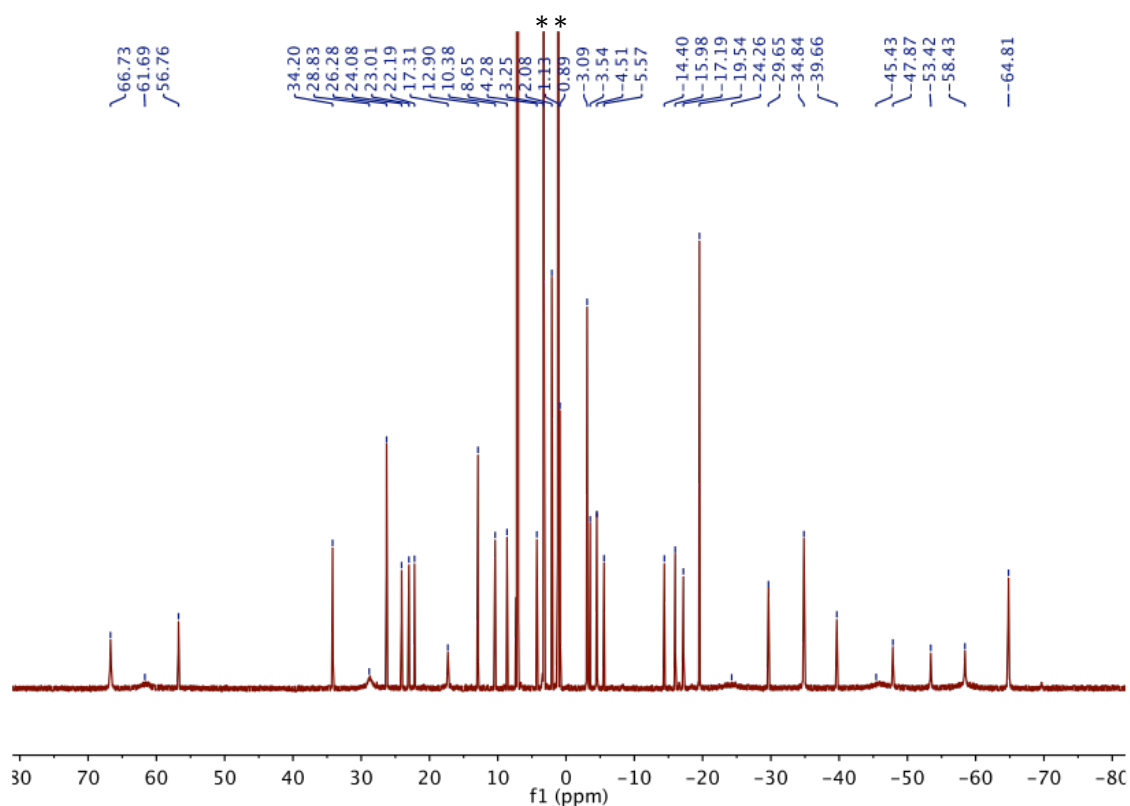


Figure 7.3. ^1H NMR spectrum of complex **7.3** in C_6D_6 . Asterisks indicate the presence of Et_2O .

7.2.3 Synthesis and Characterization of [Li][Li(Et₂O)][U(2,3-C₆H₃CH₂NMe₂)(2-C₆H₃CH₂NMe₂-3-C(Ph)=N)(2-C₆H₄CH₂NMe₂)₂] (7.4)

Nitrile insertion reactivity of complex **7.1** was investigated with MeCN, ^tBuCN, and PhCN. Although both MeCN and ^tBuCN appeared to react with complex **7.1**, based on obvious color changes to red-brown, and the observations of new paramagnetic products in the *in situ* ¹H NMR spectra, products from these reactions were never crystallized. However, similar to the benzophenone reactivity, addition of 2 equiv of PhCN to complex **7.1** results in formation of an insertion product, specifically the U(IV) ketimide complex, [Li][Li(Et₂O)][U(2,3-C₆H₃CH₂NMe₂)(2-C₆H₃CH₂NMe₂-3-C(Ph)=N)(2-C₆H₄CH₂NMe₂)₂] (**7.4**), which can be isolated as a green-brown crystalline solid in 21% yield after work-up (Scheme 7.7). Comparable nitrile insertion reactivity has been observed previously for the actinides. For example, reaction of (η⁵-Cp*)₂ThPh₂ or (η⁵-Cp*)₂UMe₂ with excess PhCN yields the ketimide complexes, (η⁵-Cp*)₂Th(N=CPh₂)₂ and (η⁵-Cp*)₂U(N=CPhMe)₂, respectively.⁵⁴ Similarly, reaction of [η⁵-1,2,4-(Me₃C)₃C₅H₂]₂Th(η²-C₂Ph₂) with PhCN, generates the azametallacycle, [η⁵-1,2,4-(Me₃C)₃C₅H₂]₂Th[N=C(Ph)C(Ph)=C(Ph)].³⁹ Likewise, reaction of (η⁵-Cp*)₂Th(η⁴-C₄Ph₂) with PhCN, affords the azametallacycle, (η⁵-Cp*)₂Th[N=C(Ph)(C₄Ph₂)C(Ph)=N].⁵⁵ Curiously, the isolation of **7.4** in reasonable yields requires the addition of two equiv of PhCN, but only one equiv is incorporated into the final product. It is not entirely clear why the second equivalent of PhCN is needed, but we speculate that it may coordinate to a Li cation in **7.1**, which changes the steric profile of the benzyne ligand and allows for the insertion to occur.

Complex **7.4** crystallizes in the monoclinic space group $P2_1/n$ (Figure 7.4). The eight-coordinate U(IV) center features two N,C- κ^2 bound arylamine ligands, one C,C- η^2 bound benzyne ligand, and one N,C- κ^2 bound aryl-ketimide ligand. The stereochemistry of nitrile insertion is the same as that observed in complex **7.3**. Also present in the structure are two Li cations. One Li cation is bound to an *ipso*-carbon of the arylamine ligand, the C2 carbon of the benzyne ligand (see Scheme 7.7 for numbering convention), the nitrogen atom of the aryl ketimide ligand, and the nitrogen atom of a dimethylamino group. The other Li cation is bound to the *ipso*-carbon of the aryl ketimide ligand, the C3 carbon of the benzyne ligand, the nitrogen atom of a dimethylamino group, and a molecule of diethyl ether. The U1-N4 bond distance (2.37(1) Å) is comparable to other U(IV)-N_{ketimide} bond lengths.^{54,56} The N4-C38 distance (1.27(2) Å) is indicative of a double bond, and also supports the formation of the ketimide functional group.⁵⁷ Finally, the U-C_{aryl} bond lengths in **7.4** are 2.57(2), 2.62(2) and 2.68(1) Å, which are similar to those found in complex **7.3**.

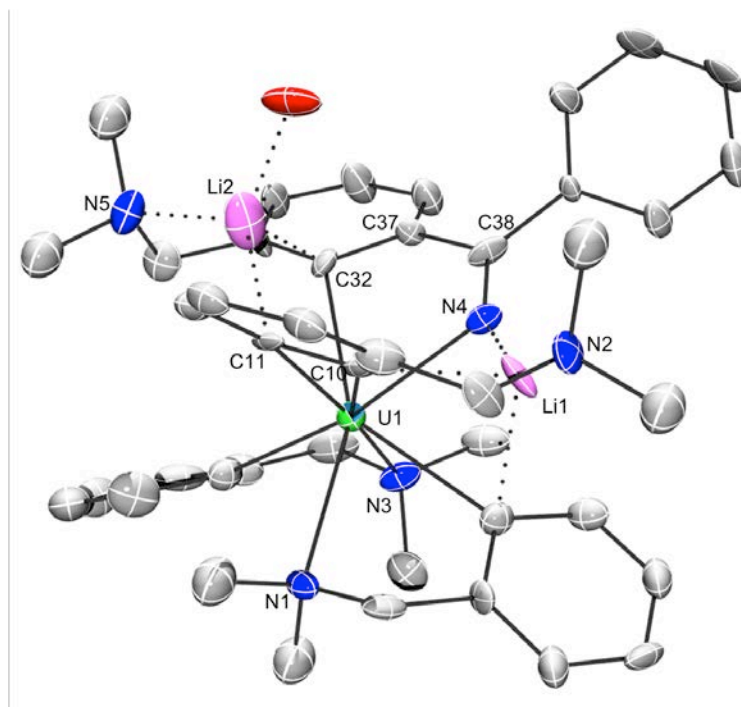


Figure 7.4. Solid-state structure of $[\text{Li}][\text{Li}(\text{Et}_2\text{O})][\text{U}(2,3\text{-C}_6\text{H}_3\text{CH}_2\text{NMe}_2)(2\text{-C}_6\text{H}_3\text{CH}_2\text{NMe}_2\text{-3-C(Ph)=N})(2\text{-C}_6\text{H}_4\text{CH}_2\text{NMe}_2)_2]$ (**7.4**) with 50% probability ellipsoids. Et_2O carbons and all hydrogen atoms have been removed for clarity. Selected bond lengths (\AA) and angles (deg): $\text{U1-N4} = 2.37(1)$, $\text{N4-C38} = 1.27(2)$, $\text{C37-C38} = 1.51(2)$, $\text{U1-C1} = 2.62(2)$, $\text{U1-C10} = 2.45(1)$, $\text{U1-C11} = 2.39(1)$, $\text{U1-C23} = 2.57(2)$, $\text{U1-C32} = 2.68(1)$, $\text{C10-C11} = 1.41(2)$, $\text{U1-C32} = 2.68(1)$, $\text{C10-U1-C11} = 33.7(5)$, $\text{C32-U1-N4} = 67.4(4)$.

The ^1H NMR spectrum of complex **7.4** features 29 paramagnetically shifted resonances ranging from 44.68 to -46.36 ppm, consistent with the C_1 symmetric structure observed in the solid state. The $^7\text{Li}\{^1\text{H}\}$ NMR spectrum, as anticipated for the C_1 symmetric structure, features two highly shifted resonances at 182.26 and -69.42 ppm, in a 1:1 ratio. The near-IR spectrum of **7.4** is similar to complexes **7.1** and **7.3**, as

well as other U(IV) complexes, supporting the presence of a $5f^2$ ion, and indicating that its remaining benzyne ligand is still in the dianionic resonance form.^{11,45,46}

7.2.4 Synthesis and Characterization of $[\text{Li}][\text{Li}(\text{Et}_2\text{O})][\text{U}(\text{2,3-C}_6\text{H}_3\text{CH}_2\text{NMe}_2)(\text{5-C}_6\text{H}_3\text{CH}_2\text{NMe}_2\text{-2-S})(\text{2-C}_6\text{H}_4\text{CH}_2\text{NMe}_2)_2]$ (7.5)

During these investigations, we also explored the reactivity of **7.1** with ethylene sulfide, a common sulfur source.^{58,59} Thus, reaction of complex **7.1** with excess ethylene sulfide in Et_2O , resulted in a red solution, from which a few red crystals of $[\text{Li}]_2[\text{U}(\text{2,3-C}_6\text{H}_3\text{CH}_2\text{NMe}_2)(\text{5-C}_6\text{H}_3\text{CH}_2\text{NMe}_2\text{-2-S})(\text{2-C}_6\text{H}_4\text{CH}_2\text{NMe}_2)_2]$ (**7.5**) were isolated in one instance (Scheme 7.7). Complex **7.5** forms as a result of sulfur insertion into the U-C3 bond of one of the benzyne ligands (see Scheme 7.7 for numbering convention), forming a new aryl thiolate ligand. Comparable sulfur insertion reactivity has been observed previously for transition metal benzynes. For example, reaction of $\text{Ge}(\text{Tbt})(\text{Dipp})(\text{C}_6\text{H}_4)$ with elemental sulfur, results in the formation of the germanium-metallacycle, $\text{Ge}(\text{Tbt})(\text{Dipp})(\kappa^2\text{-C}_6\text{H}_4\text{S})$ (Scheme 7.3b).²⁵ Interestingly, even in the presence of excess ethylene sulfide, only the mono-insertion product (**7.5**) is formed.

Complex **7.5** crystallizes in the monoclinic space group $P2_1/n$ (Figure 7.5). The eight-coordinate U(IV) center features two N,C- κ^2 bound arylamine ligands, one C,C- η^2 bound benzyne ligand, and one S,C- κ^2 bound aryl thiolate ligand. The stereochemistry of nitrile insertion is the same as that observed in complexes **7.3** and **7.4**. Also present in the structure are two Li cations. One Li cation is bound to sulfur atom of the aryl thiolate ligand, the C2 carbon of the benzyne ligand (see Scheme 7.7 for numbering

convention), the *ipso*-carbon of the arylamine ligand and the nitrogen atom of a dimethylamino group. The other Li cation is bound to the *ipso*-carbon of the aryl thiolate ligand, the C3 carbon of the benzyne ligand, the nitrogen atom of a dimethylamino group, and a molecule of diethyl ether. The U1-S1 bond distance (2.887(2) Å) is on the longer side of typical U(IV)-S single bonds. For example, the U(IV) trisulfide complex, [K(18-crown-6)][U(η^3 -S₃)(N(SiMe₃)₂)₃] exhibits U-S bond lengths of 2.835(1), 2.819(1), and 2.760(1) Å,⁶⁰ and the U(IV) bridging chalcogenide complex, [((Me₃Si)₂N)₃U]₂(μ -S)], exhibits an av. U-S distance of 2.662 Å.⁶¹ The C1-S1 distance in **7.5** (1.780(9) Å) is indicative of a single bond, and comparable to other aryl thiolate ligands.^{25,62} For example, the Co(III) complex, Co(CH₃)(PMe₃)₃(κ^2 -C₆H₄S), exhibits a C-S bond length of 1.765(3) Å,⁶² and the germanium-metallacycle complex, Ge(Tbt)(Dipp)(κ^2 -C₆H₄S), exhibits a C-S bond length of 1.783(4) Å.²⁵ Finally, the U-C_{aryl} bond lengths in **7.5** are 2.591(9), 2.62(1) and 2.562(9) Å, which are similar to those found in complex **7.4**.

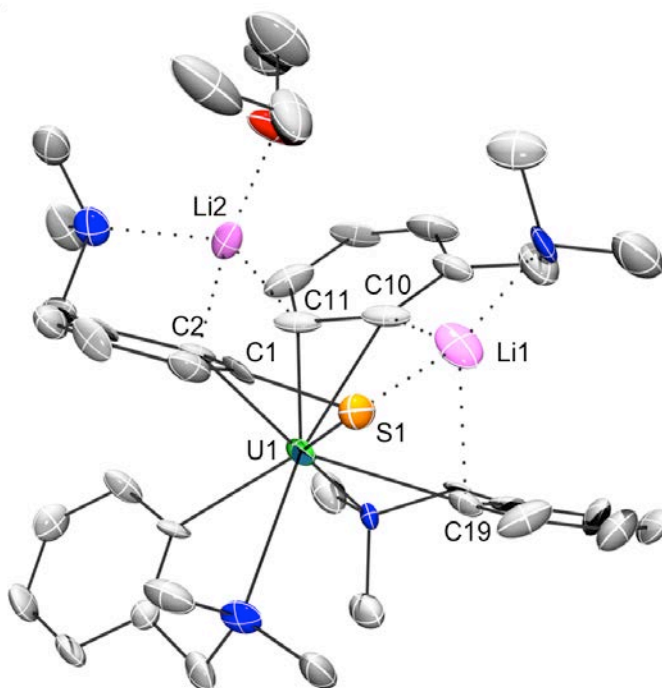


Figure 7.5. Solid-state structure of $[\text{Li}][\text{Li}(\text{Et}_2\text{O})][\text{U}(2,3\text{-C}_6\text{H}_3\text{CH}_2\text{NMe}_2)(5\text{-C}_6\text{H}_3\text{CH}_2\text{NMe}_2\text{-}2\text{-S})(2\text{-C}_6\text{H}_4\text{CH}_2\text{NMe}_2)_2]$ (**7.5**) with 50% probability ellipsoids. All hydrogens have been removed for clarity. Selected bond lengths (\AA) and angles (deg): $\text{U1-S1} = 2.887(2)$, $\text{U1-C2} = 2.591(9)$, $\text{U1-C10} = 2.531(9)$, $\text{U1-C11} = 2.44(1)$, $\text{U1-C19} = 2.62(1)$, $\text{U1-C28} = 2.562(9)$, $\text{C1-S1} = 1.780(9)$, $\text{S1-Li1} = 2.40(2)$, $\text{C2-U1-S1} = 59.3(2)$, $\text{C10-U1-C11} = 36.3(3)$.

7.2.5 Reactivity of **7.1** with Unsaturated Hydrocarbons

We also probed the reactivity of **7.1** with alkenes and alkynes. Surprisingly, we observe no reaction between **7.1** and a wide variety of unsaturated hydrocarbons, including cyclopentene, cyclooctene, tetracyanoethylene, phenylacetylene, diphenylacetylene, and norbornene. This contrasts dramatically with the reactivity

observed for transition metal benzyne complexes, which readily react with alkynes and alkenes.^{19,20,22,23,26} To explain this observation we suggest that the presence of the dimethylamino arms in **7.1**, as well as its inner sphere Li cations, provide sufficient steric protection to the benzyne carbons to prevent insertion. The ejection of 2-Li-C₆H₄CH₂NMe₂ during the formation of complex **7.3**, which presumably occurs to relieve steric pressure upon insertion of benzophenone, is consistent with this hypothesis.

7.2.6 Synthesis and Characterization of [Li(12-crown-4)₂][Li][U(2-C₆H₃CH₂NMe₂-3-(N-N=N-Ad))₂(2-C₆H₄CH₂NMe₂)₂] (**7.6**)

Finally, the reactivity of **7.1** with a variety of oxidants was probed. For example, reaction of complex **7.1** with 2 equiv of AdN₃, followed by addition of 2 equiv of 12-crown-4, results in formation of [Li(12-crown-4)₂][Li][U(2-C₆H₃CH₂NMe₂-3-(N-N=N-Ad))₂(2-C₆H₄CH₂NMe₂)₂] (**7.6**), which can be isolated as a red crystalline solid in 42% yield after work up (Scheme 7.7). Complex **7.6** forms as a result of azide insertion into each U-C3 bond of the benzyne ligands (see Scheme 7.7 for numbering convention), forming two aryl triazenido ligands. Insertion of an organoazide into a U-C bond to form a triazenido ligand has been observed previously.^{7,48,63} Also of note, in contrast to the reaction of U(CH₂C₆H₅)₄ with 4 equiv of AdN₃ (Scheme 7.8),⁴⁸ where two AdN₃ serve to oxidize the uranium center, while the remaining two undergo U-C bond insertion,⁴⁸ we observe no evidence for oxidation of the metal center and formation of a U(VI) imido complex in this reaction. Interestingly, similar to the reactivity of **7.1** with benzophenone, reaction of **7.1** with only 1 equiv of AdN₃ does not result in a

mono-inserted product, but rather complexes **7.1** and **7.6** in a 1:1 ratio, respectively, as determined by inspection of the ^1H and $^7\text{Li}\{^1\text{H}\}$ NMR spectra of the reaction mixture.

Complex **7.6** crystallizes in the monoclinic space group $P2_1/n$, as a discrete cation/anion pair. Its solid-state molecular structure is shown in Figure 7.6. The eight-coordinate U(IV) anion features two N,C- κ^2 bound arylamine ligands, as well as two N,C- κ^2 bound aryl triazenido ligands, formed from azide insertion in the U-C3 benzyne linkage. Notably, the stereochemistry of azide insertion is the same as those observed in complexes **7.3**, **7.4** and **7.5**. Also present in the structure is a Li cation, which is bound to one *ipso*-carbon of an arylamine ligand, and four nitrogen atoms of the aryl triazenido ligands in a N,N- κ^2 arrangement. Interestingly, the U-N1 (2.742(8) Å) and U-N4 (2.515(7) Å) distances are longer than those observed for other uranium triazenido complexes.^{48,63} This discrepancy is likely due to the presence of the Li cation, which also competes for triazenido electron density. In addition, the variation in the N-N bond lengths (N1-N2 = 1.34(1), N2-N3 = 1.29(1), N4-N5 = 1.33(1), N5-N6 = 1.23(1) Å), suggests that the triazenido fragment features localized π -bonding. Furthermore, the new C-N bond lengths between the former benzyne ligands and the inserted AdN₃ ligands are 1.40(1) and 1.45(1) Å. Finally, the U-C_{aryl} bond lengths in **7.6** range from 2.50(1) to 2.613(9) Å, and are similar to those found in complexes **7.3**, **7.4** and **7.5**.

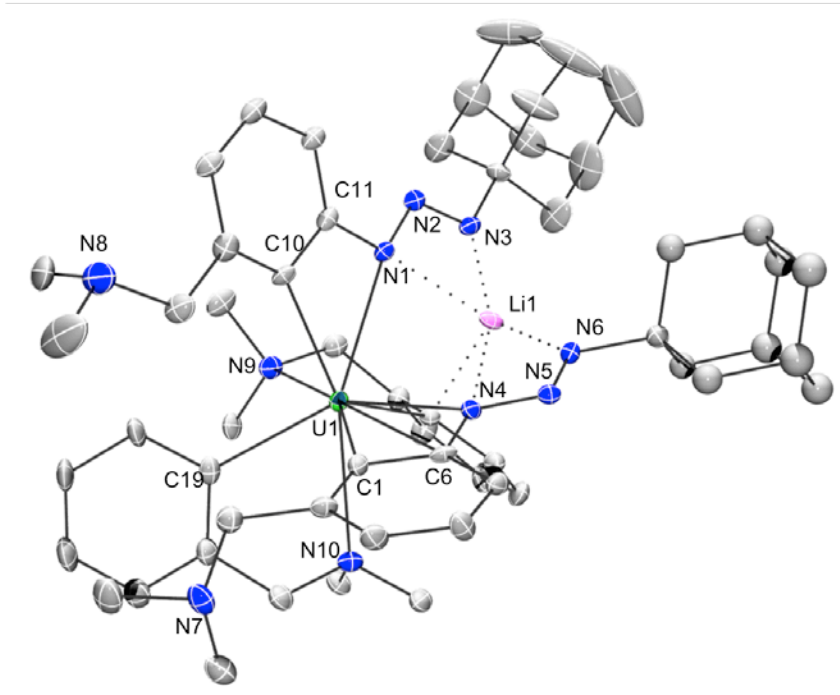


Figure 7.6. Solid-state structure of $[\text{Li}(12\text{-crown-}4)_2][\text{Li}][\text{U}(2\text{-C}_6\text{H}_3\text{CH}_2\text{NMe}_2\text{-}3\text{-(N=N-Ad)})_2(2\text{-C}_6\text{H}_4\text{CH}_2\text{NMe}_2)_2]\cdot\text{OC}_4\text{H}_{10}$ (**7.6** $\cdot\text{OC}_4\text{H}_{10}$) with 50% probability ellipsoids. The $[\text{Li}(12\text{-crown-}4)_2]^+$ cation, the Et_2O solvate, and all hydrogen atoms have been removed for clarity. Selected bond lengths (\AA) and angles (deg): $\text{U1-C1} = 2.52(1)$, $\text{U1-C10} = 2.520(9)$, $\text{U1-C19} = 2.50(1)$, $\text{U1-C28} = 2.613(9)$, $\text{U1-N1} = 2.742(8)$, $\text{U1-N4} = 2.515(7)$, $\text{N1-N2} = 1.34(1)$, $\text{N2-N3} = 1.29(1)$, $\text{N4-N5} = 1.33(1)$, $\text{N5-N6} = 1.23(1)$, $\text{C11-N1} = 1.40(1)$, $\text{N1-N2} = 1.34(1)$, $\text{N2-N3} = 1.29(1)$, $\text{N4-N5} = 1.33(1)$, $\text{N5-N6} = 1.23(1)$, $\text{C11-N1} = 1.40(1)$, $\text{C6-N4} = 1.44(1)$, $\text{C1-U1-N4} = 55.9(3)$, $\text{C10-U1-N1} = 52.8(3)$, $\text{N1-N2-N3} = 114.3(7)$, $\text{N4-N5-N6} = 114.1(7)$.

The $^7\text{Li}\{^1\text{H}\}$ NMR spectrum of complex **7.6** in $\text{THF-}d_8$ displays two resonances at 75.15 and -44.63 ppm, in a roughly 1:1 ratio. Also present in the spectrum is a less intense resonance at 0.98 ppm (featuring ca. 40% of the intensity of the other two resonances), which is assignable to the $[\text{Li}(12\text{-crown-}4)_2]$ moiety. The observation of

two highly paramagnetically-shifted resonances in this spectrum, when only one is expected, indicates that a structural change has occurred upon dissolution of **7.6** in THF-*d*₈. This structural change most likely involves the incorporation of two Li cations, with different coordination environments, into the secondary coordination sphere of the uranium ion. Interestingly, addition of a several-fold excess of 12-crown-4 to this sample, in an attempt to favor the separated ion pair structure, results only in the slight growth of the [Li(12-crown-4)₂] resonance. Even under these conditions, the resonances at 75.15 and -44.63 ppm are still the major resonances in the spectrum. Despite the complexity of the ⁷Li{¹H} NMR spectrum, the ¹H NMR spectrum of complex **7.6** only features 35 paramagnetically shifted resonances, which range from 48.68 to -62.70 ppm. This is close to the 39 resonances predicted from inspection of the solid-state structure. In addition, only one broad resonance is observed for the 12-crown-4 methylene protons (at 3.58 ppm), likely due to fast exchange of Li between free 12-crown-4 and Li-coordinated 12-crown-4. Finally, the near-IR spectrum of **7.6** is consistent with the presence of a 5f² ion, supporting the U(IV) oxidation state assignment.^{11,45,52,53}

We also probed the reactivity of **7.1** with Me₃SiN₃, but surprisingly, we observed no reaction. In contrast, complex **7.1** rapidly reacts with I₂ to generate dark red-brown solutions, but no tractable products could be isolated from these mixtures. The reactions of **7.1** with other oxidants, such as AgPF₆, [Fc][PF₆], S₈, and PhSSPh, also lead to intractable mixtures. Reaction of **7.1** with oxygen-atom transfer reagents, such as TEMPO (TEMPO = (2,2,6,6-tetramethylpiperidin-1-yl)oxyl), pyridine-*N*-oxide, and morpholine-*N*-oxide, generate dark orange brown solutions, however, these also

proved to be intractable. In summary, our attempts to generate a U(VI) benzyne complex were unsuccessful, which is perhaps not surprising considering that a high valent uranium benzyne is likely to be much more reactive than complex **7.1**.

7.3 Summary

Reaction of UCl_4 with 2-Li- $\text{C}_6\text{H}_4\text{CH}_2\text{NMe}_2$ results in formation of the U(IV) dibenzyne complex, $[\text{Li}]_2[\text{U}(2,3\text{-C}_6\text{H}_3\text{CH}_2\text{NMe}_2)_2(2\text{-C}_6\text{H}_4\text{CH}_2\text{NMe}_2)_2]$ (**7.1**), in good yields. Complex **7.1** is a rare example of a dibenzyne complex, and has proven to be an excellent substrate for probing the reactivity of the actinide-benzyne linkage. Complex **7.1** reacts with a variety of electrophiles, such as benzophenone, benzonitrile and ethylene sulfide, to give the insertion products, $[\text{Li}][\text{U}(2\text{-C}_6\text{H}_3\text{CH}_2\text{NMe}_2\text{-3-COPh})_2(2\text{-C}_6\text{H}_4\text{CH}_2\text{NMe}_2)]$ (**7.3**), $[\text{Li}][\text{Li}(\text{Et}_2\text{O})][\text{U}(2,3\text{-C}_6\text{H}_3\text{CH}_2\text{NMe}_2)(2\text{-C}_6\text{H}_3\text{CH}_2\text{NMe}_2\text{-3-C(Ph)=N})(2\text{-C}_6\text{H}_4\text{CH}_2\text{NMe}_2)_2]$ (**7.4**), and $[\text{Li}][\text{Li}(\text{Et}_2\text{O})][\text{U}(2,3\text{-C}_6\text{H}_3\text{CH}_2\text{NMe}_2)(5\text{-C}_6\text{H}_3\text{CH}_2\text{NMe}_2\text{-2-S})(2\text{-C}_6\text{H}_4\text{CH}_2\text{NMe}_2)_2]$ (**7.5**), respectively. Reaction of complex **7.1** with the AdN_3 also results in an insertion product, $[\text{Li}(12\text{-crown-4})_2][\text{Li}][\text{U}(2\text{-C}_6\text{H}_3\text{CH}_2\text{NMe}_2\text{-3-(N-N=N-Ad)})_2(2\text{-C}_6\text{H}_4\text{CH}_2\text{NMe}_2)_2]$ (**7.6**). Overall, our study demonstrates that actinide benzynes generally behave like early metal benzynes. This observation is probably not surprising, given that both uranium and the early transition metals are similarly electropositive and likely feature electronically similar $\text{M-C}_{\text{benzyne}}$ interactions. However, one contrast between our U(IV) benzyne and those of Groups 4 and 5, is that oxidation of the metal center is possible for **7.1**. Despite this difference, we see no evidence for the oxidation of **7.1** with the use of oxidizing

substrates (e.g., organoazides). Nonetheless, oxidation of the uranium center in **7.1** is possible, and is also of significant interest, given that high valent metal benzynes could feature different reactivity than their lower valent counterparts. In this regard, we will continue to probe the reactivity of **7.1** in an effort to discover novel actinide benzyne reactivity.

7.4 Experimental

7.4.1 General Procedures. All reactions and subsequent manipulations were performed under anaerobic and anhydrous conditions under an atmosphere of nitrogen or argon. Hexanes, Et₂O, THF and toluene were dried by passage over activated molecular sieves using a Vacuum Atmospheres solvent purification system. C₆D₆ and THF-*d*₈, were dried over activated 3Å molecular sieves for 24 h before use. UCl₄ and 2-Li-C₆H₄CH₂NMe₂ were prepared according to literature procedures.^{64,65} All other reagents were purchased from commercial suppliers and used as received.

NMR spectra were recorded on a Varian UNITY INOVA 400 spectrometer or an Agilent Technologies 400-MR DD2 spectrometer. ¹H NMR spectra were referenced to external SiMe₄ using the residual protio solvent peaks as internal standards. The chemical shifts of ⁷Li{¹H} were referenced indirectly with the ¹H resonance of SiMe₄ at 0 ppm, according to IUPAC standard.^{66,67} IR spectra were recorded on a Mattson Genesis FTIR/Raman spectrometer. UV-vis/NIR experiments were performed on a UV-3600 Shimadzu spectrophotometer. Elemental analyses were performed by the Microanalytical Laboratory at UC Berkeley.

7.4.2 Synthesis of [Li]₂[U(2,3-C₆H₃CH₂NMe₂)₂(2-C₆H₄CH₂NMe₂)₂] (7.1). To a stirring green solution of UCl₄ (128 mg, 0.337 mmol) in THF (2 mL), was added a light yellow suspension of 2-Li-C₆H₄CH₂NMe₂ (286 mg, 2.03 mmol) in Et₂O (4 mL). The red-orange mixture was allowed to stir for 24 h at 25 °C, which resulted in formation of a dark brown solution concomitant with the deposition of a grey precipitate. All the volatiles were removed *in vacuo*, which generated a dark red-brown solid. The solid

was then extracted into Et₂O (8 mL), and the resulting solution was filtered through a Celite column (2 cm × 0.5 cm) supported on glass wool. The volume of the dark brown filtrate was then reduced *in vacuo* and the concentrated solution was stored at -25 °C for 24 h, which resulted in the deposition of a blue solid of **7.1** (106.6 mg, 40% yield). In a handful of instances, a few brown crystals were also isolated from the reaction mixture. These were confirmed to be [Li][Li(THF)₂][U(2,3-C₆H₃CH₂NMe₂)₂(2-C₆H₄CH₂NMe₂)₂] (**7.2**) by X-ray crystallography. Anal. Calcd for ULi₂N₄C₃₆H₄₆: C, 54.96; H, 5.89; N, 7.12. Found: C, 55.12; H, 5.57; N, 6.75. ¹H NMR (C₆D₆, 25 °C, 400 MHz): δ 75.43 (s, 1H), 31.30 (s, 1H), 25.85 (s, 1H), 22.88 (s, 1H), 18.47 (s, 3H), 17.22 (d, *J*_{HH} = 8.0 Hz, 1H), 13.07 (d, *J*_{HH} = 9.3 Hz, 1H), 6.95 (s, 1H), 3.70 (s, 1H), 2.65 (d, *J*_{HH} = 8.8 Hz, 1H), 0.73 (d, *J*_{HH} = 8.2 Hz, 1H), -1.98 (s, 3H), -11.53 (s, 1H), -42.66 (s, 3H), -42.86 (s, 3H). ⁷Li{¹H} NMR (C₆D₆, 25 °C, 155 MHz): δ 48.03 (s). ¹H NMR (THF-*d*₈, 25 °C, 500 MHz): δ 36.79 (s, 1H), 34.95 (s, 1H), 20.48 (t, *J*_{HH} = 8.4 Hz, 1H), 20.18 (d, *J*_{HH} = 5.8 Hz, 1H), 20.13 (d, *J*_{HH} = 7.9 Hz, 1H), 20.07 (t, *J*_{HH} = 7.5 Hz, 1H), 19.74 (d, *J*_{HH} = 7.1 Hz, 1H), 17.69 (d, *J*_{HH} = 10.1 Hz, 1H), 17.04 (d, *J*_{HH} = 5.2 Hz, 1H), 16.69 (d, *J*_{HH} = 6.8 Hz, 1H), 11.27 (d, *J*_{HH} = 4.0 Hz, 1H), 9.79 (br s, 3H), 8.41 (t, *J*_{HH} = 5.4 Hz, 1H), 8.16 (t, *J*_{HH} = 5.6 Hz, 1H), 6.92 (d, *J*_{HH} = 9.6 Hz, 1H), 6.63 (d, *J*_{HH} = 4.5 Hz, 1H), 5.71 (d, *J*_{HH} = 5.7 Hz, 1H), 5.51 (s, 1H), 5.21 (br s, 3H), -3.06 (d, *J*_{HH} = 9.3 Hz, 1H), -4.17 (br s, 1H), -4.36 (d, *J*_{HH} = 10.2 Hz, 1H), -6.90 (br s, 1H), -10.37 (br s, 1H), -19.79 (s, 3H), -20.06 (s, 3H), -38.32 (s, 3H), -42.32 (s, 3H). Two of the CH₃ resonances were not observed, possibly due to paramagnetic broadening. ⁷Li{¹H} NMR (THF-*d*₈, 25 °C, 155 MHz): δ 7.72 (s, 1Li), 2.95 (s, 1Li). UV-vis/NIR (C₆H₆, 4.19 × 10⁻³ M, L·mol⁻¹·cm⁻¹): 586 (ε = 1081), 598 (ε = 1109), 602 (ε = 1106), 700 (sh, ε = 146), 734 (sh, ε = 101), 914 (ε = 45), 958 (ε = 55), 1094 (ε = 99), 1148 (sh, ε = 110),

1212 ($\epsilon = 158$), 1424 ($\epsilon = 105$), 1544 ($\epsilon = 104$). IR (KBr pellet, cm^{-1}): 3039 (w), 3004 (m), 2945 (m), 2854 (m), 2816 (s), 2775 (s), 2698 (w), 1597 (w), 1585 (sh w), 1562 (w), 1520 (w), 1479 (sh m), 1463 (sh m), 1454 (vs), 1421 (sh m), 1413 (m), 1389 (w), 1362 (m), 1282 (w), 1273 (m), 1267 (m), 1230 (m), 1235 (m), 1207 (w), 1171 (m), 1146 (m), 1111 (w), 1092 (m), 1070 (w), 1043 (m), 1030 (s), 1001 (s), 966 (w), 887 (w), 864 (w), 845 (s), 823 (sh m), 795 (w), 760 (s), 740 (s), 700 (m), 698 (m), 625 (w), 525 (w), 450 (w).

7.4.3 Synthesis of [Li][U(2-C₆H₃CH₂NMe₂-3-COPh₂)₂(2-C₆H₄CH₂NMe₂)] (7.3). To a dark blue solution of complex **7.1** (60.2 mg, 0.077 mmol) in Et₂O (3 mL), was added a solution of benzophenone (28.3 mg, 0.155 mmol) in Et₂O (1 mL). After addition, the solution quickly changed to a red-orange color, concomitant with the deposition of a pale yellow precipitate. The suspension was allowed to stir for 15 min, whereupon it was filtered through a Celite column (2 cm × 0.5 cm) supported on glass wool. The resulting red filtrate was collected and its volume was reduced *in vacuo* to ca. 2 mL. Storage of this solution at -25 °C for 24 h resulted in the deposition of a red-orange solid (47.4 mg, 61% yield). X-ray quality crystals were grown from a concentrated Et₂O solution that contained a few drops of hexanes, and which was stored at -25 °C for 24 h. Anal. Calcd for ULiN₃O₂C₅₃H₅₄: C, 63.03; H, 5.39; N, 4.16. Found: C, 62.79; H, 5.55; N, 3.89. ¹H NMR (C₆D₆, 25 °C, 400 MHz): δ 66.73 (s, 2H, aryl CH), 61.69 (br s, 2H, aryl CH), 56.76 (s, 1H), 34.20 (s, 2H, aryl CH), 28.83 (br s, 2H, aryl CH), 26.28 (s, 3H, CH₃), 24.08 (s, 1H), 23.01 (s, 1H), 22.19 (s, 1H), 17.31 (s, 1H), 12.90 (s, 3H, CH₃), 10.38 (s, 1H), 8.65 (s, 1H), 0.89 (s, 1H), -3.09 (s, 3H, CH₃), -3.54 (s, 1H), -4.51 (s, 1H), -5.57 (s, 1H), -14.40 (s, 1H), -15.98 (1H), -17.19 (s, 1H), -19.54 (s, 3H, CH₃), -24.26 (br s, 2H, aryl

CH), -29.65 (s, 1H), -34.84 (s, 3H, CH₃), -39.66 (s, 1H), -45.43 (br s, 2H, aryl CH), -47.87 (s, 1H), -53.42 (s, 1H), -58.43 (s, 1H), -58.47 (br s, 2H, aryl CH), -64.81 (s, 3H, CH₃). One CH resonance, integrating to 1H, and one aryl CH resonance, integrating to 2H, were not observed. ⁷Li{¹H} NMR (C₆D₆, 25 °C, 155 MHz): δ -117.68 (s). UV-vis/NIR (C₆H₆, 6.23 × 10⁻³ M, L·mol⁻¹·cm⁻¹): 516 (sh, ε = 22), 546 (ε = 21), 572 (sh, ε = 14), 622 (sh, ε = 10), 678 (ε = 25), 752 (ε = 5), 832 (ε = 5), 952 (sh, ε = 14), 1034 (ε = 30), 1066 (ε = 30), 1150 (ε = 48), 1290 (ε = 25), 1448 (ε = 14), 1570 (ε = 11), 1774 (ε = 8), 1818 (sh, ε = 7). IR (KBr pellet, cm⁻¹): 3070 (w), 3040 (w), 3027 (m), 2954 (sh m), 2956 (m), 2852 (m), 2819 (m), 2777 (m), 2686 (sh w), 1595 (w), 1489 (m), 1462 (sh m), 1456 (m), 1444 (s), 1402 (w), 1381 (w), 1358 (sh w), 1352 (w), 1309 (w), 1282 (w), 1261 (w), 1234 (w), 1173 (m), 1153 (w), 1140 (w), 1113 (w), 1093 (w), 1082 (w), 1036 (s), 1028 (s), 1007 (sh s), 1001 (s), 931 (w), 910 (w), 895 (w), 845 (m), 841 (sh m), 823 (w), 785 (m), 764 (m), 756 (s), 746 (m), 723 (w), 700 (vs), 673 (w), 642 (m), 644 (m), 632 (w), 617 (w), 567 (w), 528 (w), 472 (w), 441 (w), 426 (w).

7.4.4 Synthesis of [Li][Li(Et₂O)][U(2,3-C₆H₃CH₂NMe₂)(2-C₆H₃CH₂NMe₂-3-C(Ph)=N)(2-C₆H₄CH₂NMe₂)₂] (7.4). To a cold (-25 °C) stirring dark blue solution of complex **7.1** (83.2 mg, 0.106 mmol) in Et₂O (2 mL) was added cold (-25 °C) PhCN (22 μL, 0.213 mmol) via microsyringe. The solution turned a dark green-brown color within seconds of addition. The solution was allowed to warm to room temperature, with stirring. After 30 min, the volatiles were removed *in vacuo* to produce a tacky dark brown solid. This material was extracted into Et₂O (2.5 mL), and the resulting brown solution was quickly filtered through a Celite column (2 cm × 0.5 cm) supported on glass wool. The volume of the dark green-brown filtrate was then reduced *in vacuo*

to ca. 1 mL. Storage of this solution at -25 °C for 2 weeks resulted in the deposition of dark green-brown crystals of **7.4** (20.9 mg, 21% yield). Anal. Calcd for $\text{ULi}_2\text{N}_5\text{OC}_{47}\text{H}_{61}$: C, 58.56; H, 6.38; N, 7.27. Found: C, 58.93; H, 6.34; N, 7.45. ^1H NMR (C_6D_6 , 25 °C, 400 MHz): δ 44.68 (br s, 1H), 34.69 (s, 1H), 28.19 (s, 1H), 27.52 (s, 1H), 27.03 (s, 1H), 26.05 (s, 3H), 24.91 (s, 1H), 24.41 (s, 1H), 20.13 (s, 2H), 18.80 (s, 3H), 14.82 (s, 1H), 13.43 (s, 1H), 9.79 (s, 1H), 9.36 (s, 1H), 9.04 (s, 1H), 6.86 (s, 3H), 6.37 (s, 3H), 4.99 (s, 1H), 0.96 (s, 3H), -0.30 (s, 1H), -1.07 (s, 1H), -5.86 (s, 3H), -6.04 (s, 1H), -10.93 (s, 1H), -22.53 (br s, 2H, aryl CH), -28.87 (s, 1H), -30.97 (s, 1H), -32.00 (s, 3H), -46.36 (br s, 2H, aryl CH). One CH_3 resonance, three CH resonances, and the Et_2O resonances were not assigned. $^7\text{Li}\{^1\text{H}\}$ NMR (C_6D_6 , 25 °C, 155 MHz): δ 182.26 (s, 1Li), -69.42 (s, 1Li). UV-vis/NIR (Et_2O , 1.99×10^{-3} M, $\text{L}\cdot\text{mol}^{-1}\cdot\text{cm}^{-1}$): 718 ($\epsilon = 606$), 1114 ($\epsilon = 167$), 1164 ($\epsilon = 176$), 1224 ($\epsilon = 150$), 1444 ($\epsilon = 78$), 1610 ($\epsilon = 63$). IR (KBr pellet, cm^{-1}): 3026 (w), 2966 (m), 2949 (m), 2831 (m), 2818 (s), 2775 (s), 2702 (w), 1599 (s), 1589 (sh m), 1570 (m), 1541 (w), 1481 (m), 1464 (sh vs), 1454 (vs), 1429 (sh m), 1362 (m), 1275 (m), 1261 (m), 1242 (m), 1173 (m), 1146 (w), 1093 (m), 1070 (w), 1039 (sh m), 1028 (s), 1005 (s), 989 (sh m), 881 (w), 850 (s), 827 (m), 802 (m), 771 (sh m), 758 (m), 742 (s), 702 (s), 646 (w), 617 (w).

7.4.5 Synthesis of $[\text{Li}][\text{Li}(\text{Et}_2\text{O})][\text{U}(\text{2,3-C}_6\text{H}_3\text{CH}_2\text{NMe}_2)(\text{5-C}_6\text{H}_3\text{CH}_2\text{NMe}_2\text{-2-S})(\text{2-C}_6\text{H}_4\text{CH}_2\text{NMe}_2)_2]$ (7.5**).** To a cold (-25 °C) stirring dark blue solution of complex **7.1** (36.2 mg, 0.046 mmol) in Et_2O (2 mL), was added cold (-25 °C) ethylene sulfide (11.0 μL , 0.185 mmol) via microsyringe. The solution quickly changed to a vibrant red color after addition. The solution was allowed to warm to room temperature, with stirring. After 20 min, the red solution was filtered through a Celite column (2 cm \times 0.5 cm)

supported on glass wool. The resulting red filtrate was concentrated *in vacuo*, and stored at -25 °C for 24 h. This resulted in the deposition of a few red crystals of complex 7.5.

7.4.6 Synthesis of [Li(12-crown-4)₂][Li][U(2-C₆H₃CH₂NMe₂-3-(N-N=N-Ad))₂(2-C₆H₄CH₂NMe₂)₂] (7.6). To a cold (-25 °C) stirring dark blue solution of complex 7.1 (70.4 mg, 0.089 mmol) in Et₂O (2 mL), was added a cold (-25 °C) solution of AdN₃ (32.1 mg, 0.181 mmol) in Et₂O (1 mL). The solution quickly changed to a vibrant red color after addition. The solution was allowed to warm to room temperature, with stirring. After 10 min, 12-crown-4 (29 μL, 0.179 mmol) was added to the solution via microsyringe, which resulted in no visible change. The red solution was then filtered through a Celite column (2 cm × 0.5 cm) supported on glass wool. The resulting red filtrate was transferred to a 4mL scintillation vial that was placed inside a 20mL scintillation vial. Toluene (2 mL) was then added to the outer vial. Storage of this two vial system at -25 °C for 72 h afforded red crystals, which were isolated by decanting off the supernatant (55.8 mg, 42% yield). Anal. Calcd for ULi₂N₁₀O₈C₇₂H₁₀₈: C, 57.90; H, 7.29; N, 9.38. Found: C, 57.52; H, 6.88; N, 9.59. ¹H NMR (THF-*d*₈, 25 °C, 400 MHz): δ 48.68 (s, 1H), 40.32 (s, 1H), 26.34 (br s, 1H), 25.50 (s, 1H), 24.09 (s, 1H), 23.79 (s, 1H), 22.82 (s, 1H), 22.67 (s, 1H), 17.68 (s, 1H), 13.71 (s, 3H), 12.44 (s, 1H), 10.47 (s, 3H), 10.04 (s, 1H), 7.83 (br d, *J*_{HH} = 9.2 Hz, 1H), 5.86 (s, 3H), 5.42 (d, *J*_{HH} = 11.0 Hz, 3H), 4.47 (d, *J*_{HH} = 10.9 Hz, 3H), 3.74 (s, 1H), 3.58 (s, 32H, crown), 3.22 (s, 1H), 2.29 (s, 1H), 2.05 (s, 1H), 0.88 (s, 1H), 0.76 (br s, 3H), 0.55 (s, 1H), 0.09 (s, 1H), -1.42 (d, *J*_{HH} = 7.6 Hz, 3H), -2.13 (s, 3H), -2.53 (d, *J*_{HH} = 8.8 Hz, 3H), -7.93 (br s, 1H), -8.08 (d, *J*_{HH} = 9.4 Hz, 3H), -8.16 (d, *J*_{HH} = 11.6 Hz, 3H), -22.36 (s, 1H), -23.50 (s, 3H), -62.70 (s, 3H). One CH resonance,

integrating to 1H, one CH₃ resonance, integrating to 3H, and two CH₃ resonances, integrating to 6H, were not assigned. ⁷Li{¹H} NMR (THF-*d*₈, 25 °C, 155 MHz): δ 75.15 (s), 0.98 (s), -44.63 (s). UV-vis/NIR (Et₂O, 4.97 × 10⁻³ M, L·mol⁻¹·cm⁻¹): 730 (ε = 57), 900 (ε = 3.6), 964 (ε = 4.2), 1066 (ε = 37.7), 1112 (ε = 75.6), 1176 (ε = 117.3), 1212 (ε = 99.6), 1426 (ε = 41.1), 1592 (ε = 19). IR (KBr pellet, cm⁻¹): 3028 (w), 2952 (sh m), 2922 (sh s), 2900 (s), 2846 (s), 2814 (m), 2765 (m), 1603 (sh w), 1591 (w), 1545 (w), 1489 (sh w), 1475 (sh w), 1460 (sh m), 1450 (s), 1421 (m), 1379 (s), 1363 (s), 1342 (m), 1306 (m), 1288 (m), 1254 (sh s), 1244 (s), 1201 (m), 1169 (m), 1132 (vs), 1093 (vs), 1039 (sh m), 1024 (s), 1005 (m), 976 (w), 922 (m), 849 (m), 814 (w), 783 (w), 741 (w), 731 (sh w), 696 (w), 665 (w), 636 (w), 552 (w), 463 (w).

7.4.7 X-ray Crystallography. The solid-state molecular structures of complexes **7.1** – **7.6** were determined similarly with exceptions noted in the following paragraph. Crystals were mounted on a cryoloop under Paratone-N oil. Data collection was carried out on a Bruker KAPPA APEX II diffractometer equipped with an APEX II CCD detector using a TRIUMPH monochromator with a Mo K α X-ray source ($\alpha = 0.71073 \text{ \AA}$). Data for **7.1** – **7.6** were collected at 100(2) K, using an Oxford nitrogen gas cryostream system. A hemisphere of data was collected using ω scans with 0.3° frame widths. Frame exposures of 30, 20, 10, 10, 30 and 30 seconds were used for complexes **7.1**, **7.2**, **7.3**, **7.4**, **7.5** and **7.6**, respectively. Data collection and cell parameter determination were conducted using the SMART program.⁶⁸ Integration of the data frames and final cell parameter refinement were performed using SAINT software.⁶⁹ Absorption correction of the data was carried out using the multi-scan method SADABS.⁷⁰ Subsequent

calculations were carried out using SHELXTL.⁷¹ Structure determination was done using direct or Patterson methods and difference Fourier techniques. All hydrogen atom positions were idealized, and rode on the atom of attachment. However, hydrogen atoms were not assigned to the disordered carbon atoms. Structure solution, refinement, graphics, and creation of publication materials were performed using SHELXTL.⁷¹

Complex **7.3** contains a hexane solvent molecule that exhibits mild positional disorder. Hydrogen atoms were not assigned to these carbon atoms. Complex **7.4** contains an Et₂O solvent molecule within the main residue that exhibits positional disorder of the CH₃ groups. The positional disorder was addressed by modeling the CH₃ groups in two orientations in a 50:50 ratio. The Et₂O carbon atoms were not refined anisotropically and were constrained with the EADP, DFIX, and FLAT commands. Complex **7.6** exhibits positional disorder of one 1-adamantyl group. The positional disorder was addressed by modeling the adamantyl group in two orientations in a 50:50 ratio. The EADP and DFIX commands were used to constrain both orientations. Complex **7.6** also contains an Et₂O solvent molecule that exhibited positional disorder, which was address by modeling the molecule in two orientations in a 50:50 ratio. Disordered atoms of the 1-adamantyl group and the Et₂O solvent molecule were not refined anisotropically and were constrained with the EADP, DFIX, and FLAT commands. Complex **7.6** also exhibits some mild positional disorder of the carbon atoms in one of the 12-crown-4 moieties. These atoms were constrained with the EADP and DFIX commands. A summary of relevant crystallographic data for **7.1-7.6** is presented in Tables 7.2 – 7.3.

Table 7.2. X-ray Crystallographic Information for **7.1** – **7.3**

	7.1	7.2	7.3·0.5C₆H₁₄
empirical formula	ULi ₂ N ₄ C ₃₆ H ₄₆	ULi ₂ N ₄ O ₂ C ₄₄ H ₆₂	ULiN ₃ O ₂ C ₅₆ H ₆₁
Crystal habit, color	square, blue	rod, brown	plate, red-orange
crystal size (mm)	0.10 × 0.10 × 0.05	0.1 × 0.05 × 0.04	0.30 × 0.20 × 0.05
crystal system	monoclinic	monoclinic	monoclinic
space group	<i>C2/c</i>	<i>P2₁/n</i>	<i>P2₁/c</i>
vol (Å ³)	3413.5(2)	4203(2)	4523.3(3)
a (Å)	25.7342(8)	21.494(5)	17.3133(7)
b (Å)	9.9023(4)	10.946(2)	13.2031(6)
c (Å)	18.1648(9)	18.895(4)	20.2884(8)
α (deg)	90	90	90
β (deg)	132.487(2)	109.009(4)	102.751(2)
γ (deg)	90	90	90
Z	4	4	4
fw (g/mol)	786.68	930.89	1053.05
density (calcd) (Mg/m ³)	1.531	1.471	1.546
abs coeff (mm ⁻¹)	4.789	3.901	3.635
F ₀₀₀	1552	1872	2116
Total no. reflections	11593	26296	31161
Unique reflections	3491	8565	11212
final R indices [I > 2σ(I)]	R ₁ = 0.0263 wR ₂ = 0.0501	R ₁ = 0.0419 wR ₂ = 0.0614	R ₁ = 0.0356 wR ₂ = 0.0734
largest diff peak and hole (e ⁻ Å ⁻³)	1.119 and -0.720	1.665 and -1.737	2.748 and -2.687
GOF	0.995	0.929	1.010

Table 7.3. X-ray Crystallographic Information for **7.4 – 7.6**

	7.4	7.5	7.6·OC₄H₁₀
empirical formula	ULi ₂ N ₅ OC ₄₇ H ₆₁	ULi ₂ N ₄ OSC ₄₀ H ₅₆	ULi ₂ N ₁₀ O ₉ C ₇₆ H ₁₀₅
Crystal habit, color	shard, brown	plate, red	plate, red
crystal size (mm)	0.05 × 0.025 × 0.01	0.20 × 0.10 × 0.05	0.1 × 0.05 × 0.025
crystal system	monoclinic	monoclinic	monoclinic
space group	<i>P</i> 2 ₁ / <i>n</i>	<i>P</i> 2 ₁ / <i>n</i>	<i>P</i> 2 ₁ / <i>n</i>
vol (Å ³)	4310(2)	8923.0(5)	8115(4)
a (Å)	9.993(3)	11.6066(8)	11.966(3)
b (Å)	19.938(4)	17.008(1)	26.333(7)
c (Å)	22.005(6)	19.985(2)	25.774(7)
α (deg)	90	90	90
β (deg)	100.579(8)	96.068(5)	92.425(5)
γ (deg)	90	90	90
Z	4	4	4
fw (g/mol)	953.84	892.86	1554.60
density (calcd) (Mg/m ³)	1.470	1.512	1.273
abs coeff (mm ⁻¹)	3.806	4.226	2.057
F ₀₀₀	1896	1784	3204
Total no. reflections	16676	90457	36957
Unique reflections	7409	17260	16552
final R indices [I > 2σ(I)]	R ₁ = 0.0722 wR ₂ = 0.1245	R ₁ = 0.0648 wR ₂ = 0.0807	R ₁ = 0.0806 wR ₂ = 0.2109
largest diff peak and hole (e ⁻ Å ⁻³)	1.506 and -1.135	3.349 and -1.868	3.162 and -2.924
GOF	0.959	1.257	1.035

7.5 Acknowledgements

I would like to thank Dr. Lani Seaman for pioneering this research project, by obtaining the solid-state structures of complexes **7.1** and **7.2**, and for performing some preliminary reactivity studies before she graduated. Additionally, I would like to thank my undergraduate student, Joshua Scott, for synthesizing complexes **7.4** and **7.5**, as well as my other undergraduate student, Leonel Griego, for both the synthesis and characterization of complex **7.3**.

7.6 References

- (1) Graves, C. R.; Schelter, E. J.; Cantat, T.; Scott, B. L.; Kiplinger, J. L. *Organometallics* **2008**, *27*, 5371.
- (2) Evans, W. J.; Miller, K. A.; Ziller, J. W.; DiPasquale, A. G.; Heroux, K. J.; Rheingold, A. L. *Organometallics* **2007**, *26*, 4287.
- (3) Montalvo, E.; Ziller, J. W.; DiPasquale, A. G.; Rheingold, A. L.; Evans, W. J. *Organometallics* **2010**, *29*, 2104.
- (4) Ren, W.; Zhou, E.; Fang, B.; Zi, G.; Fang, D.-C.; Walter, M. D. *Chem. Sci.* **2014**, *5*, 3165.
- (5) Korobkov, I.; Arunachalampillai, A.; Gambarotta, S. *Organometallics* **2004**, *23*, 6248.
- (6) Korobkov, I.; Gorelsky, S.; Gambarotta, S. *J. Am. Chem. Soc.* **2009**, *131*, 10406.
- (7) Evans, W. J.; Walensky, J. R.; Ziller, J. W.; Rheingold, A. L. *Organometallics* **2009**, *28*, 3350.
- (8) Evans, W. J.; Kozimor, S. A.; Hillman, W. R.; Ziller, J. W. *Organometallics* **2005**, *24*, 4676.
- (9) Fagan, P. J.; Manriquez, J. M.; Maatta, E. A.; Seyam, A. M.; Marks, T. J. *J. Am. Chem. Soc.* **1981**, *103*, 6650.
- (10) Pedrick, E. A.; Hrobarik, P.; Seaman, L. A.; Wu, G.; Hayton, T. W. *Chem. Commun.* **2016**, *52*, 689.

- (11) Seaman, L. A.; Pedrick, E. A.; Tsuchiya, T.; Wu, G.; Jakubikova, E.; Hayton, T. W. *Angew. Chem. Int. Ed.* **2013**, *52*, 10589.
- (12) Petrov, A. R.; Rufanov, K. A.; Harms, K.; Sundermeyer, J. J. *Organomet. Chem.* **2009**, *694*, 1212.
- (13) Boker, C.; Noltemeyer, M.; Gornitzka, H.; Kneisel, B. O.; Teichert, M.; Herbst-Irmer, R.; Meller, A. *Main Group Met. Chem.* **1998**, *21*, 565.
- (14) Cotton, F. A.; Mott, G. N. *Inorg. Chem.* **1981**, *20*, 3896.
- (15) Manzer, L. E.; Gearhart, R. C.; Guggenberger, L. J.; Whitney, J. F. *Chem. Commun.* **1976**, 942.
- (16) Khan, O. F. Z.; Frigo, D. M.; O'Brien, P.; Howes, A.; Hursthouse, M. B. *J. Organomet. Chem.* **1987**, *334*, C27.
- (17) Silva, M.; Domingos, A.; Pires de Matos, A.; Marques, N.; Trofimenko, S. *Dalton Trans.* **2000**, 4628.
- (18) Tadross, P. M.; Stoltz, B. M. *Chem. Rev.* **2012**, *112*, 3550.
- (19) Erker, G.; Kropp, K. *J. Am. Chem. Soc.* **1979**, *101*, 3659.
- (20) Buchwald, S. L.; Watson, B. T.; Huffman, J. C. *J. Am. Chem. Soc.* **1986**, *108*, 7411.
- (21) Aseman, M. D.; Roselli, C. A.; Gagné, M. R. *Organometallics* **2015**, *34*, 2707.
- (22) McLain, S. J.; Schrock, R. R.; Sharp, P. R.; Churchill, M. R.; Youngs, W. J. *J. Am. Chem. Soc.* **1979**, *101*, 263.
- (23) Bennett, M. A.; Hambley, T. W.; Roberts, N. K.; Robertson, G. B. *Organometallics* **1985**, *4*, 1992.
- (24) Bartlett, R. A.; Power, P. P.; Shoner, S. C. *J. Am. Chem. Soc.* **1988**, *110*, 1966.
- (25) Sasamori, T.; Sasaki, T.; Takeda, N.; Tokitoh, N. *Organometallics* **2005**, *24*, 612.
- (26) Buijink, J. K. F.; Kloetstra, K. R.; Meetsma, A.; Teuben, J. H.; Smeets, W. J. J.; Spek, A. L. *Organometallics* **1996**, *15*, 2523.
- (27) Churchill, M. R.; Youngs, W. J. *Inorg. Chem.* **1979**, *18*, 1697.
- (28) Appleton, T. G.; Bennett, M. A.; Singh, A.; Yoshida, T. *J. Organomet. Chem.* **1978**, *154*, 369.
- (29) Sato, Y.; Tamura, T.; Mori, M. *Angew. Chem., Int. Ed.* **2004**, *43*, 2436.
- (30) Deaton, K. R.; Gin, M. S. *Org. Lett.* **2003**, *5*, 2477.
- (31) Bennett, M. A.; Wenger, E. *Organometallics* **1995**, *14*, 1267.
- (32) Bennett, M. A.; Wenger, E. *Organometallics* **1996**, *15*, 5536.
- (33) Gevorgyan, V.; Radhakrishnan, U.; Takeda, A.; Rubina, M.; Rubin, M.; Yamamoto, Y. *J. Org. Chem.* **2001**, *66*, 2835.
- (34) Sugihara, T.; Wakabayashi, A.; Nagai, Y.; Takao, H.; Imagawa, H.; Nishizawa, M. *Chem. Commun.* **2002**, 576.
- (35) Wang, W.; Peng, X.; Qin, X.; Zhao, X.; Ma, C.; Tung, C.-H.; Xu, Z. *J. Org. Chem.* **2015**, *80*, 2835.
- (36) Bennett, M. A.; Schwemlein, H. P. *Angew. Chem. Int. Ed. Engl.* **1989**, *28*, 1296.
- (37) Hartwig, J. F.; Andersen, R. A.; Bergman, R. G. *J. Am. Chem. Soc.* **1989**, *111*, 2717.

- (38) Hartwig, J. F.; Bergman, R. G.; Andersen, R. A. *J. Am. Chem. Soc.* **1991**, *113*, 3404.
- (39) Fang, B.; Ren, W.; Hou, G.; Zi, G.; Fang, D.-C.; Maron, L.; Walter, M. D. *J. Am. Chem. Soc.* **2014**, *136*, 17249.
- (40) Fang, B.; Zhang, L.; Hou, G.; Zi, G.; Fang, D.-C.; Walter, M. D. *Chem. Sci.* **2015**, *6*, 4897.
- (41) Sarry, B.; Schön, M. *J. Organomet. Chem.* **1968**, *13*, 9.
- (42) Sarry, B.; Grossmann, H. *Z. Anorg. Allg. Chem.* **1968**, *359*, 234.
- (43) Sarry, B.; Velling, P. *Z. Anorg. Allg. Chem.* **1983**, *500*, 199.
- (44) Sarry, B.; Schaffernicht, R. *Z. Naturforsch.* **1981**, *B36*, 1238.
- (45) Pedrick, E. A.; Wu, G.; Hayton, T. W. *Inorg. Chem.* **2015**, *54*, 7038.
- (46) Fortier, S.; Walensky, J. R.; Wu, G.; Hayton, T. W. *J. Am. Chem. Soc.* **2011**, *133*, 11732.
- (47) Wu, J. Y.; Stanzl, B. N.; Ritter, T. *J. Am. Chem. Soc.* **2010**, *132*, 13214.
- (48) Kraft, S. J.; Fanwick, P. E.; Bart, S. C. *Organometallics* **2013**, *32*, 3279.
- (49) Kiernicki, J. J.; Newell, B. S.; Matson, E. M.; Anderson, N. H.; Fanwick, P. E.; Shores, M. P.; Bart, S. C. *Inorg. Chem.* **2014**, *53*, 3730.
- (50) Villiers, C.; Adam, R.; Lance, M.; Nierlich, M.; Vigner, J.; Ephritikhine, M. *Chem. Commun.* **1991**, 1144.
- (51) Lam, O. P.; Anthon, C.; Heinemann, F. W.; O'Connor, J. M.; Meyer, K. *J. Am. Chem. Soc.* **2008**, *130*, 6567.
- (52) Cohen, D.; Carnall, W. T. *J. Phys. Chem.* **1960**, *64*, 1933
- (53) Monreal, M. J.; Diaconescu, P. L. *Organometallics* **2008**, *27*, 1702.
- (54) Jantunen, K. C.; Burns, C. J.; Castro-Rodriguez, I.; Da Re, R. E.; Golden, J. T.; Morris, D. E.; Scott, B. L.; Taw, F. L.; Kiplinger, J. L. *Organometallics* **2004**, *23*, 4682.
- (55) Fang, B.; Zhang, L.; Hou, G.; Zi, G.; Fang, D.-C.; Walter, M. D. *Organometallics* **2015**, *34*, 5669.
- (56) Seaman, L. A.; Wu, G.; Edelstein, N. M.; Lukens, W. W.; Magnani, N.; Hayton, T. W. *J. Am. Chem. Soc.* **2012**, *134*, 4931.
- (57) Lewis, R. A.; Wu, G.; Hayton, T. W. *J. Am. Chem. Soc.* **2010**, *132*, 12814.
- (58) Beuter, G.; Drobnik, S.; Lorenz, I.-P.; Lubik, A. *Chem. Ber.* **1992**, *125*, 2363.
- (59) Proulx, G.; Bergman, R. G. *Organometallics* **1996**, *15*, 133.
- (60) Smiles, D. E.; Wu, G.; Hayton, T. W. *Inorg. Chem.* **2014**, *53*, 12683.
- (61) Brown, J. L.; Wu, G.; Hayton, T. W. *Organometallics* **2013**, *32*, 1193.
- (62) Beck, R.; Frey, M.; Camadanli, S.; Klein, H.-F. *Dalton Trans.* **2008**, 4981.
- (63) Evans, W. J.; Walensky, J. R.; Ziller, J. W. *Organometallics* **2010**, *29*, 101.
- (64) Kiplinger, J. L.; Morris, D. E.; Scott, B. L.; Burns, C. J. *Organometallics* **2002**, *21*, 5978.
- (65) Jones, F. N.; Zinn, M. F.; Hauser, C. R. *J. Org. Chem.* **1963**, *28*, 663.
- (66) Harris, R. K.; Becker, E. D.; Cabral De Menezes, S. M.; Goodfellow, R.; Granger, P. *Pure Appl. Chem.* **2001**, *73*, 1795.
- (67) Harris, R. K.; Becker, E. D.; Cabral De Menezes, S. M.; Granger, P.; Hoffman, R. E.; Zilm, K. W. *Pure Appl. Chem.* **2008**, *80*, 59.
- (68) SMART, Apex II, Version 2.1; Bruker AXS Inc.: Madison, WI, 2005.
- (69) SAINT, Software User's Guide, Version 7.34a; Bruker AXS Inc.: Madison, WI, 2005.

- (70) Sheldrick, G. M. *SADABS*, University of Gottingen: Germany, 2005.
- (71) *SHELXTL PC*, Version 6.12; Bruker AXS Inc.: Madison, WI, 2005.

Appendix A

Table A.1. Electrochemical parameters for $\text{UO}_2(\text{dbm})_2(\text{THF})$ (**2.1**) in CH_2Cl_2 (vs. Fc/Fc^+ , $[\text{NBu}_4][\text{PF}_6]$ as supporting electrolyte).

Reduction feature	Scan rate, V/s	$E_{p,c}$, V		
	0.025	-1.167		
	0.05	-1.154		
	0.1	-1.189		
	0.25	-1.206		
	0.5	-1.230		
	0.75	-1.248		
	1	-1.283		
Ferrocene	Scan rate, V/s	$E_{p,a}$, V	ΔE_p, V	$i_{p,c}/i_{p,a}$
	0.025	0.052	0.089	1.06
	0.05	0.062	0.094	1.06
	0.1	0.051	0.109	1.05
	0.25	0.059	0.132	1.07
	0.5	0.072	0.160	1.09
	0.75	0.082	0.155	1.13
	1	0.086	0.200	1.15

ΔE_p is defined as the potential difference between the cathodic wave and the anodic wave generated after the change in sweep direction.

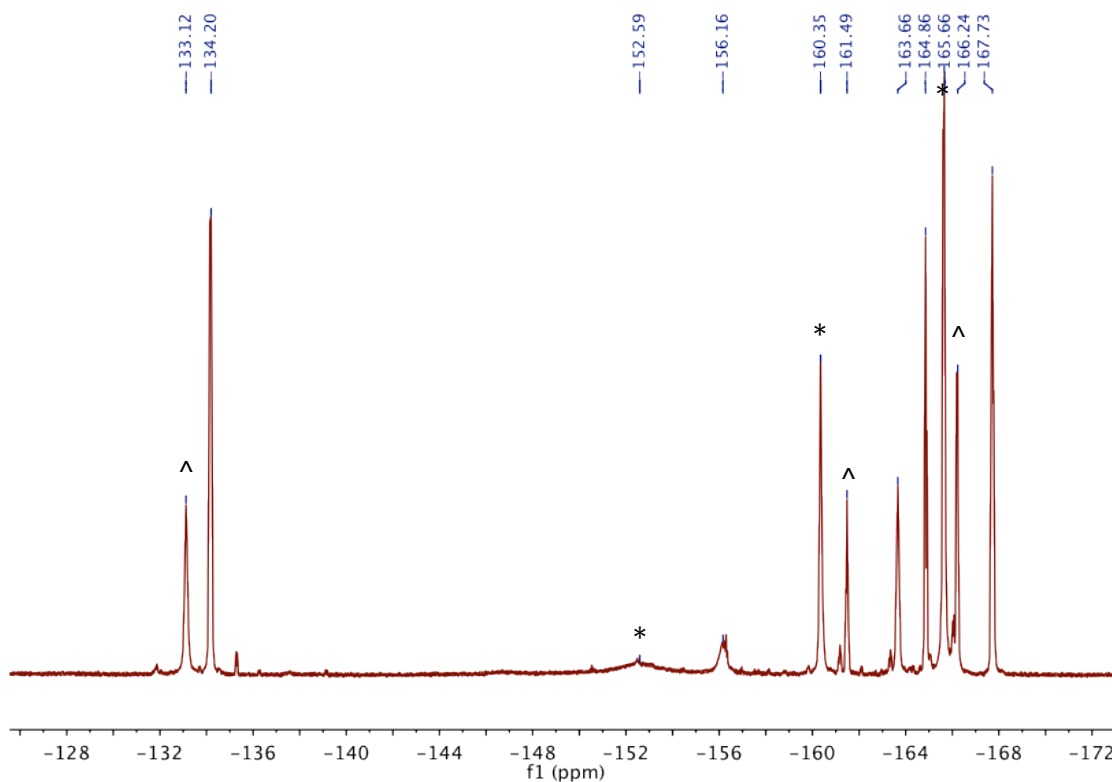


Figure A.1. $^{19}\text{F}\{^1\text{H}\}$ NMR spectrum of the *in situ* reaction of $\text{UO}_2(\text{dbm})_2(\text{THF})$ with 1 equiv of $\text{B}(\text{C}_6\text{F}_5)_3$ and 2 equiv HSiEt_3 in CD_2Cl_2 ; after 24 h at 25 °C. **Experimental Details:** To an orange CD_2Cl_2 solution (1 mL) containing $\text{UO}_2(\text{dbm})_2(\text{THF})$ (24.1 mg, 0.030 mmol) was added dropwise a colorless CD_2Cl_2 solution (0.75 mL) of $\text{B}(\text{C}_6\text{F}_5)_3$ (16.0 mg, 0.031 mmol) and HSiEt_3 (10 μL , 0.061 mmol), resulting in a color change to deep red. The tube was sealed, and the ^1H and $^{19}\text{F}\{^1\text{H}\}$ NMR spectra were recorded after standing at room temperature for 24 h (^{19}F spectrum shown above). These spectra revealed the formation of **2.3** and **2.4**, in a 1:2 ratio, which was determined by comparing the integrations of the *meta* C–F resonances in the ^{19}F NMR spectrum. Asterisks indicate resonances assignable to complex **2.4**, while ^ indicates resonances assignable to complex **2.3**. Several other ^{19}F resonances are observed that were not assignable to any known species.

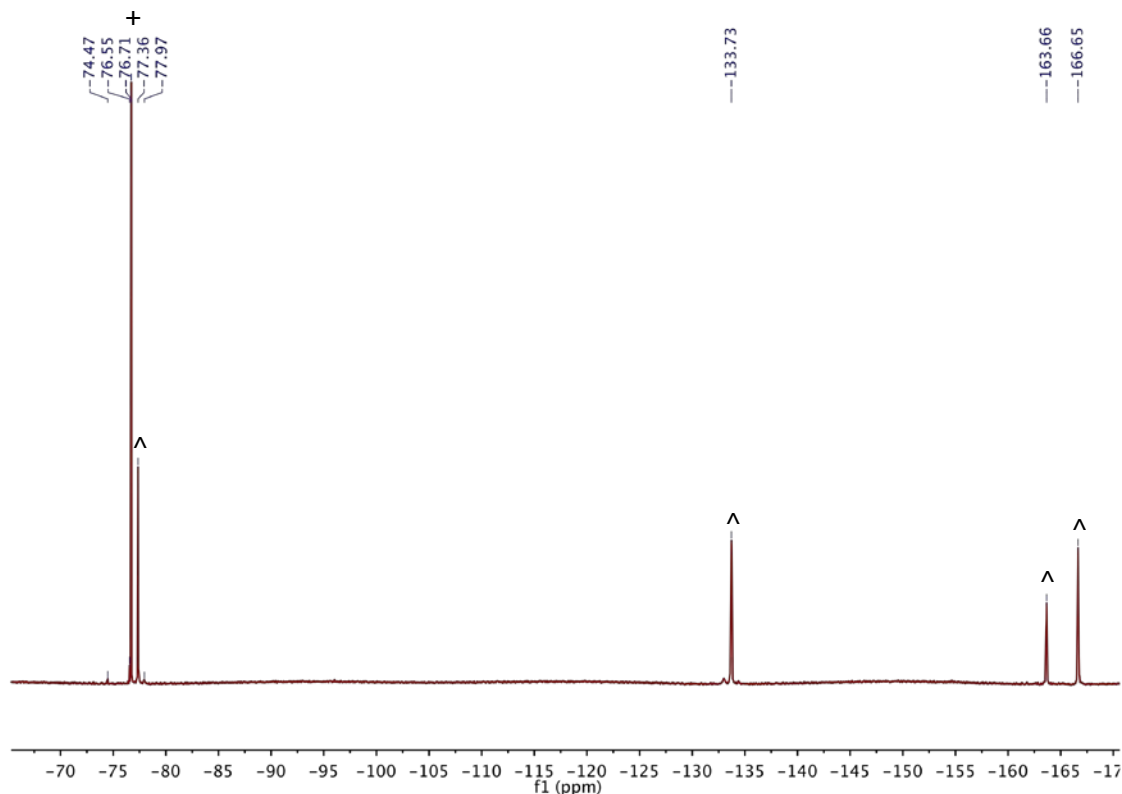


Figure A.2. $^{19}\text{F}\{^1\text{H}\}$ NMR spectrum of the *in situ* reaction of $[\text{UO}_2(\text{dppmo})_2\text{OTf}][\text{OTf}]$ with 2 equiv Ph_3SiH and $\text{B}(\text{C}_6\text{F}_5)_3$ in $\text{TCE-}d_2$; after 5 min at 25 °C. **Experimental Details:** A pale yellow $\text{TCE-}d_2$ solution (1 mL) containing $[\text{UO}_2(\text{dppmo})_2\text{OTf}][\text{OTf}]$ (31.0 mg, 0.022 mmol) was sealed in a J. Young NMR tube, and the ^1H , $^{19}\text{F}\{^1\text{H}\}$, and $^{31}\text{P}\{^1\text{H}\}$ NMR spectra was recorded. Then a colorless CD_2Cl_2 solution (1 mL) of Ph_3SiH (12.1 mg, 0.046 mmol) and $\text{B}(\text{C}_6\text{F}_5)_3$ (23.5 mg, 0.046 mmol) was added dropwise, resulting in a pale yellow solution. The tube was sealed, and the ^1H , ^{11}B , $^{19}\text{F}\{^1\text{H}\}$, and $^{31}\text{P}\{^1\text{H}\}$ NMR spectra were recorded after standing at room temperature for 5 min (^{19}F spectrum shown above). The J. Young NMR tube was then thermolyzed for 72 h at 105 °C, whereupon a color change to pale green is observed and the ^1H , ^{11}B , $^{19}\text{F}\{^1\text{H}\}$, and $^{31}\text{P}\{^1\text{H}\}$ NMR spectra were recorded again. ^ indicates resonances assignable to $[\text{UO}_2(\text{dppmo})_2\text{OTf}][\text{H}(\text{BC}_6\text{F}_5)_3]$, and + indicates resonances assignable to Ph_3SiOTf .

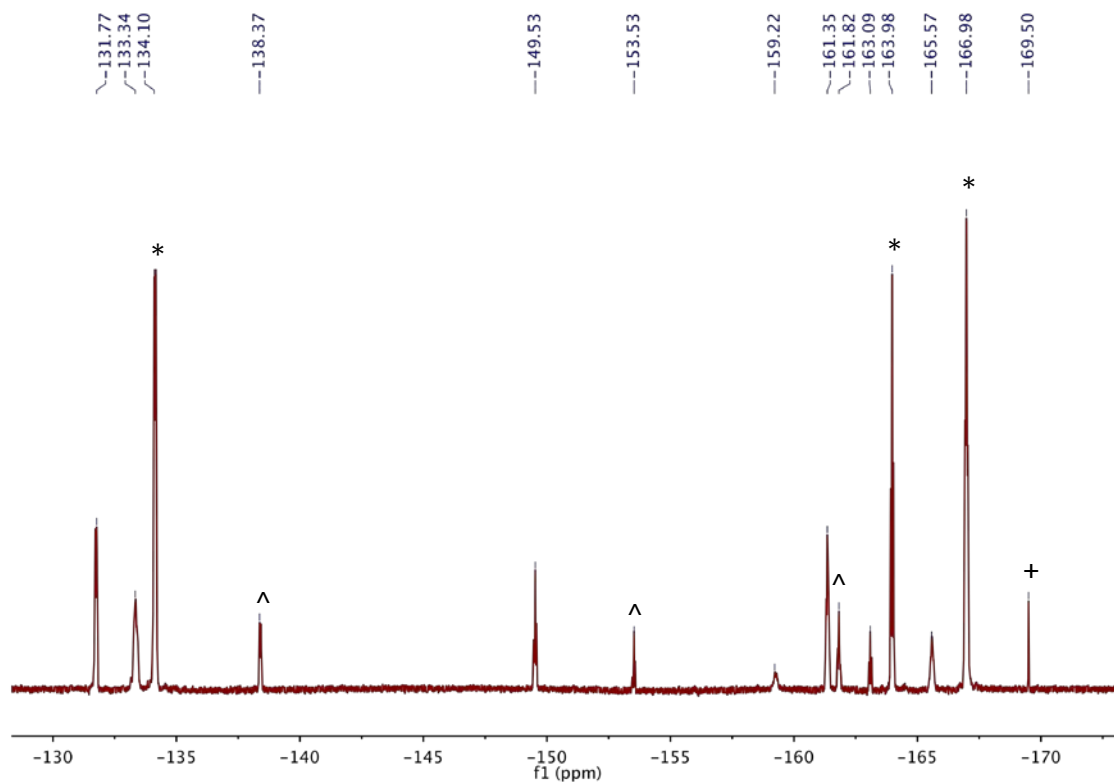


Figure A.3. Partial $^{19}\text{F}\{^1\text{H}\}$ NMR spectrum of the *in situ* reaction of $[\text{UO}_2(\text{dppmo})_2\text{OTf}][\text{OTf}]$ with 2 equiv Ph_3SiH and $\text{B}(\text{C}_6\text{F}_5)_3$ in $\text{TCE-}d_2$; after 72 h at 105 °C. **Experimental Details:** See Figure A.2. Astericks indicates resonances assignable to $[\text{B}(\text{C}_6\text{F}_5)_4]^-$, ^ indicates resonances assignable to pentafluorobenzene, and + indicates resonances assignable to Ph_3SiF .

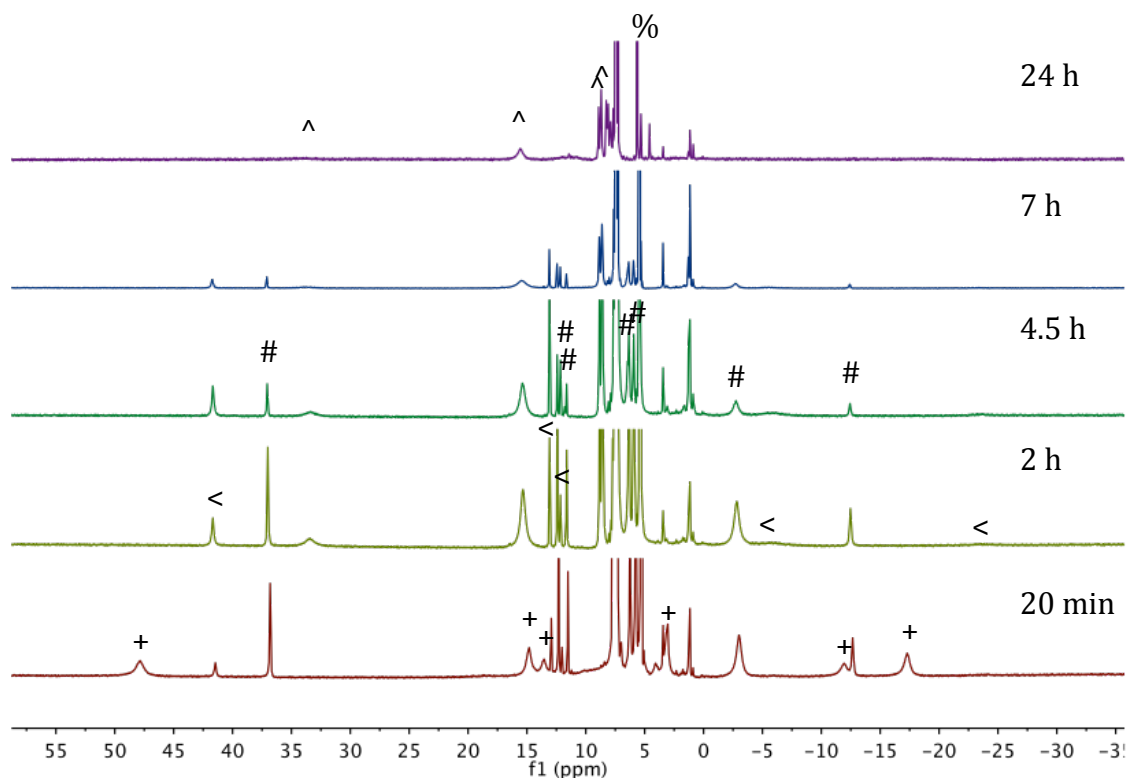


Figure A.4. ^1H NMR spectra of the *in situ* reaction of $[\text{UO}_2(\text{dppmo})_2(\text{OTf})][\text{OTf}]$ with 4 equiv of Ph_3SiOTf and 2 equiv of Cp_2Co in CD_2Cl_2 . **Experimental Details:** To a stirring pale yellow CD_2Cl_2 solution (1 mL) containing $[\text{UO}_2(\text{dppmo})_2(\text{OTf})][\text{OTf}]$ (34.3 mg, 0.025 mmol), was added dropwise a light brown CD_2Cl_2 solution (1 mL) of Ph_3SiOTf (41.4 mg, 0.101 mmol) and Cp_2Co (9.3 mg, 0.051 mmol). This resulted in an immediate color change to yellow-green. After 20 min, the reaction mixture was transferred to a J. Young NMR tube, and the ^1H , $^{19}\text{F}\{^1\text{H}\}$, and $^{31}\text{P}\{^1\text{H}\}$ NMR spectra were recorded. The NMR solution was returned to the vial, and stirring was continued. ^1H , $^{19}\text{F}\{^1\text{H}\}$, and $^{31}\text{P}\{^1\text{H}\}$ NMR spectra were similarly recorded after 2 h, 4.5 h, 7 h, and 24 h of stirring at room temperature. In addition, a green precipitate began to form in the reaction mixture after 4 h. # indicates resonances assignable to complex **3.1**, + indicates resonances assignable to complex **3.4**, % indicates resonances assignable to

[Cp₂Co][OTf], ^ indicates resonances assignable to complex **3.3**, and < indicates the resonances of an unidentified U(IV) silyloxy-containing species.

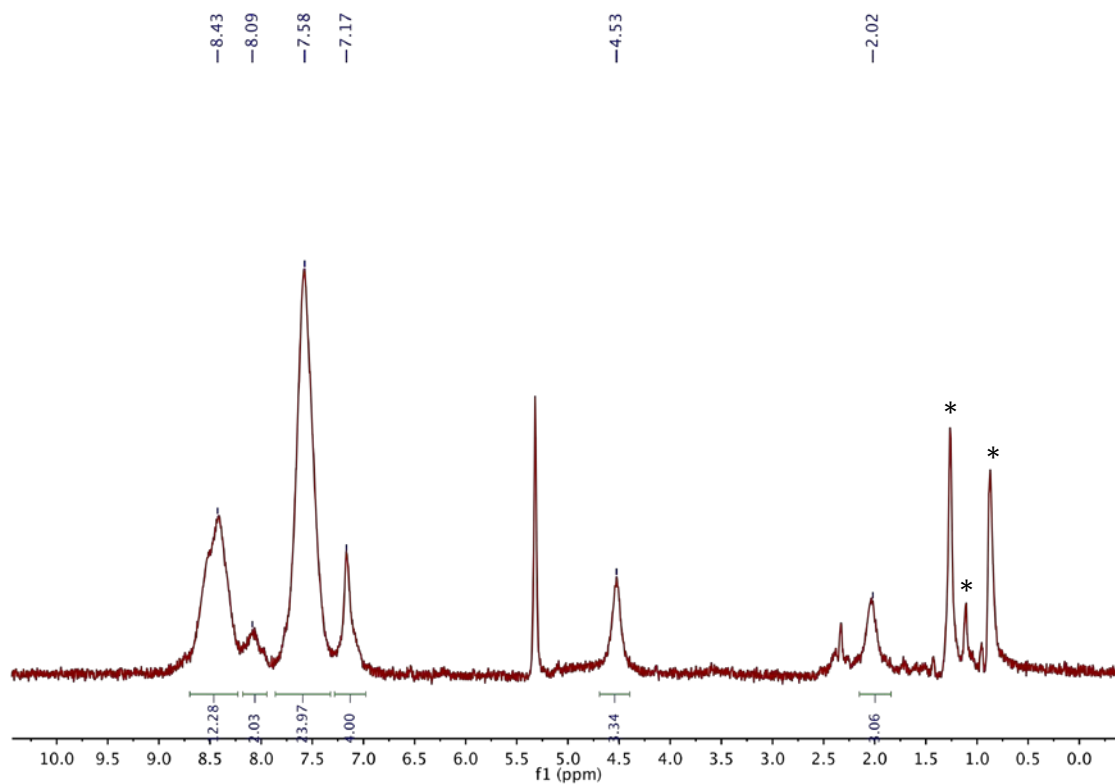


Figure A.5. ¹H NMR spectrum of “[U(OSiMe₃)₂(dbm)₂(THF)][OTf]” in CD₂Cl₂ at 25 °C. Asterisks indicate the presence of hexanes.

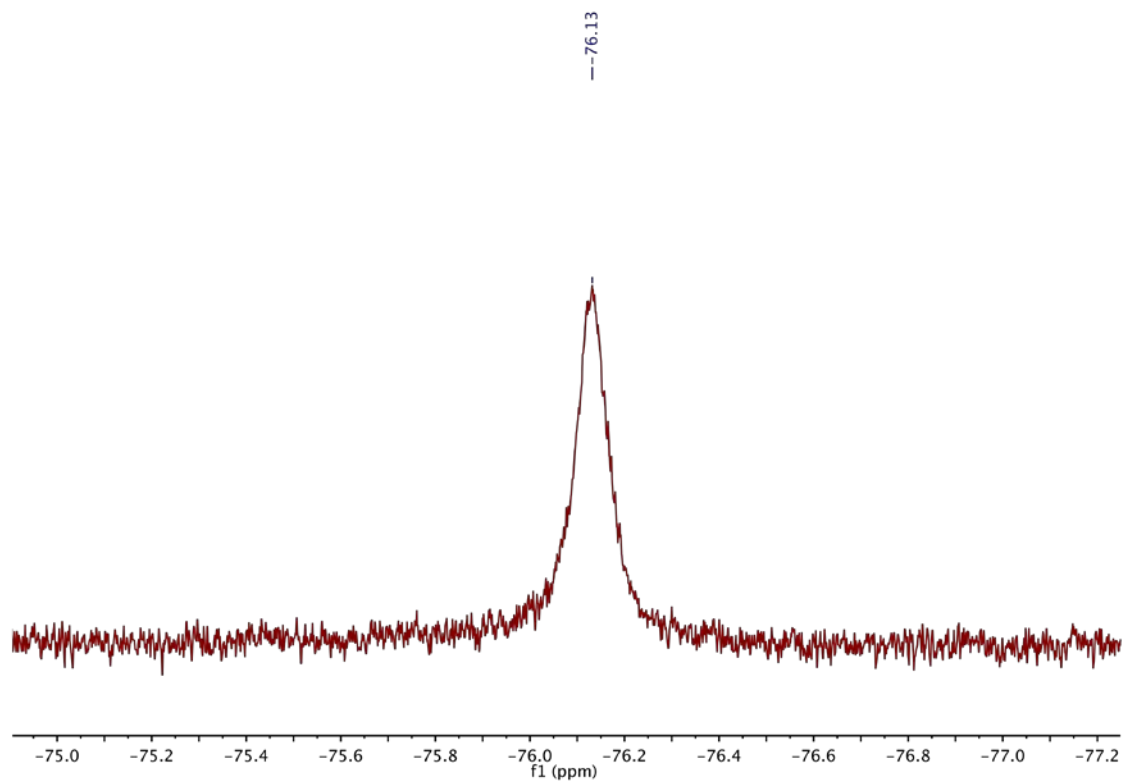


Figure A.6. $^{19}\text{F}\{^1\text{H}\}$ NMR spectrum of “[U(OSiMe₃)₂(dbm)₂(THF)][OTf]” in CD₂Cl₂ at 25 °C.

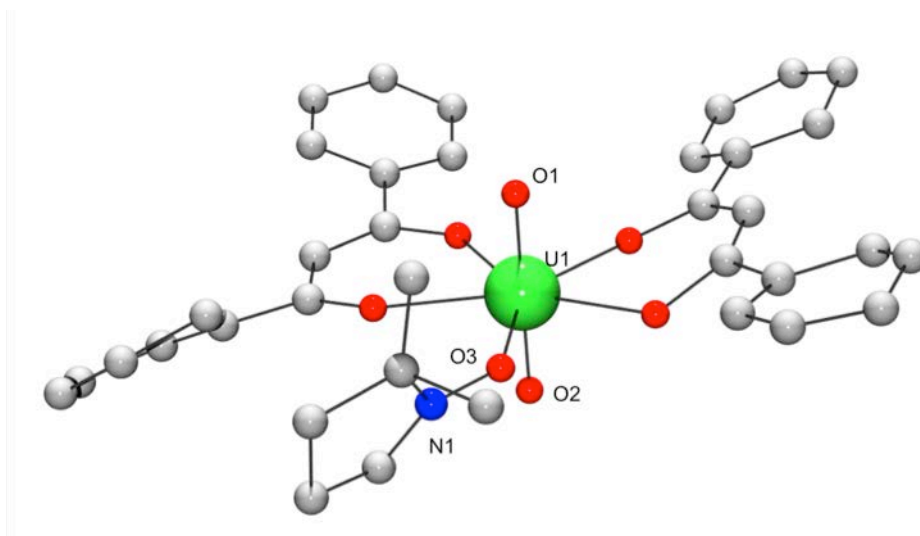


Figure A.7. Solid-state ball and stick structure of $\text{UO}_2(\text{dbm})_2(\text{DMPO})$ (**4.5**). Complex **4.5** crystallizes in the monoclinic space group $P2_1/n$, with the unit cell parameters: $a = 13.709(1) \text{ \AA}$, $b = 15.876(1) \text{ \AA}$, $c = 16.617(1) \text{ \AA}$, $\alpha = 90^\circ$, $\beta = 101.017(7)^\circ$, $\gamma = 90^\circ$, Volume = $3550.1(5)$. Only connectivity could be confirmed from this structure.

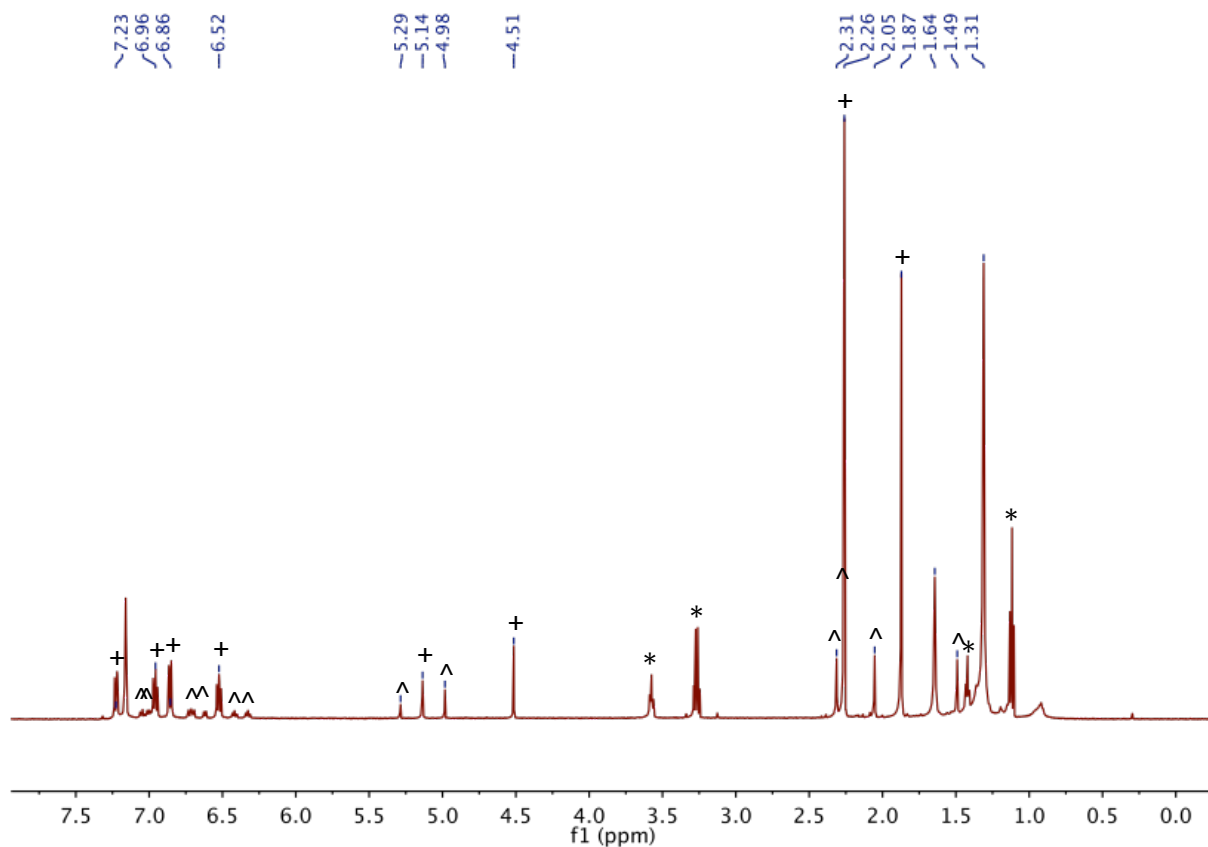


Figure A.8. ^1H NMR spectrum of a mixture of the two isomers of $\text{C}_{22}\text{H}_{22}\text{N}_4$ (*Z*-isomer: **5.3**; *E*-isomer: **5.4**) in a 2:3 ratio in C_6D_6 . ^ indicates resonances assignable to compound **5.3**, + indicates resonances assignable to compound **5.4**, and asterisks indicate the presence of Et_2O and THF.

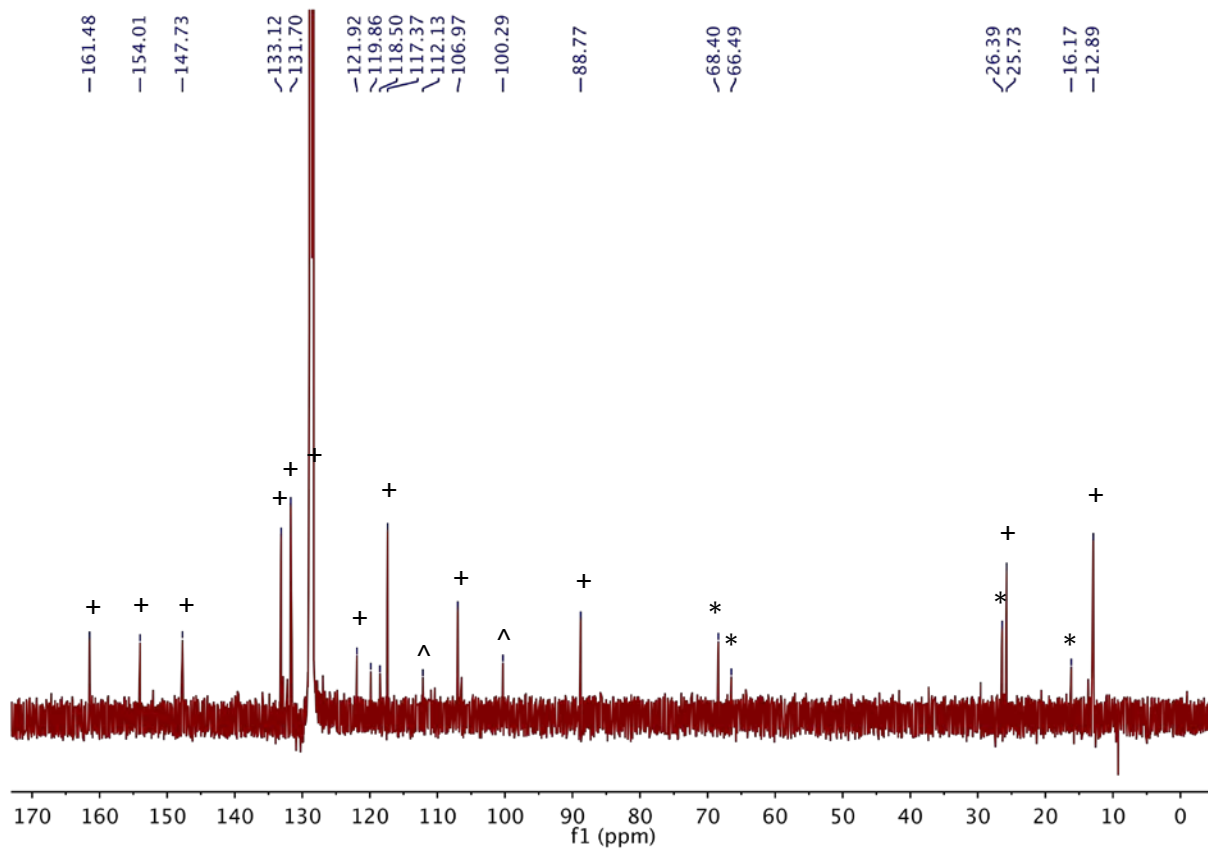


Figure A.9. $^{13}\text{C}\{^1\text{H}\}$ NMR spectrum of a mixture the two isomers of $\text{C}_{22}\text{H}_{22}\text{N}_4$ (*Z*-isomer: **5.3**; *E*-isomer: **5.4**) in a 2:3 ratio in C_6D_6 . ^ indicates resonances assignable to compound **5.3**, + indicates resonances assignable to compound **5.4**, and asterisks indicate the presence of Et_2O .

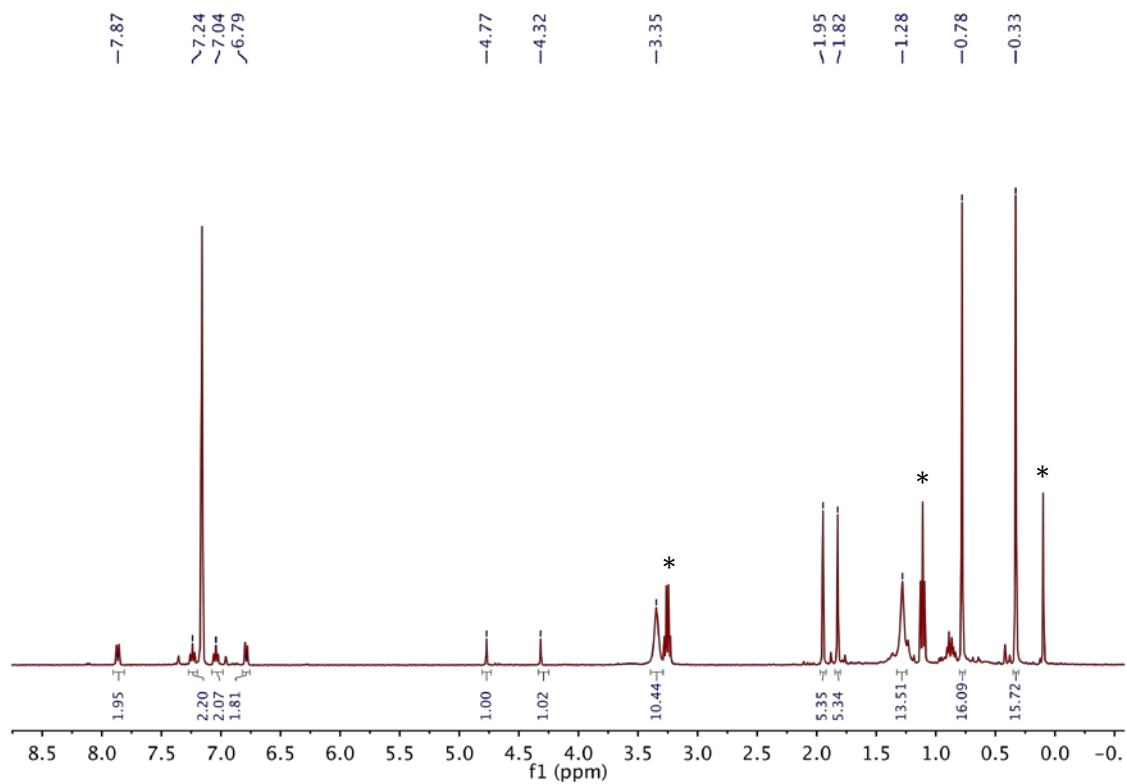


Figure A.10. ¹H NMR spectrum of [Li(THF)₂[UO₂(N(SiMe₃)₂)₂(tmtaa)]] (**5.6**) in C₆D₆ at 25 °C. Asterisks indicate the presence of Et₂O and HN(SiMe₃)₂.

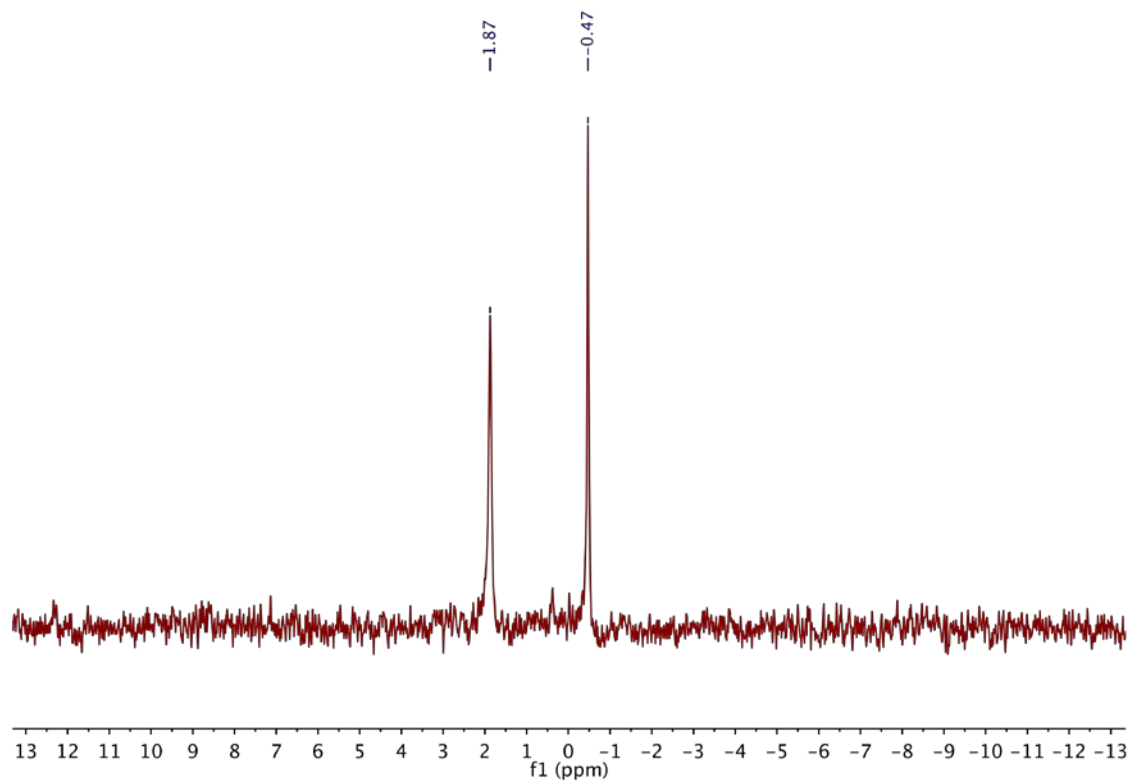


Figure A.11. ${}^7\text{Li}\{{}^1\text{H}\}$ NMR spectrum of $[\text{Li}(\text{THF})_2[\text{UO}_2(\text{N}(\text{SiMe}_3)_2)_2(\text{tmtaa})]]$ (**5.6**) in C_6D_6 at 25 °C.

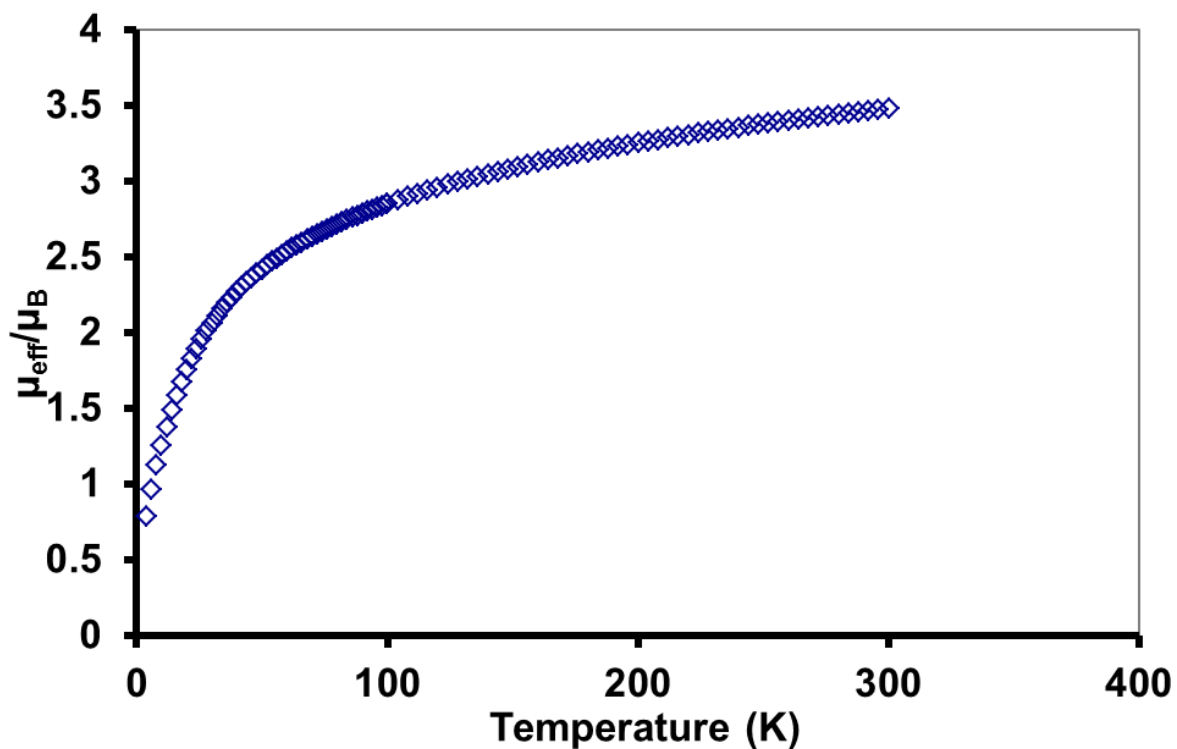


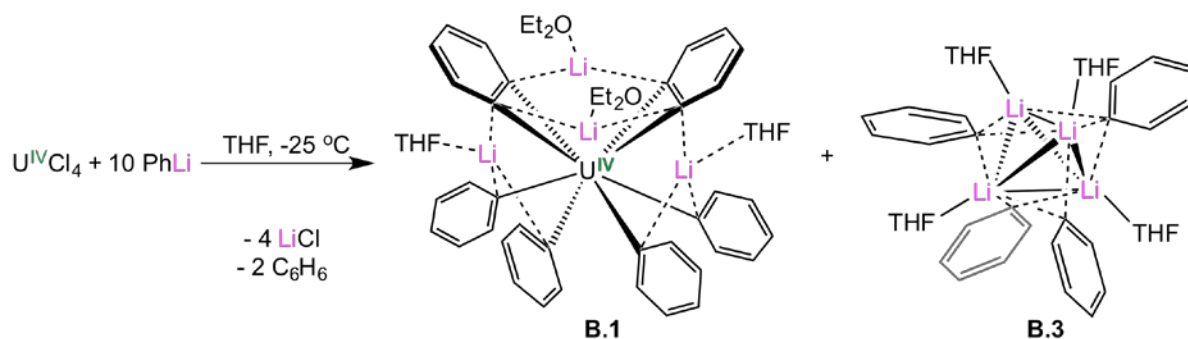
Figure A.12. Temperature dependence of μ_{eff} for $[\text{Li}][\text{U}(2,3\text{-C}_6\text{H}_3\text{CH}_2\text{NMe}_2)(2\text{-C}_6\text{H}_4\text{CH}_2\text{NMe}_2)_3]$ from 4 K to 300 K ($\chi_{\text{dia}} = -3.73 \times 10^{-4} \text{ cm}^3 \cdot \text{mol}^{-1}$, mass = 18.2 mg, $M = 780.75 \text{ g/mol}$). **Magnetism Measurements:** Magnetism data were recorded using a Quantum Design MPMS 5XL SQUID magnetometer. The complex, $[\text{Li}][\text{U}(2,3\text{-C}_6\text{H}_3\text{CH}_2\text{NMe}_2)(2\text{-C}_6\text{H}_4\text{CH}_2\text{NMe}_2)_3]$, was analyzed using 18.2 mg of powdered crystalline material loaded into a NMR tube, which was subsequently flame sealed. The solid was kept in place with $\sim 45 \text{ mg}$ quartz wool packed on either side of the sample. Data for $[\text{Li}][\text{U}(2,3\text{-C}_6\text{H}_3\text{CH}_2\text{NMe}_2)(2\text{-C}_6\text{H}_4\text{CH}_2\text{NMe}_2)_3]$ was collected using a 5 T field between 4 K and 300 K. Diamagnetic correction for 2, $\chi_{\text{dia}} = -3.73 \times 10^{-4} \text{ cm}^3 \cdot \text{mol}^{-1}$, was made using Pascal's constants.¹

(1) Bain, G. A.; Berry, J. F. *J. Chem. Educ.* **2008**, *85*, 532.

Appendix B. Synthesis of U(IV) Aryl Complexes and Sc(III) Ketimide Complexes

B.1. Synthesis of $[\text{Li}(\text{Et}_2\text{O})]_2[\text{Li}(\text{THF})_2]_2[\text{U}(\text{C}_6\text{H}_4)_2(\text{C}_6\text{H}_5)_4]$ (B.1)	267
B.2. Synthesis of $[\text{Li}(\text{Et}_2\text{O})]_4[\text{LiCl}][\text{U}(\text{C}_6\text{H}_4)_2(\text{C}_6\text{H}_5)_3(\text{OC}_4\text{H}_9)]$ (B.2)	269
B.3. Synthesis of $\text{Sc}^{\text{III}}(\text{L1})(\text{N}=\text{C}^t\text{Bu}_2)(\text{Cl})$ (B.4).....	272
B.4. Synthesis of $[\text{Sc}^{\text{III}}(\text{N}=\text{C}^t\text{Bu}_2)_3]_2$ (B.5).....	275
B.5. X-ray Crystallography	278
B.6. References	281

B.1 Synthesis of [Li(Et₂O)]₂[Li(THF)]₂[U(C₆H₄)₂(C₆H₅)₄] (B.1). To a cold (-25 °C), stirring green solution of UCl₄ (101.1 mg, 0.266 mmol) in THF (2 mL) was added cold (-25 °C) PhLi (1.30 mL, 2.66 mmol). The solution immediately turned dark orange-brown and the solvent was removed *in vacuo* to give a very dark brown oil. The oil was extracted into pre-cooled diethyl ether (-25 °C). A grey precipitate was immediately removed by filtration through a Celite column (2 cm × 0.5 cm) supported on glass wool. The resulting brown filtrate was concentrated *in vacuo*. Storage of the solution at -25 °C for 44 d resulted in the formation of a few emerald green crystals of complex **B.1**. These crystals were only isolated once. In one instance, a few emerald green crystals of [Li(Et₂O)]₄[LiCl][U(C₆H₄)₂(C₆H₅)₃(OC₄H₉)] (**B.2**), were isolated from a similar reaction mixture, although the yield was again very low. Other attempts to repeat this synthesis lead to the isolation of many colorless crystals of [Li(THF)]₄[C₆H₅]₄ (**B.3**) (See Below).



Scheme B.1. Synthesis of **B.1** and **B.3**.

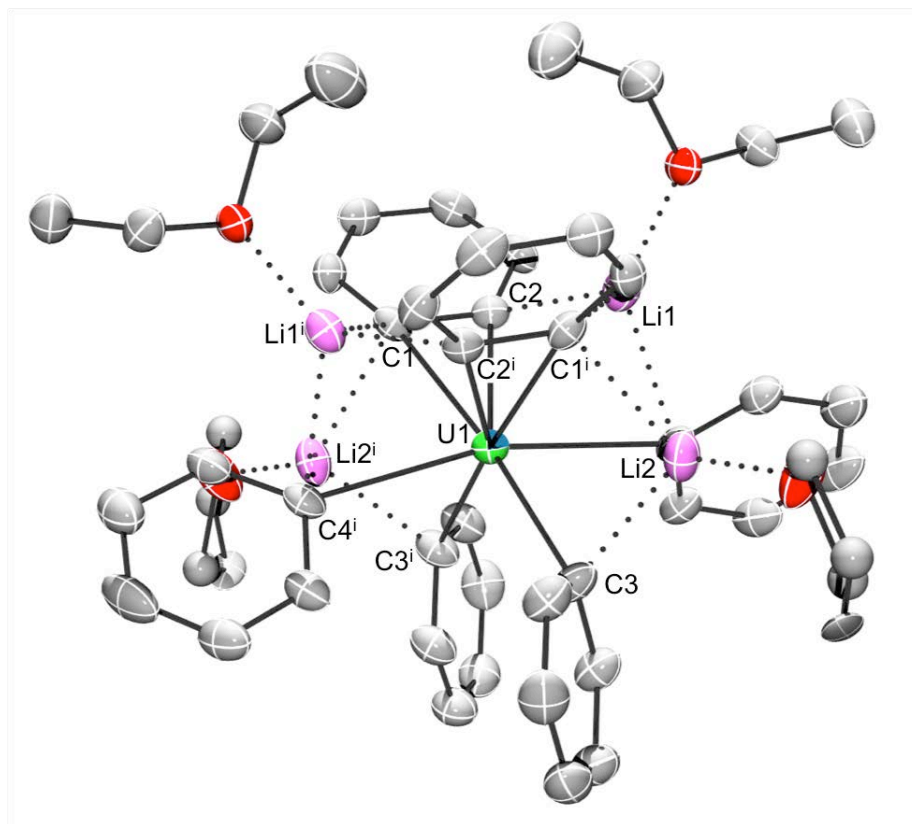
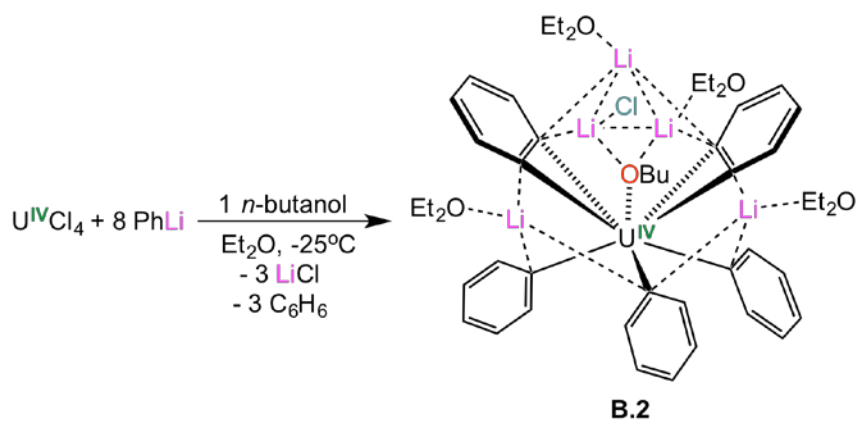


Figure B.1. Solid-state structure of $[\text{Li}(\text{Et}_2\text{O})]_2[\text{Li}(\text{THF})_2]_2[\text{U}(\text{C}_6\text{H}_4)_2(\text{C}_6\text{H}_5)_4]$ (**B.1**), with 50% probability ellipsoids. Hydrogen atoms omitted for clarity. Selected bond lengths (\AA) and angles (deg): $\text{U1-C1} = 2.542(5)$, $\text{U1-C2} = 2.435(3)$, $\text{U1-C3} = 2.629(4)$, $\text{U1-C4} = 2.715(4)$, $\text{C1-C2} = 1.420(6)$, $\text{C1-U1-C2} = 33.1(1)$, $\text{C1-U1-C2}^i = 86.3(1)$, $\text{C3-U1-C3}^i = 101.1(2)$, $\text{C4-U1-C4}^i = 165.2(2)$.

B.2 Synthesis of [Li(Et₂O)]₄[LiCl][U(C₆H₄)₂(C₆H₅)₃(OC₄H₉)] (B.2). To a cold (-25 °C), stirring green solution of UCl₄ (66.9 mg, 0.176 mmol) in THF (2 mL) was added cold (-25 °C) PhLi (0.78 mL, 0.176 mmol), which resulted in a dark red brown solution. Then, *n*-butanol (16.5 μL, 0.180 mmol) was immediately added via microsyringe, which did not result in any visible change. The solution was quickly filtered through a Celite column (2 cm × 0.5 cm) supported on glass wool, which afforded a dark brown filtrate and a black-brown plug. The filter was rinsed with Et₂O (<1 mL) to dissolve most of the plug. The volume of the filtrate was reduced *in vacuo* (ca. 1.5 mL), and storage of the solution at -25 °C for 3 h resulted in the formation of a few colorless crystals, which were removed by decanting the solution. The dark brown mother liquor was quickly filtered again through a Celite (2 cm × 0.5 cm) supported on glass wool. The resulting dark brown filtrate was transferred to a 4mL scintillation vial that was placed inside a 20mL scintillation vial. Hexanes (2 mL) was then added to the outer vial. Storage of this two vial system at -25 °C for 30 d afforded a few green rhombic crystals towards the mouth of the inner vial. The identity of the green rhombic crystals were confirmed twice from two separate reactions by a unit cell determination of a green rhombic crystal: $a = 23.56 \text{ \AA}$, $b = 12.70 \text{ \AA}$, $c = 35.40 \text{ \AA}$; $\alpha = 90^\circ$, $\beta = 99.30^\circ$, $\gamma = 90^\circ$, as well as $a = 23.68 \text{ \AA}$, $b = 12.89 \text{ \AA}$, $c = 35.62 \text{ \AA}$; $\alpha = 90^\circ$, $\beta = 98.72^\circ$, $\gamma = 90^\circ$, which both match the unit cell originally obtained for **B.2** (Table B.1).



Scheme B.2. Synthesis of complex **B.2**.

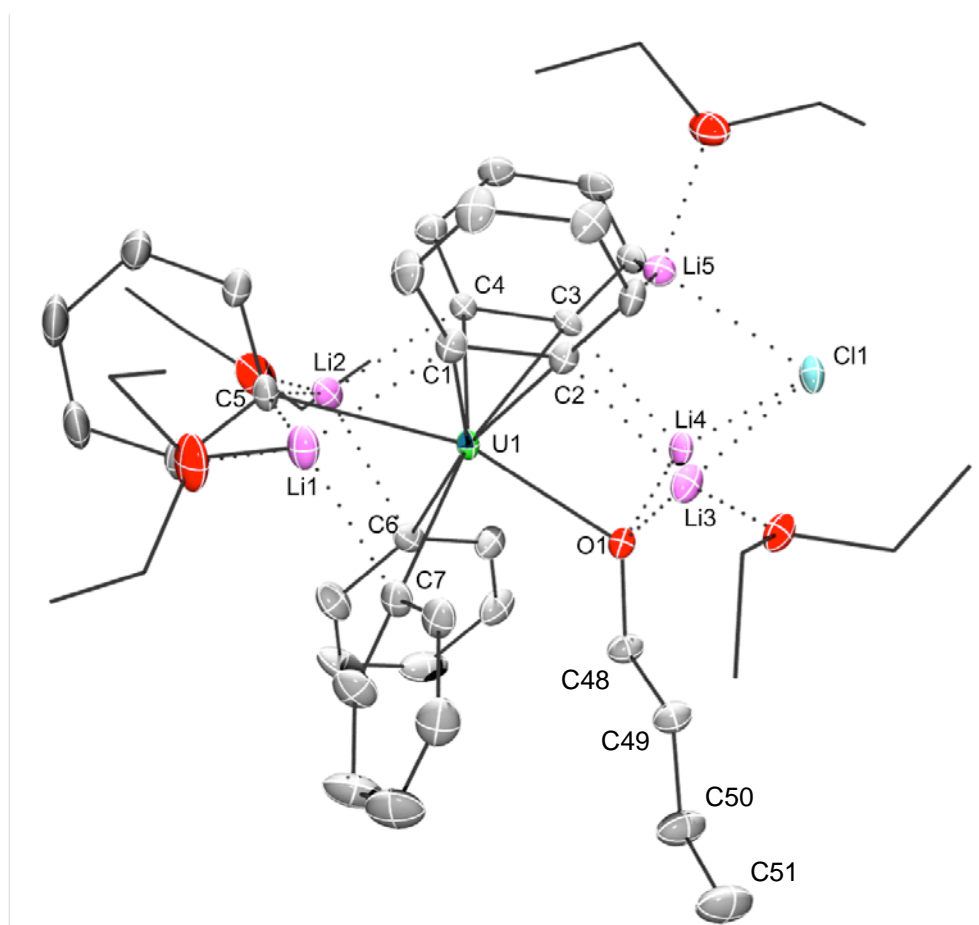


Figure B.2. Solid-state structure of $[\text{Li}(\text{Et}_2\text{O})]_4[\text{LiCl}][\text{U}(\text{C}_6\text{H}_4)_2(\text{C}_6\text{H}_5)_3(\text{OC}_4\text{H}_9)]$ (**B.2**) with 50% probability ellipsoids. Hydrogen atoms omitted for clarity. Selected bond

lengths (Å) and angles (deg): U1-C1 = 2.440(5), U1-C2 = 2.555(5), U1-C3 = 2.559(5), U1-C4 = 2.447(5), U1-C5 = 2.701(5), U1-C6 = 2.659(5), U1-C7 = 2.656(5), U1-O1 = 2.371(3), C1-C2 = 1.404(7), C3-C4 = 1.428(7), O1-C48 = 1.418(6), C48-C49 = 1.513(7), C49-C50 = 1.487(8), C50-C51 = 1.504(9).

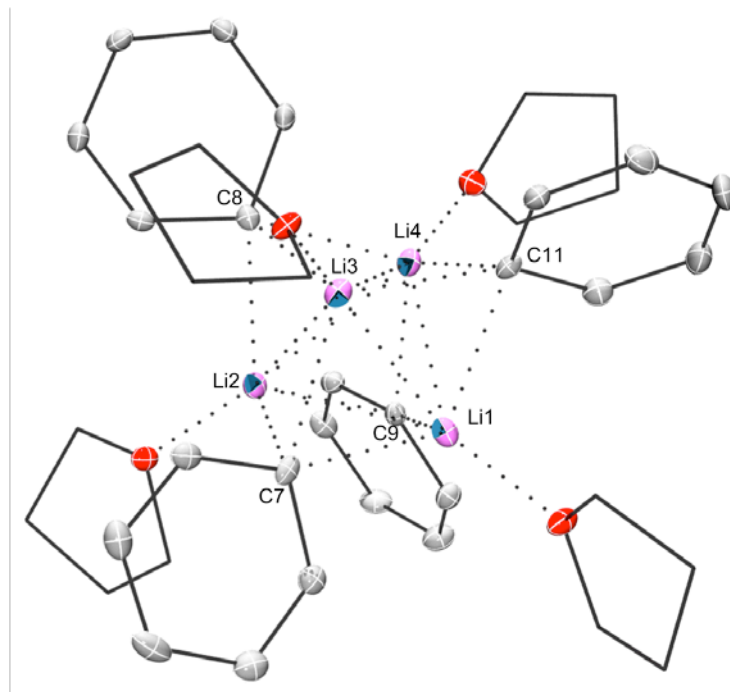
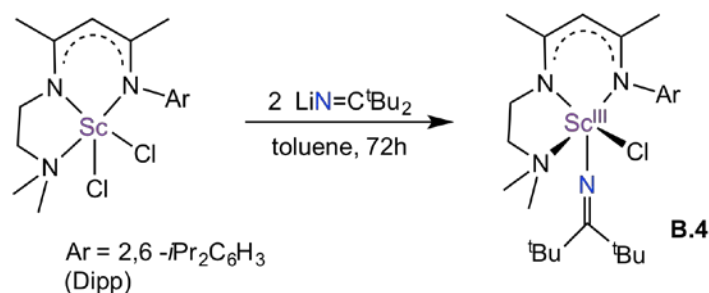


Figure B.3. Solid-state structure of $[\text{Li}(\text{THF})]_4[\text{C}_6\text{H}_5]_4$ (**B.3**), with 50% probability ellipsoids for the phenyl carbons. Hydrogen atoms omitted for clarity. Selected bond lengths (Å): Li1-C7 = 2.311(4), Li1-C9 = 2.260(4), Li1-C11 = 2.341(4), Li2-C7 = 2.257(4), Li2-C8 = 2.249(4), Li2-C9 = 2.304(4), Li1-Li2 = 2.700(5), Li1-Li3 = 2.500(5), Li1-Li4 = 2.628(5), Li2-Li3 = 2.585(5), Li2-Li4 = 2.661(5), Li3-Li4 = 2.622(5), Li1-O2 = 2.016(4).

B.3 Synthesis of Sc^{III}(L1)(N=C^tBu₂)(Cl) (B.4). To a stirring yellow solution of (L1)ScCl₂ [L1 = CH₃C(2-6-(*i*Pr)₂-C₆H₃N)CHC(CH₃)(NCH₂CH₂NMe₂)]¹ (100.4 mg, 0.226 mmol) in toluene (~3 mL), was added a yellow slurry of LiN=C^tBu₂ (66.5 mg, 0.452 mmol) in toluene (~3 mL). The slurry was allowed to stir at room temperature for 10 min, whereupon the color of the slurry took on an orange hue. The slurry was allowed to stir for an additional 72 h, whereupon a yellow-orange solution was generated, concomitant with the deposition of a very fine white precipitate. The fine white solid was removed via centrifugation. The volatiles of the resulting light orange solution were removed *in vacuo*. The resulting orange oil was triturated with hexanes (1 mL), which resulted in a mixture of orange solid and orange oil. The oil was extracted in hexanes (3 mL), decanted away from the solid and discarded. The orange solid was dried *in vacuo* (97.9 mg, 79% yield). X-ray quality crystals were grown out of a concentrated toluene solution stored at -25 °C for 24 h. ¹H NMR (C₆D₆, 25 °C, 400 MHz): δ 7.24 (m, 3H, Dipp), 5.00 (s, 1H, γ-CH), 3.37 (m, 2H, CH₂), 2.86 (m, 2H, CH₂), 2.34 (s, 3H, CH₃), 2.15 (s, 3H, CH₃), 1.66 (s, 6H, *i*Pr-Dipp), 1.62 (s, 6H, *i*Pr-Dipp), 1.51 (d, *J*_{HH} = 9 Hz, 3H, CH₃), 1.30 (s, 18H, *t*Bu) 1.20 (d, *J*_{HH} = 9 Hz, 3H, CH₃).



Scheme B.3. Synthesis of complex B.4.

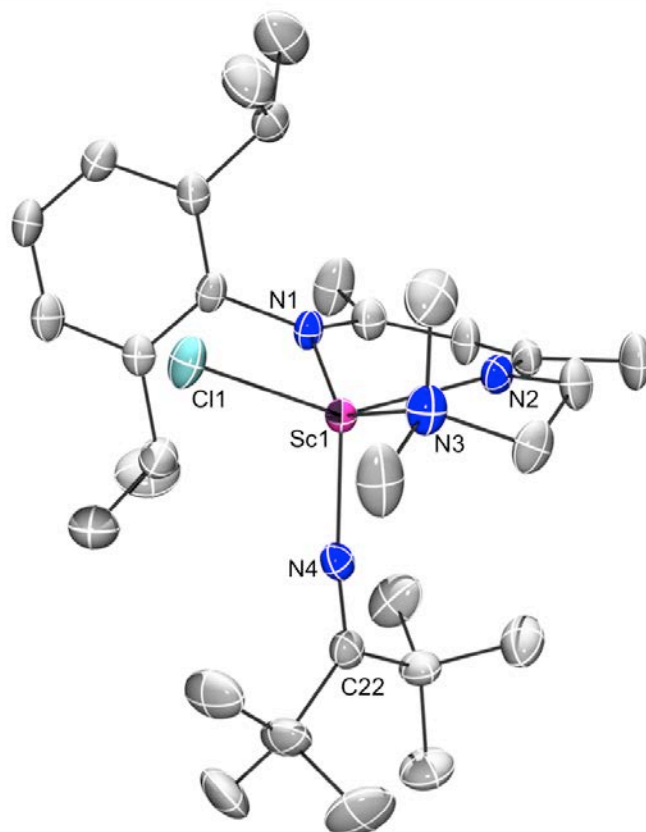


Figure B.4. Solid-state structure of $\text{Sc}^{\text{III}}(\text{L1})(\text{N}=\text{C}^t\text{Bu}_2)(\text{Cl})$ (**B.4**) with 50% probability ellipsoids. All hydrogen atoms have been removed for clarity. Complex **B.4** crystallizes with two independent molecules in the asymmetric unit; only one is shown here for clarity. Selected bond lengths (\AA) and angles (deg): $\text{Sc1-N1} = 2.184(5)$, $\text{Sc1-N2} = 2.194(4)$, $\text{Sc1-N3} = 2.343(5)$, $\text{Sc1-N4} = 1.988(4)$, $\text{N4-C22} = 1.243(6)$, $\text{Sc1-Cl1} = 2.424(2)$, $\text{Sc1-N4-C22} = 171.8(4)$. The $\text{Sc-N}_{\text{ketimide}}$ bond length ($1.988(4) \text{ \AA}$) falls in between the Sc-N bond lengths in the complexes $\text{Sc}^{\text{III}}(\text{L1})(\text{HNDipp})(\text{Me})$ ($\text{Sc-NH}_{\text{Dipp}} = 2.047(3) \text{ \AA}$) and $\text{Sc}^{\text{III}}(\text{L1})(\text{NDipp})(\text{DMAP})$ ($\text{Sc}=\text{N}_{\text{Dipp}} = 1.881(5) \text{ \AA}$).¹

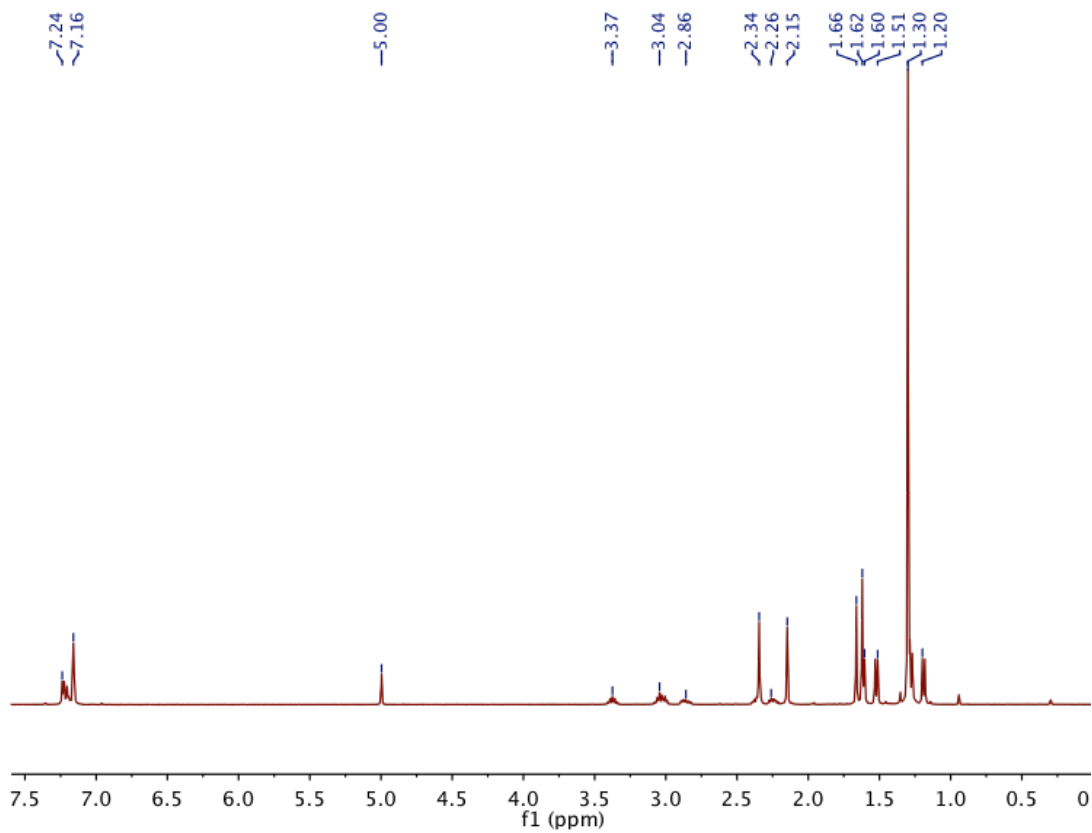
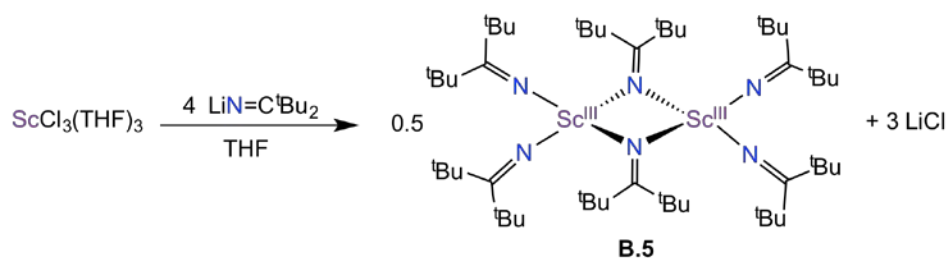


Figure B.5. ^1H NMR spectrum of complex **B.4** in C_6D_6 .

B.4 Synthesis of [Sc^{III}(N=C^tBu₂)₃]₂ (B.5). To a stirring, off white slurry of ScCl₃(THF)₃ (100.5 mg, 0.273 mmol) in THF (2 mL), was added a white slurry of LiN=C^tBu₂ (159.9 mg, 1.086 mmol) in THF (3 mL), which resulted in an immediate change to a yellow slurry. After stirring at room temperature for 15 min, the solid completely dissolved. The resulting yellow solution was allowed to stir for an additional 1.33 h, whereupon all the volatiles were removed *in vacuo*. The resulting yellow solid was triturated with hexanes (2 mL), and extracted into hexanes (5 mL). The resulting yellow slurry was filtered through a Celite column (2 cm × 0.5 cm) supported on glass wool. All the volatiles were removed from the yellow filtrate *in vacuo*, which afforded a yellow oil. The yellow oil was dried *in vacuo* for 3 h, which resulted in the formation of a yellow oil concomitant with a yellow solid. Several drops of cold (-25 °C) hexanes were added to the mixture. Storage of the mixture at -25 °C for 1 h, resulted in formation of a yellow solution concomitant with a yellow solid. The supernatant was decanted quickly from the solid and discarded. The solid was dried *in vacuo*, and then extracted into hexanes (~2 mL). The resulting yellow solution was concentrated *in vacuo* (ca. 1.5 mL), and storage of the solution at -25 °C for 24 h, afforded yellow crystals (82.6 mg, 65% yield). ¹H NMR (C₆D₆, 25 °C, 400 MHz): δ 1.40 (s, 36H, ^tBu), 1.37 (s, 72H, ^tBu).



Scheme B.4. Synthesis of complex **B.5**.

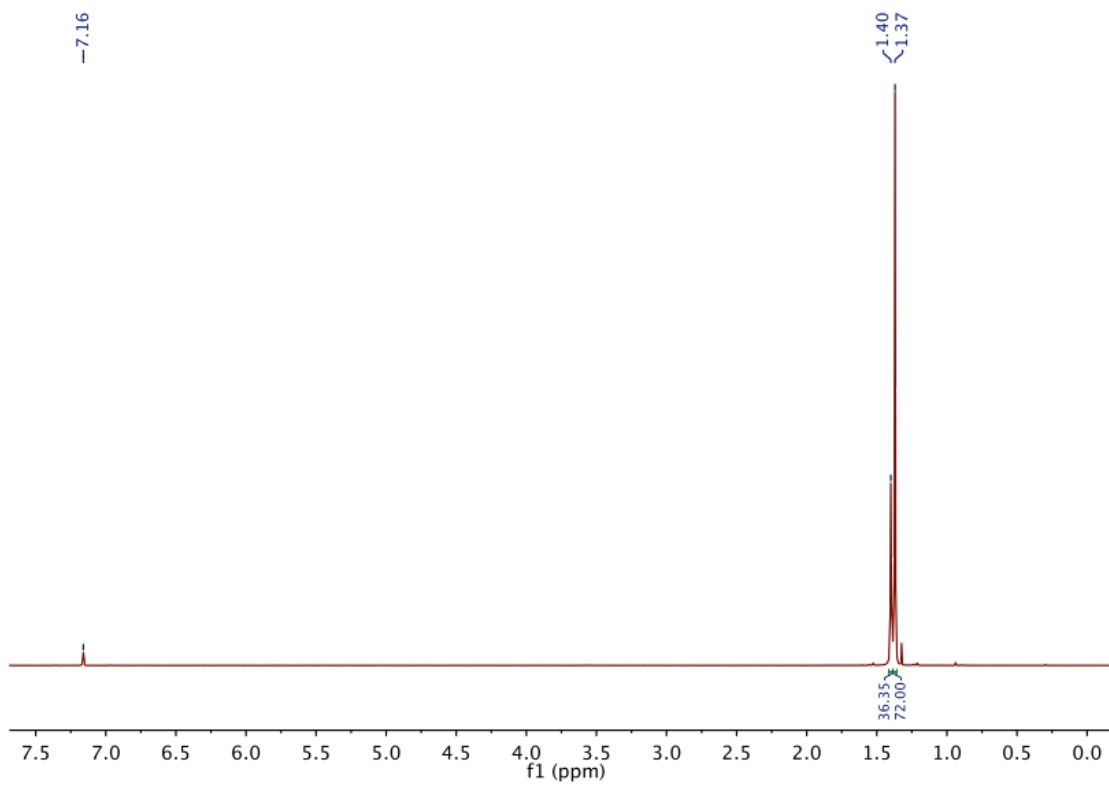


Figure B.7. ^1H NMR spectrum of complex **B.5** in C_6D_6 .

B.5 X-ray Crystallography. The solid-state molecular structures of complexes **B.1 – B.5** were determined similarly with exceptions noted in the following paragraph. Crystals were mounted on a cryoloop under Paratone-N oil. Data collection was carried out on a Bruker KAPPA APEX II diffractometer equipped with an APEX II CCD detector using a TRIUMPH monochromater with a Mo K α X-ray source ($\lambda = 0.71073 \text{ \AA}$). Data for **B.1 – B.3** were collected at 100(2) K, data for **B.4** were collected at 173(2) K, and data for **B.5** were collected at 140(2) K, using an Oxford nitrogen gas cryostream system. A hemisphere of data was collected using ω scans with 0.5° frame widths. Frame exposures 10 seconds were used for complexes **B.1 - B.5**. Data collection and cell parameter determination were conducted using the SMART program.² Integration of the data frames and final cell parameter refinement were performed using SAINT software.³ Absorption correction of the data was carried out using the multi-scan method SADABS.⁴ Subsequent calculations were carried out using SHELXTL.⁵ Structure determination was done using direct or Patterson methods and difference Fourier techniques. All hydrogen atom positions were idealized, and rode on the atom of attachment. Structure solution, refinement, graphics, and creation of publication materials were performed using SHELXTL.⁵ A summary of relevant crystallographic data for complexes **B.1–B.5** are presented in Tables B.1-B.2.

Table B.1. X-ray Crystallographic Information for **B.1**, **B.2** and **B.3**

	B.1	B.2	B.3
empirical formula	C ₄₈ H ₅₆ Li ₄ O ₄ U	C ₁₀₀ H ₁₄₂ Cl ₂ Li ₁₀ O ₁₀ U ₂	C ₄₀ H ₅₂ Li ₄ O ₄
Crystal habit, color	plate, green	diamond, green	needle, colorless
crystal size (mm)	0.20 × 0.1 × 0.05	0.1 × 0.05 × 0.25	0.30 × 0.05 × 0.05
crystal system	orthorhombic	monoclinic	triclinic
space group	<i>Pbcn</i>	<i>C2/c</i>	<i>P-1</i>
vol (Å ³)	4824.3(2)	10331.8(7)	1826.0(5)
a (Å)	14.0716(4)	23.4693(9)	9.242(1)
b (Å)	18.4128(5)	12.6104(4)	10.202(2)
c (Å)	18.6195(5)	35.308(2)	20.017(3)
α (deg)	90	90	85.338(5)
β (deg)	90	98.614(2)	83.932(4)
γ (deg)	90	90	77.091(5)
Z	4	4	2
fw (g/mol)	962.72	2120.50	624.60
density (calcd) (Mg/m ³)	1.325	1.363	1.468
abs coeff (mm ⁻¹)	3.402	3.234	0.068
F ₀₀₀	1920	4280	642
Total no. reflections	10469	45118	7314
Unique reflections	5302	13345	4647
final R indices [I > 2σ(I)]	R ₁ = 0.0404 wR ₂ = 0.1239	R ₁ = 0.0467 wR ₂ = 0.0975	R ₁ = 0.0549 wR ₂ = 0.1183
largest diff peak and hole (e ⁻ Å ⁻³)	1.963 and -0.971	1.685 and -1.530	0.403 and -0.399
GOF	0.976	1.053	1.020

Table B.2. X-ray Crystallographic Information for **B.4** and **B.5**

	B.4	B.5
empirical formula	C ₃₀ H ₅₂ ClN ₄ Sc	C ₅₄ H ₁₀₆ N ₆ Sc ₂
Crystal habit, color	block, yellow	block, pale-yellow
crystal size (mm)	0.26 × 0.10 × 0.05	0.26 × 0.25 × 0.20
crystal system	triclinic	monoclinic
space group	<i>P</i> -1	<i>P</i> 2 ₁ / <i>n</i>
vol (Å ³)	3245(2)	5885(2)
a (Å)	10.683(4)	12.206(3)
b (Å)	15.633(5)	22.474(5)
c (Å)	20.213(7)	21.472(5)
α (deg)	88.596(7)	90
β (deg)	89.309(7)	92.432(4)
γ (deg)	74.077(6)	90
Z	4	4
fw (g/mol)	549.16	929.36
density (calcd) (Mg/m ³)	1.124	1.049
abs coeff (mm ⁻¹)	0.332	0.267
F ₀₀₀	1192	2056
Total no. reflections	12594	10921
Unique reflections	8071	6140
final R indices [I > 2σ(I)]	R ₁ = 0.0806 wR ₂ = 0.2347	R ₁ = 0.0793 wR ₂ = 0.2113
largest diff peak and hole (e ⁻ Å ⁻³)	1.246 and -0.702	0.899 and -0.529
GOF	1.048	1.062

B.6 References

- (1) Lu, E.; Li, Y.; Chen, Y. *Chem. Commun.* **2010**, *46*, 4469.
- (2) *SMART*, Apex II, Version 2.1; Bruker AXS Inc.: Madison, WI, 2005.
- (3) *SAINT*, Software User's Guide, Version 7.34a; Bruker AXS Inc.: Madison, WI, 2005.
- (4) Sheldrick, G. M. *SADABS*, University of Gottingen: Germany, 2005.
- (5) *SHELXTL PC*, Version 6.12; Bruker AXS Inc.: Madison, WI, 2005.